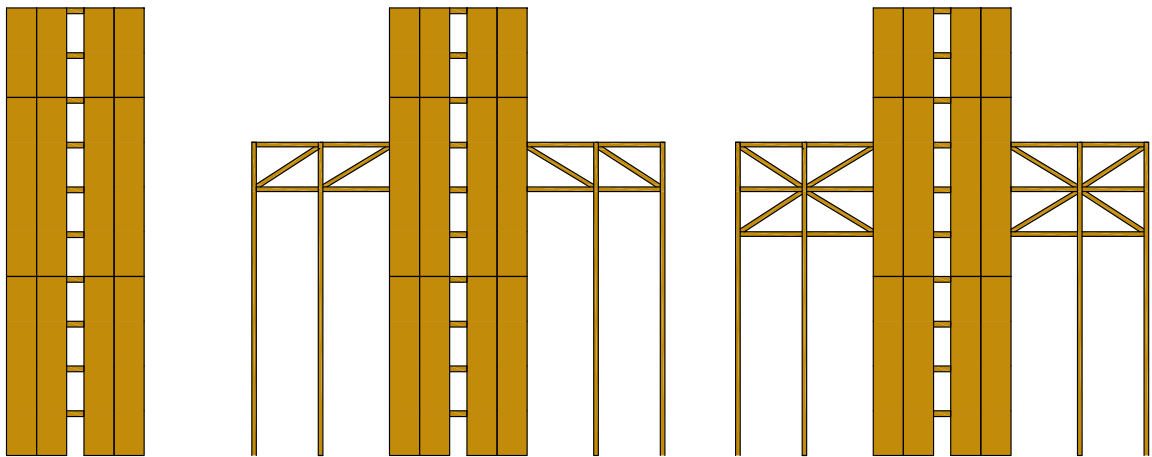


DELFT UNIVERSITY OF TECHNOLOGY

**INFLUENCE OF A TIMBER OUTRIGGER SYSTEM ON CROSS
LAMINATED TIMBER CORE BUILDINGS**



INFLUENCE OF A TIMBER OUTRIGGER SYSTEM ON CROSS LAMINATED TIMBER CORE BUILDINGS

[Master's Thesis]

by

F.F. Janssens

in partial fulfillment of the requirements for the degree of

Master of science
in civil engineering

at the Delft University of Technology,
to be defended publicly on March 15, 2023

Thesis Committee:	Dr.ir. G.J.P. Ravenshorst	TU Delft, Chairman
	Dr.ir. P.C.J. Hoogenboom	TU Delft, Supervisor
	Prof.dr.ir. J.W.G. van de Kuilen	TU Delft, Supervisor
	Ir. M. Felicita	TU Delft, Supervisor

An electronic version of this thesis is available at <http://repository.tudelft.nl/>.



Author's Declaration of Originality

I hereby certify that I am the sole author of this thesis. All the used materials, references to the literature and the work of others have been referred to. This thesis has not been presented for examination anywhere else.

Author: F.F. Janssens

07.03.2023

Abstract

The construction industry contributes significantly to global emissions. In response to the growing concern about climate change, new methods are being developed to reduce these emissions. Building with timber is one such approach, as it can be CO_2 neutral if reforestation is practiced. Timber is a lightweight and flexible material compared to traditional construction materials like steel and concrete, which can result in high accelerations and deflections, negatively affecting user comfort.

Engineered wood products such as CLT and GLT make it possible to construct larger panel sizes and spans, which can lead to more efficient building design. Many buildings utilize core systems to provide lateral stability and facilitate vertical transportation of goods and people. Therefore, replacing a conventional concrete core with a CLT core could be a viable solution to reduce the building's environmental impact.

Timber, being a flexible material, often lacks the necessary stability to meet user requirements for deflection and acceleration in high-rise buildings. An outrigger, similar to those used in concrete and steel structures, can provide the solution to enhance user comfort. The outrigger transfers bending moments from the core to the columns, reducing forces in the core and increasing overall stiffness. However it is unclear what the influence of the addition of a timber outrigger on a CLT core building is and how such a system can be improved. Therefore the purpose of this thesis is to evaluate the impact of a timber outrigger on a CLT core building, and provide guidance for structural engineers on how to improve the structural behaviour of such a system.

The impact of adding an outrigger is evaluated through comparison of numerical case studies. Case A consists of a CLT core as the lateral stability system. Case B consists of a CLT core with timber outriggers. A sensitivity analysis is performed on different design aspects for each case. In Case A, the influence of core joint design is analyzed, while in Case B, the impact of outrigger design parameters is evaluated. For a fair comparison of deflections, accelerations and force transfer, both Case A and B are designed based on ULS requirements. Finally, Case C is an optimized design based on the results of the sensitivity analyses. The different stability systems of the case studies as previously mentioned can be seen in figure 1.

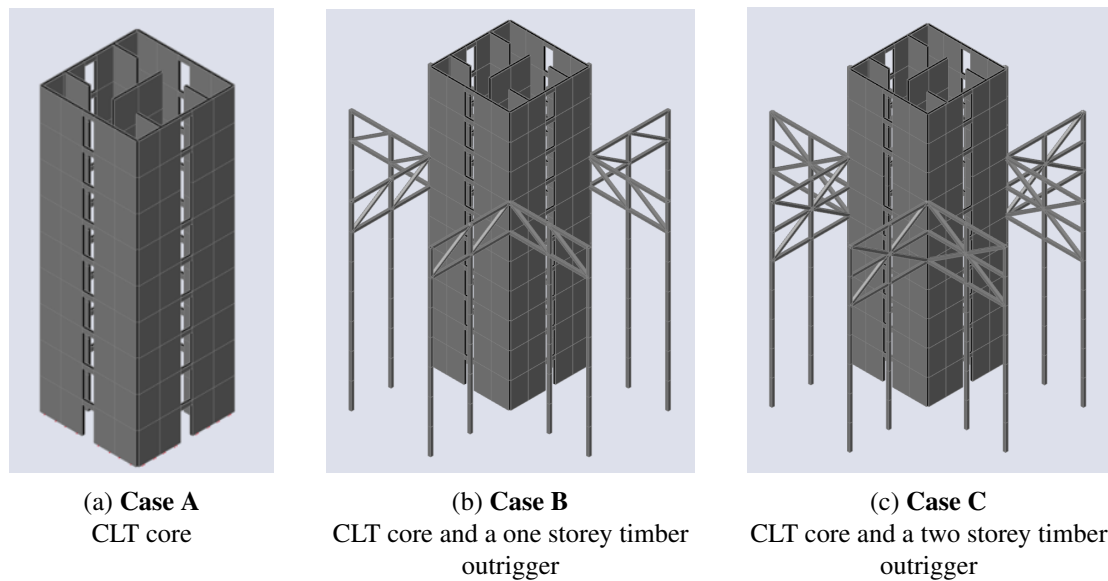


Figure 1. Numerical models of the different stability systems

By introducing a timber outrigger to a CLT core building bending moments are transferred from the core to the column, partially restricting rotation of the core. This will have the following effects on the behaviour of the structure. Firstly, the deflections due to lateral wind loading are reduced due to the increased global stiffness. In figure 2 the maximum lateral deflection of the three different case studies is shown. In which the maximum lateral deflection of case A is reduced by 14% and 35% for case B and C respectively.

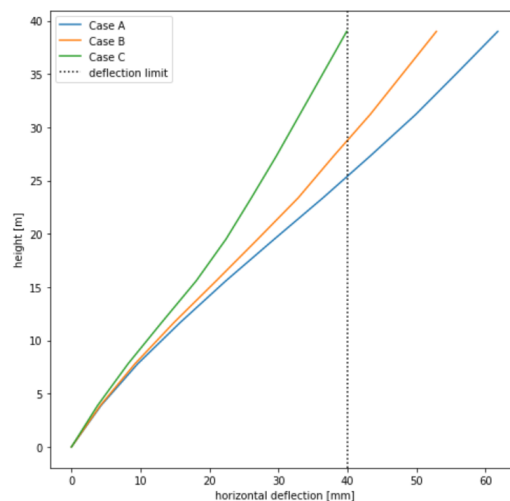


Figure 2. Lateral deflection of the different case studies

Secondly, the increased stiffness of the structure will result in a reduction of peak lateral acceleration. The peak lateral acceleration of case A is reduced by 10% and 25% for case B and C respectively compared to case A. Thirdly, by transferring loads from the core to the columns the strength requirements on the connections of the core are reduced. Finally, by introducing a timber outrigger system to a CLT core building horizontal forces are generated in the core at outrigger level, which

should be accounted for in the design phase of the vertical core joints. Increasing the stiffness of the outrigger will further reduce deflections, peak lateral acceleration and strength requirements on the core joint, however strength requirements on the vertical core joints at outrigger level will further increase.

An exponential relationship has been derived between the lateral deflections and the ratio between the effective bending stiffness of the outrigger and the effective bending stiffness of the core as can be seen figure 3a. A similar exponential relationship has been derived for the peak lateral accelerations as shown in figure 3b.

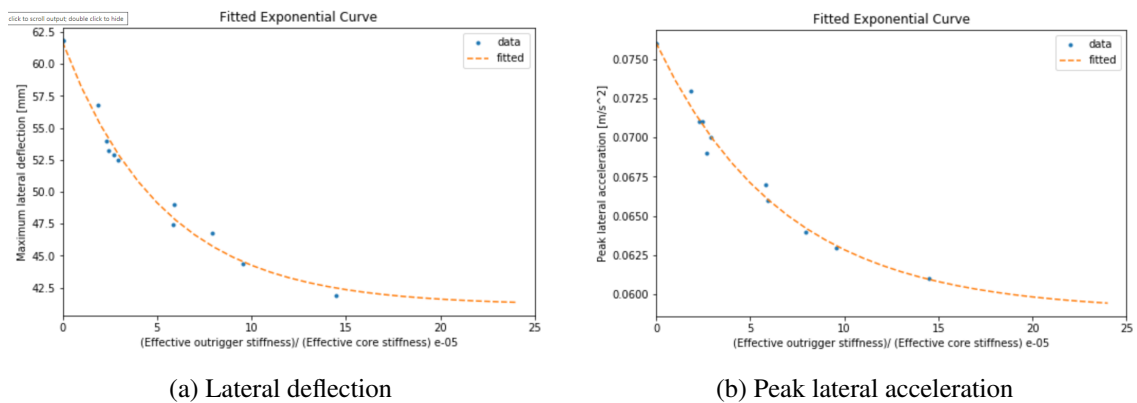


Figure 3. *Fitted curves influence of stiffness ratio*

With the previously shown exponential relationships the effectiveness of a specific outrigger design in terms of reducing deflections and lateral accelerations is determined and shown in figure 4, in which 0% effectiveness represents an outrigger with zero bending stiffness and 100% effectiveness represents an infinitely rigid outrigger.

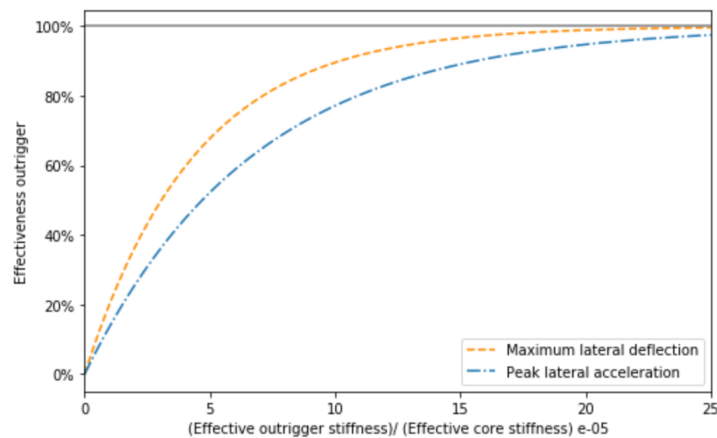


Figure 4. *Effectiveness outrigger*

Additionally it was investigated what the critical design parameters are and how the performance of a CLT core building with timber outriggers can be improved. For the design of a CLT core

the connection between the core and foundation showed to be critical, having large effects on the lateral deformation. While increasing the stiffness of the vertical connections showed to have little influence on the interaction between core walls due to their respective high interaction factors. In the design of the outrigger it was shown that a two storey outrigger is able to more than double the reduction in deflections compared to a single storey outrigger, further increasing the overall effectiveness of the system. Finally the effectiveness of the system was found to be significantly influenced by the configuration of the outrigger truss, demonstrating a greater impact than increasing member size or connection stiffness.

keywords: stability system, CLT core, timber outrigger, wind-induced behaviour, lateral deflections, dynamic behaviour

Acknowledgements

I would like to acknowledge and express my gratitude to those that have helped me write this thesis.

I would like to begin with thanking my graduation committee, Geert Ravenshorst, Jan-willem van de Kuilen, Pierre Hoogenboom and Maria Felicita. Thanks to the critical feedback provided during our meetings I was able to obtain new insights which has helped me tremendously in completing this research. I would like to mention Maria Felicita in particular as she has helped me through our numerous meetings that we have had. Because of your interest in my research topic I always had someone to talk about difficulties that occurred throughout the thesis, providing valuable feedback from start to finish.

I would like to thank my parents and family for always supporting and loving me, whatever decision I make. You have and will always be there for me and for that I am very grateful.

I would like to thank Féline, for always having my back, loving me and distracting me during stressful times. Due to you I was always motivated to do my best which has helped me a lot in writing this research. I am for always thankful for the support that you have provided during the period that I was writing this thesis.

Finally I would like to thank my friends for always keeping my spirit up.

Table of Contents

Author's Declaration of Originality	i
Abstract	ii
Acknowledgements	vi
List of Figures	x
List of Tables	xv
1 Introduction	1
1.1 Scientific relevance and research motive	1
1.2 Problem definition	3
1.3 Goals and objectives	4
1.4 Methodology	5
1.5 Scope	5
2 Literature study	7
2.1 Review of current full timber buildings	7
2.1.1 Dalston Lane, England	7
2.1.2 Treet, Norway	7
2.1.3 Mjøsa, Norway	8
2.1.4 Brockcommons, Canada	9
2.2 Materials	10
2.2.1 Cross laminated timber [CLT]	10
2.2.2 Glued laminated timber [GLT]	12
2.3 Outriggers	13
2.3.1 Timber outriggers	15
2.3.2 Outrigger truss connections	17
2.3.3 Column to foundation connection	20
2.3.4 Conclusion outriggers	21
2.4 Cross laminated timber cores	22
2.4.1 Limit state of shear walls	25
2.4.2 In-plane & orthogonal CLT connections	26
2.4.3 Horizontal CLT connection	28
2.4.4 Connection CLT core to foundation	29
2.4.5 Connections CLT core to truss	32
2.5 Timber design issues	36
2.5.1 Fire safety	36
2.5.2 Differential vertical shortening	37

2.5.3	Vibrations	38
2.6	Dynamic performance	38
2.6.1	Damping	39
2.6.2	Lateral acceleration and user discomfort	41
2.7	Numerical modelling of CLT	43
3	Case study	47
3.1	Program of requirements	47
3.2	Design aspects	48
3.3	Loads	48
3.4	Load combinations	49
3.5	Serviceability criteria	50
3.6	Design assumptions	51
3.7	Design strategy	51
3.7.1	Case A	51
3.7.2	Case B	53
3.7.3	Case C	54
3.7.4	Strategy design choices	55
3.8	Member design	55
3.8.1	CLT wall design	55
3.8.2	Column design	56
3.8.3	Floor panels	56
3.9	Connection design case A	57
3.9.1	Connection design considerations	57
3.9.2	Connection types	59
3.9.3	Vertical orthogonal connection	60
3.9.4	Vertical in-plane connection	69
3.9.5	Horizontal connection CLT panels	72
3.9.6	Column to foundation	81
3.9.7	Column to column	84
3.9.8	Connection of the beams	87
3.9.9	Connection of the floors	87
3.10	Connection design case B	87
3.10.1	Outrigger to column connection	88
3.10.2	Outrigger to core	92
4	Numerical modelling	95
4.1	Modelling assumptions	95
4.2	Validation of the numerical modelling methods	96
4.3	Numerical modelling of case A	96
4.4	Numerical modelling of case B	103
5	Results	104

5.1	Results case A	105
5.1.1	Static response	105
5.1.2	Dynamic response	108
5.1.3	Sensitivity of connection design of case A	109
5.1.4	Conclusion results case A	117
5.1.5	Discussion results case A	118
5.2	Results case B	118
5.2.1	Static response	118
5.2.2	Dynamic response	127
5.2.3	Sensitivity analysis case B	128
5.2.4	Conclusion results case B	139
5.2.5	Discussion results case B	140
5.3	Results case C	140
5.3.1	Static response	141
5.3.2	Dynamic response	144
5.3.3	Conclusion results case C	145
6	Discussion	147
7	Conclusions and recommendations	155
7.1	Conclusions	155
7.2	Recommendations	158
	References	160
Appendix A	Wind load	164
Appendix B	Analytical calculation of deflection	172
Appendix C	Behaviour of the outrigger	180
Appendix D	Contributions to the global deflection	184
Appendix E	CLT core wall design	187
Appendix F	Column design	191
Appendix G	Validation of the numerical modelling methods	196
Appendix H	Calculation methods connections	206
Appendix I	Connection of the floors	221
Appendix J	Connection of the beams	229
Appendix K	Alternative connection core to foundation	235
Appendix L	Calculation effective stiffness outrigger	237

List of Figures

1	Numerical models of the different stability systems	iii
2	Lateral deflection of the different case studies	iii
3	Fitted curves influence of stiffness ratio	iv
4	Effectiveness outrigger	iv
1.1	Building topology vs maximum height of concrete buildings with internal lateral load resisting systems[1]	2
1.2	Distribution of case studies on the topic of timber buildings and their respective number of storeys[2]	3
2.1	Dalton Lane, England [5].	7
2.2	Structural system Treet, Bergen, Norway [6]	8
2.3	Structural system Mjøstarnet, Mjøsa, Norway [7]	9
2.4	Construction sequence of mass timber elements brock commons[9]	10
2.5	Engineered wood products [12]	11
2.6	(a) Core outrigger system, (b) Bending moment line of the structure [15]	14
2.7	Lateral displacement and accelerations for a core building, one including outriggers and one including smart outriggers[19]	15
2.8	Influence of number of outrigger systems on the lateral displacement [3]	16
2.9	Outrigger-truss configurations numerically tested[20]	17
2.10	(a) Nailed plywood gusset connection, (b) Nailed steel gusset connection[21]	18
2.11	Glulam connection using dowels and slotted in steel plates [22]	19
2.12	(a) Direct epoxied glued-in rebars connection, (b) Indirect epoxied glued-in rebars connection [23]	19
2.13	Glued glulam connection [21]	20
2.14	Column to foundation connection using dowels and steel plates [7]	21
2.15	Column to foundation connection using internal dissipation [25]	21
2.16	Experimental test setup of a C-shaped CLT core system [27]	23
2.17	Experimental test setup and deformations: (a) Pres-lam system with 46.1% pre-stress ratio; (b) Conventional shear wall system using hold-downs[29]	24
2.18	Limit states CLT shear walls: (a) Decompression; (b) Effective linear limit [29]	25
2.19	STS configurations of in plane and orthogonal joint experimentally tested by Brown, et al.[27]	26
2.20	X-bracket panel to panel joint[34]	27
2.21	Configuration of dovetail (a) Mortise part, (b) Tenon part, (c) Self-tapping screws[35]	28
2.22	Castellated joint design for the connection between upper and lower segments of CLT panels[27]	29
2.23	Perforated steel plate geometry [37]	30
2.24	Example modified HSK connection [37]	30

2.25	<i>Angle bracket and hold-down connection of a CLT panel [38]</i>	31
2.26	<i>CLT glued-in steel rod connection [41]</i>	32
2.27	<i>Experimental results of multiple CLT glued-in steel rods [43]</i>	33
2.28	<i>Minimum spacing distances of a glued-in rod in a beam according to the GIROD-proposal [44]</i>	34
2.29	<i>CLT dowel connection [45]</i>	34
2.30	<i>Loading of the experimentally tested dowelled CLT connection[46]</i>	35
2.31	<i>Correct truss to core connection location [3]</i>	36
2.32	<i>Relation building height vs natural frequency[50]</i>	39
2.33	<i>Damping codes vs results from vibration tests[51]</i>	40
2.34	<i>Damping ratio vs frequency[50]</i>	41
2.35	<i>Effect of lateral accelerations on humans [52]</i>	41
2.36	<i>Requirements on maximum lateral acceleration</i>	42
2.37	<i>(a) Convention of different stiffness directions, (b) Planes and directions associated to each stiffness matrix element [54]</i>	46
3.1	<i>Floor plan proposal case study</i>	48
3.2	<i>CLT 5-ply floor system[57]</i>	49
3.3	<i>Workflow of case A</i>	52
3.4	<i>Numerical model case A</i>	52
3.5	<i>Numerical model case B</i>	54
3.6	<i>Workflow case studies</i>	54
3.7	<i>Numerical model case C</i>	55
3.8	<i>Layup CLT top view [0/0/90/0/90/0/90/0/0]</i>	56
3.9	<i>CLT floor panel layup</i>	57
3.10	<i>Workflow of the connection design</i>	59
3.11	<i>Connection types of the CLT core</i>	60
3.12	<i>Connection types of the columns and beams</i>	60
3.13	<i>STS connection of CLT panels and their angle notation[32]</i>	61
3.14	<i>Shear force in the vertical orthogonal connection</i>	61
3.15	<i>Scia coordinate system joint on a 2D member edge</i>	67
3.16	<i>Vertical orthogonal connection CLT panels mixed angle STS</i>	68
3.17	<i>Shear force in the vertical in-plane connection</i>	69
3.18	<i>Vertical in-plane connection CLT panels mixed angle STS</i>	71
3.19	<i>Forces on the horizontal connection between CLT panels or CLT to foundation</i>	72
3.20	<i>In-plane shear loading castellated joint[58]</i>	74
3.21	<i>Analytical spring model 5-layer CLT [58]</i>	75
3.22	<i>Composite spring model horizontal joint</i>	78
3.23	<i>Horizontal dowelled and castellated connection CLT panel</i>	79
3.24	<i>Horizontal dowelled and castellated connection CLT panel to foundation</i>	80
3.25	<i>Loading of the bonded-in rods</i>	82
3.26	<i>Column to foundation connection steel shoe and internal bonded-in rods</i>	83
3.27	<i>SCIA coordinate system hinge on a 1D member</i>	84

3.28	<i>Column to column connection steel connector and internal bonded-in rods</i>	86
3.29	<i>Beam to column joint</i>	87
3.30	<i>Forces in the outrigger</i>	88
3.31	<i>Failure mode of a dowel under four shear planes</i>	89
3.32	<i>Resulting force in the outrigger to column connection</i>	90
3.33	<i>Outrigger to column connection</i>	91
3.34	<i>Resulting force in the core</i>	92
3.35	<i>Outrigger to core connection</i>	94
4.1	<i>Workflow numerical modelling</i>	97
4.2	<i>Numerical model groundfloor</i>	99
4.3	<i>Orientation of CLT floors</i>	99
4.4	<i>Locale coordinate systems joints SCIA</i>	100
4.5	<i>Example of modelling a hinge on 2d member on the orthogonal core connection</i>	100
4.6	<i>Numerical model case A</i>	102
5.1	<i>Workflow sensitivity analysis design parameters</i>	104
5.2	<i>Horizontal deflection of case A</i>	105
5.3	<i>Global displacement case A of the core at groundfloor level, SLS loading, vertical deflection</i>	106
5.4	<i>Origin of translations case A</i>	107
5.5	<i>Dynamic response case A</i>	109
5.6	<i>Overview horizontal connection</i>	110
5.7	<i>Influence of the amount of dowels in the horizontal connection on the lateral deflection</i>	111
5.8	<i>Influence of the castellations on the lateral deflection</i>	112
5.9	<i>Overview vertical orthogonal connection</i>	114
5.10	<i>Influence of the vertical orthogonal connection on the lateral deflection</i>	114
5.11	<i>Overview vertical in-plane connection</i>	115
5.12	<i>Influence of the vertical in-plane connection on the lateral deflection</i>	116
5.13	<i>Influence of variably distributed vertical connections on the lateral deflection</i>	117
5.14	<i>Deflection of case B</i>	119
5.15	<i>Origin of translations case B</i>	120
5.16	<i>Vertical displacement of the outrigger</i>	123
5.17	<i>Forces in members of the outrigger</i>	124
5.18	<i>Horizontal axial forces n_y in the core at outrigger level</i>	125
5.19	<i>Force transfer outrigger to core , top view</i>	126
5.20	<i>Dynamic response case B</i>	127
5.21	<i>Columns connected to the outrigger</i>	129
5.22	<i>Overview outrigger connections</i>	130
5.23	<i>Influence of the connection stiffness of the outrigger on lateral deflection</i>	131
5.24	<i>Deflection of CLT the shear wall outrigger</i>	133
5.25	<i>Horizontal force in the outrigger to core connection</i>	134
5.26	<i>Lateral deflection of the structure with different heights of the outrigger</i>	134

5.27	<i>One storey outrigger configurations</i>	135
5.28	<i>Lateral deflection of the outrigger truss configurations</i>	135
5.29	<i>Two storey outrigger configurations</i>	136
5.30	<i>Lateral deflection of the two storey tall outrigger truss configurations</i>	137
5.31	<i>Fitted curves influence of stiffness ratio</i>	138
5.32	<i>Effectiveness outrigger</i>	139
5.33	<i>Deflection case C</i>	141
5.34	<i>Forces in members of the outrigger of case C</i>	143
5.35	<i>Horizontal axial forces n_y in the core at outrigger level, case C</i>	144
5.36	<i>Dynamic response case C</i>	145
5.37	<i>Effectiveness outrigger</i>	148
5.38	<i>Outrigger with a single diagonal connecting core to column</i>	149
5.39	<i>Interaction factors CLT core</i>	151
5.40	<i>Effect of zero interaction of the vertical connections of the core</i>	152
5.41	<i>Deflection of case A with and without floors</i>	153
A.1	<i>Force coefficient for rectangular cross section with sharp corners</i>	168
A.2	<i>Reference height according to NEN1991-1</i>	169
B.1	<i>Test setup used to determine the effective width of a CLT-LVL composite beam [59]</i>	172
B.2	<i>Mechanically jointed beam according to NEN-EN1995-1-1</i>	173
B.3	<i>Shear lag effect CLT core</i>	174
B.4	<i>Matrixframe outrigger structure</i>	176
B.5	<i>Bending stiffness outrigger</i>	177
B.6	<i>Results matrixframe outrigger beam model</i>	177
B.7	<i>Matrixframe outrigger structure with truss</i>	178
B.8	<i>Results matrixframe outrigger truss model</i>	179
C.1	<i>Vertical displacement of the outrigger nodes</i>	181
C.2	<i>Vertical displacement of the outrigger</i>	182
C.3	<i>Forces in members of the outrigger</i>	183
D.1	<i>Origin of translations case A</i>	185
D.2	<i>Origin of translations case B</i>	186
G.1	<i>Dimensions of the experimental test setup [27]</i>	197
G.2	<i>Spring placement (pink) in the numerical model</i>	199
G.3	<i>Support on the numerical verification model</i>	200
G.4	<i>Loads on the numerical validation model</i>	201
G.5	<i>C-shaped CLT wall numerical model</i>	202
G.6	<i>Orientation joint degree of freedoms SCIA</i>	202
G.7	<i>Global displacement of the C-shaped CLT wall</i>	203
G.8	<i>(a) Shear deformation in-plane joint, (b) Tensile deformation vertical springs</i>	204
H.1	<i>Failure modes of a fastener loaded in single shear</i>	206
H.2	<i>Angle between fastener and fibre direction</i>	208
H.3	<i>Failure mode of a dowel in 4 shear planes embeded in CLT</i>	211

H.4	<i>Definition of angle α</i>	212
H.5	<i>Spacing and edge distances for fasteners in timber</i>	213
H.6	<i>Effective area for glued in rods</i>	216
H.7	<i>Spacing notation bonded-in rods</i>	217
I.1	<i>Floor to beam connection of a single floor panel</i>	222
I.2	<i>Floor to beam connection of two floor panels</i>	223
I.3	<i>Floor to floor connection</i>	225
I.4	<i>Floor to core connection</i>	227
J.1	<i>Beam to column joint</i>	229
J.2	<i>Beam to column joint</i>	231
J.3	<i>Beam to core connection</i>	233
J.1	<i>Procedure for calculating the deflections due to bending of the outrigger</i>	238
J.2	<i>Deflection vs stiffness ratio</i>	240
J.3	<i>Fitted curve deflection vs stiffness ratio</i>	241
J.4	<i>Normalized fitted curve deflection vs stiffness ratio</i>	242
J.5	<i>Fitted curves influence of stiffness ratio on peak lateral accelerations</i>	243

List of Tables

2.1	<i>Characteristic strength and stiffness CLT for class CL24 (prEN1995-1)</i>	12
2.2	<i>Characteristic strength and stiffness properties and densities for homogenous glulam (NEN-EN 14080:2013)</i>	13
2.3	<i>Numerical results of member forces of different outrigger-truss configurations[20]</i>	17
2.4	<i>Strength and stiffness of STS connection experimentally tested by Brown et al.[27]</i>	26
2.5	<i>Obtained shear strengths and stiffness of X-bracket[34]</i>	28
2.6	<i>Shear strength and stiffnesses of experimental tests on angle brackets[38]</i>	31
2.7	<i>Structural damping coefficients according to Eurocode</i>	39
2.8	<i>Shear correction factor for different number of layers[55].</i>	44
3.1	<i>General requirements</i>	47
3.2	<i>Characteristic variable loading</i>	49
3.3	<i>Self-weight 5-ply CLT floor system</i>	49
3.4	<i>Characteristic permanent loading</i>	49
3.5	<i>ψ-values</i>	50
3.6	<i>Forces in the column at ground floor</i>	56
3.7	<i>Force in vertical orthogonal connection</i>	62
3.8	<i>Input data orthogonal STS connection calculation</i>	66
3.9	<i>Output data orthogonal STS connection</i>	67
3.10	<i>Numerical boundary conditions vertical orthogonal joint</i>	67
3.11	<i>Vertical in-plane forces, SCIA</i>	69
3.12	<i>Input data vertical in-plane STS connection</i>	70
3.13	<i>Output data vertical in-plane STS connection</i>	70
3.14	<i>Numerical boundary conditions in-plane vertical joint</i>	72
3.15	<i>Axial forces in vertical direction in the CLT core, SCIA</i>	73
3.16	<i>Input data doweled connection</i>	73
3.17	<i>Output dowelled horizontal connection</i>	74
3.18	<i>In plane shear forces, SCIA</i>	74
3.19	<i>Input data castellated joint</i>	77
3.20	<i>Output data castellated joint</i>	77
3.21	<i>Numerical boundary conditions horizontal joint</i>	78
3.22	<i>Numerical boundary conditions horizontal connection core to foundation</i>	81
3.23	<i>Maximum normal and shear force in the column to foundation connection, SCIA</i>	81
3.24	<i>Input data glued-in rod connection</i>	82
3.25	<i>Output glued-in rod connection</i>	82
3.26	<i>Numerical boundary conditions column to foundation connection</i>	84
3.27	<i>Maximum force in the column to column connection, SCIA</i>	84
3.28	<i>Numerical boundary conditions column to column connection</i>	85

3.29	<i>Forces in the outrigger to column connection</i>	89
3.30	<i>Input data outrigger to column connection</i>	90
3.31	<i>Output data outrigger to column connection</i>	90
3.32	<i>Stiffness modelling assumptions outrigger to column connection</i>	91
3.33	<i>Forces in the outrigger to core connection</i>	92
3.34	<i>Input data outrigger to core connection</i>	93
3.35	<i>Output data outrigger to core connection</i>	93
3.36	<i>Stiffness modelling assumptions outrigger to core connection</i>	94
4.1	<i>Overview connection stiffness's numerical model case A</i>	101
4.2	<i>Overview connection stiffnesses numerical model case B</i>	101
5.1	<i>Result analytical calculation</i>	108
5.2	<i>Result analytical vs numerical calculation</i>	108
5.3	<i>Boundary conditions horizontal connection core to core and core to foundation, sensitivity analysis</i>	111
5.4	<i>Boundary conditions horizontal connection core to core, sensitivity analysis castellations</i>	112
5.5	<i>Influence of the horizontal connection on the lateral deflection</i>	112
5.6	<i>Boundary conditions vertical orthogonal connection, sensitivity analysis</i>	113
5.7	<i>Influence of the vertical orthogonal connection on the lateral deflection</i>	115
5.8	<i>Boundary conditions vertical in-plane connection, sensitivity analysis</i>	116
5.9	<i>Influence of the vertical orthogonal connection on the lateral deflection</i>	116
5.10	<i>Maximum values of the lateral deflection for tapered vertical connections</i>	117
5.11	<i>Maximum axial force horizontal connections</i>	121
5.12	<i>Maximum shear force horizontal connections</i>	121
5.13	<i>Maximum shear force vertical connections</i>	121
5.14	<i>Interaction factors</i>	121
5.15	<i>Vertical displacements of the outrigger</i>	122
5.16	<i>Eigenfrequencies lateral sway modes case B</i>	127
5.17	<i>Peak lateral acceleration case B</i>	128
5.18	<i>Result analytical vs numerical calculation outrigger</i>	128
5.19	<i>Influence of the column size on the lateral deflection</i>	129
5.20	<i>Influence of the outrigger size on the lateral deflection</i>	129
5.21	<i>Boundary conditions outrigger connection, sensitivity analysis</i>	130
5.22	<i>Influence of the connection stiffness of the outrigger on the lateral deflection</i>	131
5.23	<i>Boundary conditions outrigger connection, sensitivity analysis</i>	131
5.24	<i>Influence of the connection stiffness of the outrigger on the lateral deflection</i>	132
5.25	<i>Influence of the location of the outrigger on the lateral deflection</i>	134
5.26	<i>Influence of the location of the outrigger on the lateral deflection</i>	136
5.27	<i>Influence of the location of the outrigger on the lateral deflection</i>	137
5.28	<i>Maximum deflections of case studies</i>	141
5.29	<i>Maximum axial force horizontal connections, case C</i>	142

5.30	<i>Maximum shear force horizontal connections, case C</i>	142
5.31	<i>Maximum shear force vertical connections, case C</i>	142
5.32	<i>Eigenfrequencies lateral sway modes case C</i>	145
5.33	<i>Peak lateral acceleration case C</i>	145
5.34	<i>Influence of connection stiffness on interaction factors</i>	151
A.1	<i>Results Peak wind pressure calculation</i>	165
A.2	<i>Results calculation windpressure</i>	170
B.1	<i>Interaction factors</i>	174
B.2	<i>Result analytical calculation</i>	175
B.3	<i>Result analytical vs numerical calculation</i>	175
B.4	<i>Input matrixframe</i>	177
E.1	<i>Input data calculation wall section</i>	190
E.2	<i>Unity checks CLT core wall</i>	190
F.1	<i>Input data column calculation</i>	195
F.2	<i>Unity checks column</i>	195
G.1	<i>Connection stiffness experimental tests CW-6 [27]</i>	196
G.2	<i>Spring stiffness of the cables</i>	199
G.3	<i>Overview connection constraints</i>	202
H.1	<i>Recommended minimum spacing and edge distance for lateral loaded dowel connection</i>	214
H.2	<i>Characteristic bond line strength for different effective anchorage lengths</i>	214
H.3	<i>Spacing for glued-in rods</i>	217
I.1	<i>Forces acting on the floor to beam connection</i>	221
I.2	<i>Input data floor to beam connection</i>	221
I.3	<i>Output floor to beam connection</i>	222
I.4	<i>Stiffness modelling assumptions floor to beam connection</i>	223
I.5	<i>Forces acting on the floor to floor connection</i>	224
I.6	<i>Input data floor to floor connection</i>	224
I.7	<i>Output floor to floor connection</i>	224
I.8	<i>Stiffness modelling assumptions floor to floor connection</i>	225
I.9	<i>Forces acting on the floor to core connection</i>	226
I.10	<i>Input data floor to core connection</i>	226
I.11	<i>Output floor to core connection</i>	226
I.12	<i>Stiffness modelling assumptions floor to core connection</i>	228
J.1	<i>Forces on the beam to column connection</i>	229
J.2	<i>Input data beam to column</i>	230
J.3	<i>Shear resistance beam to column joint</i>	230
J.4	<i>Numerical boundary conditions column to beam connection</i>	231
J.5	<i>Forces on the beam to core connection</i>	232
J.6	<i>Input data beam to core</i>	232
J.7	<i>Shear resistance beam to column joint</i>	233

J.8	<i>Numerical boundary conditions beam to core connection</i>	234
J.1	<i>Required amount of glued in rods, placed in vertically orientated layers</i>	235
J.2	<i>Required amount of glued in rods, placed in horizontally orientated layers</i>	235
J.3	<i>Stiffness of the glued in rod connection</i>	236
J.1	<i>Vertical deflections and rotations of the column and core</i>	238
J.2	<i>Vertical forces in the column</i>	239
J.3	<i>Effective bending stiffness outrigger</i>	239
J.4	<i>Ratio effective bending stiffness outrigger vs effective bending stiffness core</i>	240

1. Introduction

1.1 Scientific relevance and research motive

In recent decades buildings have been constructed higher than ever before, this change is due to a few causes. Urbanisation has led to a growth in the number of citizens in cities while the available space has become limited, resulting in a high demand for housing in cities. New technologies and research have made it possible to reduce calculation time and increase safety of tall buildings, resulting in ever growing buildings.

The building sector is responsible for approximately 11% of the total worldwide energy consumption according to the united nations environmental programme (UNEP, 2017). This is primarily due to the fact that steel and concrete, the most used construction products, require a large amount of energy during production. Which is one of the causes for global warming which could have catastrophic consequence in the coming decades. From rising temperatures, sea level rise, extreme weather to polluted air the list goes on and on. To combat these severe changes in our climate the emission of greenhouse gasses needs to be drastically reduced. Due to increasing concerns from society on climate change there is a high demand to use more sustainable solutions in the building sector. With the possibility to sustainably harvest timber as a building material it is possible to use this renewable building material and replace other alternatives which have a high environmental footprint. Which in turn could drastically reduce the energy consumption and environmental footprint of the building sector.

Current trends for tall buildings has been assessed and summarized [1], from these trends different types of topologies are mentioned which can be used to transfer lateral loads to the foundation while also providing sufficient stiffness to provide comfort for the user. From this study it appears an outrigger structure is a solution which is regularly applied for tall steel and timber buildings. An outrigger system makes use of lever arms which are connected to a core system, reducing the bending moment in the core and increasing overall stiffness.

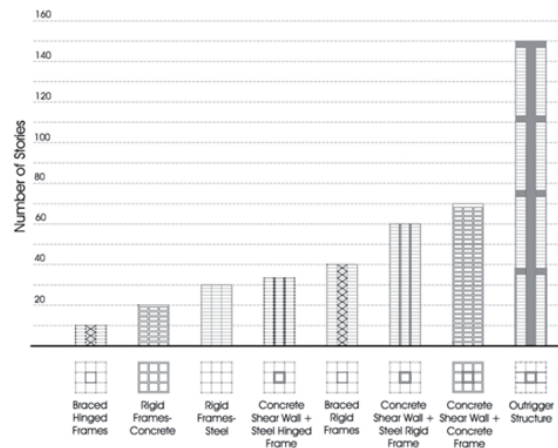


Figure 1.1. *Building topology vs maximum height of concrete buildings with internal lateral load resisting systems*[1]

Since all buildings require a form of vertical transport of personal and goods most building have a core system which is used for vertical load transfers and provide lateral stiffness. It is easy to see why outriggers are regularly applied to increase the maximum building height, since most components of outriggers systems i.e. core and columns are already present.

Timber buildings are significantly lighter than their concrete and steel counterparts, therefore increasing the overall stiffness of the building becomes interesting and is already relevant for mid-rise timber buildings. Additionally when comparing the stiffness of timber and concrete the latter has a stiffness which is between three and five times higher than that of timber, resulting in increased structural member sizes and a decreased maximum building height. This shows that it is interesting to investigate timber structural systems for mid-rise buildings.

The available literature on the topic of timber outriggers is currently fairly limited, suggesting a lot of knowledge can be gained. Combining this with the need for sustainability and an increasing urban population there is sufficient scientific and public relevance to do further research in this field. It can also be seen throughout Europe and Northern America more and more fully timber or composite timber buildings are constructed, with currently the highest building being Mjornstadt with a height of 86 meters.

An overview is given of case studies performed on timber buildings shows two distinct features over the past decade. First the total number of case studies performed annually is in a growing trend and second the height of these case studies is also in growing annually. This shows the increased interest in the topic over the past decades and the progression of structural methods used for timber buildings.

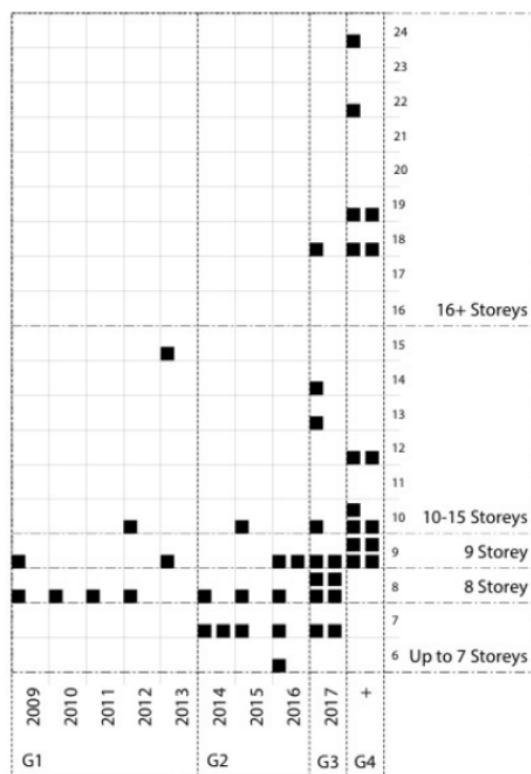


Figure 1.2. *Distribution of case studies on the topic of timber buildings and their respective number of storeys[2]*

Further research within the timber research area could provide valuable insight in structural topology regarding timber buildings and mid-rise buildings specifically. Which in turn can have beneficial influences on the environmental footprint of the construction sector and reduce global warming.

1.2 Problem definition

Available literature on the topic of timber outriggers is fairly limited however there are some papers which have discussed this or have performed research on this topic. During the thesis research of Slooten, E. C.[3] a timber outrigger structure is assessed and the influence of the addition of the outrigger system on the lateral displacement is numerically calculated. From this study it was shown that a reduction of 37% of the lateral displacement can be achieved with the addition of a single outrigger level, with more outrigger levels leading to an even higher reduction of lateral displacement. The influence of the addition of a timber outrigger system is assessed. It should be noted that the structure which is assessed in this research consists of a reinforced concrete core making the building a wood-concrete hybrid structure.

A thesis performed by Boellard, B.[4] does discuss the possibility of using a timber outrigger outrigger system on a CLT core. In this research an in depth study is done on a 20-storey building which uses a CLT core system with additional timber outriggers. This study assesses the feasibility of a CLT core building with timber outriggers, which is verified. The research consists of a single

case study design which is improved based upon ultimate limit state conditions and once again on serviceability limit state. However the influence of the addition of the timber outriggers on the structural behaviour of the CLT core system has not been assessed.

Comparing the before mentioned theses, the former assesses the influence of the addition of timber outriggers with a reinforced concrete core and the latter is a feasibility study of the use of a CLT core system with timber outriggers, however the latter does not quantify the influence the outriggers has on the structural behaviour of the CLT core system. This shows there is a knowledge gap between the topics and the influence of a timber outrigger system on a CLT core system has yet to be assessed and quantified.

1.3 Goals and objectives

Goals

The goal of this thesis is to investigate the influences of adding an outrigger system to a cross laminated timber core building and determine the effects the outrigger system has on the deflections, accelerations and internal forces etc. Additionally the goal is to optimize this system and find the best possible strategy for incorporating an outrigger system in a CLT core building.

The research topic is defined as follows:

Influence of timber outriggers system on cross laminated timber core buildings.

The research question is defined as follows:

How does a timber outrigger system influence the structural behaviour of a cross laminated core building?

Objectives

During this research the addition of a timber outrigger system to a CLT core building is assessed. The influence of adding an outrigger system could provide additional stability to a full timber building, this is numerically assessed using finite element modelling. During the research it is also assessed how the structural behaviour of the outrigger system could be improved. Optimization is performed numerically to investigate influences of different parameters. During the research different numerical models are build and compared, for instance a CLT core building without an outrigger system and one with an outrigger system. Allowing a comparisons to be made between both models in terms of force distribution, deflections, accelerations etc.

Sub research question: **What are the critical parameters of a CLT core building with timber outriggers?**

- Determine critical parameters of a CLT core building in ultimate limit state and serviceability

limit state.

- Determine critical parameters of a timber outrigger system in ultimate limit state and serviceability limit state.

Sub research question: **How can a timber outrigger system of a CLT core building be optimized?**

- Investigate the possibilities of reducing lateral acceleration of the building and potential dampening capabilities an outrigger can provide.
- Determine the influence of the critical parameters on the structural behaviour of the building.

1.4 Methodology

Literature review

An extensive literature study is performed on existing scientific literature on the topic of CLT cores with an additional timber outrigger system. Since the available literature on the topic is fairly limited the topic is subdivided into the following categories to gain a better understanding of the overarching problem. A literature study is performed on the following topics: Current timber buildings under construction/ or already constructed, Assessment of engineered wood products, Assessment of CLT core systems, Assessment of timber outriggers, large timber joints, dynamic response of timber structures and assessment of critical parameters for both CLT core systems as timber outriggers.

Numerical modelling

The main goal of the research is to assess the influence of adding outriggers to a CLT core building, therefore several numerical models are build. A preliminary design is made of a CLT core building and one of a CLT core building with timber outriggers including its respective connections. The preliminary design needs to fulfil the requirements set out by the Eurocode on ultimate limit state. When both models have been developed comparisons can be made between them. The next step is to iterate the CLT core system with timber outriggers using the critical parameters which have been previously found to optimize its stiffness, allowing the serviceability criteria to be met, which is performed manually.

1.5 Scope

The research focuses on the design of a timber outrigger and a CLT core system and its respective connections. Optimization of the design is primarily performed on structural members, connections and topology of the lateral load resisting system. In this research it is not of interest to investigate secondary components of the structure for instance facades, only main structural components are designed.

The scope of the research is limited to short term behaviour of the material. The influence of creep and other long term material behaviours has on the global structural behaviour of the design are

not taken into consideration. The research is limited to numerical experimentation (building finite element models) and literature research. Experimental test are not a part of the research and is outside the scope for this thesis.

2. Literature study

2.1 Review of current full timber buildings

In this section an overview is given of full timber buildings that have already been build or are planned for the coming years. A handful of projects will be mentioned and their respective stability systems will be discussed. There will also be an overview of the research performed on the topic of timber buildings.

2.1.1 Dalston Lane, England

The building lane, a 10-storey CLT building with a height of 33 meters, in london has set an example of the progress engineers and researchers have made in the field of CLT buildings. By using a tapered thickness of the load carrying elements throughout the height, thickness reduces while the height increases, the designers of the structure where able to reduce the amount of timber per square meter by 20% in comparison with previously buildt Stadthaus which is a 9-storey full timber building. Additionally the building only weighs a fifth of a similar building constructed out of concrete [5]. The lateral stability system consists of CLT shearwalls which are connected with metal fasteners. The basement and groundfloor are made up of concrete to reduce the influence groundwater has on the material and increase openspace on the groundfloor.



Figure 2.1. *Dalton Lane, England [5].*

2.1.2 Treet, Norway

An example of a timber building is Treet, a 14-storey tall timber building completed in 2015 [6], in Bergen Norway. The construction consist of a large glued laminated timber (glulam) frame which is responsible for the horizontal load transfer and stiffness, furthermore treet uses a particular technique for its vertical load transfer. The prefabricated residential modules consisting of mostly cross laminated timber (CLT) are stacked upon each other. The levels 1-4 are resting on the concrete

foundation slab and are independent of the glulam frame. Level 5 is referred to as a so called “power storey” consisting of a strengthened glulam frame system which is able to take up the loads of the prefabricated modules stacked on top. The levels 6-9 again are not connected to the main load bearing structure at any point besides their foundation which is a concrete level located at the top of the “power storey”. This process is repeated once more until the height of 14 storeys is reached. In figure 2.2 the structural load carrying system can be seen consisting of the glulam truss system and the location of the “power storey’s” can be seen.

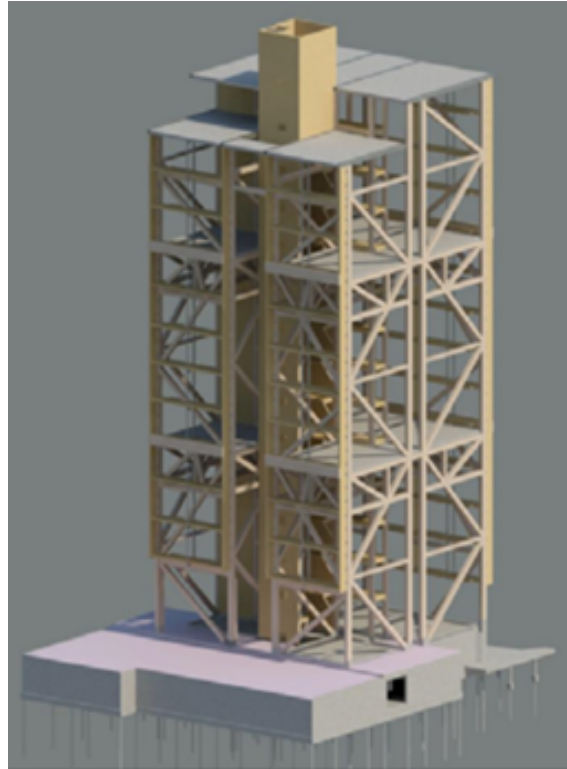


Figure 2.2. *Structural system Treet, Bergen, Norway [6]*

The concrete slabs are used to connect the glulam trusses and provide additional mass to the building to improve the dynamic behaviour. While the building has a total height of approximately 45 meters the dimensions of the diagonals are 405x405 mm. The robustness of the building is verified, if a column or other load bearing element fails a second load path is available which ensures the structure does not collapse. Connections of the glulam members primarily consist of slotted in steel plates.

2.1.3 Mjøsa, Norway

Mjøstarnet is an 18-storey tall timber building completed in 2019 [7]. The structural system consists of a large glulam frame which is responsible for carrying the horizontal load and providing stiffness to the building. Glulam columns and beams are responsible for transfer of the vertical loads, CLT walls around the lift shaft and stairs provide a secondary load path for vertical loads. In the design phase the choice has been made to apply concrete floors on the 12th until the 18th

floor. The reason for the concrete floors at these levels is to increase the mass at the top of the structure which in turn will improve the dynamic behaviour of the timber building. In figure 2.3 the structural system of Mjøstarnet can be seen with the primary lateral load resisting system being the glulam diagonals and the location of the concrete floors.

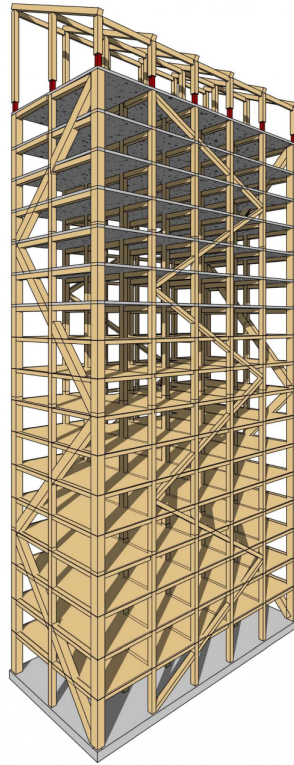


Figure 2.3. *Structural system Mjøstarnet, Mjøsa, Norway [7]*

The diagonals which are used for the building have a maximum dimension of 625x990 mm. For the connection between glulam elements the choice has been made to use slotted in steel plates with steel dowels. The structural system has been placed inside the façade to provide protection against the weather which increases durability and reduces maintenance.

2.1.4 Brockcommons, Canada

The brock commons tallwood house is a 18-storey residential building aimed to house students. The structural system consists of a hybrid structure, stability is provided by a reinforced concrete core, the vertical load carrying capacity is provided by glulam columns while the bottom columns (floor 2-5) consist of parallel-strand lumber. The floors are constructed by 5-ply CLT and the foundation is made of concrete.

Due to large the large dimensions of the load carrying elements at the bottom storeys and the requirement by the client to have an open floor plan on the ground floor the ground floor utilizes concrete to transfer loads from the first floor to the foundation [8].

The construction of the building was divided into casting of the concrete foundation, placement of the mass timber elements and finally the building envelope and interior. For the construction of the floors a three day cycle has been used, it should be noted that prior to the placement of the mass timber elements the precast concrete core has been finished[9]. The construction sequence of brock commons tallwood house can be seen in figure 2.4.



Figure 2.4. *Construction sequence of mass timber elements brock commons[9]*

2.2 Materials

Engineered wood products have attracted the attention of researcher globally over the past decades. There are many reason why engineered wood products have gained so much traction recently. A few examples are: Decreasing supply and increasing demand, increased interest to reduce emissions of the construction sector and increased geometrical possibilities in comparison with ordinary sawn timber[10]. While there are many different engineered wood products the scope of this research is limited to structural use and therefore only CLT and glulam will be discussed.

Additionally to the increasing trend in research and development of timber structures regulators have to closely follow trends in the sector and if possible stay ahead of the curve. In the current Eurocode chapter EN 1995-1 covers timber structures, however the content is fairly limited if compared to other chapters related to steel and concrete. Therefore a revised version of EN1995-1 is underway, currently the draft version is named prEN1995-1. The revised version includes more detailed calculation methods en is in general more extensive than the current version, different engineered wood products such as CLT, glulam and lvl are added. During the research use will be made of the revised draft version when possible.

2.2.1 Cross laminated timber [CLT]

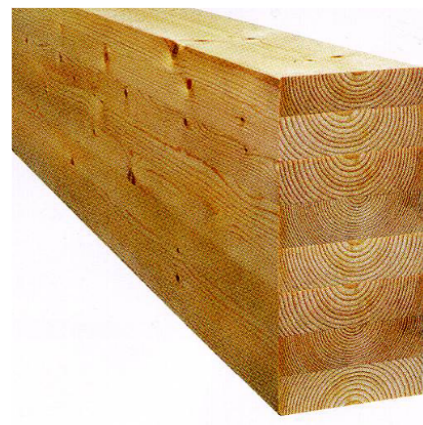
Cross laminated timber (CLT) consist of several layers glued together at an angle of 90 degrees. There are several advantages of CLT in comparison with regular timber planks. First of all the layers can provide improved material quality by spreading out defects. Secondly by using different

layers perpendicular to each other a high in-plane and out-plane strength and stiffness properties can be achieved, providing the panel with two-way action capabilities [11]. Thirdly due to the gluing of layers the CLT panel can be made into large panels unlike regular timber planks where size is restricted by tree growth.

The configuration of the layers is always symmetrical and usually in odd numbers, sometimes the choice can be made to have consecutive layers placed in the same direction for structural purposes. Commonly CLT consist of three to nine layers but more is also possible. Typical production sizes are possible up to 3 meters wide and 18 meters long and thicknesses of up to 500 mm[11]. Figure 2.5a, shows a typical CLT product consisting of 5 layers with layer 2 and 4 perpendicular to the rest.



(a) Cross laminated timber (CLT)



(b) Glued laminated timber (GLT)

Figure 2.5. *Engineered wood products [12]*

Strength and stiffness properties of cross laminated timber with strength classes CL24 can be found in table 2.1 according to prEN1995-1.

Table 2.1. Characteristic strength and stiffness CLT for class CL24 (prEN1995-1)

Property		Symbol	Unit	Strength class CL24
Bending strength	Out of plane loading	$f_{m,k}$	N/mm ²	24
	In plane loading	$f_{m,edge,k}$	N/mm ²	20,5 ^a
Tension strength	In plane loading	$f_{t,0,k}$	N/mm ²	14
	Perpendicular to plane loading	$f_{t,90,k}$	N/mm ²	0,12
Compressive strength	In plane	$f_{c,0,k}$	N/mm ²	21
	Perpendicular to plane	$f_{c,90,k}$	N/mm ²	2,5
Shear strength	Out of plane loading	$f_{v,k}$	N/mm ²	3,5
	Rolling shear	$f_{r,k}$	N/mm ²	0,7
	Perpendicular to plane loading	$f_{v,xy,k}$	N/mm ²	5,5 ^a
Modulus of elasticity	In and out of plane loading	E_{mean}	N/mm ²	11.000
	Perpendicular to plane loading	$E_{90,mean}$	N/mm ²	370
Shear modulus	Out of plane loading	G_{mean}	N/mm ²	650
	Rolling shear	$G_{r,mean}$	N/mm ²	50
	In plane loading	$G_{v,xy,mean}$	N/mm ²	250 ^a
Density		ρ_k	kg/m ³	385

2.2.2 Glued laminated timber [GLT]

Glued laminated timber (GLT) also referred to as glulam consist of layers glued together, unlike CLT layers are glued parallel to each other. Similar to CLT, the size of GLT elements can have large spans due to the connection of the different layers, up to 18 meters. The limitation in length of the GLT elements is primarily due to transportation restrictions. Due to the laminating effect strength and stiffness properties can be increased since reinforcement of defects and distribution of timber quality occurs, similar to CLT [13]. Strength properties of the strength classes GL20h up to GL32h are shown in table 2.2. In figure 2.5b a typical 8-layer cross section of GLT can be seen.

For depths of glulam elements other than 600 mm subjected to bending the characteristic 5th-percentile value of the bending strength $f_{m,k}$ should be multiplied with the factor k_h according to prEN1995-1 using equation 2.1.

$$k_h = \min \left\{ \left(\frac{600}{h} \right)^{0.1}; 1.1 \right\} \quad (2.1)$$

Where

k_h is the depth modification factor;
 h is the depth of the bending member, in mm ;

Table 2.2. *Characteristic strength and stiffness properties and densities for homogenous glulam (NEN-EN 14080:2013)*

Property	Symbol	Glulam strength class						
		GL 20h	GL 22h	GL 24h	GL 26h	GL 28h	GL 30h	GL 32h
Bending strength	$f_{m,g,k}$	20	22	24	26	28	30	32
Tensile strength	$f_{t,0,g,k}$	16	17,6	19,2	20,8	22,3	24	25,6
	$f_{t,90,g,k}$	0,5						
Compression strength	$f_{c,0,g,k}$	20	22	24	26	28	30	32
	$f_{c,90,g,k}$	2,5						
Shear strength (shear and torsion)	$f_{v,g,k}$	3,5						
Rolling shear strength	$f_{r,g,k}$	1,2						
Modulus of elasticity	$E_{0,g,mean}$	8 400	10 500	11 500	12 100	12 600	13 600	14 200
	$E_{0,g,05}$	7 000	8 800	9 600	10 100	10 500	11 300	11 800
	$E_{90,g,mean}$	300						
	$E_{90,g,05}$	250						
Shear modulus	$G_{g,mean}$	650						
	$G_{g,05}$	540						
Rolling shear modulus	$G_{r,g,mean}$	65						
	$G_{r,g,05}$	54						
Density	$\rho_{g,k}$	340	370	385	405	425	430	440
	$\rho_{g,mean}$	370	410	420	445	460	480	490

2.3 Outriggers

An outrigger belt/truss system consist of a core system, an outrigger, a belt truss and perimeter columns. The outrigger is a rigid beam which connects the core to the outer columns, normally the height of 1-2 two storeys depending on the loads that need to be transferred and spanning length. An outrigger can be made of a truss or a diaphragm wall which transfer forces from the core to the outer columns. The belt/truss systems is a truss systems which goes around the circumference of the building and is responsible for the activation of all perimeter columns. A common drawback of an outrigger system is the reduced freedom of the storey on which the outrigger truss/belt is placed.

Lateral loads on buildings will result in an overturning moment and rotations in the core. The outrigger will resist these rotations due to the connection with the perimeter columns, which will generate opposite forces. The forces in the columns will resist the rotation of the core and attached outrigger truss and will induce reverse story shear forces. This culmination of effects will cause an inflection point in the deflection curve of the building[14].

The introduction of an outrigger belt/truss to a core system providing lateral stability can have several benefits. First the outrigger system can provide a more economical solution then that of only a core since bending moments are decreased in the core. Secondly applying an outrigger system decreases the vulnerability of a building for progressive collapse[15]. Finally an outrigger system can effectively increase a buildings lateral stiffness, decrease deflections and reduce lateral accelerations, which is especially useful for tall timber structures[16].

In figure 2.6 an outrigger system can be seen which makes use of three outriggers levels, on the righthand side the bending moment diagram of the building due to wind loading can be seen.

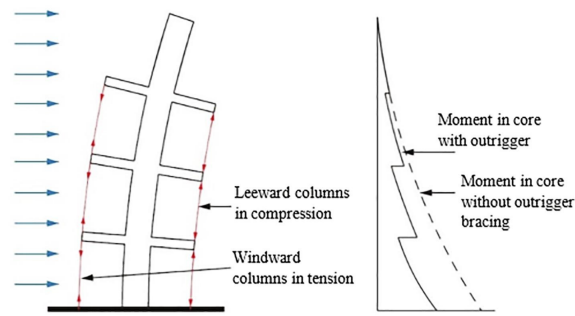


Figure 2.6. (a) Core outrigger system, (b) Bending moment line of the structure [15]

Previous studies have investigated the influence of a handful of critical parameters in the design of an outrigger systems. Factors which heavily influenced the behaviour of the system where: the location of the outrigger, number of outrigger stories and the size of the members. The relative stiffness between outrigger system components such as the relative stiffness between core and outriggers and between outrigger and perimeter columns showed to have a large influence on the structural performance of the system[15].

Optimization study performed on a steel-concrete composite building of 67-stories found that the optimum location of a single outrigger system is 35% of the building height for compliance optimization and 49% for displacement optimization. For two outrigger levels the optimum was found at 27 and 46% of the building height for compliance optimization[17].

Taranath[18] found the optimum location of a single outrigger to be at 44.5% of the building while for two outrigger levels the optimum location 31.2 and 68.5% of the height from the top of the building, for steel and concrete buildings. It should be noted that results of both optimization studies are material and case dependent and criteria on which the optimization is performed also has influence on the height of optimized outrigger location.

The influence of the addition of an outrigger system on a reinforced concrete core building has been assessed by Kim and Kang[19]. Displacement and lateral accelerations have been compared based on a dynamic time dependent wind loading. A comparison was made for a core building, a core building with outriggers and a core building with smart outriggers, which include dampers at the interface between outriggers and column. In figure 2.7 the plots for lateral displacement and lateral accelerations can be seen for the three cases. It is clearly shown that a drastic reduction in lateral displacement can be obtained with the introduction of an outrigger system especially when dampers are incorporated. For the lateral acceleration a slight reduction can be observed when the conventional outrigger system is introduced, however with the introduction of the smart outrigger system the peak accelerations are drastically reduced.

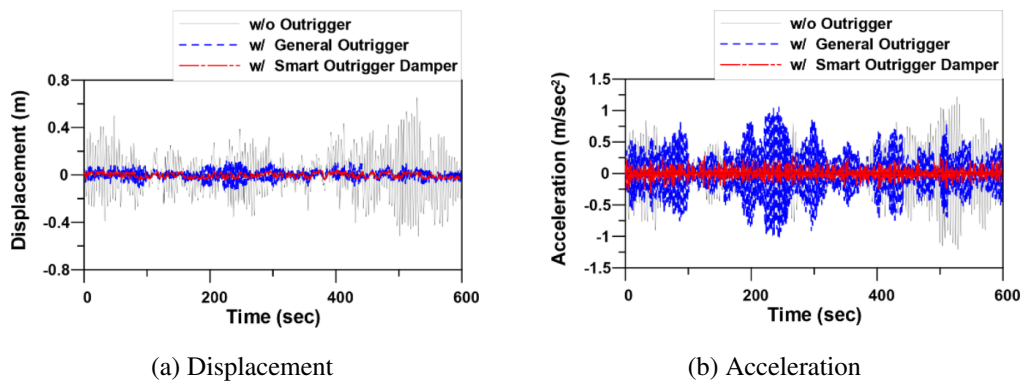


Figure 2.7. *Lateral displacement and accelerations for a core building, one including outriggers and one including smart outriggers[19]*

As mentioned before the outrigger lateral load resisting system consist of the following major structural components, a core, a belt/truss and columns. Each structural component has several connection types where design choices need to be made to optimize the structural behaviour of the building both in ultimate limit state and serviceability limit state. The different connection types for the core, which will be made of CLT, are the horizontal joint connection, the orthogonal joint connection and the in-plane joint connection which will be discussed in section 2.4.2. The connection types for the belt/truss connection consists of the truss connection itself, the truss to column connection and the truss to core connection which will be discussed in sections 2.3.2, ?? and 2.4.5 respectively. Furthermore in the follow section 2.3.1 the timber outrigger system will be discussed and in section 2.4 the CLT core system will be discussed.

2.3.1 Timber outriggers

Research performed by Boellaard[4] discusses and verifies a 20-storey building which uses a CLT core in combination with an outrigger system. In this research the influence of the addition of a timber outrigger system on the CLT core is not assessed. Design of the structure has been initially based on ultimate limit state conditions to obtain initial dimensions of structural members. The design has been improved based on serviceability limit state which seemed to be governing for the design. The design utilizes slotted in steel plates with dowels for the connection between beams and columns of the outriggers. The research concluded that the connection design is as relevant as the design of structural elements and the whole stability system.

Research performed by Slooten[3] investigated the influence of several design parameters on the behaviour of a wood-concrete hybrid 300 meter supertall building. The building utilizes a concrete core in combination with mass-timber outriggers to provide stability against lateral wind loads. The design satisfied both serviceability and ultimate limit state conditions imposed by the Eurocode, however to avoid peak accelerations measures need to be taken to reduce the dynamic behaviour, possibilities are shape optimization and implementation of a tuned mass damper. The connections of the outrigger have been designed as slotted-in steel plates and dowels.

In the before mentioned study optimization of the following parameters concerning the timber outriggers has been performed: number of outrigger levels, orientation of the outriggers, number of column rows, stiffness of the connections and size of the columns and core walls. The influence of the number of outrigger levels showed that increasing the number of outriggers reduces the lateral displacement, however adding a second outrigger level has a smaller reduction than adding the first outrigger level as can be seen in figure 2.8. The addition of one outrigger level to the reinforced concrete core has an effect of 37% reduction on the lateral displacement while the addition of two outrigger levels has an effect of 54% reduction. It should be noted that the addition of multiple outrigger levels increases cost of construction while reducing usable free floor area. Therefore it is important to consider the positive and negative effects of adding multiple outrigger levels during the design phase.

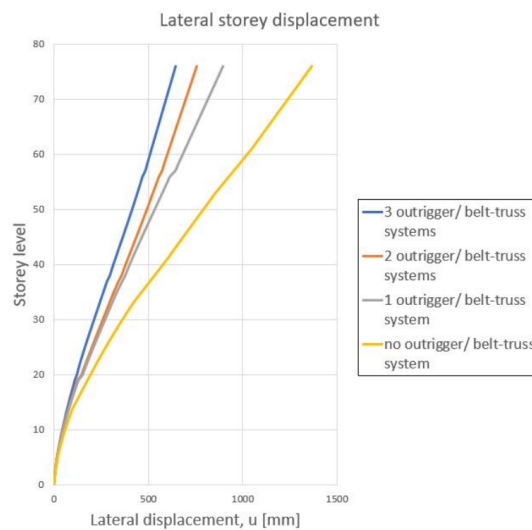


Figure 2.8. Influence of number of outrigger systems on the lateral displacement [3]

The orientation of the outriggers placement orthogonal and diagonal, where the diagonal placement provides a connection from the core to the corner columns, showed that the orthogonal placement can reduce lateral displacement by 15% more than diagonal. It was shown that the orthogonal orientation of the outriggers provided a stiffer connection and distributed forces more evenly.

The addition of an extra column row showed a reduction of 10% of the lateral displacement, this however comes at a cost of decreasing the open floor plan. However introducing an extra column row decreases the floor span and therefore reduces strength requirements of the floor i.e. thinner/lighter floors can be used.

Size of the columns and core walls show to reduce lateral displacement as stiffness of the building increases. The influence of increasing dimensions of columns and walls needs to be re-evaluated for a CLT core wall system and timber outriggers since connections again play a more significant role than for the reinforced concrete core case.

Numerical research on the topology of different configurations of the outrigger-truss of a 20-storey CLT core building was performed by Tesfamariam and Das[20]. During the numerical study maximum member forces and bending moments of a beam, X-bracing, V-bracing, chevron bracing and regular truss were determined. From the numerical results the benefits of the different configurations were shown, which can be seen in Table 2.3. The different configurations of the outrigger can be seen in figure 2.9. It can be seen that force transfer from core to columns was highest with the truss system resulting in the lowest bending moment in the core, while axial force in the core was lowest for the chevron bracing.

Table 2.3. Numerical results of member forces of different outrigger-truss configurations[20]

Member	Force	Configuration				
		Outrigger Beam	X-Bracing	Chevron Bracing	V-Bracing	Truss
Beam	Shear Force (kN)	120	120	92	118	41
	Moment (kNm)	140	128	114	122	63
Column	Axial Force(C) (kN)	3650	3403	3378	3387	3286
	Axial Force(T) (kN)	215	370	375	400	437
	Shear Force (kN)	49	58	47	45	66
	Moment (kNm)	157	96	89	94	106
Bracing	Axial Force(C) (kN)	-	760	960	904	577
	Axial Force(T) (kN)	-	730	840	815	478
Core	Axial Force (kN)	7910	7818	7811	7917	7853
	Moment (kNm)	375	338	200	323	199

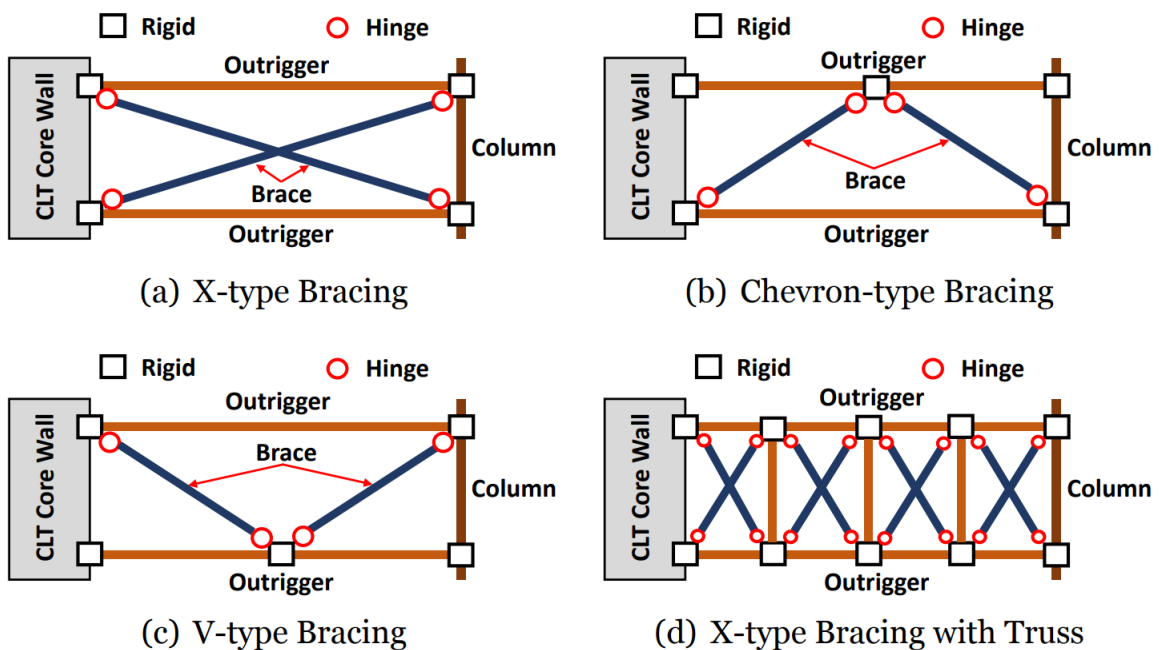


Figure 2.9. Outrigger-truss configurations numerically tested[20]

2.3.2 Outrigger truss connections

Design of the truss connections should be determined on different aspects for example strength, stiffness and displacement capacity/ dissipation of energy. In the following section the different

alternatives will be discussed and their benefits/drawbacks will be mentioned.

Nailed connection

Connecting truss elements using nails can provide rotational stiffness. The rotational stiffness is primarily due to the fact no hole clearance is present for the nails which translates into zero initial slip in combination with the large number of nails used for the connection. Since a large number of nails are necessary to ensure adequate strength and stiffness assembly can be time consuming and costly. The connection has minimal fire resistance unless protection is used [21]. Connections are primarily made using plywood or steel gusset plates. Figure 2.10 shows nailed connections using (a) plywood gusset and (b) steel gusset.

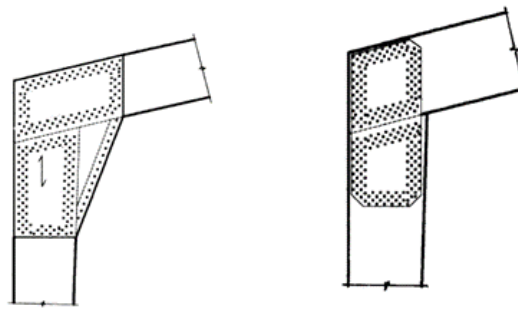


Figure 2.10. (a) *Nailed plywood gusset connection*, (b) *Nailed steel gusset connection*[21]

Doweled connection

A dowel connection consist of steel dowels which connect truss members. The connection can take place by direct contact of the truss members or by use of slotted-in steel plate. Hole clearance for the dowel holes is adopted for practical reasons to reduce the effort needed for assembly, this however causes initial joint slip when loading is applied. The doweled connection needs to be designed in such a way that ductile failure occurs instead of brittle failure according to design rules of Eurocode 5. Figure 2.11 shows a doweled connection at the intersection of multiple members under different angles which has been established for the building Treet in Norway. Doweled connections are able to provide high strength and stiffness while being able to provide sufficient ductility to allow energy to dissipate.

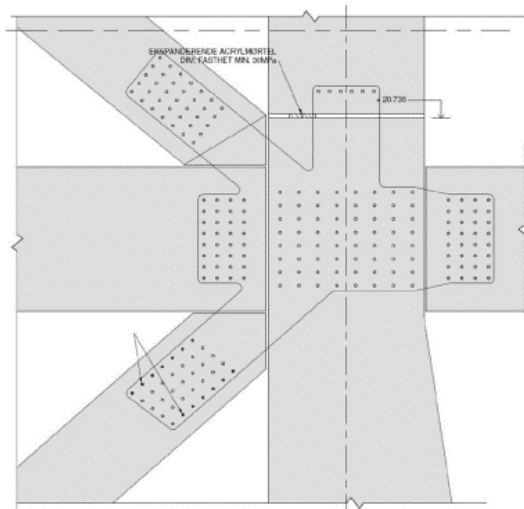


Figure 2.11. *Glulam connection using dowels and slotted in steel plates [22]*

Epoxyed glued-in rebar connection

Epoxyed glued-in rebars connect truss members by placement of steel rods in pre-drilled holes where the connection between steel and truss member is provided by an epoxy layer. Epoxyed glued-in rebars have high strength similar to the strength capacity of the truss members. The connection can provide a ductile failure mechanisms if the steel rods are designed so that yielding of the steel occurs before failure of the truss member[23]. Ling et al. verified that with proper design a glued-in rebar connection can provide sufficient ductility to the joint[24]. Figure 2.37 shows two different types of epoxyed joints, a direct and an indirect connection making use of a steel hollow section.

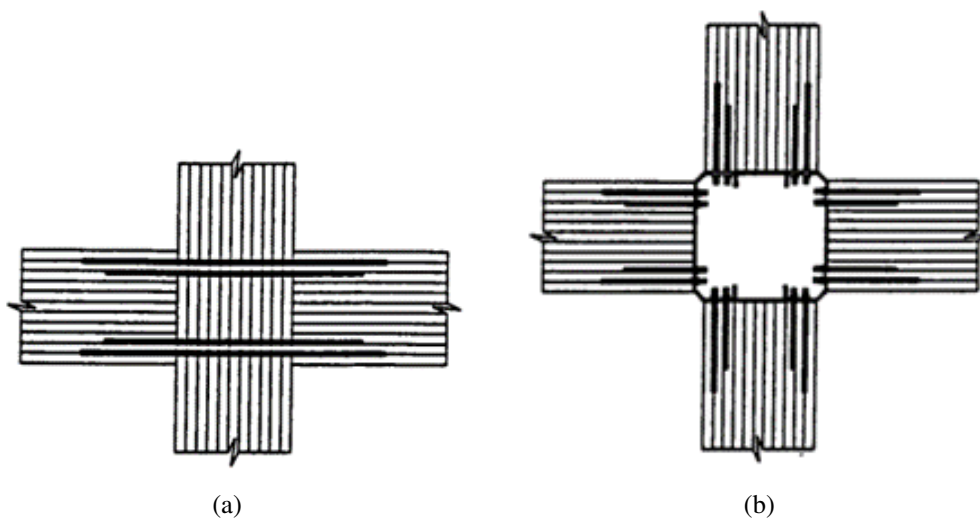


Figure 2.12. (a) *Direct epoxyed glued-in rebars connection, (b) Indirect epoxyed glued-in rebars connection [23]*

Glued connection

It is possible to connect glulam or LVL elements using glue, making use of an intertwining pattern of the layers allows the members to be glued together. However this connection type has to be made in the factory, due to controllable conditions needed to cure and assemble the glued joint, which reduces the possible size of the connected elements due to factory and transportation limitations. Glued connections are characterized by having full-strength moment resisting joints, failure of the joint will be brittle[21]. Figure 2.13 shows the intertwining pattern of the glued glulam connection.

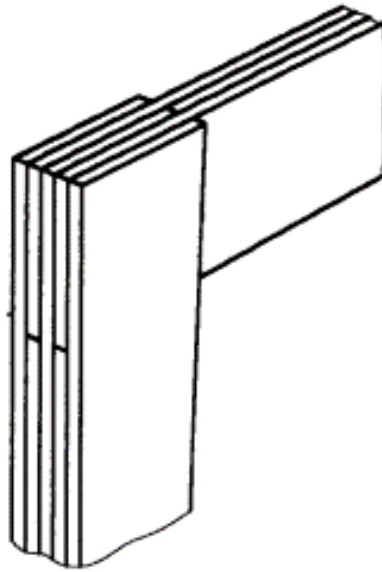


Figure 2.13. *Glued glulam connection [21]*

2.3.3 Column to foundation connection

The connection between the columns and foundation should be able to transfer the shear and normal forces and the bending moment from the column to the foundation.

Doweled connection

A solution which is currently being applied in timber structures is to connect the timber columns and/or diagonals, depending on the type of structure, using steel plates and dowels. The benefits of this type of connection is already discussed in section 2.3.2. The connection type can be constructed of multiple steel plates increasing its strength. Figure 2.14 shows the connection to the foundation used in Mjøstårnet.

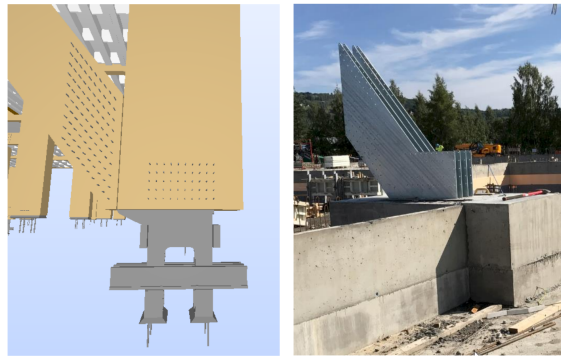


Figure 2.14. *Column to foundation connection using dowels and steel plates [7]*

Steel dissipaters and shoe

A possible connection between the columns and foundation is by using a steel shoe in combination with internal dissipaters. The steel dissipaters embedded in the walls and columns as shown in figure 2.15 could allow for limited residual structural deformation. Design of the steel dissipaters should be done in such a way that stresses in the steel remain elastic. The proposed solution by Smith et al. [25] allows for easy construction since the steel shoe can be attached to the column during manufacturing and only needs to be bolted down on site.

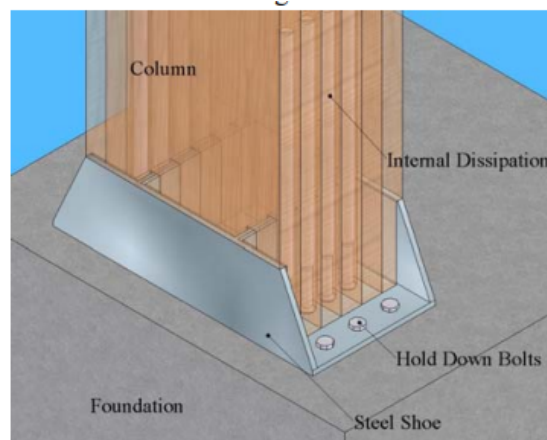


Figure 2.15. *Column to foundation connection using internal dissipation [25]*

If post-tensioning cables are applied to counteract the uplifting forces in the column due to wind loading a large concrete foundation is necessary so that the cables can be directly grouted in the concrete[25].

2.3.4 Conclusion outriggers

While the above mentioned connection are all able to provide sufficient strength to the structure and are able to be designed in such a way that forces are able to be transferred to the foundation. However there are some distinctions between the joint types when it comes down to constructability. The connections in the truss can be intricate, as multiple members converge at a single junction,

making a glued connection challenging to implement. Similar problems occur when epoxied glued-in rebars are used to connect multiple members.

When comparing the nailed and doweled connection the mayor difference is construction time. Especially for large timber joints a large number of nails are required to transfer loads between members, resulting in a large construction time. Doweled connections have pre-drilled holes and only the dowels need to be placed on site, drastically reducing construction time.

For the connection between truss elements of the outrigger the doweled connection is chosen due to its relatively fast construction time, high strength and ductility.

2.4 Cross laminated timber cores

With vertical transport of personal and goods being essential in multiple floor buildings, a regularly applied solution is to bundle the transports together and encase the vertical transport with interconnected shear walls, also known as a core. The core system is able to provide lateral stiffness to a building and transfer horizontal loads to the foundation. This solution can also be applied by using timber as a building material instead of reinforced concrete or steel. A engineered wood product which stand out to be used for this stability system is CLT due to its homogeneous material properties and large panel sizes.

In recent years the interest in cross laminated timber cores has grown. Unlike reinforced concrete walls a CLT core cannot be built up of a single homogeneous material but instead consist of several wall segments which have to be connected to provide interaction. The main reason for the decreased size is manufacturing and transportation to the building site, while reinforced concrete core can be made in-situ, CLT segments have to be pre made in factories which limit the size up to a maximum of approximately 3 by 18 meters according to the CLT handbook [11]. Research has shown that connections between the wall elements tend to be critical and governing for the interaction behaviour of CLT wall systems[26].

Experimental tests performed by Brown et al. [27] have shown valuable insights in the behaviour of a prestressed C-shaped CLT core wall system. During the experimental study different connection types are implemented to assess the influence the connections have on the interaction of the different wall segments, stiffness of the connections, strength of the connections and ductility of the connections. The interaction is calculated using the following formula.

$$\%CA_{\delta} = \frac{F_{Test,\delta} - F_{0\%,\delta}}{F_{100\%,\delta} - F_{0\%,\delta}} \quad (2.2)$$

Where $F_{100\%,\delta}$ is the theoretical force for a fully composite section for a given drift, $F_{0\%,\delta}$ is the

theoretical force for a fully non-composite section for a given drift and $F_{T_{est,\delta}}$ is the experimental force for a given drift. The highest interaction factor which was obtained was 65% for a specific combination of connections, which will be discussed in detail further on. It should however be noted that the obtained interaction factor is geometry specific and therefore the obtained interaction factor cannot be used for other geometries then that of the C shaped wall. It does however give an indication of the interaction of wall segments that can be achieved by applying specific connections.

To increase the composite interaction of the wall segments and reduce uplifting forces a pres-lam system is implemented. A pres-lam system is a system where prestressed cables are internally placed in CLT to apply compressive forces in the members, which counteract the tensile uplifting forces[28]. From the experimental study it has been shown that by applying a pres-lam system an increased interaction of different wall segments can be achieved and as a results the overall stiffness of the system is increased. The C-shaped CLT core wall which has been experimentally tested can be seen in figure 2.16.

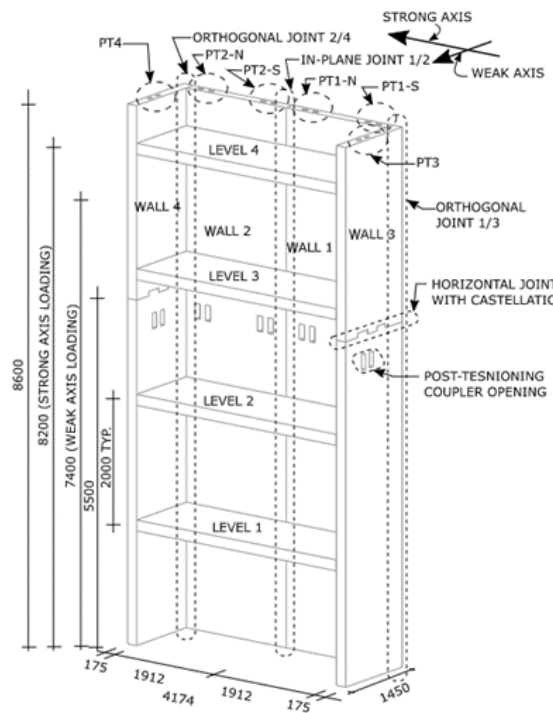


Figure 2.16. *Experimental test setup of a C-shaped CLT core system [27]*

From the experimental data obtained the different contribution to the total lateral deflections are calculated at a peak inter-storey drift of 2.3%. The contributions are subdivided into rocking deformation caused by rigid body rotation, sliding deformation caused by rigid body translation, and shear and bending deformation. The contributions are respectively 61%, 4% and 35%. This has shown the importance of incorporating connections early in the design phase of a CLT core system and its numerical assessment.

Additional to the before mentioned experimental research on C-shaped prestressed CLT core systems experimental test have been performed on CLT shear walls using a pres-lam system and a conventional system [29]. The conventional CLT shear wall systems makes use of hold downs to provide tensile resistance to the connection while the pres-lam system makes use of prestressed cables integrated in the CLT wall segments. The experimental tests where performed on wall systems with different prestressing ratios, prestressing force divided by the yield strength of the cable, a ratio of 15.4%, 30.7% and 46.1% where tested. From the experimental test it was shown that a higher prestressing force leads to lower percentage of prestress losses, 21.4%, 18.0% and 16.6% respectively.

Comparing the lowest prestress force applied to the conventional system which uses hold-downs it has been shown that for a similar applied force the maximum inter-storey is 2.5% and 6.2% respectively, using a pres-lam system lead to a reduction of inter-storey drift by a factor 2.5. This is partly due to the fact the wall segments have a better interaction and behave more as a single unit whereas the conventional system shows rigid body rotations of the different wall segments and had a gap opening between elements of 7.5mm while this was only 0.43mm for the prestress ratio, which can be seen in figure 2.17.

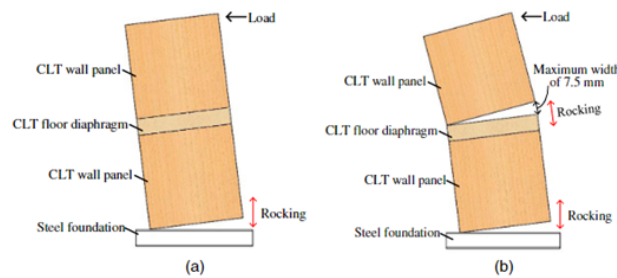


Figure 2.17. Experimental test setup and deformations: (a) Pres-lam system with 46.1% prestress ratio; (b) Conventional shear wall system using hold-downs[29]

From the experimental test it was shown that for a drift level of 2.5% the pres-lam systems showed no damage in the CLT segments due to repeated loading cycles, however some damage occurred in the connections. A friction coefficient of 0.32 was recommended by the authors to be used for the interface between the CLT segments and the steel foundation. Additionally for high enough prestress force the friction force proofed large enough to transfer the shear forces present and therefore additional shear keys where not needed. As a final remark it was shown that the pres-lam system showed excellent lateral performance and self-centering capabilities in comparison with the conventional models and can be accurately simulated using numerical software.

Since the core needs to accessible to occupants openings will be needed to allow passage from and to the core. These openings will have a negative effect on the stiffness of the CLT wall, which need to be taken into account. The calculation for the in-plane stiffness of a CLT wall with openings is shown in equation 2.3 and has been proposed by Shahnewaz et al[30] based on FEA on several different configurations of openings.

$$K_{opening} = K_{full} \left[1 - \frac{r_{o/w}(A_o/A_w)}{\sqrt{r_{o/w} + r_o(A_o/A_w) - 2(r_{off}/r_w)}} \right] \quad (2.3)$$

Where

- A_o is the area of the opening;
- A_w is the area of the wall with opening;
- r_o is the aspect ratio of the opening (smaller to larger dimension);
- r_{off} is the wall offset to wall dimension (x_{off}/L or y_{off}/H);
- $r_{o/w}$ is the maximum aspect ratio of the wall, $\max(l_o/L; h_o/H)$;

Since openings in the core are mostly limited to doors a conservative assumption is to assume the connection between CLT wall and lintel is executed as a pinned connection transferring limited bending moment.

2.4.1 Limit state of shear walls

According to Akbas et al.[31] two structural limit states exist for pre-lam CLT shear walls. First there is the DEC limit state which is decompression of the base of the wall as can be seen in figure 2.18a. Secondly there is the effective linear limit (ELL) which indicates the end of the linear-elastic response of the CLT as can be seen in figure 2.18b.

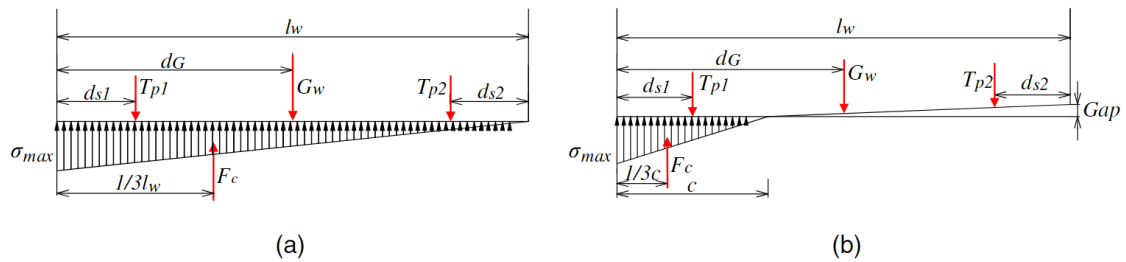


Figure 2.18. *Limit states CLT shear walls: (a) Decompression; (b) Effective linear limit [29]*

These limit states can be used to determine the dimensions of the CLT shear walls where stresses are within the elastic regime (ELL) or to determine allowable forces on the shear wall such that no tensile forces occur in the connections between segments. The latter can be especially useful for the shear wall connection design since tensile forces will result in a large gap openings between the segments and cause rigid body rotations of the segments. For tall structures these rigid body rotations will eventually lead to a large deflection of the structure under serviceability limit state loading.

2.4.2 In-plane & orthogonal CLT connections

As discussed in section 2.4 the type of connection between CLT panels can have large effects on the interaction and force transfer between different panels, therefore careful considerations between possible connection methods needs to be made to select a method which is able to maximize the strength and stiffness of the parent material.

Self-tapping screws

From experimental tests performed it is shown that mixed angle self-tapping screws provide the best combination of strength, stiffness and ductility for the orthogonal and in-plane connection[27]. It should be noted that screws under an angle of 90° provide the highest strength and stiffness while screws under an angle of 45° provide the highest ductility and as a results dissipative behaviour[32]. Strength and stiffnesses obtained for the different connection types, as shown in figure 2.16, can be found in table 2.4.

Table 2.4. *Strength and stiffness of STS connection experimentally tested by Brown et al.[27]*

	In-plane joint	Orthogonal wall 1/3 joint	Orthogonal wall joint 2/4 joint
F_y	150	68	63
K_{ser}	121	55	51

The different connections used for the in-plane and orthogonal joints can be seen in figure 2.19. A minimum spacing between STS of $a_1 = 10d$ as adopted according to Eurocode 5 (CEN).

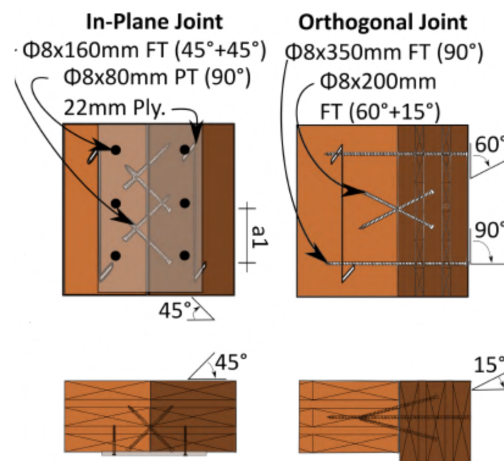


Figure 2.19. *STS configurations of in plane and orthogonal joint experimentally tested by Brown, et al.[27]*

A comparison between experimental models of different configurations of straight and double inclined screws and an analytical strength model for the same configurations gave an average overstrength of 1.1, in which the overstrength was determined by dividing the 5th percentile

strength with the analytically derived strength.

Experimental test performed by Hossain et al.[33] has shown the influence groups of self-tapping screws(STS) have on the reduction factor of the connection capacity. The reduction factor for STS acting in shear or withdraw under quasi-static monotonic loading is given in equation 2.4.

$$n_{eff} = 0.9n \quad (2.4)$$

X-bracket connection

A fairly novel connection type for the connection between CLT panels is the X-bracket connection. The X-bracket connection consists of the steel X-bracket itself, a groove in the CLT panel and dowel type fasteners coupled with punched metal plates, figure 2.20 shows a panel to panel X-bracket joint. Experimental testing on the connection type has proven that the connection is able to have similar yielding and ultimate strengths compared to conventional CLT connection methods (i.e. holddowns and angle brackets), however the X-brackets were able to provide more ductility and energy dissipation, even if the connection is subjected to coupled shear-tension behaviour[34].

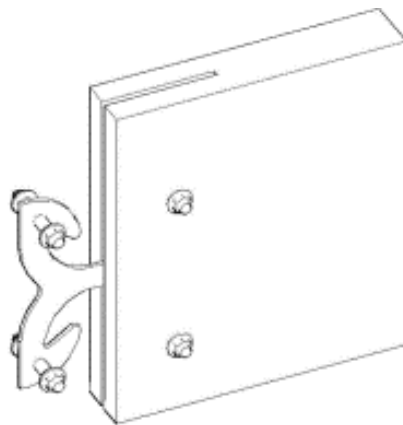


Figure 2.20. *X-bracket panel to panel joint*[34]

For an X-bracket with a height of 233 mm, a width of 303 mm and a thickness of 6 mm the obtained shear strength and stiffness can be seen in Table 2.5. It should be noted that the dimensions of the X-bracket are determined in such a way that stiffness and strength are comparable to that of conventional connection types while ductility is increased.

Table 2.5. Obtained shear strengths and stiffness of X-bracket[34]

parameters	Average	
	EN 12512 Method	equivalent elastic-plastic energy method
F_y (kN)	28.9	28.04
V_y (mm)	3.46	3.86
F_u (kN)	29.03	28.04
k_{el} (kN/mm)	8.53	7.73
k_{pl} (kN/mm)	0.02	0.00
μ ($V_u = 50mm$)	15.33	13.84
DuctilityClass	H	H

One of the main concerns for the application of X-brackets in the design of a CLT core is the orthogonal connection. Current experimental tests performed are only based on in-plane joints and horizontal joints. Especially the out of plane embedding of the X-bracket could provide difficulties since the thickness and end distance of the CLT are limited.

Steel dovetail connection

Another new connection type is the steel dovetail connection, the connection consists of a mortise part, a tenon part and self-tapping screws, introduced by Li et al. [35]. The assembly can be largely done in the factory, providing quick assembly and a high level of control over the construction process, an example of such a connection can be seen in figure 2.21.

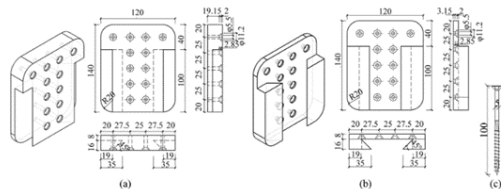


Figure 2.21. Configuration of dovetail (a) Mortise part, (b) Tenon part, (c) Self-tapping screws[35]

Under experimental testing the dovetail connection showed to have high strength and elastic stiffness, which was largely due to the tight and reliable interlocking of the mortise and tenon part. However a major drawback of the dovetail connection is that only a single longitudinal direction can give strength and stiffness, in the other direction sliding will occur. Additionally the dovetail connection achieved a rather low ductility factor under hysteresis loading.

2.4.3 Horizontal CLT connection

A relatively simple method to provide shear transfer and stiffness to a horizontal CLT connection is to use castellations. From experimental research by Brown et al. [27], [36] it has been shown that a castellated joint is able to take up high shear forces while deflections of the castellations remain limited. With their strength and stiffness values being 2.5 and 7 times great respectively compared

to a similar joint connected by steel angle brackets. Figure 2.22 shows the castellated joints for the horizontal shear transfer between vertical CLT panels. It should be noted that in the fabrication procedure a margin of 2 mm on all sides of the castellations are used, allowing easy construction. This will however result in a rigid body translation of the CLT of 4mm in either directions since the wall section is able to move freely.

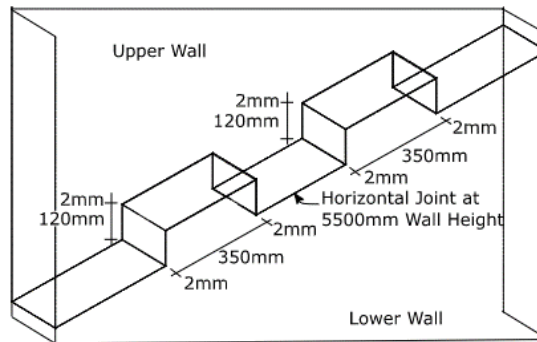


Figure 2.22. Castellated joint design for the connection between upper and lower segments of CLT panels[27]

While the horizontal force transfer of the core is able to transfer through the castellations additional measures need to be taken to allow the transfer of vertical tensile forces. Which can either be transferred by a dowelled connection using internal steel plates, tension cables or external steel plates.

2.4.4 Connection CLT core to foundation

Connections between the core or columns and foundation should be able to transfer high shear forces and hinder possible uplifting of the construction due to bending moments induced by wind loading. This section will discuss the possible solution for providing such connections.

High strength hold-downs(HSK)

To provide a stiff connection between the foundation and the CLT core a so called Holz-Stahl-Komposit-System (HSK) can be used. The requirements of the system is that forces are able to flow to the foundation and limited translations and rotations of the CLT core occur due to lateral forces. The HSK system consists of a perforated steel plate which is inserted in the CLT after which the holes are filled with adhesive. Within these holes “adhesive dowels” are formed (AD) and connections with adjacent AD’s are formed through “steel links” (SL). Figure 2.24 shows the geometry of the perforated steel plates and the position of AD and SL.

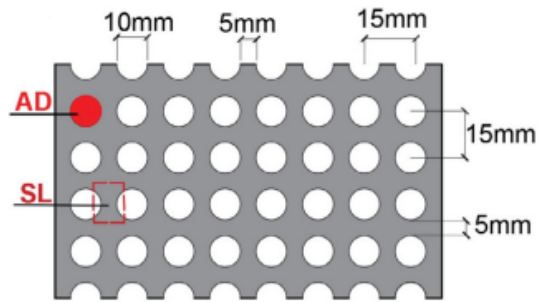


Figure 2.23. *Perforated steel plate geometry [37]*

Zhang et al.[37] proposed to modify the HSK system as mentioned above. The modification is in the form of covering the outer row of perforated steel plate with duct tape, ensuring no adhesive penetrates to holes and forms AD's. This will increase the ductility of the connection and provide more dissipative behaviour. In figure 2.24 an example can be found of the modified HSK connection.

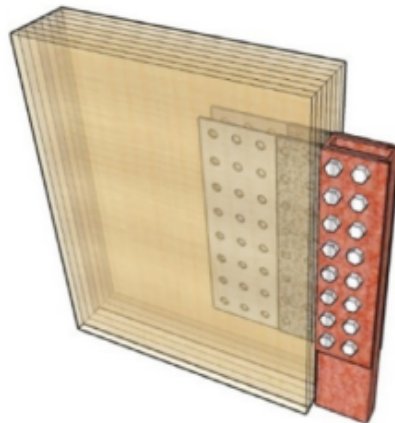


Figure 2.24. *Example modified HSK connection [37]*

From experimental testing it has been shown a hsk system is able to be designed in such a way that ductile failure will occur. By changing the numbers of AD and SL the capacity, stiffness and ductility of the joint can be regulated. The shear yield strength of a individual SL is equal to 2.1 kN while the ultimate shear strength is equal to 4 kN. The connection properties are independent of the orientation of the CLT layer in which the composite HSK is embedded. The researchers concluded that the modified HSK system can provide strong, stiff and ductile hold-downs which are able to dissipate large amounts of energy and can therefore be used in tall timber buildings.

Angle brackets and hold-downs

Angle brackets and hold-downs are able to connect CLT panels to floors or foundations by using steel plates and self-tapping screws. Currently angle brackets hold-downs are widely used in the construction sector for the connection of CLT panels in in low rise buildings. The angle brackets are largely responsible for taking up the shear force while the hold-downs are responsible for carrying

vertical tensile loading. A typical angle bracket and hold-down connection can be seen in figure 2.25.

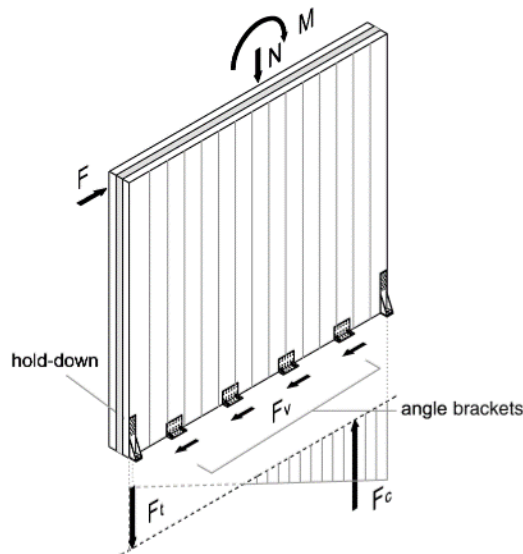


Figure 2.25. Angle bracket and hold-down connection of a CLT panel [38]

Experimental testing of different angle brackets by Tomasi and Smith[38] has determined the maximum shear strength and stiffnesses of the angle brackets, as can be seen in table 2.6.

Table 2.6. Shear strength and stiffnesses of experimental tests on angle brackets[38]

	F_{max} [kN]	K_{tot} [kN/mm]
AB200	75.52	5.04
AB110	27.3	1.84
AB90	20.98	0.84

Research has shown the complex behaviour of steel angle brackets and there failure modes, it has been proposed to only use experimental testing to determine strength and stiffness of a specific connection [38].

However for the connection between CLT and the foundation the choice to use steel angle brackets is unlikely due to its limited stiffness. This would result in large rigid body rotations and translations which result in large lateral deformations. The overturning moment induced by earthquake loading on mid-rise buildings causes tensile forces to occur in the hold-down connections with the foundation. It is stated by Polastri et al.[39] that the forces induced by earthquake loading will already be too large for conventional hold-downs for a 8-storey building.

pres-lam

As stated in section 2.4 applying a pres-lam system to a CLT core brings major benefits. Construction of a pres-lam system will be fast with cost kept to a minimum, while displacements during

dynamic earthquake or wind loading will be minimized. However careful attention should be given to the connection between the pre-lam system and the foundation, similar to the connection between columns and foundation in section 2.3.3 the post-tensioning cables need to be directly grouted in the concrete foundation, which results in a large concrete slab depth.

2.4.5 Connections CLT core to truss

The connection between the CLT elements and the truss elements can be executed in several different solutions. For this research, the main interest is to provide a connection between the CLT core and the truss outriggers. These connection have to be able to transfer large forces from the core to the outrigger, since large bending moments need to be transferred from the core through the outrigger truss to the columns.

Glued-in steel rods

Research has been performed on the use of glued-in rods for the connection of CLT elements. However these studies only provide a numerical assessment of in-plane CLT connections, out-of-plane connections where not considered. It was stated that the glued-in rods provided the connection with high strength and high stiffness and connections where the glued in rods are placed perpendicular to the grain direction of that layer have higher load bearing capacity then when the rods are placed in layers parallel to the rod direction[40], which is in line with previous experimental results. Additionally it was shown that increasing the length and thickness of the rod generally increased the axial resistance of the connection. However after a certain rod thickness is reached only small changes in the axial resistance are obtained, primarily due to a shift in failure mode to the bond connection between CLT layers.

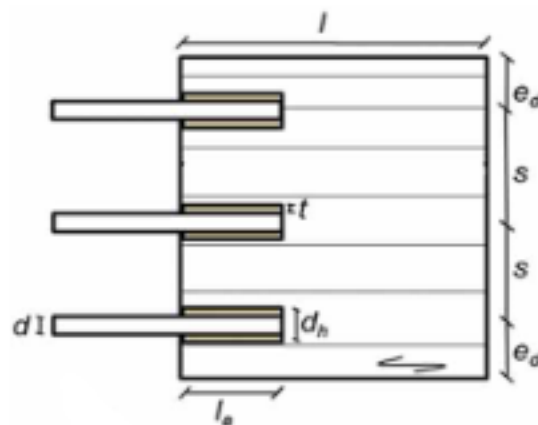


Figure 2.26. CLT glued-in steel rod connection [41]

Research performed by Ayansola et al.[41] stated that equation 2.5 provided by the GIROD project[42] is only accurate in predicting the load carrying capacity of the glued in rods parallel to

the grain. The influence of multiple glued-in steel rods on the strength of the connection has been experimentally tested by Ayansola et al[43]. From this study the influence of the anchorage length, the spacing between the steel rods and the number of steel rods was assessed, results are shown in figure 2.27.

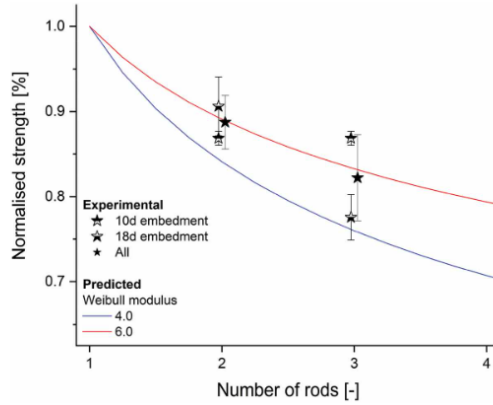


Figure 2.27. Experimental results of multiple CLT glued-in steel rods [43]

$$R_{ax} = (\pi d_H l_a) \tau_f \frac{\tanh \omega}{\omega} \quad (2.5)$$

with: $\omega = \sqrt{\frac{l_{geo}}{l_m}}$; $l_{geo} = \frac{\pi d_H l_a^2}{2} \left(\frac{1}{A_r} + \frac{E_r/E_w}{A_w} \right)$; $l_m = \frac{E_r G_f}{\tau_f^2}$;

where

- l_{geo} is a geometrical length parameter;
- l_m is a material length parameter;
- A_r is the rod cross-sectional area;
- A_w is the wood cross-sectional area;
- E_r is the rod moduli of elasticity;
- E_w is the wood moduli of elasticity;
- G_f is the fracture energy calculated from l_m ;

For the truss beam the governing equation for the characteristic pull-out load, $R_{ax,k}$, is shown in eq. 2.6 according to the GIROD-approach.

$$R_{ax,k} = f_{ax,k} \pi d_{equ} l \frac{\tanh(\omega)}{\omega} \quad (2.6)$$

with: $\omega = 0.017l / \sqrt{d_{equ}}$

where

- d_{equ} is the equivalent rod diameter, in mm ;
- l is the glued in length, in mm ;
- $f_{ax,k}$ is the formal shear strength, in N/mm^2 ;

The suggested minimum spacing of the rods can be seen in fig. 2.28.

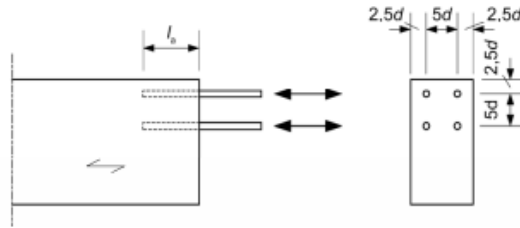


Figure 2.28. Minimum spacing distances of a glued-in rod in a beam according to the GIROD-proposal [44]

The current draft version of the eurocode prEN1995-1-1 includes calculation methods for the use of glued in rods in CLT as well as in GLT.

Dowel connection

Another alternative to connect the CLT core to the truss is by using slotted in steel plates and dowels as the connection between CLT and beam, which can be seen in figure 2.29. From experimental testing it was found that the Johansen equation in Eurocode 5 in combination with the appropriate embedment formulas provided conservative strength predictions of the connection[45]. The research also showed the importance of overstrength factors γ_{Rd} , when the material properties were determined based on information provided by suppliers $\gamma_{Rd} = 1.91$ was obtained, while when the material properties were determined experimentally an average of $\gamma_{Rd} = 1.21$ was obtained. Additionally research showed that increasing the spacing of the dowels increased the strength and stiffness of the connection and medium to high ductility ($\mu = 4.5 - 7.1$) was obtained. From testing observation the following observation has been made. To ensure delamination of the outer layers of the CLT does not occur it is advised that bolts or threaded dowels with washers and nuts are used in the end row.

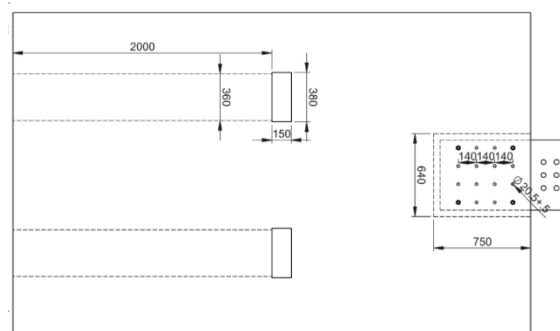


Figure 2.29. CLT dowel connection [45]

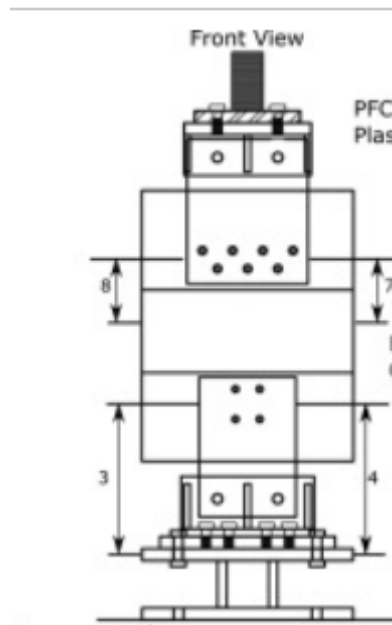


Figure 2.30. Loading of the experimentally tested dowelled CLT connection[46]

Additional experimental testing performed by Brown et al.[46] on dowelled CLT hold-down connections with increased row spacing and end distances showed that an experimental overstrength of 1.70 was achieved which was higher than the analytically calculated overstrength of 1.5. This difference could have been caused by the rather small sampling size and the variable density distribution of CLT. It should be noted that the stiffness predictions of Eurocode 5 significantly overpredicted the stiffness of the dowelled joint. Loading of the experimental tests were mainly axial as can be seen in figure 2.30.

Placement of the truss in relation to the core

The connection between the truss and CLT core should be performed in such a way that connection of the truss coincides with the in-plane direction of the CLT shear wall as can be seen in figure 2.31. If the truss is connected out of plane, for instance the center of a shear wall, large bending moments need to be transferred from the in-plane shear walls to the out-of-plane shear wall at the connection location. Connecting the truss with the out of plane direction will reduce the overall stiffness of the building and decrease its efficiency. Additional problems could occur at the connection due to limited bonding length of the rods or slotted steel plate in the CLT panels in out-of-plane direction (thickness).

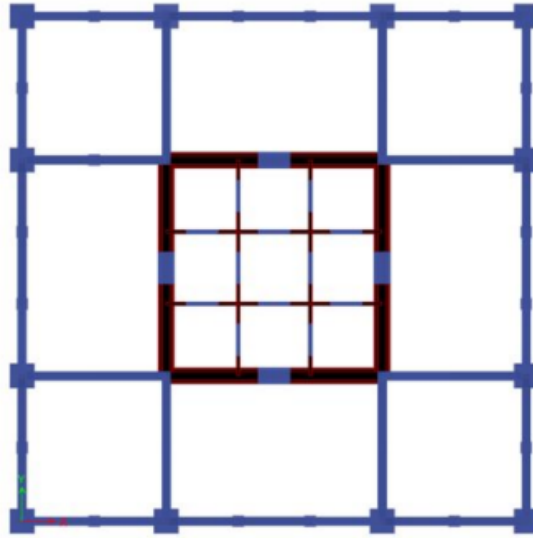


Figure 2.31. *Correct truss to core connection location [3]*

Carefull attention needs to be paid to ensure the possibilities of the before discussed connection types since it is very likely that two trusses will connect at the same corner as shown in figure 2.31, resulting in large amount of steel intersecting at the corners.

2.5 Timber design issues

When design timber structures for mid-rise to tall buildings a few design issues arise which need to be dealt with accordingly. These issues consist of fire safety, differential shortening, self-weight and vibrations and will be discussed in the following section.

2.5.1 Fire safety

One of the first topics which comes to mind when discussing the design of timber buildings is fire safety. It is important to convince the general public, regulators and project developers that fire safety can be guaranteed for mid-rise and tall timber buildings. In recent years an increasing interest has been show in research on fire safety of timber buildings[47]. The data collected in these studies could provide valuable insight in fire safety engineering of timber buildings and could allow relaxation of regulations, which are currently very strict.

Research performed by Frangi et al.[48] noted the significant difference between design concepts for mid-rise timber buildings and tall timber buildings. For mid-rise buildings it was accepted that after a defined period of time fire is able to spread through the building and collapse of the building could be accepted after a defined period of time. While for tall timber buildings the design concept differs, first of all the time needed to evacuate will increase as well as the time needed for the fire brigade to reach the fire. Secondly it is assumed that a blockade of the escape routes may occur which results in occupants being stuck on the upper floor, therefore it is not allowed that fire is able

to spread to other compartments of the building, additionally since occupants are trapped collapse of the building is not accepted.

To achieve this level of fire safety it is then stated that in such a tall timber building compartmentalization should occur. Additionally in the compartment in which the fire occurs separating and structural elements should not start charring, but a complete burn out may occur. This can be achieved by protecting the separating and structural elements with non-combustible material.

In the design of recent timber buildings a combination of fire safety measures are used, one of which is compartmentalization. In the design of Mjøstarnet a 18-storey building fire safety design consisted of achieving a 120 minute resistance of the main load bearing elements. The 120 minute fire resistance was achieved by applying the remaining cross section method after charring according to the Eurocode, allowing the large glulam columns to remain visible by the occupants. Experimental research on large glulam columns ensured the engineers of Mjøstarnet that the structural members are self-extinguishing and will prevent a building from collapse[7].

Additional measures have been taken to ensure fire safety of Mjøstarnet. Fire retardant painting was applied on all visible wood in escape routes, internal walls and elevators. Sprinklers were applied throughout the building. Fire stop is applied within the façade to ensure fire is not able to spread to adjacent floors. Steel in connections (plates or dowels) are embedded at least 85 mm and gaps between beams and columns are filled with intumescent fire strip.

In the fire safety design it is also of importance to protect the connection between structural elements against fire. This is required since heat can lower the strength and stiffness of steel connectors (screws, dowels etc.), for doweled connections this can be achieved by inserting wooden plugs or fire resistant plugs at the locations of the steel dowel to ensure the fire is not able to reach the steel.

For this research it is assumed that fire resistance can be achieved by combining the before mentioned concepts. Compartmentalization will ensure the fire is not able to spread to nearby rooms and floors, remaining cross section method will be used to ensure a 120 minute fire resistance of the main structural members, fire retardant painting will be used to secure the escape routes, sprinklers will be applied throughout the building, fire stop will be used in the façade and connections will be protected against the heat to ensure their structural integrity.

2.5.2 Differential vertical shortening

Differential shortening is caused by a difference in shortening due to shrinkage and creep of different components of a timber structure. While differential shortening might play a bigger role in composite structures where for instances columns are made of timber while the core is reinforced concrete. Differential shortening between glulam columns and CLT walls could still play a small role and could induce stresses in structural elements, however for this research it is assumed that differential shortening will not take place.

2.5.3 Vibrations

As mentioned before timber structures are light in comparison to similar steel or concrete buildings, additionally timber structures are more flexible. Dynamic loading on timber structures result in large peak accelerations which need to be minimized to allow for user comfort. This will be discussed in detail in the following section, section 2.6.

2.6 Dynamic performance

Assessing the dynamic performance of a timber building has shown to be required, since timber is a lightweight and flexible material in comparison with steel and concrete. Assessment of a timber building can be done numerically or analytically. Due to the many different elements and connections and the limited research in the topic it is preferred to make a numerical analyses to determine the dynamic performance of a timber building.

Research performed by Zhao et al.[49], has done a numerical analysis on the serviceability behaviour of tall CLT buildings. In this study the deflections, acceleration and eigenfrequency is determined for a 30-storey 105 meter tall building using a CLT core and CLT shear wall for stability. It should be noted that connections are not incorporated in this numerical study and rigid connection are assumed throughout the model. The first three lowest modal frequencies are evaluated, the first vibrational mode occurs at 0.525 Hz for the weak direction, the second vibrational mode occurs at 0.579 for the strong direction and finally the third vibrational mode occurs at 0.678 Hz for rotations.

The fundamental flexural frequency of a multi-storey building for a height greater than 50 meters can be estimated with the following formula according to BS EN 1991-1-4.

$$f_1 = \frac{46}{h} \quad (2.7)$$

This formula is based on the response of tall steel and concrete buildings. However the formula does take into account the influence connections and timber as a structural material have on the fundamental flexural frequency. Therefore Reynolds et al.[50] proposed a formula to approximate the fundamental flexural frequency for timber buildings without the influence of connections.

$$f_1 = \frac{55}{h} \quad (2.8)$$

The approximations provided by Reynolds showed similar results to that of the numerical calculation by Zhao et al.

The first two fundamental frequencies of Treet have been estimated and are determined to be equal to 0.75 and 0.89 Hz for the first and second mode respectively[22]. In situ experimental dynamic tests have been performed by Reynolds et al.[50] on a total of 11 timber buildings in Europe and the UK quantifying their damping ratio and natural frequencies in the fundamental mode of vibration. In figure 2.32 the relation between the height and natural frequency can be found. It is interesting to notice that the frequencies found for the building Treet are within the upper and lower approximations for steel and concrete buildings taller than 50 meters and the approximation proposed by Reynolds et al. in equation 2.8.

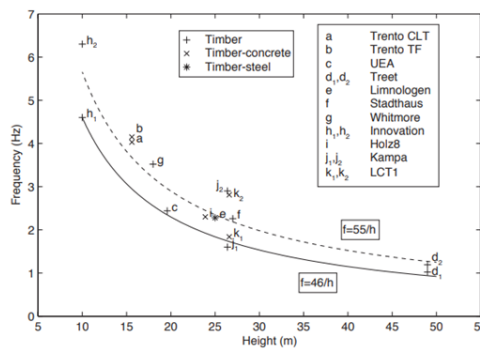


Figure 2.32. Relation building height vs natural frequency[50]

During the numerical study by Zhao et al. the influence of different parameters on the lateral acceleration has been assessed. The parameters which have been assessed are the timber grade, building mass and stiffness of the building. Increasing the timber grade from C16 to C36 resulted in a 26.4% decrease of the lateral acceleration, increasing the building mass by 40% resulted in a 29.6% reduction of the lateral acceleration and finally increasing the stiffness by 40% reduces the lateral acceleration by 36.8%. It has also been stated by Polastri et al.[39] that base anchoring of the core will be of mayor significance in timber buildings and could limit the buildings performance.

2.6.1 Damping

A structure is able to dissipate energy of vibrations by damping, this will result in the decay of vibrations in a structure over time. For several structures the structural damping is determined by the Eurocode, however timber buildings is not including in this table. The referred table can be found below in Table 2.7.

Structure	ξ_s	δ_s
Reinforced concrete buildings	1.59%	0.1
Steel buildings	0.8%	0.05
Composite buildings	1.28%	0.08
Timber bridges	0.96 - 1.91%	0.06 - 0.12

Table 2.7. Structural damping coefficients according to Eurocode

The timber buildings which have been experimentally tested in figure 2.33 had a damping ratio in the range of 1.4% - 5.6%, showing there is a large scatter in damping ratios for different building types.

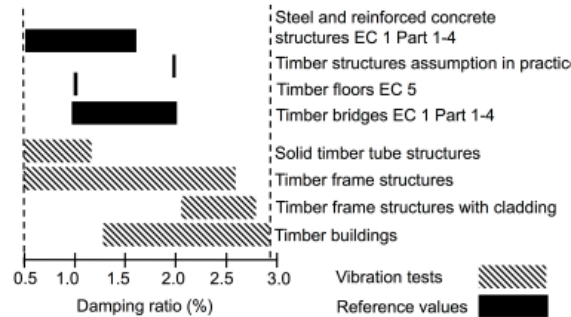


Figure 2.33. *Damping codes vs results from vibration tests*[51]

The structural damping coefficient is highly dependent on the type of structure, material and connection type. Material damping of timber can be estimated at 0.4-0.8% according to Feldman et al.[51] with concrete having similar material damping and steel having only 0.1 – 0.3% material damping. The connection type shows to have large influences on the overall damping of the structure. A dowel type connection has a material damping of 0.6-0.8% and a glued connections only has 0.2- 0.4%. Finally the supports give a contribution of 0.1-0.3% to the overall damping, resulting in an estimated damping ratio of 1.1-1.9% for timber buildings with dowel type connection and 0.7-1.5% for timber buildings with glued elements.

Since the number of full timber buildings is currently fairly limited it is not possible to collect a large sample of experimental data on the structural damping coefficient for these type of buildings. However one can use previously calculated damping ratio of for example the building Treet to approximate the damping ratio of a timber structure which utilizes slotted in steel plates and glulam trusses. For the building Treet the structural damping ratio has been determined at $\xi = 0.019$ for the final design. This damping ratio was estimated based on the fact glulam could provide a contribution in the range of $\xi = 0.005 - 0.01$ and the doweled connections $\xi = 0.01 - 0.02$ [22]. The design for Mjøstårnet incorporated a similar damping ratio of 1.9% as was used for Treet[7].

It should be noted that the prefab modules which are placed in the Treet structure where experimental tested to obtain the damping ratio of the 2x2 prefab modules. The lower bound value of the damping ratio was determined to be equal to 2.8%[22].

Reynolds et al.[50] proposed to have a lower bound approximation of the damping ratio based on the natural frequency of the building, which can be calculated according to the following formula.

$$\xi = 0.5f + 0.5 \quad (2.9)$$

The lower bound approximation was determined based on experimental testing on the same data set as the one used in figure 2.32. Figure 2.34 shows the variation of damping with frequency for each mode for the different buildings of the data set. It should be noted that however a large scatter occurs in damping ratios for high frequencies, lower frequencies tend to group together and can be better estimated using the lower bound approximation as mentioned before.

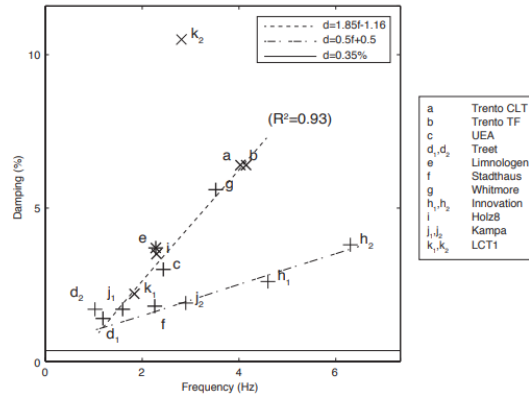


Figure 2.34. *Damping ratio vs frequency*[50]

2.6.2 Lateral acceleration and user discomfort

Dynamic loading on a structure can cause discomfort to the user, dynamic wind loading or earthquakes are the main sources of dynamic loads. The effect of sway and lateral accelerations of buildings on humans has been assessed by Smith and Coull[52], as can be seen in figure 2.35.

Range	Acceleration [m/s^2]	Effect
1	< 0.05	Humans cannot perceive motion.
2	0.05 – 0.10	Sensitive people can perceive motion; hanging object may move slightly.
3	0.10 – 0.25	Majority of people will perceive motion; level of motion may affect desk work; long-term exposure may produce motion sickness.
4	0.25 – 0.40	Desk work becomes difficult; ambulation still possible.
5	0.40 – 0.50	People strongly perceive motion.
6	0.50 – 0.60	Most people cannot tolerate motion and are unable to walk naturally.
7	0.60 – 0.70	People cannot walk or tolerate motion.
8	> 0.85	Objects begin to fall and people may be injured.

Figure 2.35. *Effect of lateral accelerations on humans* [52]

The Eurocode provides maximum values for the lateral acceleration during serviceability limit state for office buildings(region 1) and residential buildings (region 2) according to the dutch national annex NEN -EN 1990, which can be seen in figure 2.36.

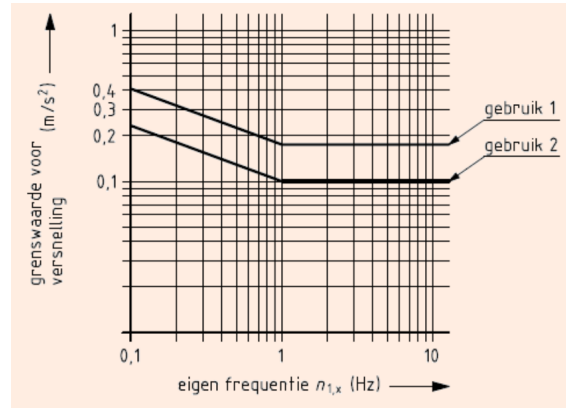


Figure 2.36. Requirements on maximum lateral acceleration

From numerical models or hand rules the fundamental frequencies of a building can be estimated. It should be noted that since the sample size of mid-rise and tall-timber buildings is limited numerical assesment will give more accurate results compared to hand rules.

Lateral acceleration

The lateral acceleration of a building in the along-wind direction can be estimated according to Eurocode EN1991-4 from eq. 2.10.

$$a_{max}(y, z) = \sigma_{a,x}(y, z)k_p \quad (2.10)$$

where

- $\sigma_{a,x}(y, z)$ is the standard deviation of the characteristic along-wind acceleration;
- k_p is the gust peak factor;

The standard deviation of the characteristic along-wind acceleration can be calculated using eq. 2.11, according to Eurocode EN1991-4.

$$\sigma_{a,x}(y, z) = c_f \rho I_v(z) v_m^2 R \frac{K_y K_z \phi(y, z)}{\mu_{ref} \phi_{max}} \quad (2.11)$$

where

- c_f is the force coefficient;
- ρ is the air density;
- $I_v(z)$ is the turbulence intensity at a specific height above ground level;

v_m	is the characteristic mean wind velocity at a specific height above ground level;
R	is the square root of the resonant response;
μ_{ref}	is the reference mass per unit area;
$\phi(y, z)$	is the mode shape;
ϕ_{max}	is the mode shape value at the point of maximum amplitude;
K_y	is the size reduction coefficient;
K_z	is the size reduction coefficient;

2.7 Numerical modelling of CLT

As previously described CLT has a orthotropic materials properties in the different directions depending on the number of layers, thickness of the layers, orientation of the layers and strength of the layers. Modelling of individual layers is very time consuming and costly, therefore it is proposed to utilize a equivalent orthotropic shell model. The equivalent orthotropic shell model is used to create a stiffness matrix which can be inputted in the FE-models, calculations are based on the equivalent bending stiffness and shear stiffness. Since the CLT panels will be primarily used for the CLT core it is useful to incorporate shear deformations in the numerical analysis, therefore Mindlin plate theory should be used[53].

Bending stiffness in the in-plane direction can be calculated using the following formula where an average is taken of the elasticity moduli in the board layers. It should be noted that in this equation an average is taken over the area instead of over the moment of inertia of the different layers. This is done because it is expected the element will be loaded in plane and will behave as a shear wall[54].

$$E_x = \frac{\sum_{i=1,3,..}^n E_0 A_i + \sum_{i=2,4,..}^{n-1} E_{90} A_j}{A_{tot}} \quad (2.12)$$

$$E_y = \frac{\sum_{i=1,3,..}^n E_{90} A_i + \sum_{i=2,4,..}^{n-1} E_0 A_j}{A_{tot}} \quad (2.13)$$

The in-plane shear stiffness G_{xy} is able to utilize different reduction factors one for torsion k_{33} and one for shear k_{88} . The in-plane shear stiffness is calculated as an average of the mean shear stiffness of the boards. For this research the assumption is made that k_{33} is equal to 1 for edge glued CLT elements and k_{88} is also equal to 1 for edge glued CLT elements.

Shear stiffness G_{yz} and G_{xz} can be calculated using the equivalent thicknesses of the layers and their respective shear modulus. For the calculation of the shear stiffness a reduction factor k needs to be used. This reduction factor can be calculated using different strategies either the laminate shear correction factor which considers coupling proposed by Gustafsson et al. (2019) and Wallner-Novak

et al.[55] or the theory of virtual work proposed by Aondio et al.[53].

$$k = \frac{(\sum(EI + EAa^2))^2}{\sum G_i b t_i \int_h \frac{S^2(z) E^2(z)}{G(z) b(z)} dz} \quad (2.14)$$

However this calculation can be rather tedious if it needs to be performed for multiple CLT configurations therefore approximation have been made by Wallner-novak et al.[55]. The approximations are valid for symmetrical CLT panels, of equal laminate thickness and should have a shear modulus ratio of $\frac{G_{90}}{G_0} = 0.1$.

Table 2.8. *Shear correction factor for different number of layers*[55].

Number of layers	1	3	5	7	9
k	0.83	0.21	0.24	0.26	0.27

Using the shear correction factors mentioned in table 2.8 the shear moduli can be calculated with the following formula's.

$$G_{yz} = k_y \frac{\sum_{i=1,3,..}^n G_0 t_i + \sum_{i=2,4,..}^{n-1} G_{90} t_j}{t_{tot}} \quad (2.15)$$

$$G_{xz} = k_x \frac{\sum_{i=1,3,..}^n G_{90} t_i + \sum_{i=2,4,..}^{n-1} G_0 t_j}{t_{tot}} \quad (2.16)$$

Poisson ratio v_{xy} and v_{yx} can be assumed to be equal to zero according to Aondio et al.[53]. Since CLT consist of a build-up which is symmetrical the stiffness matrix can be reduced to a diagonal matrix, given the assumption that the poisson ratio is 0 in all directions. The terms on the diagonal can be calculated using the following formulas.

$$D_{11} = \frac{E_x d^3}{12(1 - v_{xy} v_{yx})} \quad (2.17)$$

$$D_{22} = \frac{E_y d^3}{12(1 - v_{xy} v_{yx})} \quad (2.18)$$

$$D_{33} = \frac{G_{xy}d^3}{12} \quad (2.19)$$

$$D_{44} = \frac{5}{6}G_{xz}d \quad (2.20)$$

$$D_{55} = \frac{5}{6}G_{yz}d \quad (2.21)$$

$$D_{66} = \frac{E_x d}{1 - \nu_{xy}\nu_{yx}} \quad (2.22)$$

$$D_{77} = \frac{E_y d}{1 - \nu_{xy}\nu_{yx}} \quad (2.23)$$

$$D_{88} = G_{xy}d \quad (2.24)$$

Combining the above mentioned stiffness the following stiffness matrix can be obtained which is able to accurately describe the behaviour of CLT of various thicknesses.

$$M = \begin{bmatrix} D_{11} & 0 & 0 & 0 & 0 & 0 & 0 & 0 \\ 0 & D_{22} & 0 & 0 & 0 & 0 & 0 & 0 \\ 0 & 0 & D_{33} & 0 & 0 & 0 & 0 & 0 \\ 0 & 0 & 0 & D_{44} & 0 & 0 & 0 & 0 \\ 0 & 0 & 0 & 0 & D_{55} & 0 & 0 & 0 \\ 0 & 0 & 0 & 0 & 0 & D_{66} & 0 & 0 \\ 0 & 0 & 0 & 0 & 0 & 0 & D_{77} & 0 \\ 0 & 0 & 0 & 0 & 0 & 0 & 0 & D_{88} \end{bmatrix} \quad (2.25)$$

Careful attention should be given to assign correct local coordinate systems so that the inputted stiffness matrix correctly represent the material it is supposed to model. This will be primarily the case for the CLT plates which will be used for the CLT cores. Figure 2.37a and 2.37b show the intended stiffness directions and local coordinate system which correctly coincides with the calculated stiffness matrix.

3. Case study

This chapter will discuss the case study which will be used further on for the numerical evaluation, additionally the design choices and assumption will be discussed.

3.1 Program of requirements

During the program of requirements some requirements are set for the initial design, however these requirements are subjected to change once the initial design is finished. For the case study design A will consist of a cross laminated timber core, in design B will consist of the outrigger system. Initially the core design A will be checked and verified to ensure requirements are met in serviceability limit state and ultimate limit state.

For design A the following requirements will be used. The functions of the building are mainly offices, this is chosen since the requirements for office buildings are looser than that of a residential building, however for office buildings open spaces are required, reducing the possibilities to add shear walls outside the core. The foot print of the building will be rectangular to ensure stiffness and loads in both lateral directions are similar, a foot print of 36 by 36 meters is assumed. Location for the case study is the city of Rotterdam, over recent years the amount of tall buildings in Rotterdam has grown significantly, therefore it is more likely that a mid-rise to tall timber building will be placed somewhere in Rotterdam. The height of the initial building is 41.1 meters with a storey height of 3.9 meters and a ground floor-to-floor height of 6 meters ($9 \times 3.9 + 6$), this initial height is based on a previous study where a post-tensioned CLT core of 6 by 8 meters which is almost twice as small as the core proposed in the current case study had a maximum height of 8 storeys [56]. Overview of the general requirements can be found in table 3.1.

Table 3.1. *General requirements*

Requirements	
Function	Office
Location	Rotterdam
Height	41.4 m
average storey height	3.9 m
Footprint	36 x 36 m

Furthermore some initial requirements need to be given with regard to the size of the core and spacing of the columns. A grid size is chosen of 6x6 or 6x6 m with a core of 12x12 m, allowing the edges of core to be in line with the grid. The openings of the door have been chosen at 1.5 m to allow multiple occupants to enter and leave the core simultaneous. Figure 3.1 shows the floor plan of the case study. It can be seen from the figure that columns and core shear walls are inline, allowing the outrigger truss to be directly connected to the shear walls in plane.

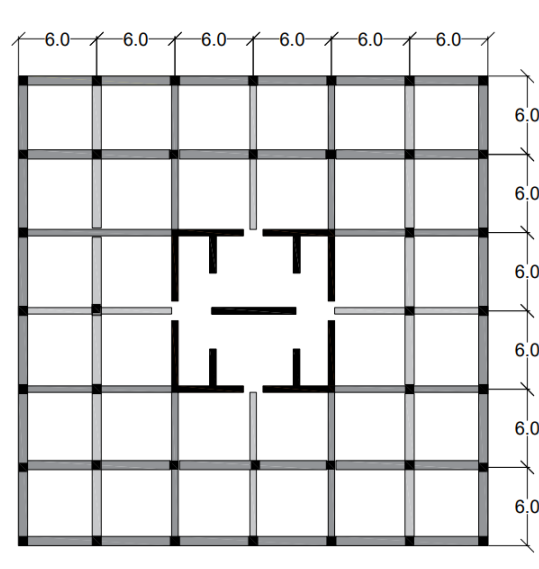


Figure 3.1. *Floor plan proposal case study*

3.2 Design aspects

As mentioned before the main goal is to determine the dimensions of the load bearing elements due to vertical gravity loading and lateral wind or earthquake loading. therefore the following elements will be considered for design A.

- Core wall layout
- Core wall thickness
- Column dimensions
- Connections core
- Connections column

Furthermore for design B the following aspects will be designed

- Outrigger/belt-truss layout
- Truss dimensions
- Truss connection
- Truss to core connection
- truss to column connection

3.3 Loads

The loads on the structure consist of vertical gravity loading and lateral wind loading. The gravity loading consists of permanent loads, due to selfweight of the structure, and variable loading, due to users and snow loading. Recommended values for the variable loading for office buildings are given in NEN-EN1991, which can be found in table 3.2.

Table 3.2. *Characteristic variable loading*

floor load offices	2.5 kN/m^2
floor load communal area	2.5 kN/m^2
snow load	0.56 kN/m^2

The floor system which will be used in the case study can be seen in figure 3.2 and consists of a 5-ply CLT, gypsum boards, sound insulation and laminate flooring, which has been tested and verified in the CLT handbook [57]. The weight of the floor system components are shown in table 3.3 where the total self-weight is equal to 2.3 kN/m^2 .

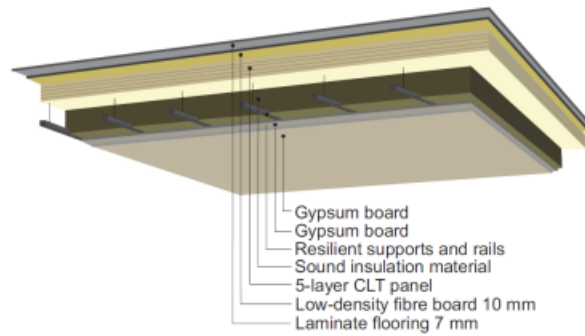


Figure 3.2. *CLT 5-ply floor system*[57]

Table 3.3. *Self-weight 5-ply CLT floor system*

CLT	1.50
Gypsum boards	0.065
Laminate flooring	0.60
Sound insulation and finishings	0.10

Table 3.4. *Characteristic permanent loading*

Self-weight floor system	2.3 kN/m^2
Interior Walls	0.5 kN/m^2
Ceiling	0.3 kN/m^2

3.4 Load combinations

Load combinations are determined according to NEN-EN1990 in combination with dutch national annexes. The consequence class has been determined at CC3, since the building is taller than 70 meters. The consequence class gives an indication of the risk associated to the collapse of the structure and the affiliated loss of human life and economic loss. The load combinations for ultimate limit state are given in eq. 3.1 and 3.2.

$$1.1(1.35G'' + \sum_{i \geq 1} 1.5\psi_{0,1}Q_{k,i}) = 1.49G'' + \sum_{i \geq 1} 1.65\psi_{0,1}Q_{k,i} \quad (3.1)$$

$$1.1(1.2G'' + 1.5Q_{k,1}'' + \sum_{i \geq 1} 1.5\psi_{0,1}Q_{k,i}) = 1.32G'' + 1.65Q_{k,1}'' + \sum_{i \geq 1} 1.65\psi_{0,1}Q_{k,i} \quad (3.2)$$

The load combinations which need to be considered for the serviceability loading are the characteristic loading, frequent loading and quasi-permanent loading, and are given in eq. 3.3, 3.4 and 3.5 respectively.

$$\sum_{j \geq 1} G_{k,j}'' + P'' + Q_{k,1}'' + \sum_{i > 1} \psi_{0,i}Q_{k,i} \quad (3.3)$$

$$\sum_{j \geq 1} G_{k,j}'' + P'' + \psi_{1,1}Q_{k,1}'' + \sum_{i > 1} \psi_{2,1}Q_{k,i} \quad (3.4)$$

$$\sum_{j \geq 1} G_{k,j}'' + P'' + \sum_{i \geq 1} \psi_{2,i}Q_{k,i} \quad (3.5)$$

Table 3.5 contains the used ψ -values for the different load combinations.

Table 3.5. ψ -values

	ψ_0	ψ_1	ψ_2
category B offices	0.5	0.5	0.3
wind	0	0.2	0
snow	0	0.2	0

3.5 Serviceability criteria

As discussed in section 2.6 the serviceability requirements play a large role in the design of timber structure. The requirements for the lateral peak response acceleration is dependent on the natural frequency and the requirement needs to be satisfied accordingly, see figure 2.36 for the requirements. Furthermore requirements on the lateral deformation of the structure are mentioned in NEN-EN1990, the total lateral displacement may not exceed $H/500$ and the lateral storey drift may not exceed $h/300$, where H is the total building height and h is the storey height.

3.6 Design assumptions

Fire safety

As discussed in section in section 2.5.1 fire safety of a tall timber building can be achieved in multiple ways. For this research it has been assumed that fire resistance can be achieved by combining compartmentalization, remaining cross section method, fire retardant painting, sprinklers, fire stop and fire protection of the connections allowing the structural integrity of the timber building for at least 120 minutes.

Foundation

The design of the foundation and its respective rotational stiffness will have a big effect on lateral deformations of the structure. The design of a foundation is dependent on several parameters such as the number of piles, local ground conditions, leading to complex and project specific designs. Therefore it is not in the interest of this thesis to go in depth in the design of the foundation. The assumption the foundation is a clamped base could lead to an overestimation of the capacity of the structure, therefore it is proposed that the foundation is responsible for 50% of the lateral deflection and the sls requirement is changed from $H/500$ to $H/1000$.

3.7 Design strategy

In this section the design strategy will be discussed. The design strategy of the three different cases A, B and C will be discussed in detail and reasoning behind strategy choices will be highlighted.

3.7.1 Case A

Initially case A will be designed based on handcalculations for ULS loading conditions. This will give some indication of the dimensions needed to transfer the loads. After the column and core dimensions are determined the connections are designed. The initial design of the connections is based on an assumed force in the detail. After the initial connection detail has been designed a numerical model will be build incorporating the springstiffnesses of the initial connections. From the numerical model the forces in the members and connections can be determined with a higher degree of accuracy. With the forces extracted from the numerical model the connections and members can be checked so that sufficient strength is available, if not the connection can be redesigned. It is possible to use optimization software within SCIA to increase or decrease the member sizes of the column and beams so that their unity check is approximately one. The workflow used for case A can be seen in figure 3.3. The numerical model of case A can be seen in figure 3.4 with a 3D view, a side view and the stability system as shown in figures 3.4a, 3.4b and 3.4c respectively.

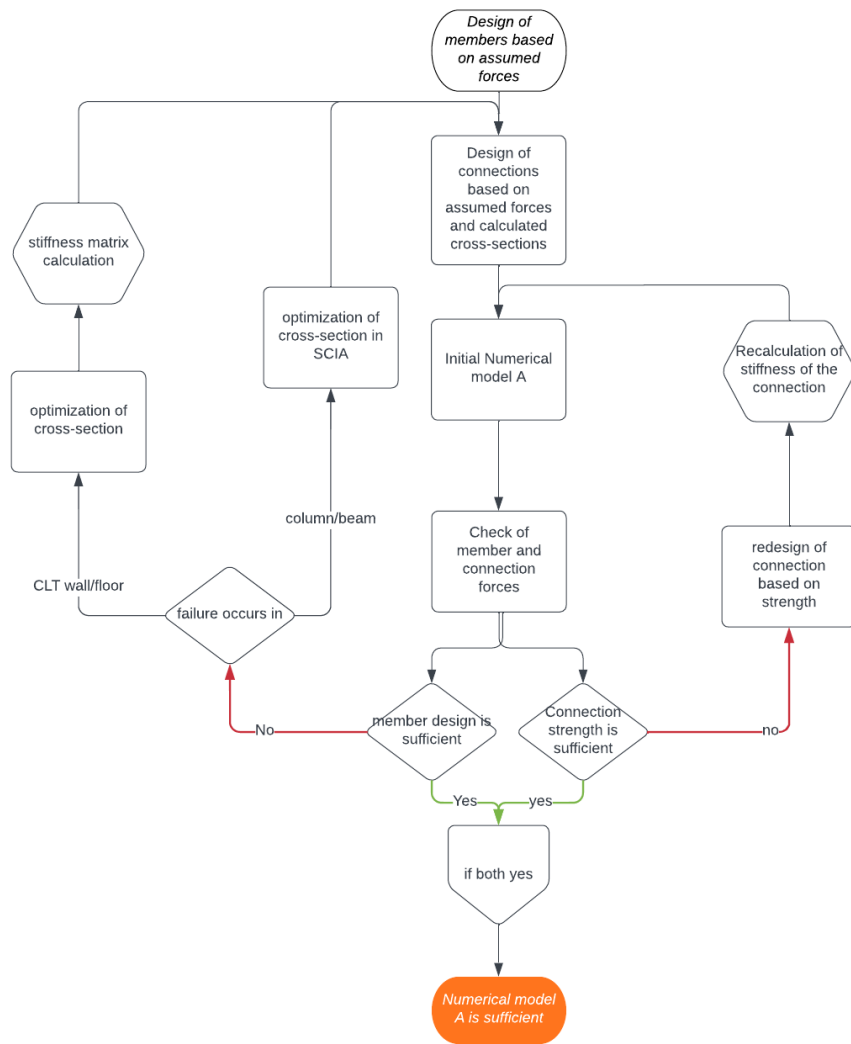


Figure 3.3. Workflow of case A

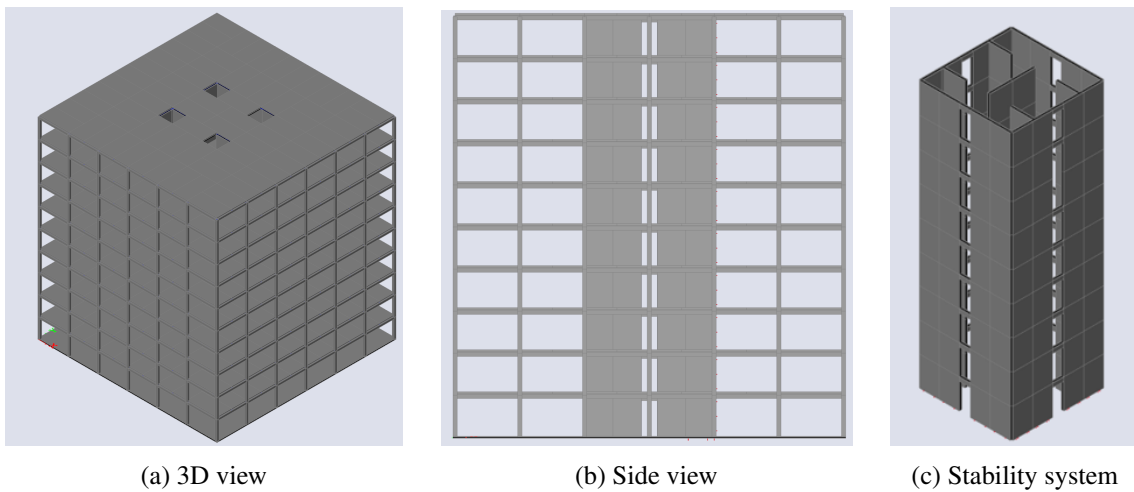


Figure 3.4. Numerical model case A

3.7.2 Case B

Once the design for case A satisfies the requirements on ULS set out by the Eurocode design of case B will commence. In this initial design of case B the goal is to not make changes on the core system as determined in case A, but simply add the outriggers and provide interaction between the core and columns. The outrigger is to be designed in such a way that SLS requirements are verified in the case B design. This will provide a good comparison between both cases allowing a clear view of the influence of a timber outrigger on a CLT core building. The comparison between both case may consist of the following aspects.

- dynamic response and peak lateral acceleration
- lateral deflection and respective contributions to the total deflection
- member forces in CLT walls and columns
- base shear between core and foundation
- strength requirements of connections of the core

After the influence of the addition of an outrigger system is assessed design B can be improved further. To show the potential an outrigger system has the influence of several design parameters will be changed. Additionally the influence of connection design of the CLT core is assessed

- assess influence of outrigger configuration on the effectiveness of the outrigger system.
- assess influence of outrigger connection stiffness on the effectiveness of the outrigger system.
- assess influence of outrigger member size on the effectiveness of the outrigger system.
- assess influence of outrigger height on the effectiveness of the outrigger system.
- assess influence of the type of outrigger on the effectiveness of the outrigger system.
- assess influence of connection design of the core.

In the second phase of the design of case B the influence of several different connection types will be assessed. The different connection types which will be assessed will be the connection between truss elements, the connection between truss and CLT core and the connection between the belt/truss and the columns.

The numerical model of case C can be seen in figure 3.5 with a 3D view, a side view and the stability system as shown in figures 3.5a, 3.5b and 3.5c respectively.

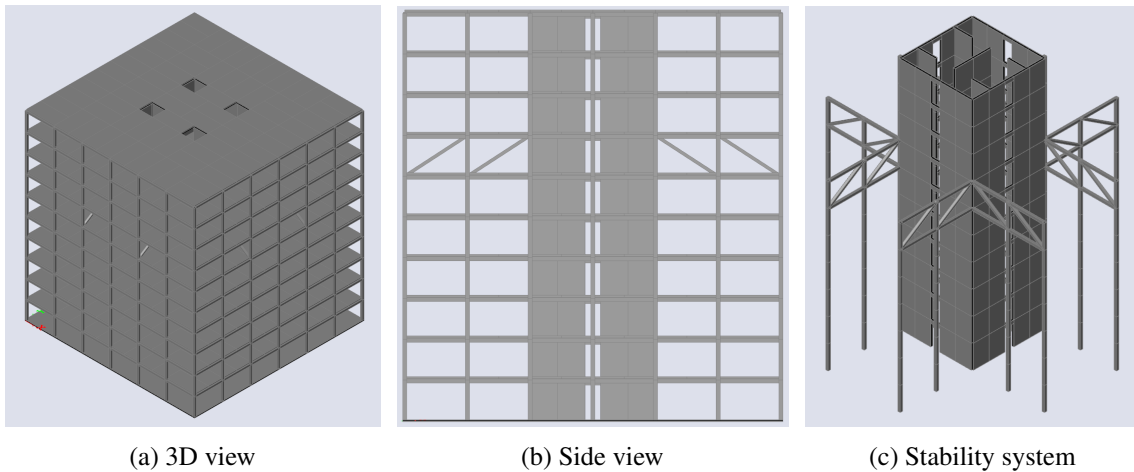


Figure 3.5. Numerical model case B

3.7.3 Case C

As a final case study the results of the influence of the different connection types will be used to build case C, this case will be a culmination of the previously found results and will consist of the highest performing connections previously found, additionally the height of this case will be increased until boundaries of the requirements are reached. This will give an indication of the possibilities of a high-performance timber outrigger building in comparison to a CLT core building. Figure 3.6 shows the adopted design strategy for the different case studies and the workflow used throughout this research.

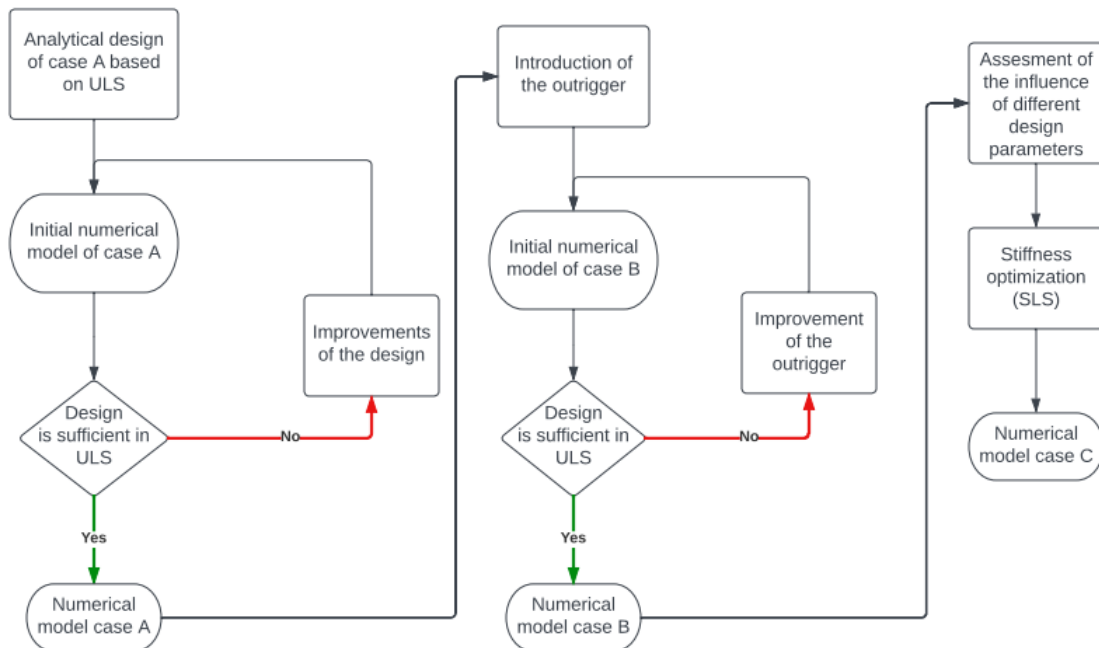


Figure 3.6. Workflow case studies

The numerical model of case C can be seen in figure 3.7 with a 3D view, a side view and the stability system as shown in figures 3.7a, 3.7b and 3.7c respectively.

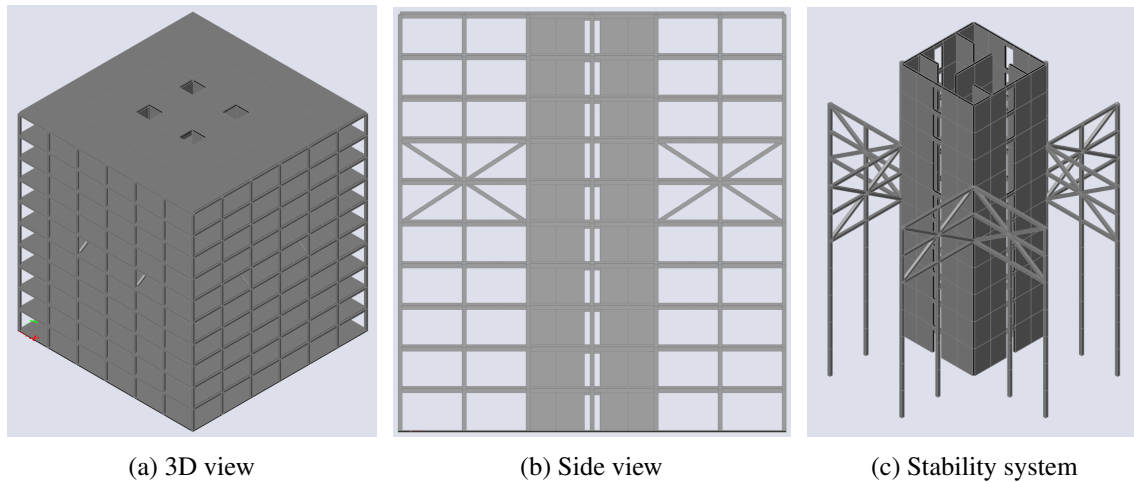


Figure 3.7. Numerical model case C

3.7.4 Strategy design choices

The reason that case A is calculated using only ULS criteria instead of a combination of ULS and SLS is the following. The goal of case A and case B is to investigate the influence a timber outrigger has on a CLT core building. Therefore it is proposed to have similar core layouts so that an equal comparison can be made between the cases when only the outrigger is added. This will give insight in the differences in force distribution of the models, global stiffness and overall behaviour of the structures and the sub-components. If case A were to be designed using both SLS and ULS criteria the addition of an outrigger to an already strong and stiff enough building would lead to an oversized core which increases material use for the structure. It is therefore proposed to have an undersized case A in terms of SLS so that when the outrigger is added sufficient global stiffness can be achieved to meet the SLS requirements.

3.8 Member design

This section will discuss the design of members such as the CLT walls used for the cores, columns and floor plates.

3.8.1 CLT wall design

The dimensions on of the wall are determined using handcalculation methods provided in the draft version of the eurocode, however it should be noted that the draft version prEN1995-1-1 is limited when it comes down to vertically loaded shear walls. The following assumptions have been used to calculate the strength of the CLT.

- It is assumed only the core takes up the bending moment and shear force in the initial design

which excludes the outriggers, therefore columns are only responsible for transfer of vertical loads.

- Vertical load transfer is determined based on equal distance between columns and cores.
- It is assumed the bending moment is only taken up by the core walls which are in-plane with the bending moment.
- Maximum and minimum normal force in the core is determined based on the maximum and minimum stress in the in-plane core wall and extrapolated over the full area of a wall section to determine the maximum and minimum normal force.
- forces are iteratively extracted from SCIA
- second order effects are not incorporated into the initial hand design.

During the design the layup used is that of a 9-layer CLT with 40 mm thick laminates. The lay up can be seen in figure 3.8 with the two most outer layers both being orientated in vertical direction to increase compressive and tensile strength, the latter will be governing in the design.



Figure 3.8. Layup CLT top view [0/0/90/0/90/0/90/0/0]

3.8.2 Column design

The design and verification of columns can be done based on equations provided in prEN1995-1-1. The forces in the column can be seen in table 3.6.

Table 3.6. Forces in the column at ground floor

axial compressive force	2772 kN
shear force	19.7 kN

By having a column cross section of 400x400 mm the governing design criteria related to flexural buckling will have a unity check of 0.9 as can be seen in table F.2.

3.8.3 Floor panels

This section will calculate the required thickness of the floor panels during ULS loading. During the initial design it is assumed that only vertical q-load is acting on the CLT panels, however in the actual loading an additional compression component is present due to the lateral wind loading which needs to be transferred from the perimeter of the building to the core. This transfer of lateral loading is partially transferred through the beams and partially through the floor panels due to

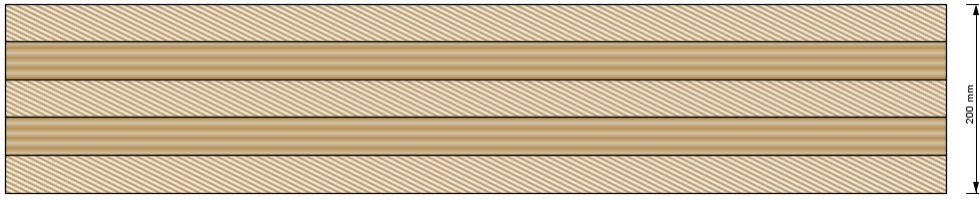


Figure 3.9. CLT floor panel layup

diaphragm action.

The calculation of the bending resistance of the floor panels is based on the same methods used for the vertical walls which are used for the core, as shown in section 3.8.1.

A CL24 (0/90/0/90/0) with a 40mm laminate thickness, a total thickness of 200mm and a width of 3 meters has a bending resistance of 1057 kNm. While the acting permanent and variable loading only result in a bending moment of 354 kNm. The reason to not reduce the thickness of the floor panels is to leave enough capacity for the transfer of lateral loads from core to column.

The stiffness matrix of the CLT floor panel is shown in equation 3.6, which has been calculated using the equations shown in 2.7. The floor panel layup can be seen in figure 3.9.

$$M = \begin{bmatrix} 5.8 & 0 & 0 & 0 & 0 & 0 & 0 & 0 \\ 0 & 1.5 & 0 & 0 & 0 & 0 & 0 & 0 \\ 0 & 0 & 0.35 & 0 & 0 & 0 & 0 & 0 \\ 0 & 0 & 0 & 20.20 & 0 & 0 & 0 & 0 \\ 0 & 0 & 0 & 0 & 11.30 & 0 & 0 & 0 \\ 0 & 0 & 0 & 0 & 0 & 1320.00 & 0 & 0 \\ 0 & 0 & 0 & 0 & 0 & 0 & 880.00 & 0 \\ 0 & 0 & 0 & 0 & 0 & 0 & 0 & 87.7 \end{bmatrix} \quad (3.6)$$

**Units are in MN and m*

3.9 Connection design case A

This section will discuss the connections details used for case A.

3.9.1 Connection design considerations

As shown in the literature study the effects of connections play a rather large roll in the design of a timber structure. The connection stiffness determines the force distribution throughout the building. Additionally the effects of connection stiffness on the displacements and accelerations

of the structure are therefore critical in the design of the structure. When a connection shows excessive deformations the structural behaviour and force distribution of the structure which could have drastic effects, for instance local failure of a member.

Ductility, strength and stiffness

The connections of the structure need to be able to provide sufficient strength and stiffness so that excessive deformations of the joint do not occur. Ductility describes the amount of energy that can be dissipated during dynamic excitations. During ductile behaviour of a timber and steel joint a phenomenon called pinching occurs in the timber. Pinching is the result of crushing of the wood which causes the steel connector to lose contact with the timber in reversed loading, and results in an empty space between the steel connector and the timber member. Pinching could cause premature failure of the connection due to local failure of the timber by introduction of splitting forces. Additionally taking into account the pinching effect the total amount of energy dissipation under hysteresis loading reduces.

However during the static and dynamic analysis due to lateral windloading the assumption has been made that the entire structure is within the elastic regime and no plastic deformations occur. It is therefore not desired that connections behave ductily and have plastic deformations.

Workflow

Throughout the designs of the different connections a similar workflow is used which can be seen in figure 3.10. The initial design of the connection is based on forces derived from handcalculations. From this initial design a stiffness of the connection is determined which can later be used to implement in the numerical model. After running the numerical model a better estimation of the forces flowing through the connections can be obtained. The design of a specific connection can then be verified based on ULS requirements and the forces obtained from the numerical model. If the connection fails in ULS a redesign of the connection needs to be made so that the requirements are met.

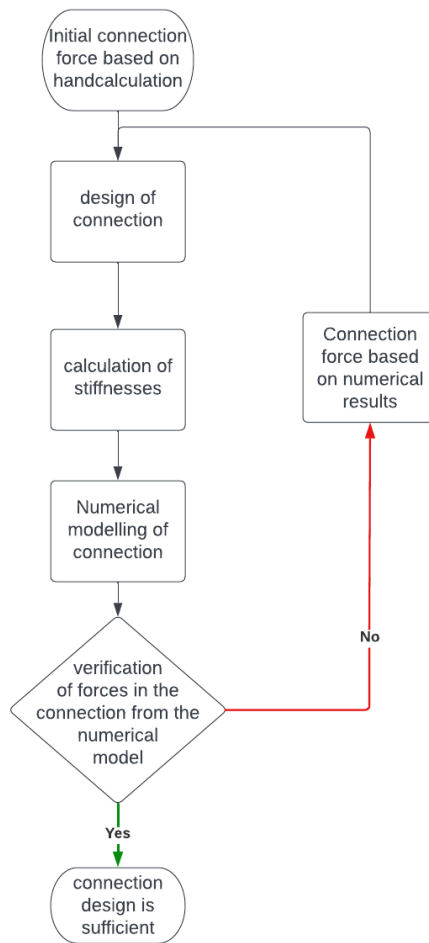


Figure 3.10. *Workflow of the connection design*

3.9.2 Connection types

The different connection types as discussed in section 2.4 are the horizontal, vertical in-plane and vertical orthogonal connection as can be seen in figure 3.11.

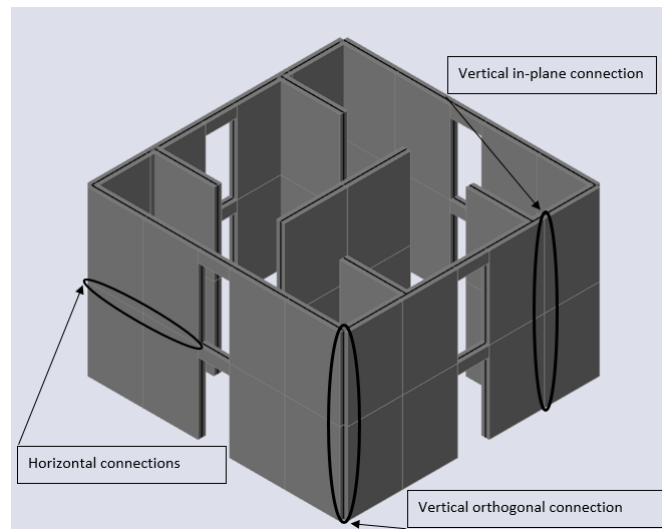


Figure 3.11. *Connection types of the CLT core*

Furthermore the connection types for the columns and beams consist of the column to column and beam, column to foundation and beam to CLT core wall. An overview of these connection types are shown in figure 3.12.

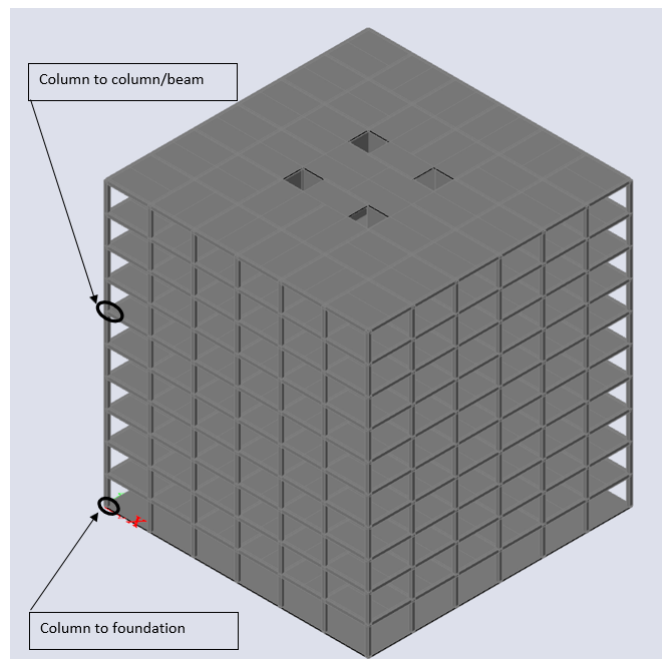


Figure 3.12. *Connection types of the columns and beams*

3.9.3 Vertical orthogonal connection

For the vertical orthogonal connection the design choice has been made to use self-tapping screws(STS) under mixed angle, due to their combination of high strength and stiffness.

For the analytical strength verification of mixed angle screws it is proposed to follow the method provided by Brown et al[32]. The analytical strength model used are a combination of the work of several authors mentioned by Brown et al, similar to the derivation of the stiffness model used. It is preferred to use the strength and stiffness models provided by Brown over that provided in the draft version of the eurocode since the latter is rather limited for inclined screws.

For the STS connection it is of importance to check whether the shear strength is not exceeded, additionally the shear stiffness will play a significant role in the global stiffness of the building as seen in chapter 2.4 as it will enable the out of plane walls to partially carry the loads due to bending of the core. The lateral loading of the vertical orthogonal connection can be seen in figure 3.13c.

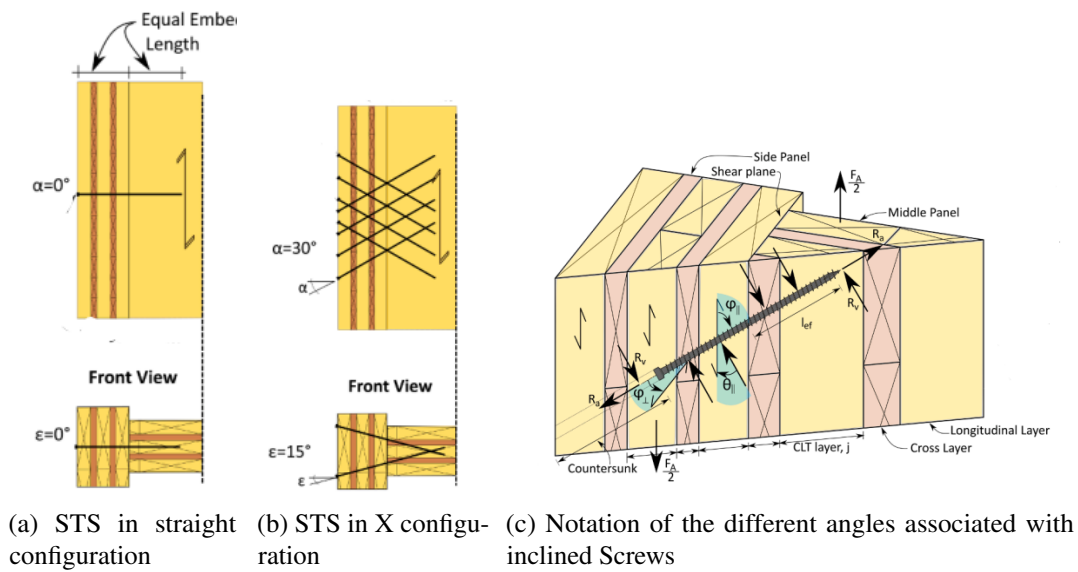


Figure 3.13. STS connection of CLT panels and their angle notation[32]

The primary force that needs to be checked is a vertical in-plane shear force which is present due to lateral windloading as can be seen in figure 3.14.

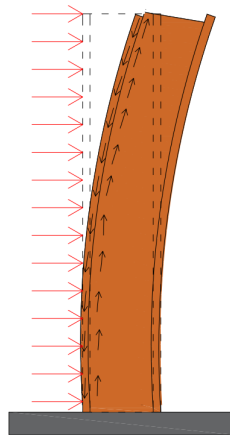


Figure 3.14. Shear force in the vertical orthogonal connection

The force on the connection extracted from SCIA can be seen in table 3.7.

Table 3.7. Force in vertical orthogonal connection

Vertical In-plane shear force	[kN/m]
	250

The strength of the different screw configuration will first be calculated separately and later combined into a single strength. The different screw configurations consist of the shear compression screw (SC) and the shear tension screw (ST), both SC and ST are part of the X configuration. If an X configuration with minimum spacing is not sufficiently strong an straight screws can be added to every row to increase the strength.

The shear strength of straight screws can be calculated in the following method and its respective angles can be seen in figure 3.13a.

The yield moment M_y is calculated using equation 3.7.

$$M_y = 0.15(600)d^{2.6} \quad (3.7)$$

where d is the outer thread diameter of the screw;

The embedment strength for all 90° straight screws $f_{h,s}$ is calculated using equation 3.8.

$$f_{h,s} = 20d^{-0.5} \quad (3.8)$$

The effective diameter of the screw d_{ef} is calculated using equation 3.9.

$$d_{ef} = 1.1d_c \quad (3.9)$$

where

d_c is the screw diameter of the core;

The shear strength of the dowel action for straight screws $R_{v,straight,i}$ is calculated using equation 3.10.

$$R_{v,straight,i} = \sqrt{\frac{2\beta}{1+\beta}} \sqrt{2M_y d_{ef} f_{h,s}} \quad (3.10)$$

where

β is the ratio between embedments strength of the different panels, assumed equal to 1;
 i is the side of the panel in-plane or out-of plane, depending if an orthogonal or in-plane connection is designed.

The axial strength of the straight screws $R_{a,straight,i}$ is calculated using equation 3.11.

$$R_{a,straight,i} = \min \left\{ \frac{f_1 d l_{ef}}{1.2 \cos^2(\phi) + \sin^2(\phi)} \left(\frac{\rho_k}{350} \right)^{0.8}, R_{tension} \right\} \quad (3.11)$$

where

f_1 is the withdrawal strength parameter, 12 MPa and 11 MPa for 8 mm and 12 mm STS respectively;
 l_{ef} is the screw thread length in each panel, $l_t/2$, where l_t is the screw thread length;
 ρ_k is the characteristic density of CLT;
 $R_{tension}$ is the tensile yield strength of the screw;

The strength of the straight screws can be calculated using equation 3.12.

$$F_{A,S,i} = R_{v,straight,i} + \min \left\{ R_{v,straight,i}, \frac{R_{a,straight,i}}{4} \right\} \quad (3.12)$$

The configuration of the X screws, consisting of SC and ST screws can be calculated using the following equations. An example of a X configuration of screws can be seen in figure 3.13b.

The yield bending moment M_y is similar to the one used for straight screws and can be calculated using equation 3.7. Similarly the effective diameter of the screw can be calculated using equation 3.9.

$$k_{90} = 1.35 - 0.015d \quad (3.13)$$

The embedment strength for inclined screws $f_{h,\phi}$ is calculated using equation 3.14.

$$f_{h,\phi} = \frac{0.082 \rho_k (1 - 0.01d)}{(1.5 \cos^2(\phi) + \sin^2(\phi)) (k_{90} \sin^2(\theta) + \cos^2(\theta))} \quad (3.14)$$

The shear strength of the dowel action for inclined ST screws $R_{v,ST,i}$ is calculated using equation

3.15.

$$R_{v,ST,i} = \sqrt{\frac{2\beta}{1+\beta}} \sqrt{2M_y d_{ef} f_{h,\phi}} \quad (3.15)$$

The axial strength for inclined ST screws $R_{a,ST,i}$ is calculated using equation 3.16.

$$R_{a,ST,i} = \min \left\{ \begin{array}{l} \frac{f_1 d_{ef}}{1.2 \cos^2(\phi) + \sin^2(\phi)} \left(\frac{\rho_k}{350} \right)^{0.8} \\ R_{tension} \end{array} \right. \quad (3.16)$$

For the calculation of the SC STS a zone exist in which zero stress exists x_1 , therefore the effective length l_{ef} is reduced by x_1 .

$$x_1 = \frac{f_{h,\phi} d_{ef}}{2 \tan(\phi) f_{rs}} \quad (3.17)$$

where

f_{rs} is the rolling shear strength of specific layers, 2.2, 1.1 or 0.9 MPa for 20, 35 and 45 mm thick CLT layers respectively;

The shear strength of the dowel action for inclined SC screws $R_{v,SC,i}^*$ is calculated using equation 3.18.

$$R_{v,SC,i}^* = \sqrt{2M_y d_{ef} f_{h,\phi} + (f_{h,\phi} d_{ef} x_1)^2} - f_{h,\phi} d_{ef} x_1 \quad (3.18)$$

The axial strength for inclined SC screws $R_{a,SC,i}^*$ is calculated using equation 3.19.

$$R_{a,SC,i}^* = \min \left\{ \begin{array}{l} \frac{f_1 d(l_{ef} - x_1)}{1.2 \cos^2(\phi) + \sin^2(\phi)} \left(\frac{\rho_k}{350} \right)^{0.8} \\ R_{tension} \end{array} \right. \quad (3.19)$$

The combined strength of the SC and ST screws in X configuration can be calculated using equation 3.20.

$$F_{A,X,i} = (R_{a,ST,i} \cos(\phi) + R_{v,ST,i} \sin(\phi)) + (R_{a,SC,i}^* \cos(\phi) + R_{v,SC,i}^* \sin(\phi)) \quad (3.20)$$

The combined strength of the STS in X and straight configuration can be calculated using equation 3.21.

$$F_{A,X+S,i} = n_x F_{A,X,i} + n_s F_{A,S,i} \quad (3.21)$$

where

n_x is the number of screws in x-configuration, as a pair one SC and one ST;

n_s is the number of screws in straight configuration;

From 3.22 the design resistance of the joint is calculated.

$$F_{RD,X+S,i} = \frac{k_{mod}}{\gamma_M} F_{A,X+S,i} \quad (3.22)$$

In the next section the stiffness model for the STS connection will be discussed.

The lateral stiffness component of a screw can be determined using equation 3.23.

$$k_{\perp} = \frac{\rho_m^{1.5} d_{ef}}{23} \quad (3.23)$$

where

ρ_m is the mean density of the CLT;

d_{ef} is the effective diameter as defined earlier;

The axial stiffness component k_{\parallel} of a screw is determined using equation 3.24.

$$k_{\parallel} = \frac{1}{\frac{1}{k_{ax,1}} + \frac{1}{k_{ax,2}}} \quad (3.24)$$

where

$k_{ax,1}$ is the axial slip modulus of panel 1;

$k_{ax,2}$ is the axial slip modulus of panel 2;

It should be noted that for equal embedment lengths axial slip modulus is the same for both CLT panels.

$$k_{ax} = 25 d l_{ef} \quad (3.25)$$

It should be noted that for SC screws the effective length of the screw l_{ef} is reduced by x_1 .

The analytical stiffness model for a specific screw configuration, straight, SC or ST, $K_{A,S}$, $K_{A,SC}$ or $K_{A,ST}$ respectively is shown in equation 3.26.

$$K_{A,STS} = k_{\perp} \sin^2(\phi) + k_{\parallel} \cos^2(\phi) \quad (3.26)$$

The overall specimen stiffness is determined using equation 3.27.

$$K_A = n_s K_{A,S} + n_{st} K_{A,ST} + n_{SC} K_{A,SC} \quad (3.27)$$

where

- n_s is the number of straight STS;
- n_{ST} is the number of ST STS;
- n_{SC} is the number of SC STS;

To compare the straight and double inclined screw a calculation was made for similar size screws where the inclined screws have a length of 1200 mm and the straight screws a length of 720 mm the following strength were obtained. For the inclined screws the strength of a combined shear tension and shear compression screw was found to be equal to 71.8 kN while for two straight screws a strength of 20.3 kN was found. Similarly a comparison was made on the stiffness of both screws types where the combined stiffness for the inclined screws was found to be equal to 89.4 kN/m while the straight screws had a combined stiffness of 6.6 kN/m. Showing the relevance of applying the inclined screws in the design for both strength and stiffness. For the design of the orthogonal connection only inclined screws are used spaced 20d apart, resulting in sufficient strength capacity to transfer the vertical shear forces present in the vertical orthogonal connection.

For this specific case study the following design has been made for the orthogonal connection where the input and output can be seen in table 3.8 and 3.9 respectively.

Table 3.8. *Input data orthogonal STS connection calculation*

	inclined screws	straight screws
d	diameter of the screw	13 mm
d_c	diameter of the core of the screw	8 mm
l	length of the fastener	1200 mm
l_t	screw thread length	1175 mm
ρ_k	characteristic density CLT	385 kg/m ³
ρ_m	mean density CLT	420 kg/m ³
f_{uk}	characteristic tensile strength	1000 N/mm ²
f_l	withdrawal strength parameter	10 Mpa
f_{rs}	rolling shear strength	0.9 Mpa
ϕ		45°
θ		24°
b	width	360 mm
n	number of screws in a single row	1*

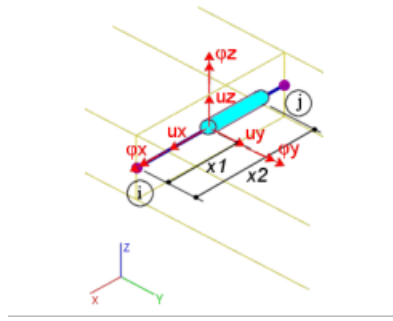


Figure 3.15. Scia coordinate system joint on a 2D member edge

*for inclined screws an X-configuration consist of a shear-tension and shear compression-screw

Table 3.9. Output data orthogonal STS connection

K_a	combined lateral shear stiffness	344 kN/mm/m
$F_{A,X+S,i}$	combined lateral shear strength	276 kN/m

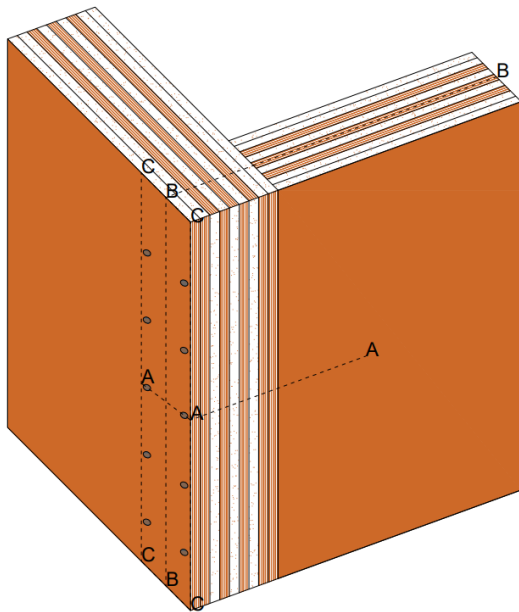
In table 3.10 the boundary conditions for the numerical modelling of the joint can be seen, figure 3.15 shows the coordinate system of a joint on a 2D member edge in SCIA. For the modelling of the vertical orthogonal connection the influence of the vertical in-plane shear stiffness is of high importance for the global stiffness of the structure as it will enable web-flange interaction. For the out-of-plane shear stiffness (u_z) it has been assumed that the influence is negligible as the lateral wind-loads will be transferred through the floor plates to the in-plane shear walls, which have a much higher stiffness than the out-of plane shear walls. The axial stiffness of the joint (u_y) is modelled as rigid as well based on the assumption that the walls will remain in contact at all times, only compressive forces present. It should be noted that this assumption might not be valid for the case B in which an outrigger is introduced as this could introduce tensile forces in the connection which could cause a gap opening. Finally the rotational stiffness of the joint ϕ_x is modelled as pinned.

Table 3.10. Numerical boundary conditions vertical orthogonal joint

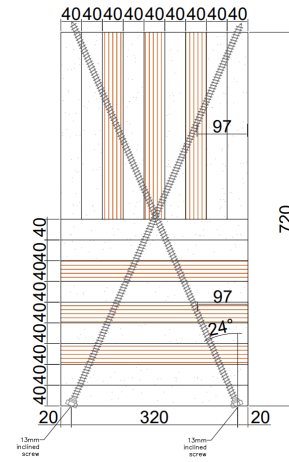
	u_x	u_y	u_z	ϕ_x
Boundary conditions	344 kN/mm/m	rigid*	rigid*	free

*it is assumed only horizontal compressive forces are present

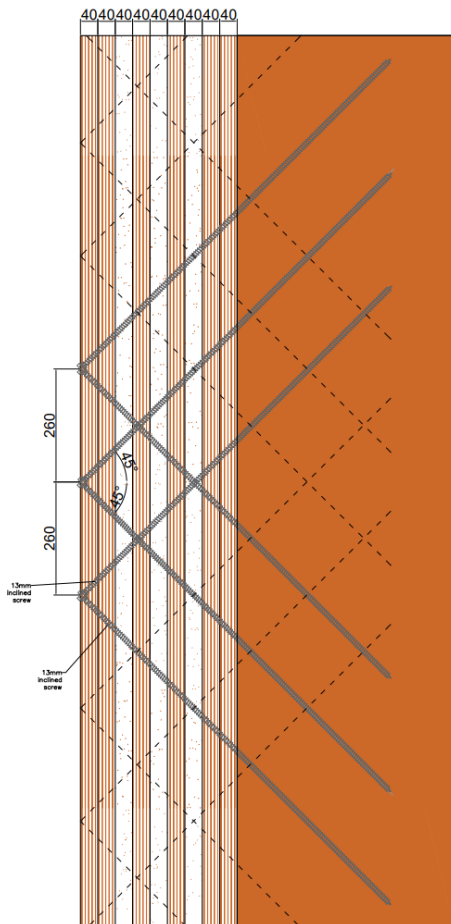
Detailed drawings of the connection are shown in figure 3.16, in which a exploded view and different 2D views are shown. it should be noted that for inclined screws spacing and edge distances should be taken form the center of gravity of a screws in a specific member, additionally the edge distance of the ends of entry points of the screws have been taken as 20 mm to ensure enough space is available for the head of the screw. According to the eurocode no requirements are given on edge distances for the head of a double inclined screw.



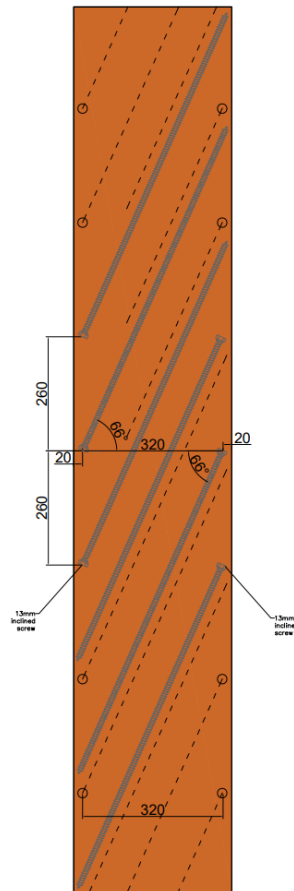
(a) Exploded view



(b) A-A



(c) B-B



(d) C-C

Figure 3.16. Vertical orthogonal connection CLT panels mixed angle STS

3.9.4 Vertical in-plane connection

The design of the vertical in-plane connection is made using STS similar to the vertical orthogonal connection. The stiffness of the vertical in-plane connection will have a rather high influence on the global behaviour of the structure, therefore it is required that the connection has a high stiffness, which the STS under combined angle can provide. Additionally the connection must be able to provide sufficient strength. Vertical in-plane loading of the connection can be seen in table 3.11 and is obtained from SCIA. The direction of loading is similar to that of the vertical orthogonal connection and can be seen in figure 3.17.

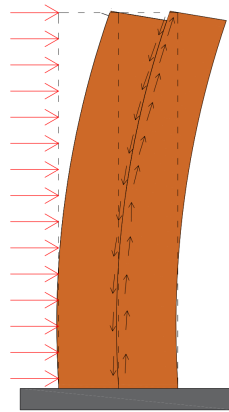


Figure 3.17. *Shear force in the vertical in-plane connection*

Table 3.11. *Vertical in-plane forces, SCIA*

	[kN/m]
Vertical in-plane shear force	328

From initial calculations it has been shown that applying only inclined screws a maximum shear strength of 311 kN/m could be obtained by applying double inclined screws spaced 10d apart. The reason for the reduced strength in comparison to the vertical orthogonal connection is the available maximum length for the inclined screws which is 1200 and 620 for the vertical orthogonal and vertical in-plane shear connections respectively. Therefore additional straight screws are placed to enhance the shear capacity of the joint. For the calculation of the shear strength of the straight screws, equations provided by the Eurocode are used and substituted in place in the strength calculation and stiffness model provided by Brown et al., [32] as shown in section 3.9.3.

For the inclined screws calculation methods provided in section 3.9.3 are used. While calculation methods for the straight screws are provided in section Vertical in-plane connection of Appendix H.

For this specific case study the following design has been made for the in-plane connection. As previously mentioned from an initial design a connection with a pair of double inclined screws did not provide sufficient strength, therefore a straight screw is added to every row. Since a straight

screw can only be added for the case that an overlapping joint is made as can be seen in figure 3.18b. By using a horizontal angle of the inclined screw θ equal to 45° spacing and edge distances to the center of gravity of a inclined screw can be guaranteed. The input data used for the calculation of the vertical in-plane connection can be seen in table 3.12.

Table 3.12. *Input data vertical in-plane STS connection*

		inclined screws	straight screws
d	diameter of the screw	13 mm	13 mm
d_{head}	diameter of the head of the screw	22 mm	22mm
d_c	diameter of the core of the screw	8 mm	8mm
l	length of the fastener	620 mm	360 mm
l_t	screw thread length	595 mm	345 mm
ρ_k	characteristic density CLT	385 kg/m ³	385 kg/m ³
ρ_m	mean density CLT	420 kg/m ³	420 kg/m ³
f_{uk}	characteristic tensile strength	1000 N/mm ²	1000 N/mm ²
f_l	withdrawal strength parameter	11.7 Mpa	11.7 Mpa
f_{rs}	rolling shear strength	0.9 Mpa	0.9 MPa
ϕ		45°	90°
θ		45°	0
b	width	360 mm	360 mm
	spacing	10d	10d
n	number of fasteners per row	1*	1

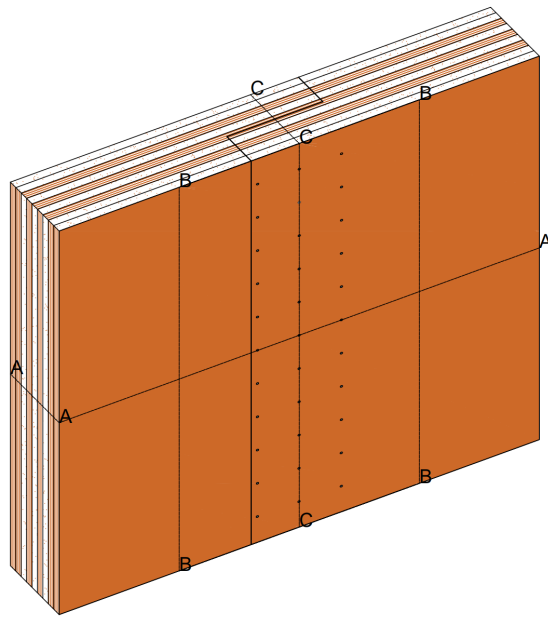
*for inclined screws an X-configuration consist of a shear-tension and shear compression-screw

The resulting combined strength and stiffness of the connection is shown in figure 3.13.

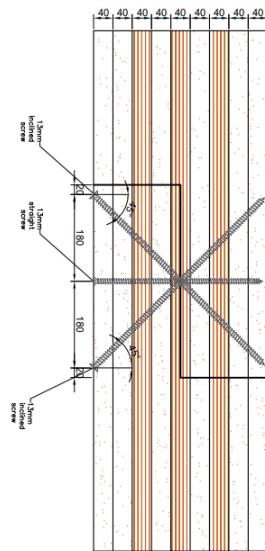
Table 3.13. *Output data vertical in-plane STS connection*

K_a	combined lateral shear stiffness	355 kN/mm/m
$F_{A,X+S,i}$	combined lateral shear strength	367.9 kN/m

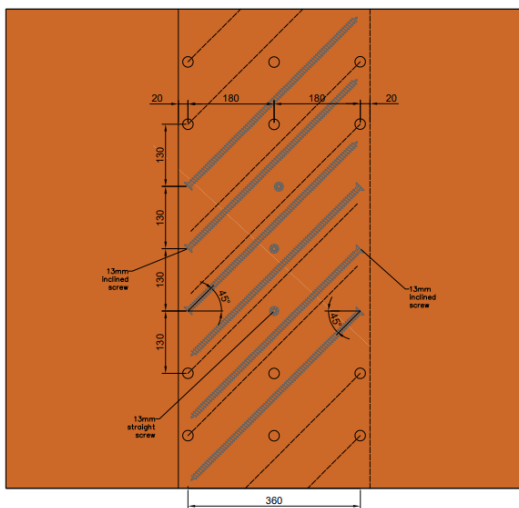
A detailed drawing of the connection is shown in figure 3.18 in which a 3d view is shown in combination with different 2d cuts of the joint.



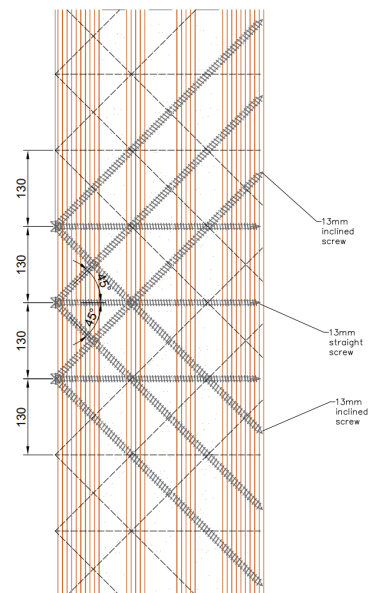
(a) Exploded view



(b) A-A



(c) B-B



(d) C-C

In table 3.14 the boundary conditions for the numerical modelling of the joint can be seen. Similar assumptions are used to that of the vertical orthogonal connection as shown in the previous section. The in-plane shear stiffness is modelled according to the obtained stiffness from the calculation while in all other directions of translation the joint is modelled as rigid, with the rotational stiffness modelled as pinned.

Table 3.14. Numerical boundary conditions in-plane vertical joint

	u_x	u_y	u_z	ϕ_x
Boundary conditions	355 kN/mm/m	rigid*	rigid*	free

*it is assumed only compressive forces are present

3.9.5 Horizontal connection CLT panels

Main function of the horizontal connection between CLT panels and that between the core and the foundation is to resist shear forces and tensile uplifting forces due to lateral wind loading as can be seen in figure 3.19a and 3.19b respectively. Additionally the connection should provide sufficient stiffness to limit rigid body rotations and translations of the core.

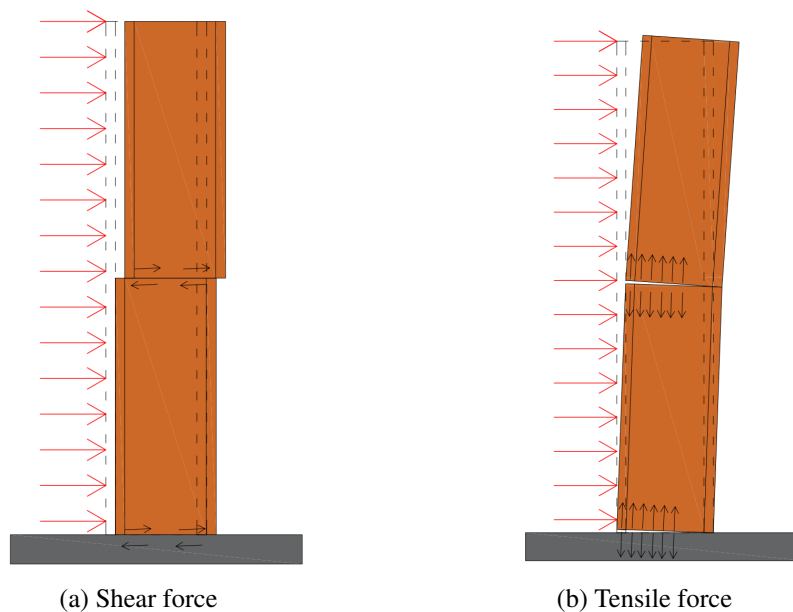


Figure 3.19. Forces on the horizontal connection between CLT panels or CLT to foundation

For the horizontal connection the design choice has been made to use a doweled connection with steel dowels and internal steel plates in combination with a castellated joint. The dowelled connection will provide axial stiffness to the connection while also providing lateral stiffness to the connection. The addition of the castellations to the horizontal joint will provide additional stiffness in lateral direction by mechanical interlocking and reduce rigid body translation, while not increasing the amount of connectors needed (only the length of the steel plates is increased).

The calculation will consist of two parts, first the dowelled connection which will provide axial and shear strength and stiffness, secondly the castellations which will increase shear stiffness of the joint. It is assumed that the out of plane shear stiffness is negligible such that the shear force in the structure is only taken up by the in-plane shear walls of the CLT core.

The forces in the horizontal connection between foundation and groundfloor core walls and at horizontal joints between corewalls at fourth to fifth floor and eight to ninth floor can be seen in figure 3.15.

Table 3.15. Axial forces in vertical direction in the CLT core, SCIA

	wind load x-direction	wind load y-direction
tensile force		
groundfloor	1405 kN/m	1344 kN/m
fourth to fifth floor	484 kN/m	404 kN/m
eight to ninth floor	248 kN/m	211 kN/m
compressive force		
groundfloor	2263kN/m	2176 kN/m
fourth to fifth floor	884 kN/m	803 kN/m
eight to ninth floor	401 kN/m	262 kN/m

The calculation methods used to determine the shear resistance of dowels combined with steel plates for the horizontal connections is provided in section Horizontal connection of Appendix H.

The input for the calculation of the strength and stiffness of the joints can be found in table 3.16.

Table 3.16. Input data doweled connection

d	diameter of the fastener	20 mm
ρ_{mean}	mean density	385 kg/m ³
ρ_k	characteristic density	350 kg/m ³
f_{uk}	characteristic tensile strength	500 N/mm ²
n	number of fasteners in a row	41
m	number of rows	3
α		90°/0°
b	width	360 mm
γ_M	partial safety factor	1.25
k_{mod}	modification factor taking into account duration of load and moisture content	0.9
$k_{rp,1}$		0.25
$k_{rp,2}$		0

With the output for three rows of dowels as can be seen in table 3.17. It should be noted that with regards to stiffness the result shown below is single side of the dowelled connection i.e. the steel to timber stiffness. To calculate the stiffness of a two sided doweled connection the composite stiffness needs to be calculated as springs in series.

Table 3.17. *Output dowelled horizontal connection*

	number of dowel rows	3	2	1
$F_{t,D}$ [kN/m]	Tensile resistance	1819	1213	606
$F_{v,D}$ [kN/m]	In-plane shear resistance	1451	967	483
K_{ser} [kN/mm/m]	Tensile and in-plane shear stiffness	1231	820	410

Based on the strengths found above the following conclusions can be made. For a design based on ULS the connection between the core and foundation needs to have three rows of dowels to provide sufficient strength while for the connection between CLT panels at the fourth to fifth storey and eight to ninth one row of dowels will suffice.

Horizontal connection - castellation

To increase the in-plane shear stiffness the following section will discuss the design of a castellated joint which will be performed in combination with the dowelled connection as calculated in the previous section. From experimental tests it has been shown that the stiffness of a castellated joint is high enough in comparison to that of steel fasteners that deformations due to the castellated joint can be assumed to be negligible [27]. Showing the relevance of applying a castellated joint and its respective effects on stiffness. The in-plane shear force loading of the castellated joint can be seen in figure 3.20 and 3.19a. The in-plane shear force transfer in the horizontal connections between CLT panels can be found in table 3.18 below.

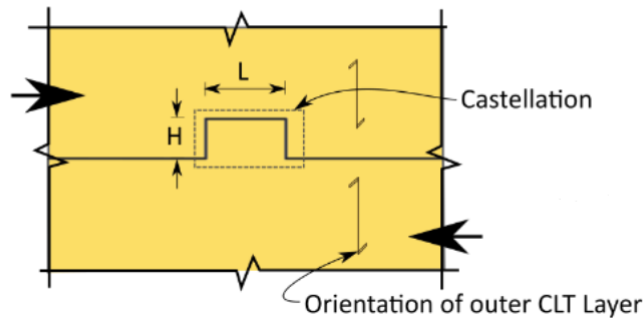


Figure 3.20. *In-plane shear loading castellated joint*[58]

Table 3.18. *In plane shear forces, SCIA*

	In-plane shear force
fourth to fifth floor	264 kN/m
eight to ninth floor	123 kN/m

The strength and stiffness model used in this section are obtained from the Brown et al. [36]. The stiffness model consist of approximating the behaviour of the joint by simplifying the different layers in to springs which then consist of several components as described in the following section. The model used to represent individual layers is shown in figure 3.21, the model shown is for a

5-layer [0/90/0/90/0] CLT panel.

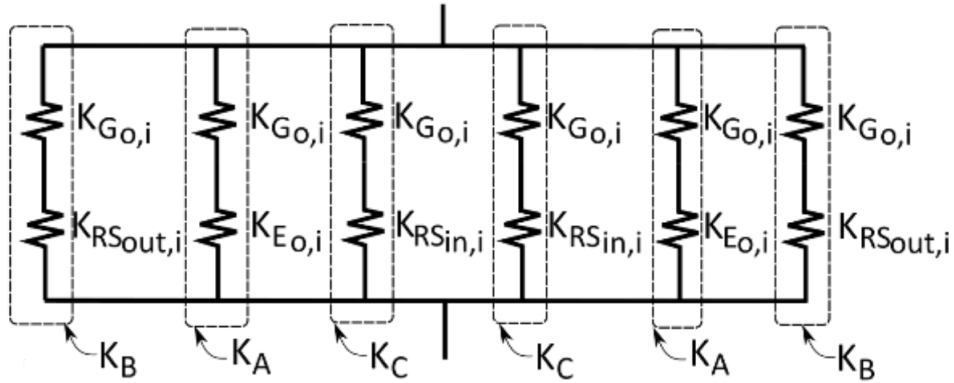


Figure 3.21. Analytical spring model 5-layer CLT [58]

The axial stiffness of the CLT layers loaded parallel to the grain $K_{E,0,i}$ as shown in equation 3.28.

$$K_{E,0,i} = \frac{E_{0,i} H_T T_{L,0,i}}{L_T} \quad (3.28)$$

where

- $E_{0,i}$ is the modulus of elasticity for layer i.
- H_T is the height of the castellation.
- $T_{L,0,i}$ is the thickness of the CLT layer.
- L_T is the length of the castellation.

The castellated longitudinal shear stiffness $K_{G,0,i}$ as shown in equation 3.29

$$K_{G,0,i} = \frac{G_{0,i} L_T T_{L,0,i}}{\frac{H_{T,i}}{2}} \quad (3.29)$$

where

- $G_{0,i}$ is the shear modulus for layer i.

The rolling shear stiffness of the outer and inner layers $K_{Grs,out,i}$ and $K_{Grs,in,i}$ as shown in equation 3.30 and 3.31 respectively.

$$K_{Grs,out,i} = \frac{G_{RS,out,i} L_T H_T}{T_{L90,i}} \quad (3.30)$$

$$K_{Gr_s,in,i} = \frac{G_{RS,in,i}L_T H_T}{\frac{T_{L90,i}}{2}} \quad (3.31)$$

where

$G_{RS,out,i}$ is the rolling shear modulus of the outer layer.

$G_{RS,in,i}$ is the rolling shear modulus of the inner layer.

$T_{L90,i}$ is the thickness of the CLt layer in rolling shear deformation.

For the layers loaded in parallel to the grain it has been assumed that deformation occur due to compression and longitudinal shear. The combined stiffness K_A of the layer is therefore calculated using equation 3.32.

$$K_A = \frac{K_{E,0,i}K_{G,0,i}}{K_{E,0,i} + K_{G,0,i}} \quad (3.32)$$

For the layers loaded in perpendicular to the grain it has been assumed that deformation occur due to rolling shear and longitudinal shear. The combined stiffness K_B and K_C of the outer and inner layer is therefore calculated using equation 3.33 and 3.34 respectively.

$$K_B = \frac{K_{RS,out,i}K_{G,0,i}}{K_{RS,out,i} + K_{G,0,i}} \quad (3.33)$$

$$K_C = \frac{K_{RS,in,i}K_{G,0,i}}{K_{RS,in,i} + K_{G,0,i}} \quad (3.34)$$

The strength of the castellations is a summation of the critical failure plane load and the loads carried by the other planes, as can be seen in equation 3.35.

$$F_J = \min \begin{cases} F_v = f_v T_{L,0} L_T n_{l,0} \left(1 + \frac{n_B K_B}{n_A K_A} + \frac{n_C K_C}{n_A K_A}\right) \\ F_{rs,out} = f_{rs,out} H_T L_T n_{s,out} \left(1 + \frac{n_A K_A}{n_B K_B} + \frac{n_C K_C}{n_B K_B}\right) \\ F_{rs,in} = f_{rs,in} H_T L_T n_{s,in} \left(1 + \frac{n_A K_A}{n_C K_C} + \frac{n_B K_B}{n_C K_C}\right) \\ F_C = f_c H_T T_{L,0} n_{L,0} \end{cases} \quad (3.35)$$

The input data used for the calculation is shown in table 3.19.

Table 3.19. *Input data castellated joint*

H_T	tenon height	300mm
L_T	tenon length	330 mm
$T_{L0,i}$	layer thickness parallel to loading	40 mm
$T_{L90,i}$	layer thickness perpendicular to loading	40 mm
$E_{0,i}$	youngs modulus	11000 Mpa
$G_{0,i}$	shear modulus	650 MPa
$G_{rs,out,i}$	rolling shear modulus outer layer	50
$G_{rs,in,i}$	rolling shear modulus inner layer	50
f_v	longitudinal shear strength	5.5 N/mm ²
$f_{rs,out}$	rolling shear strength outer layer	0.7 N/mm ²
$f_{rs,in}$	rolling shear strength inner layer	0.7 N/mm ²
f_c	compressive strength	21 N/mm ²
n_A and $n_{L,0}$	number of layers parallel to loading	3
n_B and $n_{s,out}$	number of layers perpendicular to loading not in the center	6
n_C	number of layers perpendicular to loading at the center	0
$n_{s,in}$	layer at center perpendicular to loading	0

In table 3.20 the in-plane strength and stiffness of the castellated joint is shown.

Table 3.20. *Output data castellated joint*

In-plane shear strength	846 kN/m
In-plane shear stiffness	1166 kN/mm/m

As stated in section 2.4.3 a horizontal connection between CLT panels using castallements is able to take up high shear forces while also providing a high shear stiffness. The designed joint is able to increase the shear stiffness of the dowelled horizontal connection.

overview horizontal connection panel to panel

With the above calculated strength and stiffnesses of the doweled and castellated joint the following boundary conditions will be used to numerically approximate the horizontal connection, as can be seen in table 3.21. The tensile force and stiffness in vertically direction is provided by the castellated joint alone, with the stiffness taken as composite stiffness of two single sided stiffnesses in series. For the composite stiffness in u_x the stiffness is approximated by first modelling the stiffness of the dowels as springs in series for a two sided dowelled connection. Secondly the composite stiffness of the entire joint is calculated as the composite stiffness of the dowels which are in parallel with the stiffness of the castellation, a graphical representation of the spring model is shown in figure 3.22.

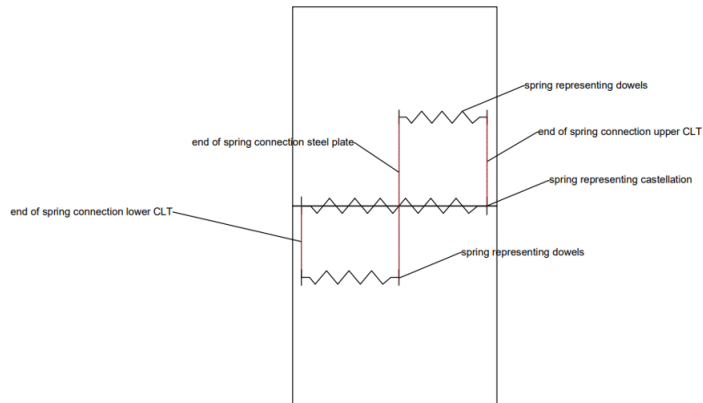


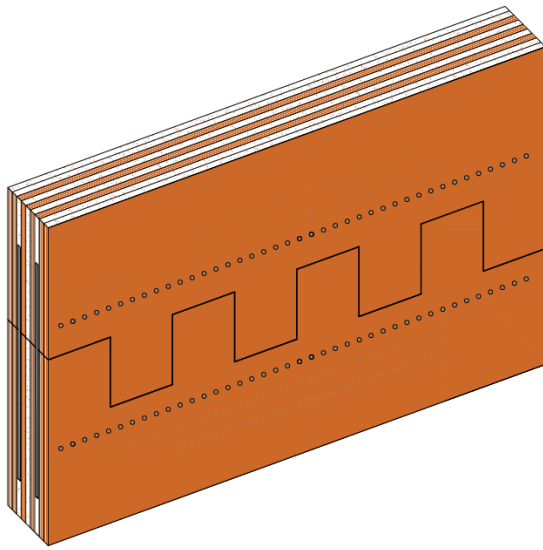
Figure 3.22. *Composite spring model horizontal joint*

Table 3.21. *Numerical boundary conditions horizontal joint*

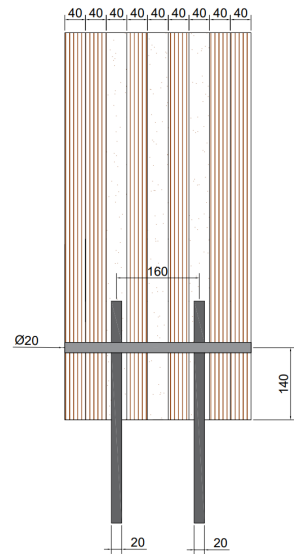
	u_x	u_y	u_z	ϕ_x
Boundary conditions	1371 kN/mm/m	205 kN/mm/m	free	free

From the stiffness in u_x direction it can be concluded that introducing a castellation to the joint design is able to effectively increase the in-plane shear stiffness from 205 to 1371 kN/mm/m.

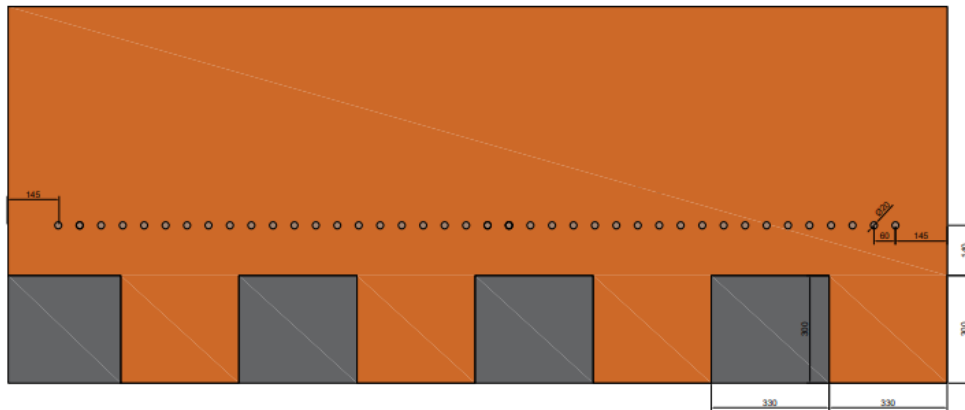
Detailed drawing of the connection between CLT panels is shown in figure 3.23, consisting of 1 row of dowels with a diameter of 20mm.



(a) 3D view



(b) Through thickness



(c) Front view

Figure 3.23. *Horizontal dowelled and castellated connection CLT panel*

overview core to foundation

The design of the core to foundation is similar to that of the CLT to CLT horizontal connection as shown in the previous section, except for the fact castellations are not applied. The reason that castellations are not applied is the uncertainty when applying timber castellations to concrete. According to table 3.17 the maximum tensile force of 1405 kN/m can be taken up by applying 3 rows of dowels, these will also provide sufficient in-plane shear strength to the joint. The tensile forces of the internal steel plate are transferred to the concrete foundation by anchorage rods.

For the the design of the anchorage rods the number of rods is determined based on the yield strength and area of the rods. For a 20mm diameter rod and a yield strength of 410 N/mm^2 and a tensile force of 1405 kN/m a total of 30 rods are needed over the length of the wall section (2.625 m).

The design of the core to foundation connection can be seen in figure 3.24 and consists of two internal steel plates and 3 rows of 20mm dowels. For the core to foundation connection the use of castellations is excluded due to uncertainties around mechanical interlocking of timber in concrete.

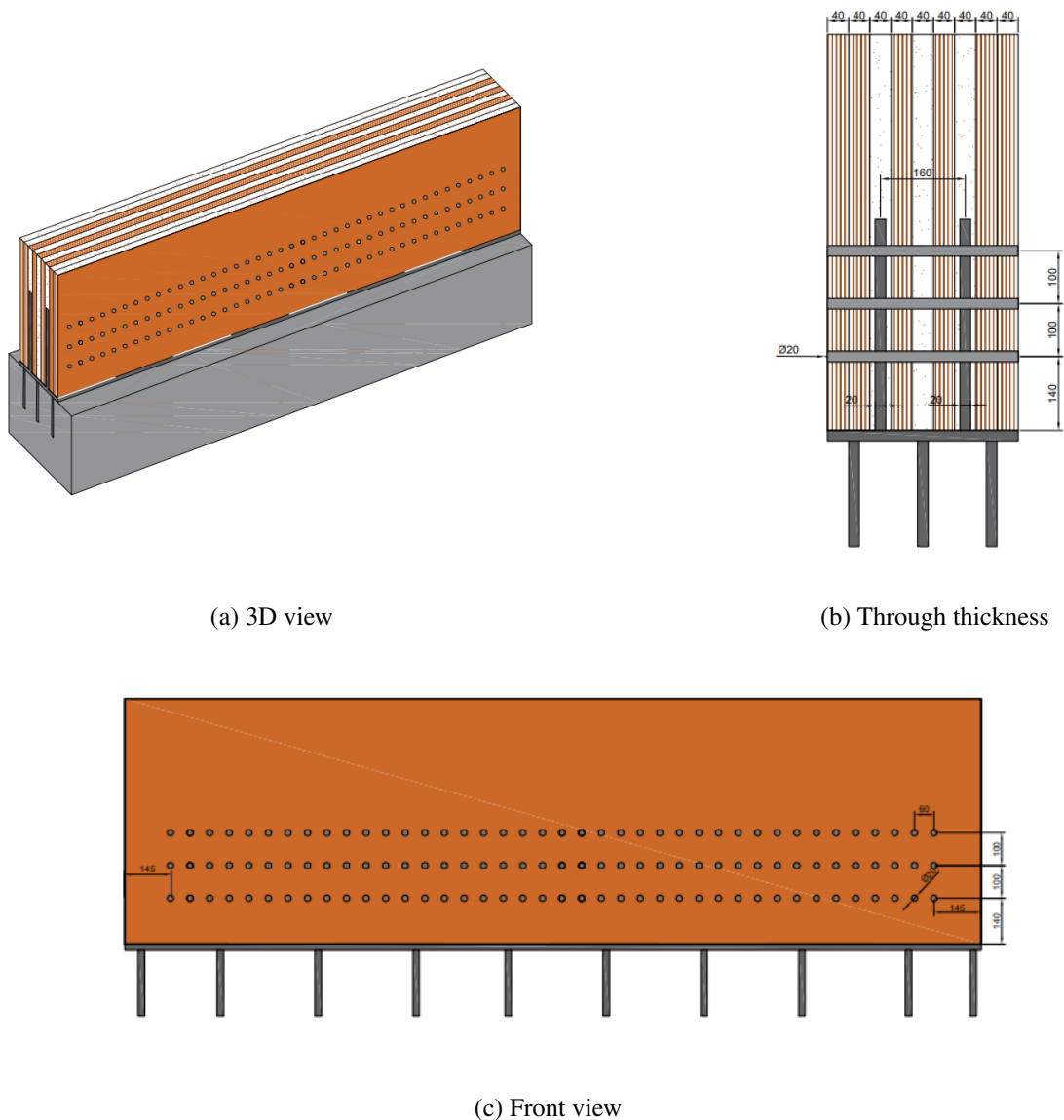


Figure 3.24. *Horizontal dowelled and castellated connection CLT panel to foundation*

The assumptions for the modelling of the core to foundation connection are given in table 3.22. The stiffness of the dowels is the same in u_x as u_y direction, while in u_z translations are assumed free and rotations assumed as pinned.

Table 3.22. Numerical boundary conditions horizontal connection core to foundation

	u_x	u_y	u_z	ϕ_x
Boundary conditions	1231 kN/mm/m	1231 kN/mm/m	free	free

For the sake of comparison an alternative design of the core to foundation connection is made making use of glued-in rods which are connected to the steel plate instead of internal steel plates and dowels. The design of the glued-in rods connection and influence on the stiffness can be found in Appendix K. Although glued-in rods may offer reduced shear stiffness, their axial stiffness is higher than that of dowelled connections, resulting in reduced global deflections. Nonetheless, the process of placing the rods can pose challenges due to the confined space and the need to maintain minimum spacing and end distances.

3.9.6 Column to foundation

The column to foundation connection can be made with a doweled connection or a steel dissipater and shoe as described in section 2.3.3. A distinction needs to be made between both connections types and the requirements needed for case A. Since no outriggers are used in case A it is expected that the forces in the columns are compressive since the overturning moment is transferred to the core. Therefore the tensile requirements of the columns is limited, additionally it is assumed shear force is mostly transferred through the core. For the case that limited tensile and shear forces are transferred a steel shoe and internal bonded-in rods acting as dissipaters and lateral and tensile resistance will suffice, according to section 2.4.5. This connection type will be easy to install since the shoe can be connected to the column of site and only needs to be bolted to the foundation. The calculation method used for the verification of the bonded in rods can be found in section Column to foundation in Appendix H.

Table 3.23. Maximum normal and shear force in the column to foundation connection, SCIA

	wind load x-direction	wind load y-direction
compressive force	2772 kN	2772 kN
tensile force	-	-
shear force	19.7 kN	12.6 kN

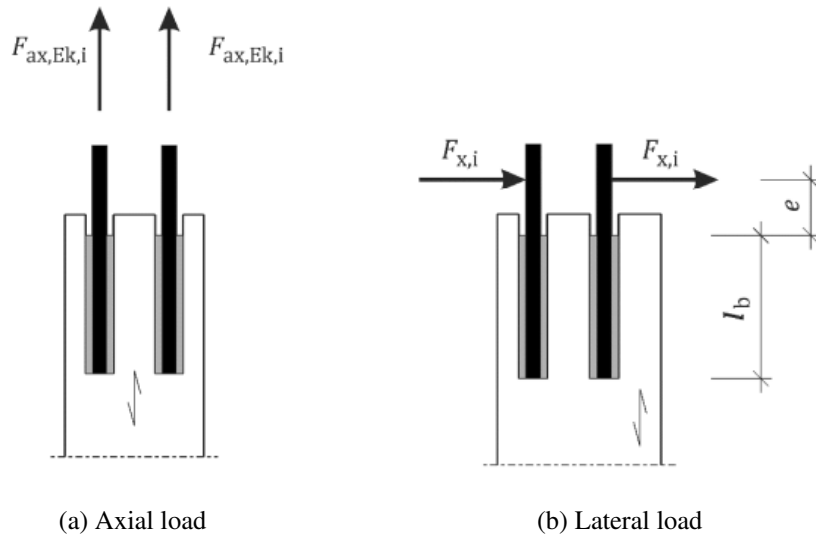


Figure 3.25. Loading of the bonded-in rods

For the calculation of the axial and shear resistance of the joint the following input is used table 3.24.

Table 3.24. Input data glued-in rod connection

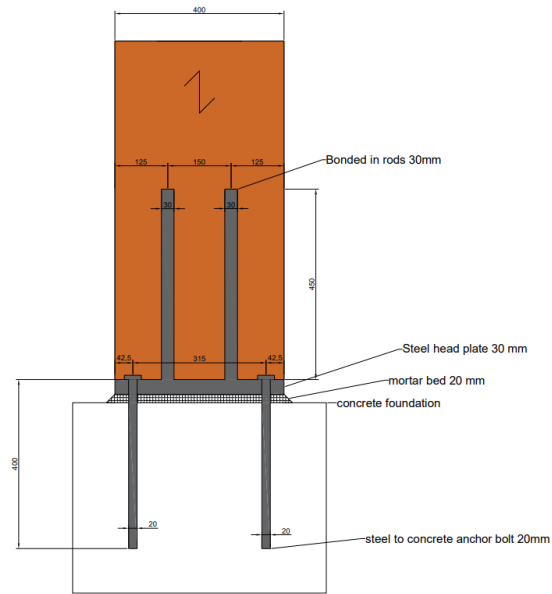
d	diameter of the rod	30 mm
$f_{y,k}$	characteristic yield strength of the rod	410 MPa
$f_{u,k}$	characteristic ultimate strength of the rod	500 Mpa
E_s	modulus of elasticity of the rod	210 Gpa
ρ_k	characteristic density of the timber	425 kg/m ³
ρ_{mean}	mean density of the timber	460 kg/m ³
α		0
γ_m	partial factor for a material property	1.25
$\epsilon_{u,timber}$	failure strain for timber parallel to the grain	2.4‰
k_{mod}	modification factor taking into account the effects of load duration and moisture	0.9
n	number of glued-in rods	4

From the input data given in table 3.24 the axial and shear resistance of the connection is calculated as can be seen in table 3.25.

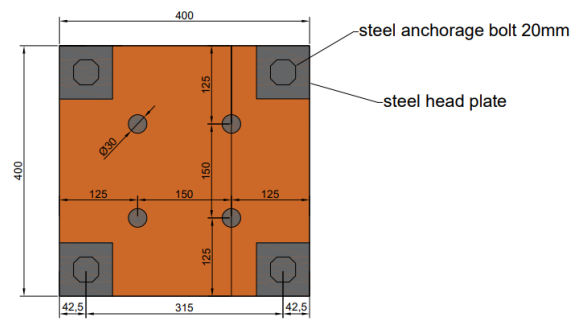
Table 3.25. Output glued-in rod connection

$F_{ax,Rd}$	axial tensile design resistance	366 kN
$F_{V,Rd}$	shear design resistance	23 kN

The current design is able to take up the lateral shear force it is subjected to according to SCIA. A detailed drawing of the column to foundation connection can be found in figure 3.26, including a side view and a top view.



(a) Side view



(b) Top view

Figure 3.26. Column to foundation connection steel shoe and internal bonded-in rods

Table 3.26. Numerical boundary conditions column to foundation connection

	u_x	u_y	u_z	ϕ_x	ϕ_y	ϕ_z
Boundary conditions	rigid	rigid	rigid	rigid	free	free

The modelling assumptions and boundary conditions for the column to foundation connection can be seen in table 3.26 with the coordinate system used in SCIA for a hinge on a 1D member as shown in figure 3.27. It should be noted that the coordinate system shown is that of the beam, for the column the coordinate system is rotated 90°. The connection is modelled as a hinged connection with translations modelled as rigid and rotations modelled as pinned, except for the rotation ϕ_x modelled as rigid which would otherwise result in free translations of the column.

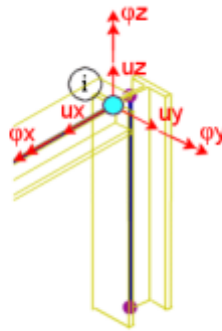


Figure 3.27. SCIA coordinate system hinge on a 1D member

3.9.7 Column to column

In the design of the column to column connection it is important to note that a high number of similar connections need to be realised throughout the structure, therefore it is required that the joint is easy to construct to reduce construction time and cost associated with both designing of the joints as well as manufacturing. Therefore a solution by Rothoblaas is proposed which is repeatable and easy to construct. The column to column connection in combination with supports for the floor systems can be provided by steel connectors designed by Rothoblaas. The connectors are able to provide up to 5000 kN of compressive force transfer between columns, however the load that the connectors are able to carry are dependent on the dimensions of the columns, floors and the steel connector itself.

Table 3.27. Maximum force in the column to column connection, SCIA

	force [kN]
compressive force	2494 kN
tensile force	-
shear force	23 kN

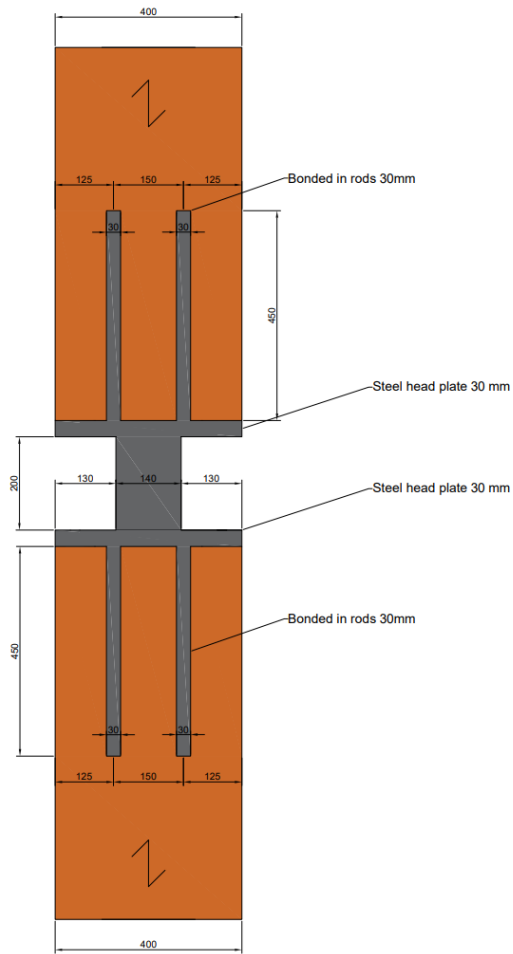
The connection is able to withstand large compressive forces however the tensile force transfer of the connection is limited, if tensile forces occur due to lateral loading additional measures need

to be taken. For instance the addition of steel plates and dowels could provide sufficient tensile capacity or the use of embedded steel rods. Therefore the design in figure 3.28 is proposed using similar bonded in rods as in the design for the column to foundation connection shown in section 3.9.6.

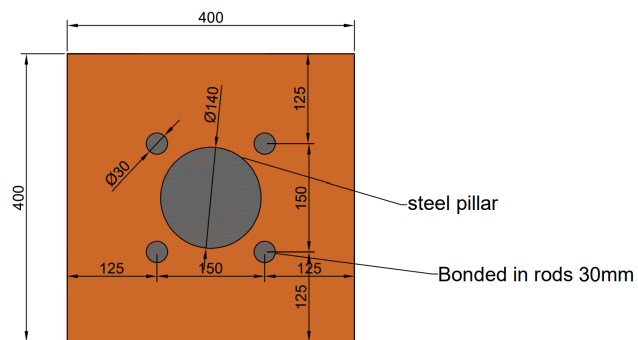
It should be noted that continuous columns of 4 storeys with similar heights as the CLT panels for the core will be used. This will drastically reduce the amount of the column to column connections and will allow construction time to be reduced. The numerically modelling of the connection will be similar to that used for the column to foundation connection and will be hinged as shown in table 3.28.

	u_x	u_y	u_z	ϕ_x	ϕ_y	ϕ_z
Boundary conditions	rigid	rigid	rigid	rigid	free	free

Table 3.28. *Numerical boundary conditions column to column connection*



(a) Side view



(b) Top view

Figure 3.28. Column to column connection steel connector and internal bonded-in rods

3.9.8 Connection of the beams

The connection of the beams will be made using steel hangers with internal wings as can be seen in figure 3.29. This connection allows for quick assembly and is relatively inexpensive for the connection of large size beams. Detailed calculations, drawings and modelling assumptions for the beam to column and beam to core connection can be found in sections Column to beam and Beam to core connection of Appendix J.



(a) 3D view



(b) Metal hanger with internal wings

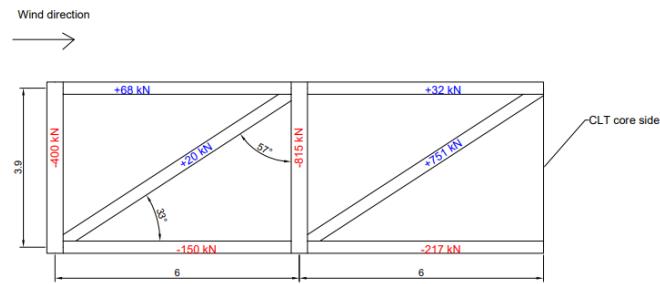
Figure 3.29. *Beam to column joint*

3.9.9 Connection of the floors

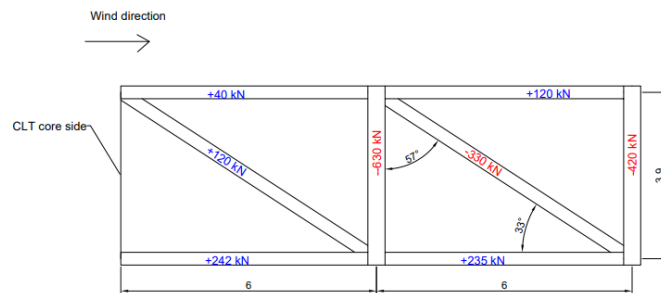
To accurately describe the behaviour of the diaphragm action of the floors under lateral loading it is important to identify the stiffnesses that the different connections have. In Appendix I the three connection types of the floors are designed and detailed drawings and modelling assumptions are shown. These connection types consist of the floor to beam, floor to floor and floor to core connection. All connections of the floor will be made using STS in X-configuration, enabling both shear tension and shear compression screws, providing high strength and stiffness to the joints.

3.10 Connection design case B

This section will discuss the connection design of case B. For the design of the outrigger the governing forces used for the verification of the connections and members of the outrigger are shown in figure 3.30, which are iteratively obtained from SCIA. The two connections which will be designed are the outrigger to column connection and the outrigger to core connection discussed in section 3.10.1 and 3.10.2 respectively.



(a) Left side of the core



(b) Right side of the core

Figure 3.30. Forces in the outrigger

The maximum force in the diagonal is a tensile force of 751 kN. The width of the diagonal is equal to 360 mm to ensure similar embedment lengths in both the dowels in the diagonal as in the core, since spacing between the plates at both sides of the connection remain the same. The height is determined based on the calculation method shown in section 3.8.2 and is equal to 300 mm.

3.10.1 Outrigger to column connection

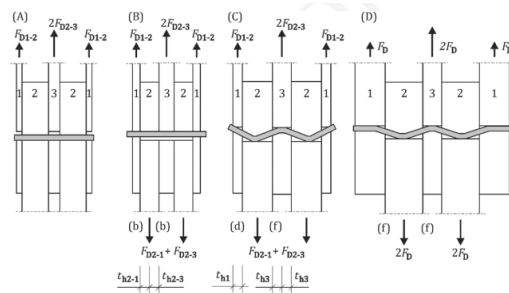
In this section the design of the outrigger to column connection will be shown. As mentioned in section 2.3.2 the connection between multiple timber members can be performed by making use of a slotted in steel plate and steel dowels, this connection type is able to connect multiple members at the same intersection and can provide high strength and stiffness, additionally ductility can be achieved by designing the connections in such a way that a ductile failure mode occurs.

At the intersection of the columns, beams and diagonals a connection needs to be designed which is able to withstand lateral wind loading and floor loading. High normal forces can be expected in the outrigger due to the transfer of bending moment from the core to the columns. The beams will carry loads due to lateral windloads and floor loads. The design for the connection will consist of two slotted in steel plates and dowels.

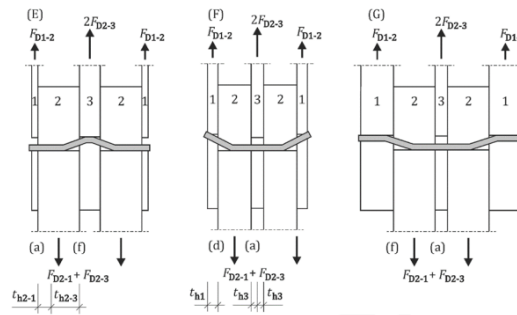
Lateral resistance of fasteners per shear plane

The characteristic lateral resistance per shear plane $F_{v,k}$ of a single fastener should be calculated according to equation H.21 and H.22. For glulam members fibres run in a single direction as

opposed to CLT, therefore the embedment strength is the same throughout the member. Similar to the design of the horizontal connection between CLT panels, compatibility between the outer and inner failure mechanisms need to be ensured, resulting in the same failure combinations, possible outer shear plane modes (a), (d) and (f) with the inner shear plane mode (a) and (f). The possible failure modes for fasteners under four shear planes can be seen in figure 3.31, where failure modes (e), (f) and (g) in figure 3.31b need to be avoided. Similar to the failure mode of the horizontal CLT connection a ductile failure mode is preferred rather than a brittle failure of the timber.



(a) Failure modes (a), (b), (c) and (d)



(b) Failure modes (e), (f) and (g)

Figure 3.31. Failure mode of a dowel under four shear planes

The characteristic embedment strength $f_{h,k}$ for dowels and bolts can be calculated according to equation H.23.

The forces used for the strength verification of the outrigger to column joint are given in table 3.33. The design of the dowels in the beam are based on the tensile force shown in the lower beam in figure 3.30b, while the diagonal is calculated based on the maximum tensile force shown in figure 3.30a. The forces present in the column side of the outrigger to column connection are based on the resulting force component under an angle to the grain as shown in figure 3.32.

Table 3.29. Forces in the outrigger to column connection

	normal force (kN)	shear force (kN)	angle to the grain
beam	242	30	83°
diagonal	751	-	0°
column	662	-	58°

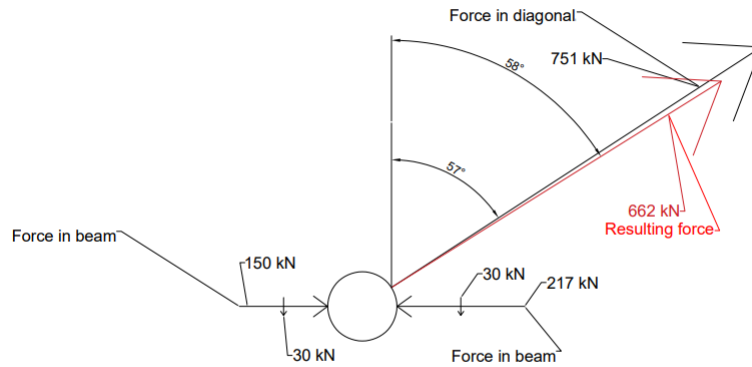


Figure 3.32. Resulting force in the outrigger to column connection

The input data for the calculation of the dowels in the diagonal, beam and column are given in table 3.30.

Table 3.30. Input data outrigger to column connection

		diagonal	beam	column
d	diameter of the fastener	20 mm	20 mm	20 mm
ρ_{mean}	mean density	385 kg/m ³	385 kg/m ³	385 kg/m ³
ρ_k	characteristic density	350 kg/m ³	350 kg/m ³	350 kg/m ³
f_{uk}	characteristic tensile strength	500 N/mm ²	500 N/mm ²	500 N/mm ²
n	number of fasteners in a row	4	5	5
m	number of rows	4	2	4
b	width	360 mm	300 mm	400 mm
γ_M	partial safety factor	1.25	1.25	1.25
k_{mod}	modification factor taking into account duration of load and moisture content	0.9	0.9	0.9
$k_{rp,1}$	factor for the rope effect	0.25	0.25	0.25
$k_{rp,2}$	limitation factor for the rope effect	0	0	0

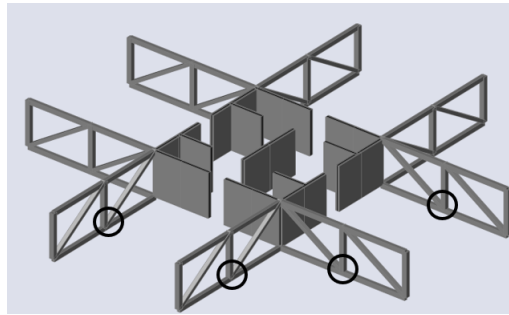
The calculated strength and stiffness of the dowels in the beam, diagonal and column are shown in table 3.31.

Table 3.31. Output data outrigger to column connection

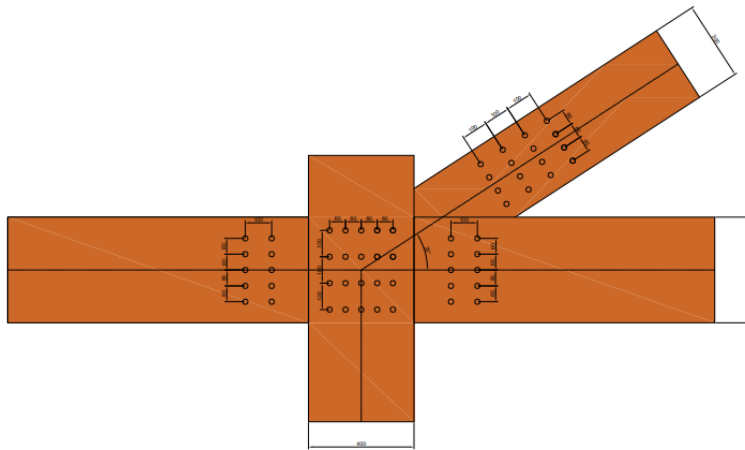
	F	K
beam	465 kN	263 kN/mm/m
diagonal	807 kN	420 kN/mm/m
column	756 kN	525 kN/mm/m

The connection between the outrigger and columns is shown in figure 3.33. A 3D view of the outrigger and core highlighting the outrigger to column connection is shown in figure 3.33a. Figure

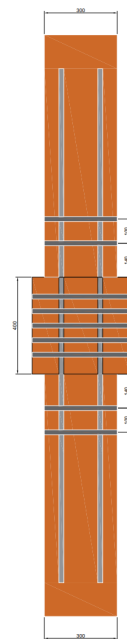
3.33b shows a side view of the connection and figure 3.33c shows a top view of the connection with the dowels of the beam to column connection.



(a) 3D view



(b) Side view



(c) Top view

Figure 3.33. *Outrigger to column connection*

The modelling assumptions used for modelling of the outrigger to column connection are given in table 3.32.

Table 3.32. *Stiffness modelling assumptions outrigger to column connection*

	u_x	u_y	u_z	ϕ_x	ϕ_y	ϕ_z
beam	263 kN/mm/m (tension only)	rigid	rigid	rigid	free	free
diagonal	420 kN/mm/m (tension only)	rigid	rigid	rigid	free	free
column	525 kN/mm/m (tension only)	rigid	rigid	rigid	free	free

3.10.2 Outrigger to core

The design of the outrigger to core connection consist of similar steel plates and dowels as the ones used for the outrigger to column connection discussed in previous section 3.10.1. The size of the diagonal has been chosen in such a way that unity checks for ULS are close to 1 while the width of the diagonal is equal to the width of the core. This has been done to increase the chance of similar type of failure modes within the diagonal and core dowels. By having a similar thickness in both members the thickness of the timber members in the outer and inner shear plane remain the same. If for instance the diagonal has a reduced width the failure mode can be shifted towards a brittle failure of the outer shear plane due to insufficient embedment length to create a plastic hinge in the dowel. The calculation of the dowelled connection within the CLT core wall is similar to the methods provided in 7.2.

The forces present in the beam and diagonal and the resulting force in the core from both members for the governing load condition are given in table 3.33. The derivation of the resulting force on the core side of the connection is shown in figure 3.34.

Table 3.33. Forces in the outrigger to core connection

	normal force (kN)	shear force (kN)	angle to the grain
beam	32	30	83°
diagonal	751	-	0°
core	792	-	56.5°

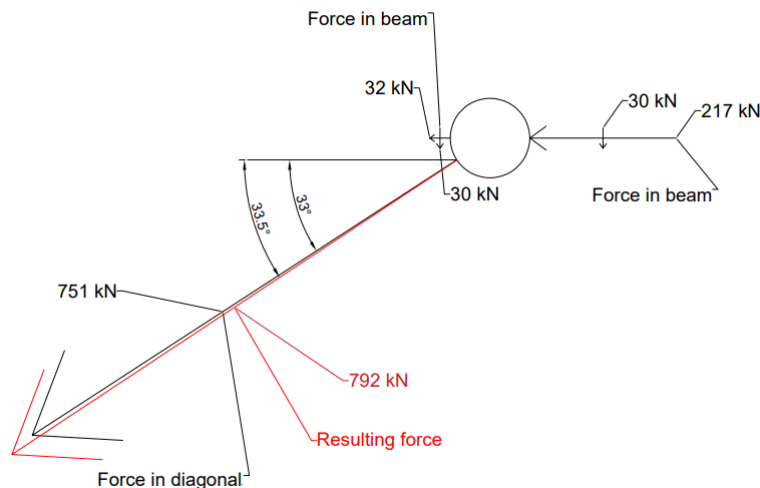


Figure 3.34. Resulting force in the core

The input data for the calculation of the dowels for the core side of the connection is given in table 3.34.

Table 3.34. *Input data outrigger to core connection*

		core
d	diameter of the fastener	20 mm
ρ_{mean}	mean density	385 kg/m ³
ρ_k	characteristic density	350 kg/m ³
f_{uk}	characteristic tensile strength	500 N/mm ²
n	number of fasteners in a row	5
m	number of rows	2
ϵ	angle between fastener and grain direction	
b	width	400 mm
γ_M	partial safety factor	1.25
k_{mod}	modification factor taking into account duration of load and moisture content	0.9
$k_{rp,1}$	factor for the rope effect	0.25
$k_{rp,2}$	limitation factor for the rope effect	0

The results of the strength and stiffness calculation of the core side of the connection is shown in table 3.35.

Table 3.35. *Output data outrigger to core connection*

	F	K
core	1197 kN	788 kN/mm/m
beam	465 kN	263 kN/mm/m
diagonal	807 kN	420 kN/mm/m

To enable a connection of the outrigger in both direction in the corner of the CLT core a cut is made in which a steel box is placed. The reason to use the steel box is to allow the transfer of compression forces between the outrigger and the core.

Detailed drawings of the outrigger to core connection are shown in 3.35. Figure 3.35a shows a 3D view of the core and outrigger with the outrigger to core connection highlighted. Figure 3.35b shows a vertical cut in which a single connection of the outrigger to core connection is shown, it should be noted perpendicular to the plane an additional connection is made of the outrigger to core. Figure 3.35c shows a horizontal cut of the connection, with the internal steel plates and box shown in figure 3.35d.

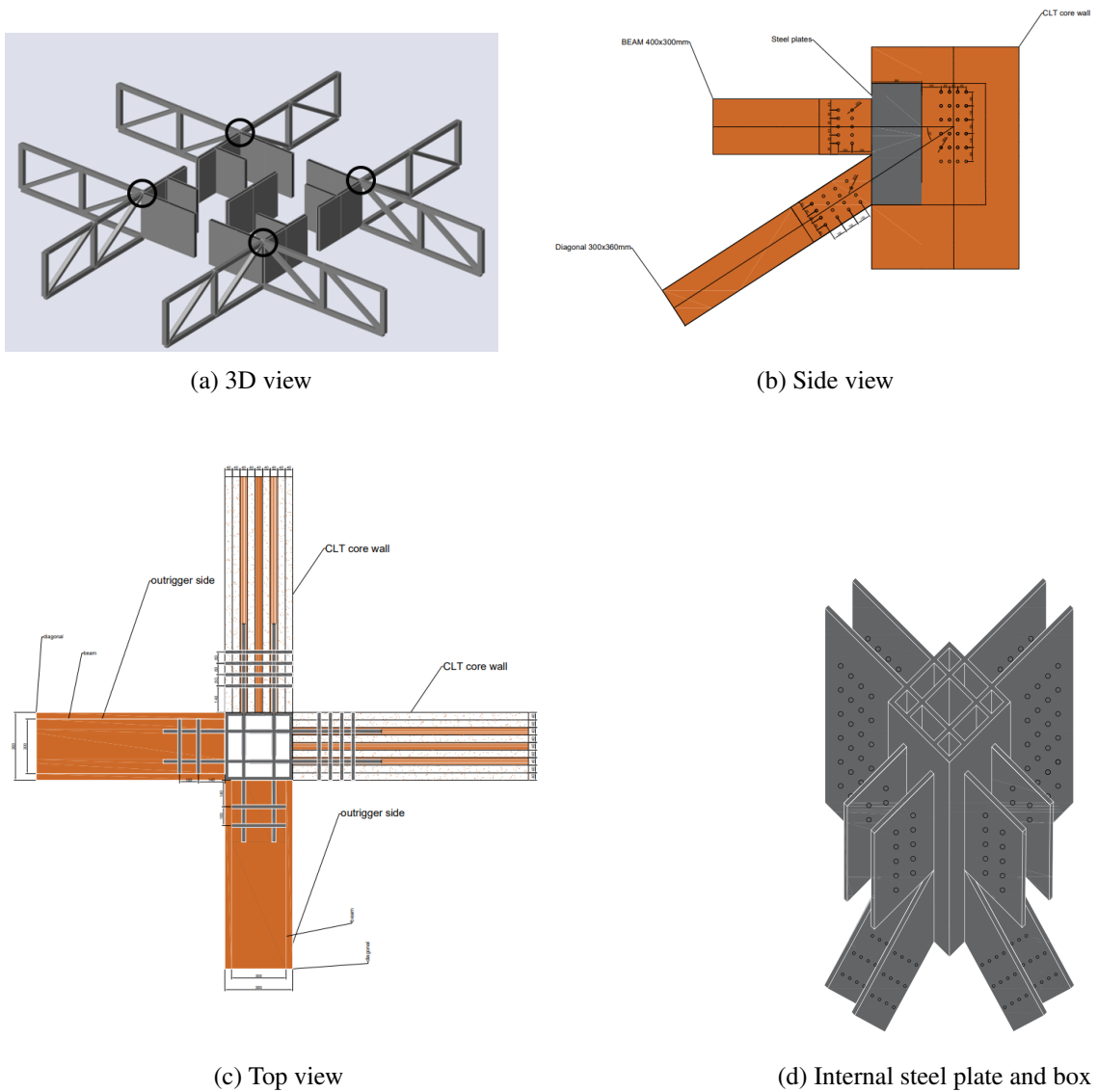


Figure 3.35. *Outrigger to core connection*

The modelling assumptions used for modelling of the outrigger to column connection are given in table 3.36

Table 3.36. *Stiffness modelling assumptions outrigger to core connection*

	u_x	u_y	u_z	ϕ_x	ϕ_y	ϕ_z
beam	263 kN/mm/m (tension only)	rigid	rigid	rigid	free	free
diagonal	420 kN/mm/m (tension only)	rigid	rigid	rigid	free	free
core	788 kN/mm/m (tension only)	rigid	rigid	rigid	free	free

4. Numerical modelling

This chapter will discuss the numerical modelling assumptions which have been made, SCIA will be used to model the different case studies. The reason for using SCIA is based on the fact SCIA already contains a lot of building materials and elements which can be used for civil/structural engineering practices while also having sufficient flexibility to be able to model new materials i.e. CLT.

4.1 Modelling assumptions

This section will discuss the assumptions which have been used to create the numerical models. Most of these assumptions are used to decrease the complexity of the models which will reduce calculation time as well as time to build the models, however this will come at a cost of reduced accuracy of the models.

Connections

Connection in the models will be constructed of translational springs or rotational springs depending on the type and location of the connection. The stiffnesses of these springs will be based on the designs made for specific details, calculations of the springs can be found in the appendixes. By defining the force displacement graph of a specific connection in SCIA it can be made possible to simulate ductility and or yielding of the connection. Additionally tendons can be modelled using translational springs which have the same stiffness as the steel tendons themselves.

CLT

As mentioned in chapter 2.7 CLT consists of numerous layers which are glued together at an angle. Modelling of the orthotropic CLT plates can be done based on the equivalent orthotropic shell model which will reduce complexity of modelling the plates itself. During the modelling of CLT the stiffness matrix will first be calculated analytically based on design parameters of the material(layer thickness, layer strength, layer orientation etc.) This matrix will then be inputted in SCIA coinciding with the correct local axis to ensure the CLT is oriented in the correct direction. For the modelling of beams, columns and diagonals SCIA already has specific material types ready to be used, therefore it is not necessary to determine the stiffness matrix for this material.

Lateral loading

Lateral loads will be modelled as line loads divided over the columns and beams on the facade. For this research it is not of importance to check the influence facade panels have on the load transfer from facade to column and eventually core.

Floors

In the models it is of importance to correctly implement floors. Floors are able to provide the structure with additional stiffness by diaphragm action, additionally this will transfer loads to the core and or outer columns. Floorloads can therefore be modelled as distributed loads over the area of the floor.

4.2 Validation of the numerical modelling methods

To ensure the methods and assumptions used in the numerical model are accurate and are able to give accurate results a validation check is done based on experimental results. A numerical model is buildt of the C-shaped CLT core wall as described in the research of Brown et al. [27] and compared to the experimental data provided in the research.

In appendix Appendix G the assumptions and results of the validation model are shown in detail. It has been concluded that with the used modelling methods and assumptions the numerical model was able to replicate the behaviour of the C-shaped CLT core with a very high accuracy.

4.3 Numerical modelling of case A

This section will describe the modelling process of case study A, consisting of the materials, dimensions, connections and loads and modelling methods. The workflow used throughout the modelling process can be seen in figure 4.1.

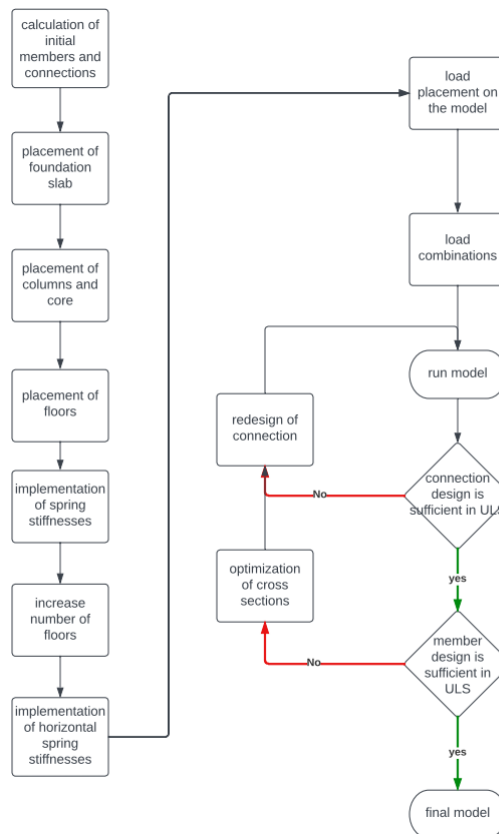


Figure 4.1. *Workflow numerical modelling*

Properties of the members

For the both the columns and beams the choice is made to use GL28h since this a material which is currently widely used and available. Higher material strengths can provide the structure with higher performance and reduce the amount of material used, however obtaining large quantities of high strength timber can prove to be difficult according to manufacturers. The material properties for GL28h are shown in table 2.2. For similar reasons the strength of the CLT laminates is chosen to be equal to CL24 as shown in table 2.1.

Initial dimensions of the walls and columns are calculated based on the calculation methods provided in section 3.8.1 and 3.8.2 respectively. Resulting in a initial wall thickness of 360 mm with a 40 mm laminate thickness and a 9-layer buildup (0/0/90/0/90/0/90/0/0). Since the vertical strength of the panels needs to be highest it is chosen to have 6 layers in vertical direction and 3 layers in horizontal direction. The dimensions of the columns are 450 mm by 450 mm. Using the stiffness matrix calculations as shown in chapter 2.7 in combination with the correct symmetrical lay-up and material properties the stiffness matrix of an equivalent shell model can be calculated, results are shown in 4.1.

$$M = \begin{bmatrix} 39.96 & 0 & 0 & 0 & 0 & 0 & 0 & 0 & MNm \\ 0 & 5.81 & 0 & 0 & 0 & 0 & 0 & 0 & MNm \\ 0 & 0 & 1.85 & 0 & 0 & 0 & 0 & 0 & MNm \\ 0 & 0 & 0 & 39.58 & 0 & 0 & 0 & 0 & MN/m \\ 0 & 0 & 0 & 0 & 20.26 & 0 & 0 & 0 & MN/m \\ 0 & 0 & 0 & 0 & 0 & 2640.00 & 0 & 0 & MN/m \\ 0 & 0 & 0 & 0 & 0 & 0 & 1320.00 & 0 & MN/m \\ 0 & 0 & 0 & 0 & 0 & 0 & 0 & 193.08 & MN/m \end{bmatrix} \quad (4.1)$$

The dimensions of the beams connecting the floor panels to the columns and to the core are calculated iteratively using the optimization software used in SCIA. The reason to use an iterative numerical calculation technique is because the beams are not only responsible for carrying the self weight of the floors and the imposed floor loads but also to transfer the wind loads from the facades to the core system. However wind loads are not only transferred using the beams but also due to the diaphragm action of the floors themselves.

Foundation plate

Since in the case studies the foundation is not of interest the groundfloor has been modelled as a plate with a very high stiffness, the plate is rigidly supported in all directions on the bottom surface. Ensuring rotations and translations of the structure are only present due to deformation of the structure itself. The plate can now be used to attach the first members.

Modelling sequence

Starting with the core each individual panel is placed according to the floorplan as shown in figure 3.1. These panels have a width of 2.625 meters and a height of 3.9 meters (equal to the story height). By enabling non-linearity in SCIA orthotropic material properties can be enabled and the stiffness matrix can be inputted. It is important to correctly set the local coordinate system so that the local x-axis follows the vertical in-plane direction, the local y-axis follows the horizontal in-plane direction and the z-axis follows the out-of-plane direction. To provide interaction between the corner section of the core system lintels are placed and modelled as beams which are hinged on both sides. The width of the lintels is equal to that of the CLT panels, 360 mm, and have a height of 500 mm. Material properties used for the lintels is equal to that of the columns and beams, GL28h. The columns are placed in a grid of 6 by 6 meters to reduce the maximum spans of the floor panels to 6 meters. In figure 4.2 the numerical model of the base floor including the columns, beams and core system is shown.

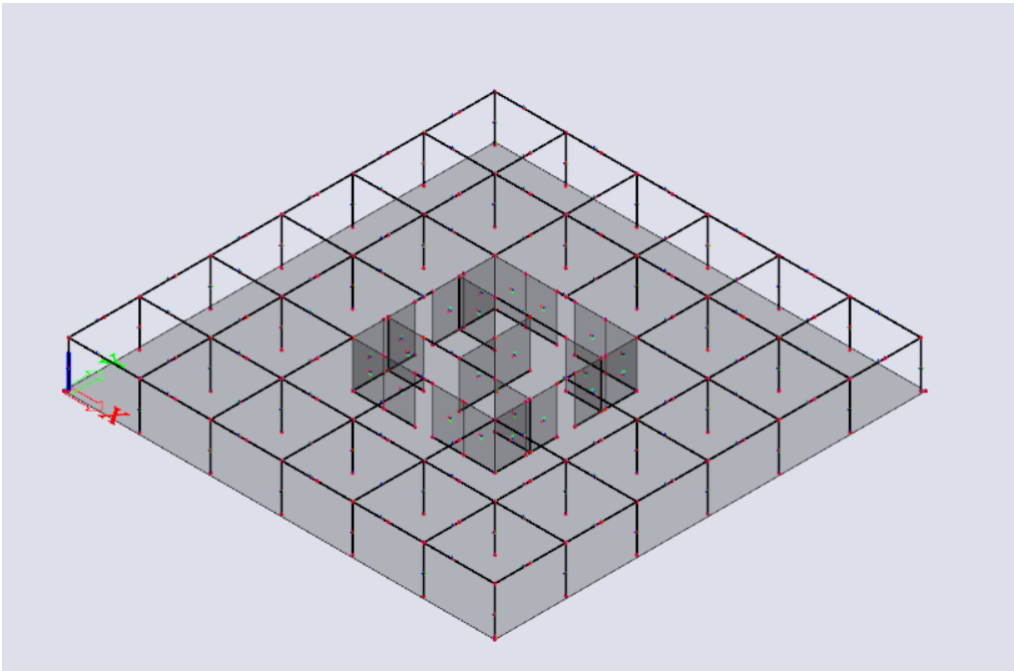


Figure 4.2. *Numerical model groundfloor*

Similar to the columns the floor plates are also modelled as hinged and have a layout as shown in figure 4.3. The layout of the floor panels is chosen in such a way to leave a total of four corners open with an area of 3 by 3 meters which can be used for the vertical transport of inhabitants. similar to the vertical CLT panels used for the core close attention needs to be paid to the locale coordinate system of the floor panels such that the LCS coincides with the intended direction as calculated in the stiffness matrix. The thickness of the CLT floor panels is based on the selfweight and imposed loads similar to the calculations used for the core systems. A thickness of 200 mm is obtained for the 6 meter span floor panels.

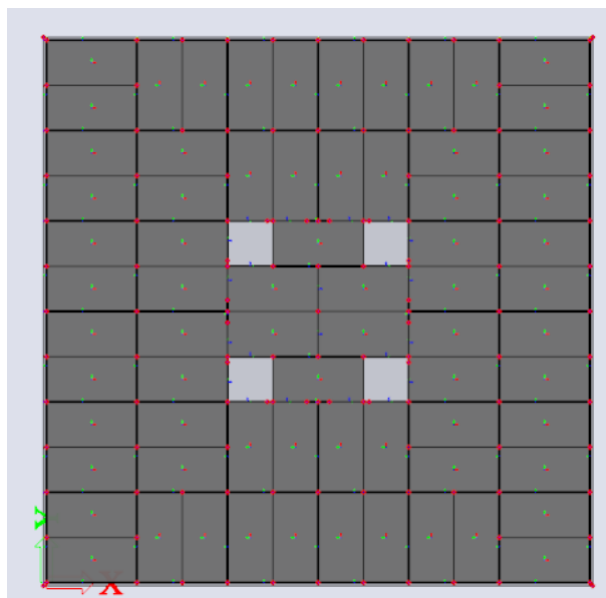


Figure 4.3. *Orientation of CLT floors*

Connections

For the design of the connections the calculation method in 3.9.3 is used for double inclined self-taping screws. For this design the choice has been made to use a combination of double inclined screws and straight screws as research has shown the combined action will provide the best combination of strength, stiffness and ductility.

By using the tool 'hinge on a 2d' the connections between the CLT panels can be modelled, while for 1D members 'hinge on a beam' is used as can be seen in figure 4.4a and 4.4b respectively. In figure 4.5 an example is given of modelling a hinge on a 2d member for the vertical orthogonal connection of the core.

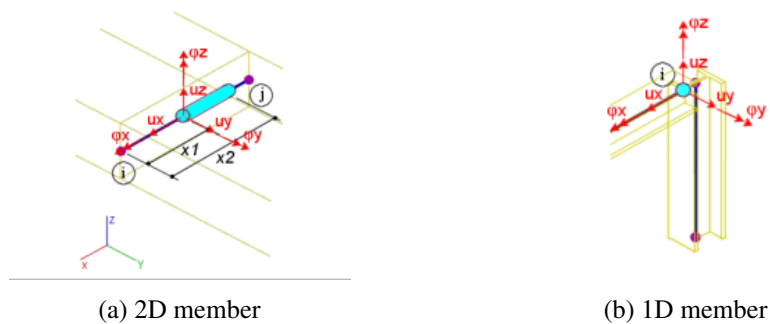


Figure 4.4. *Local coordinate systems joints SCIA*

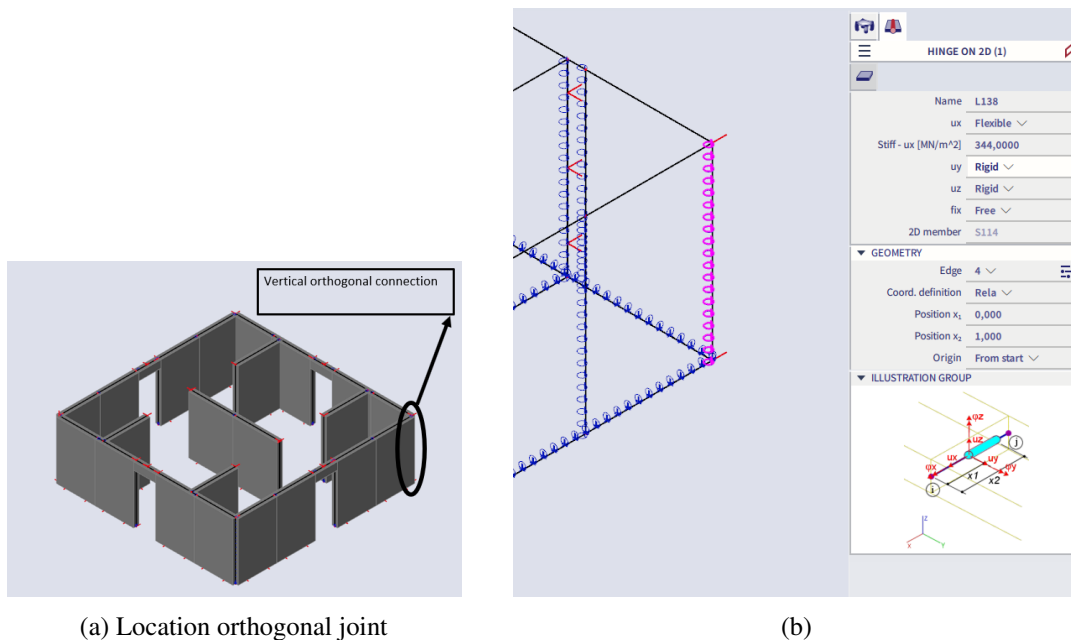


Figure 4.5. *Example of modelling a hinge on 2d member on the orthogonal core connection*

An overview of the modelling assumptions of the different connections of case A as derived in section 3.9 is shown in table 4.1. While the modelling assumptions of the different connections of case B as derived in section 3.10 is shown in table 4.2.

Table 4.1. Overview connection stiffness's numerical model case A

	u_x [kN/mm/m]	u_y [kN/mm/m]	u_z [kN/mm/m]	ϕ_x	ϕ_y	ϕ_z
connections of the core						
vertical orthogonal	344	rigid	rigid	free	-	-
vertical in-plane	355	rigid	rigid	free	-	-
horizontal CLT core to CLT core	1371	205*	free	free	-	-
horizontal CLT core to foundation	1231	1231*	free	free	-	-
connections of the columns and beams						
column to foundation	rigid	rigid	rigid	rigid	free	free
column to column	rigid	rigid	rigid	rigid	free	free
beam to column	rigid	rigid	rigid	rigid	free	free
beam to CLT core	rigid	rigid	rigid	rigid	free	free
connections of the floors						
floor to beam single	53	53	rigid	free	-	-
floor to beam double	53	56*	rigid	free	-	-
floor to floor	52	rigid	rigid	free	-	-
floor to CLT core	129	194*	rigid	free	-	-

Table 4.2. Overview connection stiffnesses numerical model case B

	u_x [kN/mm/m]	u_y [kN/mm/m]	u_z [kN/mm/m]	ϕ_x	ϕ_y	ϕ_z
connections of the outrigger						
beam	263*	rigid	rigid	rigid	free	free
diagonal	420*	rigid	rigid	rigid	free	free
column	525*	rigid	rigid	rigid	free	free
CLT core	788*	rigid	rigid	rigid	free	free

*non-linear tension only springs are implemented

Increase number of floors

During the modelling the following building sequence is used to reduce workload and increase modelling speed. The first floor is build until a height of 3.9 meters. This can then be copied and pasted including all the add-on data to increase the number of stories to 10. The entire model can be seen in figure 4.6.

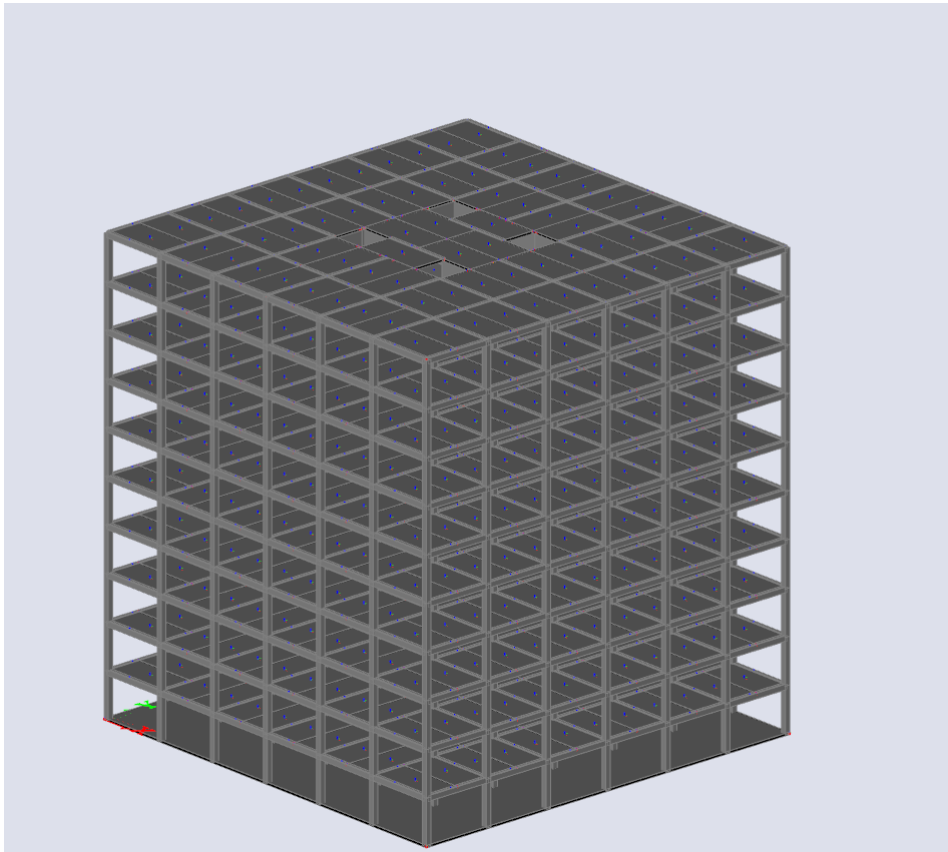


Figure 4.6. *Numerical model case A*

It is important to note that in SCIA connections of 2D panels or 1D members that do not have hinges or other constraints at the ends are modelled as rigid. This is especially important when copy pasting different stories on top of each other.

Horizontal connection

Since the maximum length of a CLT panel is 16 meters, due to manufacturing constraints, horizontal connections need to be implemented to connect the vertical panels. The choice is made to have a horizontal connection at 15.6 meters height and 31.2 meters height which coincides with floor level 4 and 8 respectively. The design of the horizontal connection consists of a doweled connection which integrates a steel plate in the center of the CLT panel. Calculation is performed based on 3.9.5 and makes use of the minimum spacing and end distances as provided in prEN1995-1. According to prEN1995-1 the stiffness of a doweled connection connecting CLT with a steel plate the stiffness may be doubled for the case that the thickness of the plate is equal to the thickness of the dowel.

Loading and load combinations

The loading of the model consist of permanent loading, variable loading and wind loading. Both the permanent and variable loading is placed on the floor panels as surface loads. In contrary the wind load is modelled as line loads on the beams placed in the facades.

Before the numerical calculation can commence it is important to note that non-linear load combinations need to be made manually to allow for a non-linear calculation. The reason to use non-linear load combinations is to be able to correctly model the tension only springs in the horizontal connection between CLT panels and to be able to use orthotropy.

element size of the CLT

The element size of the core has been chosen in such a way that the height of the element is similar to the height of the beams, between 400 and 500 mm the height of the beam and corbels respectively. If an element height greater than the height of the beam is chosen local deformations at the beam to core connection will be underestimated, while an element height smaller than the height of the beam will lead to over estimation of the local deformations. Therefore the element size has been chosen so that eight elements are used over the height of a single storey, 3.9 meters. Resulting in an element height of approximately 490 mm.

4.4 Numerical modelling of case B

This section will describe the modelling process of case study B, consisting of modelling the outrigger. The rest of the structure will remain the same as in case A shown in section 4.3.

Outrigger

The outrigger will be incorporated in the model of case A, the following changes will be made to case A.

- Introduction of outrigger diagonal
- Change of beam size of the outrigger
- Introduction of the correct connection stiffnesses as shown in table 4.2

5. Results

In this section the results of the different numerical case studies are discussed. Starting with the results of case A, followed by the results of case B and finally the results of case C. Additionally to determine the influence of design parameters a sensitivity analysis is done for the joint design of case A and the design parameters of the outrigger for case B. The workflow used throughout the sensitivity analysis can be seen in figure 5.1.

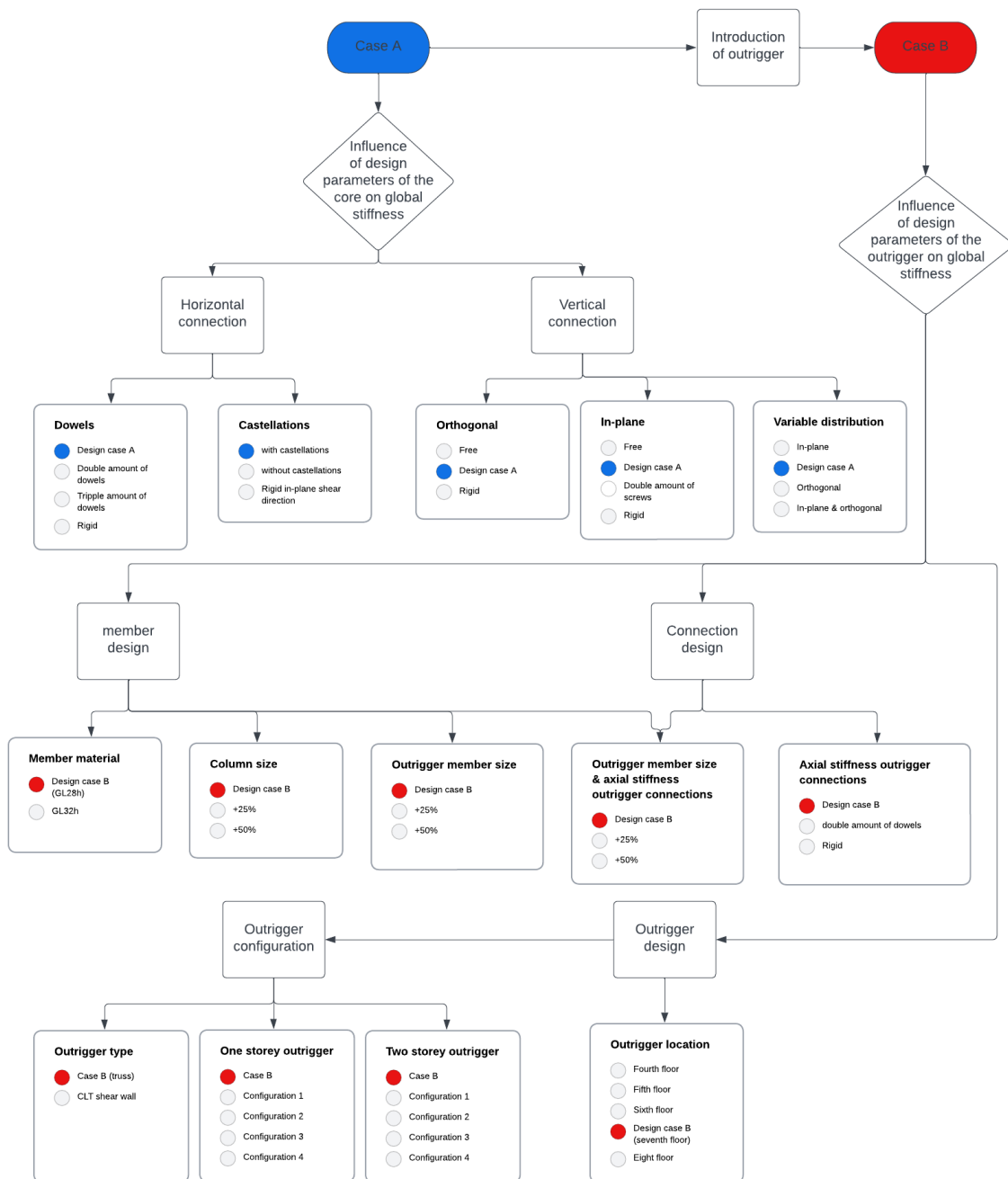


Figure 5.1. Workflow sensitivity analysis design parameters

5.1 Results case A

This section will discuss the results of the numerical simulation of case A. Initially the behaviour of the core is examined under lateral loading in SLS.

5.1.1 Static response

In this section the static behaviour of case A is discussed. The deflection of the core can be seen in figure 5.2 where the maximum deflection of the of the core is equal to 61.8 mm.

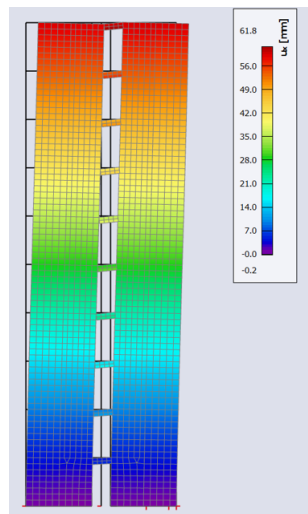


Figure 5.2. *Horizontal deflection of case A*

The maximum deflection is higher than the allowed maximum deflection limit of $h/1000$.

When looking closer at the behaviour at ground floor of the core the following topics should be noted. Figure 5.3 shows the core system at ground floor with a scaled up displacement and indicated values of the vertical displacement.

Due to the overturning moment induced by the windload, tensile forces occur in the horizontal connection between the core and the foundation resulting in a small uplifting of 1 mm at end positions of the core while the compression side remains in contact with the foundation. Additionally there is sliding which occurs between the in-plane walls which results in a small gap at the top of the panels, similarly sliding occurs at the vertical orthogonal connection.

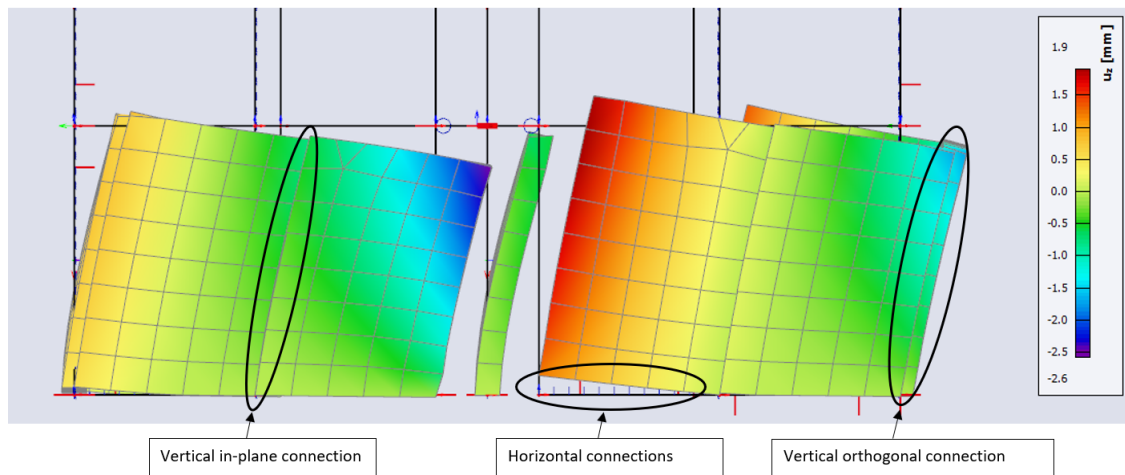


Figure 5.3. *Global displacement case A of the core at groundfloor level, SLS loading, vertical deflection*

The results show that the implementation of the different connection details provide similar results as in the verification model discussed in Results of the numerical validation model in Appendix G confirming the modelling methods used.

Contributions to the total deflection

In figure 5.4 the lateral translation of 61.8 mm for case A is subdivided into the different categories such as material and connections. It can be seen that the contribution due to bending and shear deformation is 70.6% and 18% respectively.

Secondly the contributions due to the influence of the different connections of the core is shown, which is subdivided into the horizontal and vertical connections. The total contribution of the horizontal connection towards rigid body translation is equal to 0.6% while the rigid body rotation is responsible for 8.1%. It is shown that even a slight gap opening of 0.6 mm at ground level can increase deflections by 6.8%, again highlighting the significance of providing a rigid connection at ground level. The addition of castellations in the horizontal core to core connections provided a high stiffness to the joints resulting in low rigid body translations.

Additionally the slip of the different connections is shown in the in-plane shear direction and the gap opening for the horizontal connection is given which results in rigid body rotation of the core.

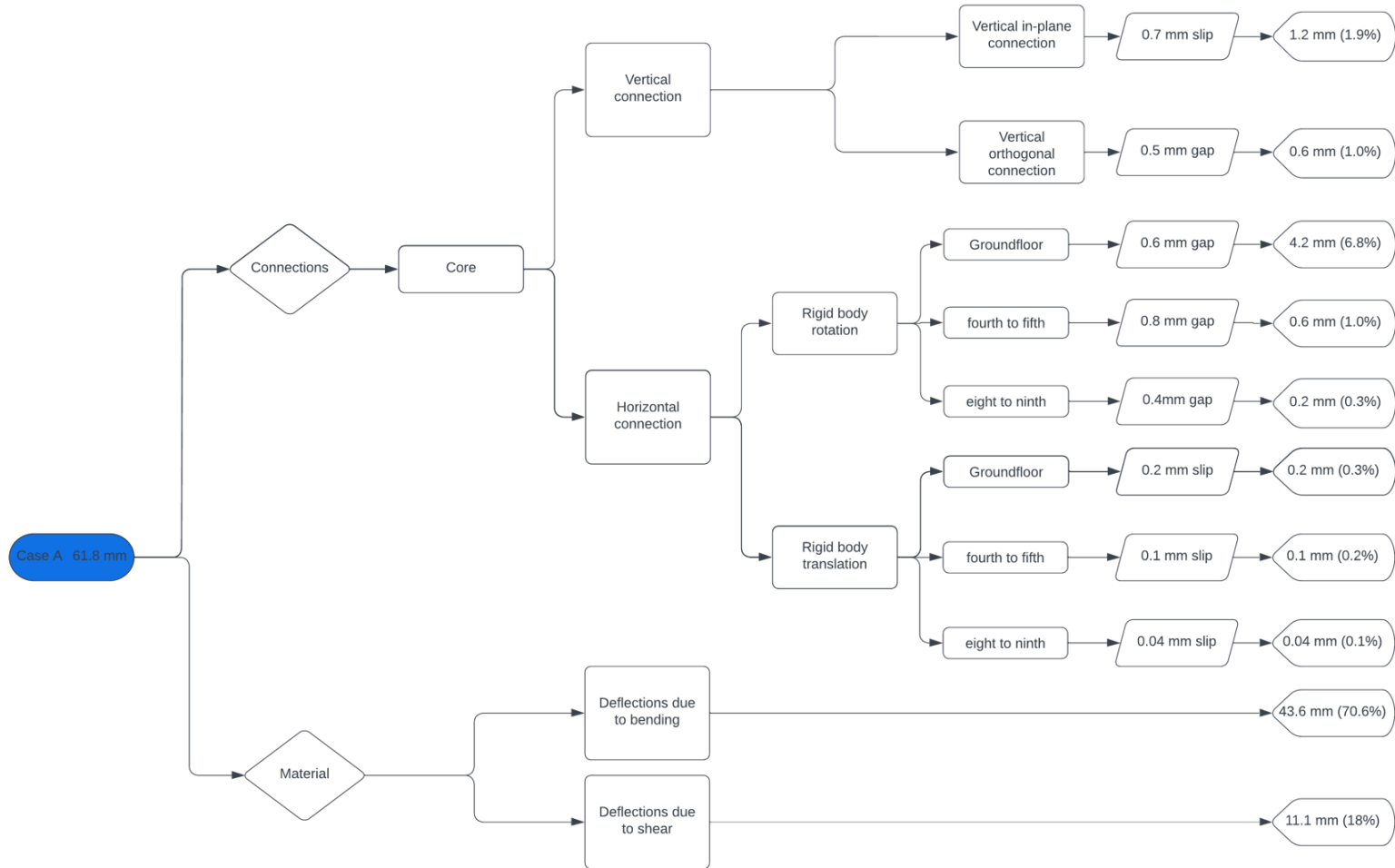


Figure 5.4. Origin of translations case A

Analytical calculation

In this section an analytical calculation is made of the deflection of the CLT core based on assumptions as shown in appendix Appendix B. By comparing analytical and numerical results a validation of both methods can be made based on results.

The deflection of a clamped beam can be calculated according to equation 5.1. The wind load is taken as distributed q-load equal to 69.84 kN/m and the bending stiffness of the core is taken as four times the individual stiffness of the corner sections as shown in figure B.3b.

$$u = \frac{ql^4}{8EI} \quad (5.1)$$

Table 5.1. Result analytical calculation

	$I_{eff} \text{ mm}^4$	deflection mm
model	$3.42 * 10^{13}$	78.6
vertical orthogonal interaction		
$\gamma = 0$	$2.06 * 10^{13}$	130.4
$\gamma = 1$	$3.44 * 10^{13}$	78.3
vertical in-plane interaction		
$\gamma = 0$	$1.46 * 10^{13}$	185.2
$\gamma = 1$	$3.47 * 10^{13}$	77.8

Table 5.2. Result analytical vs numerical calculation

type	deflection [mm]	deflection [mm]
	analytical	numerical
horizontal connections included	no	yes
model	78.6	61.8
vertical orthogonal interaction		
$\gamma = 0$	130.4(+65.9%)	94.1(+52.3%)
$\gamma = 1$	78.3 (-0.4%)	61.2(-1%)
vertical in-plane interaction		
$\gamma = 0$	185.2(+135%)	158.6(+156.6%)
$\gamma = 1$	77.8(-2.7%)	60.6(-1.9%)

The results shown in table 5.18 show that while the calculated value for the deflection is higher in the analytical model than in the numerical model the influence of the different connections can be assessed analytically with a reasonable accuracy. In both models it is shown that the influence of the vertical in-plane connection is larger than the orthogonal connection especially for the case that γ is equal to zero.

The following assumptions for the analytical model could be the cause for the difference in deflection between both models. First of all the assumption is made that the corners of the core behave separately, however in the numerical model connections of the floors to core provide some interaction between the corner sections which increases the global bending stiffness. Secondly the influence of the effective flange width of the core has a large effect on the analytical calculation of the composite bending stiffness, and since literature on the topic is relatively scarce an estimation is made with some simple numerical models.

5.1.2 Dynamic response

The dynamic response of the structure is analyzed by performing a modal analysis. The first five eigenfrequencies of case A can be seen in figure 5.5. The first eigenfrequencies for lateral sway modes are 0.86 Hz and 0.89 Hz for the x and y direction respectively. Both modes are below the approximations of the first flexural modes for steel and concrete buildings provided in the Eurocode in equation 2.6 and the approximation for timber buildings excluding connections as shown in

equation 2.8, with values 1.18 Hz and 1.41 Hz respectively.

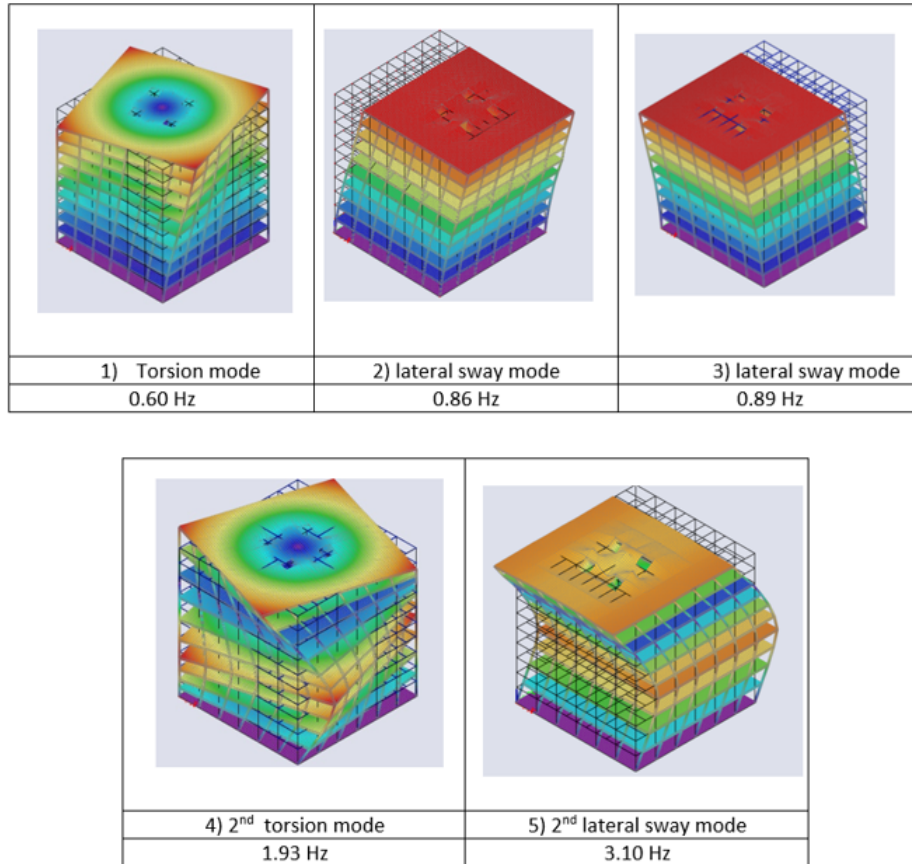


Figure 5.5. *Dynamic response case A*

The lateral acceleration of the structure due to dynamic wind loading is estimated using the equations provided in section 2.6.2. The peak acceleration is equal to 0.076 m/s^2 , which is below the maximum allowed lateral acceleration according to the eurocode as can be seen in figure 2.36, equal to 0.1 m/s^2 for region 1 (residential buildings) and 0.18 m/s^2 for region 2 (residential buildings).

It should be noted that for the calculation of the peak lateral acceleration the following assumption is used. As can be seen in figure 5.5 the first mode is a torsional mode, however since the wind load is a symmetric load the anti-symmetric torsional mode will not-hardly be excited. Therefore the first lateral sway mode, the first symmetric mode, is used in the calculation of the peak lateral accelerations in the along wind direction.

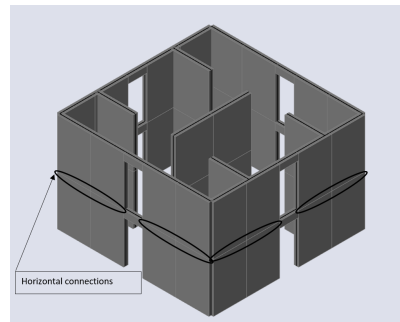
5.1.3 Sensitivity of connection design of case A

In this section a sensitivity analysis is performed. The interaction of the different wall section and thus the global stiffness of the core is large dependent on the stiffness of the connections between different segments. The influence of the stiffness of different connections of the core is assessed on

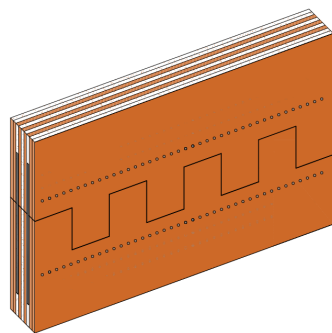
the global stiffness of the structure. Allowing the optimized design to economically make use of material while increasing the global stiffness of the structure.

Horizontal connection CLT core

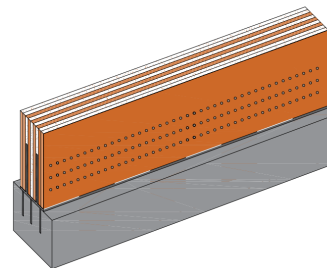
An overview of the horizontal connections with its respective displacement modes, rigid body translation and rotation can be seen in figure 5.6.



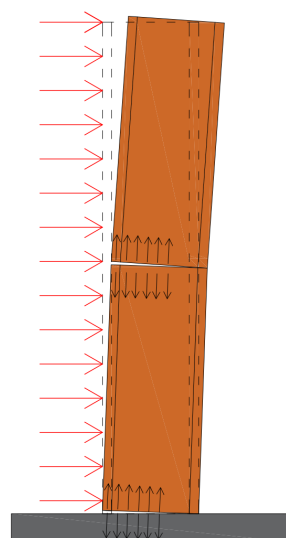
(a) Location horizontal connection



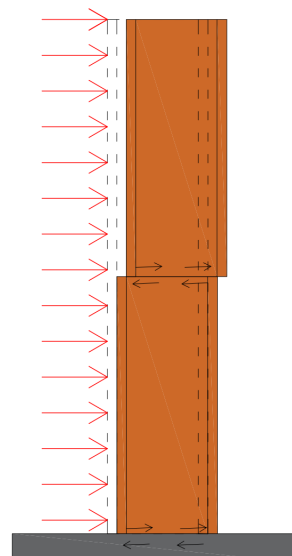
(b) Core to core



(c) Core to foundation



(d) Tensile force



(e) Shear force

Figure 5.6. Overview horizontal connection

To assess the sensitivity of the horizontal connection, i.e. the CLT panel to CLT panel connection as designed in section 3.9.5, the following design changes are made. The connection stiffness is increased by doubling and tripling the amount of dowels and finally for comparison sake the connection is modelled as rigid. The amount of dowels used in each design is six and nine rows of dowels for the core to foundation connection and two and three rows of dowels for the panel to panel connection for the double and triple stiffness models respectively. The results of the horizontal deflections of the different models are shown in figure 5.7. It should be noted that during the modelling of the increased stiffness models the castellations remain the same throughout, except for the rigid model, with the in-plane shear stiffness u_x calculated using the spring model shown in figure 3.22. Input for the different connections can be seen in table 5.3.

Table 5.3. *Boundary conditions horizontal connection core to core and core to foundation, sensitivity analysis*

	dowel rows	u_x	u_y	u_z	ϕ_x
double amount of dowels					
ground floor	6	2462 kN/mm/m	2462 kN/mm/m	free	pinned
fourth to fifth floor	2	1576 kN/mm/m	410 kN/mm/m	free	pinned
seventh to eighth floor	2	1576 kN/mm/m	410 kN/mm/m	free	pinned
triple amount of dowels					
ground floor	9	3693 kN/mm/m	3693 kN/mm/m	free	pinned
fourth to fifth floor	3	1781 kN/mm/m	615 kN/mm/m	free	pinned
seventh to eighth floor	3	1781 kN/mm/m	615 kN/mm/m	free	pinned
rigid					
-	-	rigid	rigid	free	rigid

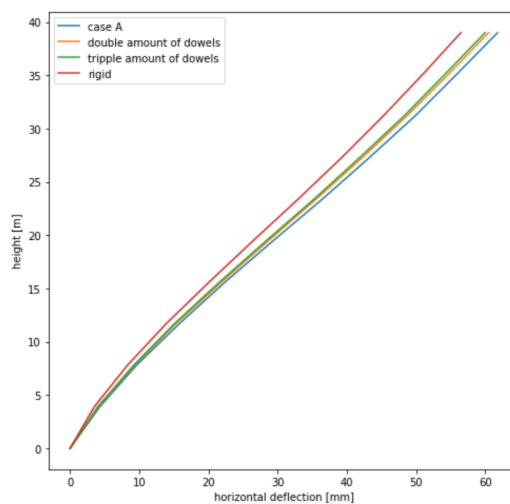


Figure 5.7. *Influence of the amount of dowels in the horizontal connection on the lateral deflection*

Additionally the influence of the castellations is assessed by comparing a model with and without castellations. The results of both models can be seen in figure 5.8. Besides the models shown in the figure below an additional model is made in which the horizontal connection is modelled as rigid in the in-plane shear direction to check the influence of rigid body translations on the global stiffness.

In table 5.4 the boundary conditions of the different models are shown used to asses the influence of the castellations.

Table 5.4. *Boundary conditions horizontal connection core to core, sensitivity analysis castelattions*

	dowel rows	u_x	u_y	u_z	ϕ_x
with castellations (case A)					
fourth to fifth floor	1	1371	205 kN/mm/m	free	rigid
seventh to eight floor	1	1371	205 kN/mm/m	free	rigid
without castellations					
fourth to fifth floor	1	205 kN/mm/m	205 kN/mm/m	free	pinned
seventh to eight floor	1	205 kN/mm/m	205 kN/mm/m	free	pinned
rigid castellation					
fourth to fifth floor	1	rigid	205 kN/mm/m	free	rigid
seventh to eight floor	1	rigid	205 kN/mm/m	free	rigid

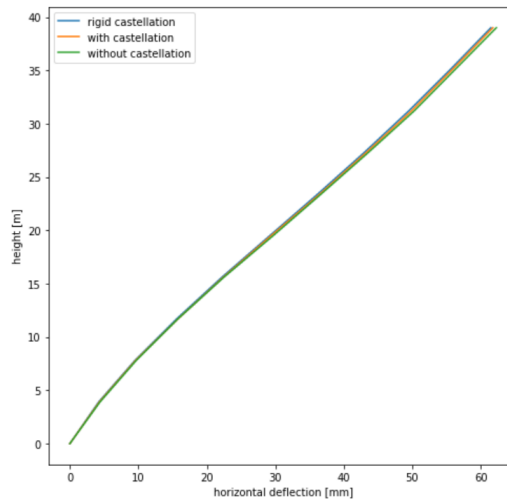


Figure 5.8. *Influence of the castellations on the lateral deflection*

In table 5.5 the maximum horizontal deflection of the different models are shown and the percentage difference between the results of case A are given.

Table 5.5. *Influence of the horizontal connection on the lateral deflection*

	deflection [mm]	% with regards to case A
Case A	61.8	-
Without castellations	62.3	+0.8%
rigid castellation	61.5	-0.5%
Double stiffness	60.5	-2.1%
Triple stiffness	60	-2.9%
Rigid	56.5	-8.6%

Comparing the results between the different cases the following observations can be made. The difference between the case A and rigid model shows a difference of 8.6%. Which is a result of

rigid body rotation and translation of the CLT panels due to stiffness of the horizontal connection. The addition of the castellations provide an increase in global stiffness and reduces deflections by 0.8%. It should be noted that case A has a height of 39 meters and has only two horizontal CLT to CLT panel connections, however if a taller building is constructed which has more horizontal panel to panel connections the effectiveness of the castellations will increase and the total amount of rigid body translations will reduce.

From the model in which the horizontal connections are modelled as rigid it is shown that 8.6% of deflections originate from rigid body translations and rotations. Taking into account the percentage of rigid body translations 0.5%, it is shown that 8.1% of the deflections originate from rigid body rotations. Which highlights the importance of reducing the rigid body rotations to increase global stiffness of a CLT core building.

Increasing the amount of dowels by double and triple the amount reduces the deflections of the structure by 2.1 % and 2.9 % respectively. However even with triple the amount of dowels, tensile forces in the core still result in rigid body rotation of the panels. Eliminating the issue could be done by introducing compressive forces in the core by making use of a pres-lam system, side effect is increased size of the panels is needed to carry compressive loads.

Vertical orthogonal connection CLT core

An overview of the vertical orthogonal connection with its respective deformation mode can be seen in figure 5.9.

The influence of the vertical orthogonal connection on the global stiffness is assessed by introducing three variation models. A model with the connection modelled as free, a model with an increased stiffness and a model with a rigid connection. The increased stiffness model has a reduced spacing of 10d instead of the 20d shown in section 3.9.3. Comparing different models allows for examination of the interaction between in-plane and out-of-plane walls and its effect on the effective flange width. The modelling assumptions for the different models are shown in table 5.6 and the deflections are shown in figure 5.10.

Table 5.6. *Boundary conditions vertical orthogonal connection , sensitivity analysis*

	u_x	u_y	u_z	ϕ_x
free	free	free	free	pinned
minimum spacing 10d	688 kN/mm/m	rigid	rigid	pinned
rigid	rigid	rigid	free	pinned

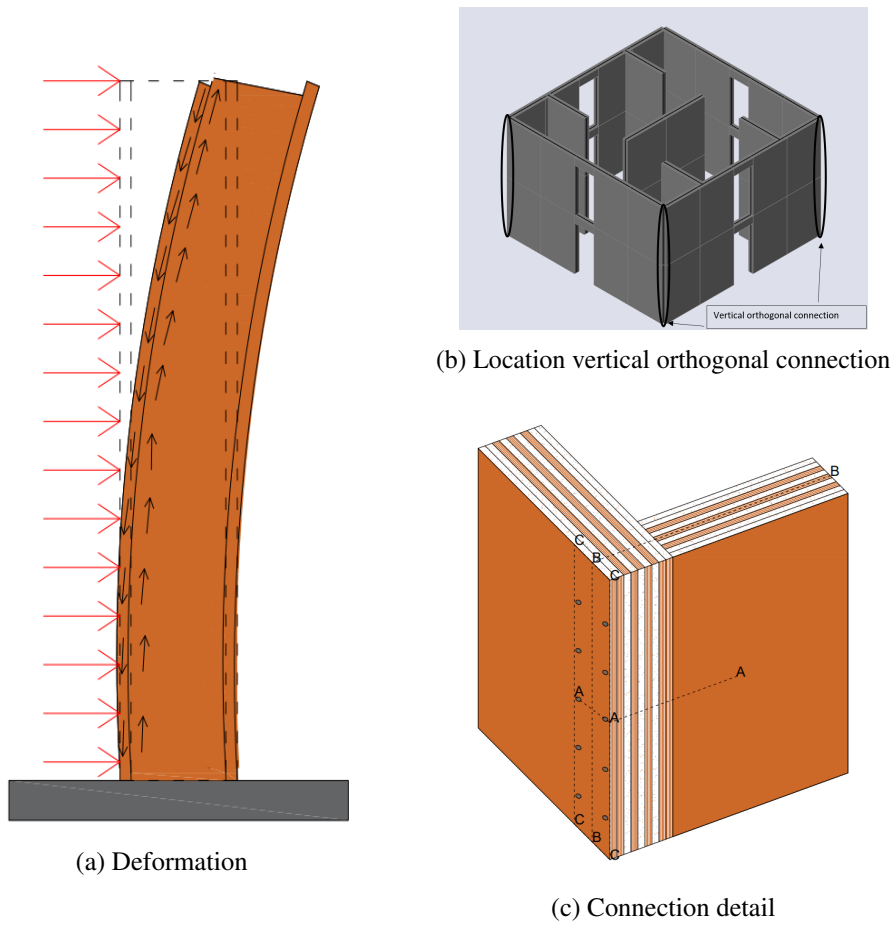


Figure 5.9. Overview vertical orthogonal connection

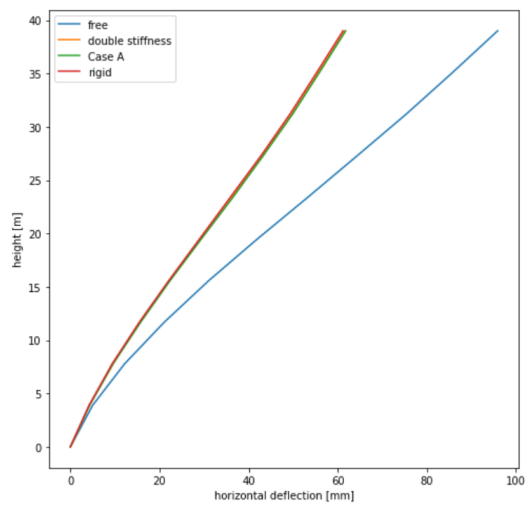


Figure 5.10. Influence of the vertical orthogonal connection on the lateral deflection

The maximum deflections are shown in table 5.7 combined with the percentage difference to case A.

Table 5.7. Influence of the vertical orthogonal connection on the lateral deflection

	deflection [mm]	% with regards to case A
Case A	61.8	-
free	94.1	+52.3%
minimum spacing 10d	61.6	-0.3%
Rigid	61.2	-1.0%

From the results shown above increasing the stiffness of the vertical orthogonal by doubling the amount of screws or modelling the connection as rigid reduces deflections by 0.3% and 1.0% respectively. This shows that the effective flange width is not greatly increased in the case of an increased stiffness in the vertical orthogonal connection.

Vertical in-plane connection CLT core

An overview of the vertical in-plane connection with its respective deformation mode can be seen in figure 5.11.

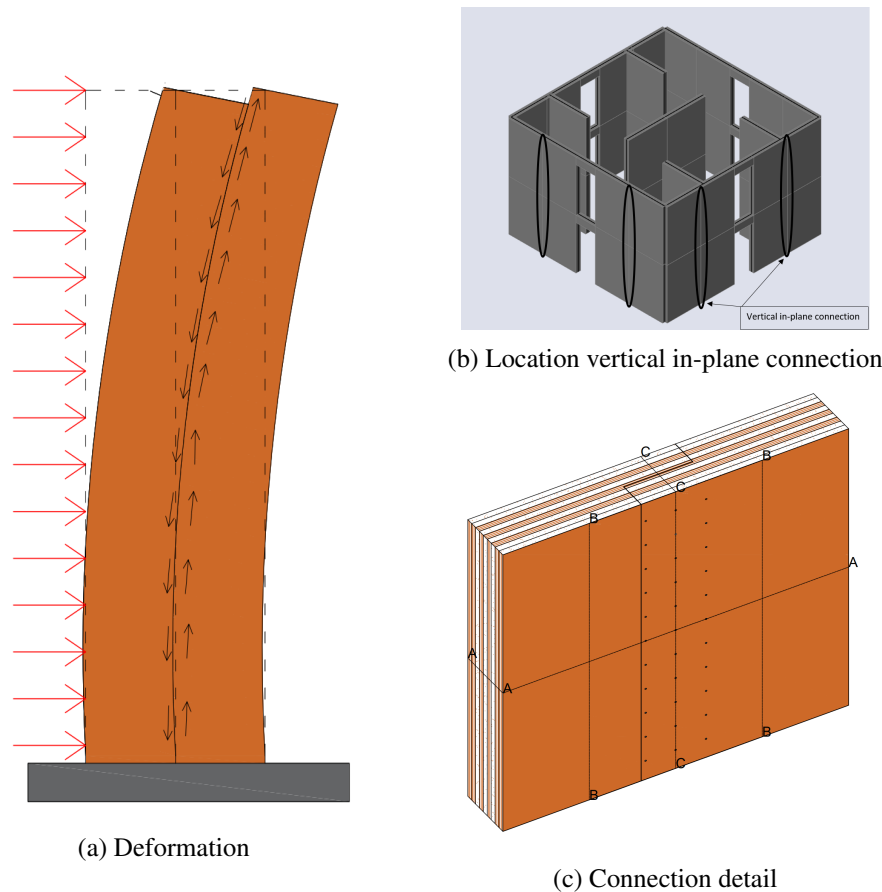


Figure 5.11. Overview vertical in-plane connection

The influence of the vertical in-plane connection on the global stiffness is assessed by introducing two boundary models. A model with the connection modelled as free and a model with the connection modelled as rigid, given the lower and upper boundary of the effects of the connection on the global stiffness. The modelling assumptions for the different models are shown in table 5.8

and the deflections are shown in figure 5.12.

Table 5.8. *Boundary conditions vertical in-plane connection , sensitivity analysis*

	u_x	u_y	u_z	ϕ_x
free	free	rigid	rigid	pinned
rigid	rigid	rigid	rigid	pinned

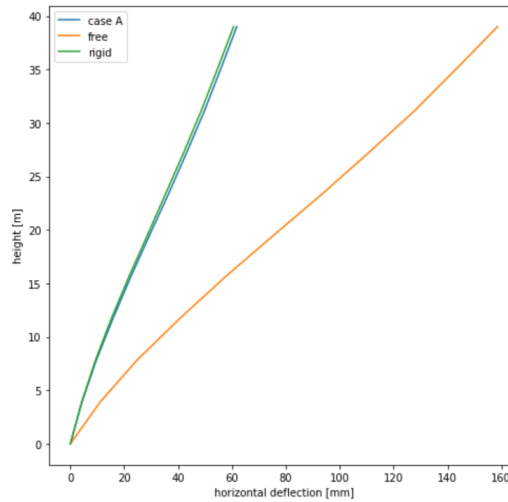


Figure 5.12. *Influence of the vertical in-plane connection on the lateral deflection*

The maximum deflections are shown in table 5.9 combined with the percentage difference to case A.

Table 5.9. *Influence of the vertical orthogonal connection on the lateral deflection*

	deflection [mm]	% with regards to case A
Case A	61.8	-
free	158.6	+156.6%
Rigid	60.6	-1.9%

Comparing the lower and upper bound value of the influence of the vertical in-plane connection it is observed that quite a large difference exist between both values, namely 98 mm. Which highlights the effect of the in-plane connection on the global stiffness of the system. Providing an in-plane connection with a high stiffness can increase the overall stiffness of the core system. The currently designed in-plane connection, based on ULS, as shown in section 3.9.4 is already close to the upper bound value. Therefore increasing the stiffness of the connection will not lead to a drastic reduction of the deflections. Additionally the connection is already designed at a minimum spacing of the screws, therefore to increase the stiffness of the connection a new joint design should be made.

Variable distribution of the vertical connections

The connections for the vertical orthogonal and vertical in-plane have been designed based upon maximum forces in ULS, in which the joint is homogeneous over the height of the structure. In this section the influence of a variable distribution of the vertical joint design is assessed. The vertical joints have a stiffness K equal to the previously designed values at ground floor, 344 and 355 kN/mm/m for the orthogonal and in-plane connection respectively, while at the 10th floor the stiffness is equal to 0, as can be seen in figure 5.13a. The deflection of for the structure with variable distributed vertical orthogonal, vertical in-plane and a combination of both can be seen in figure 5.13b with maximum values shown in table 5.10.

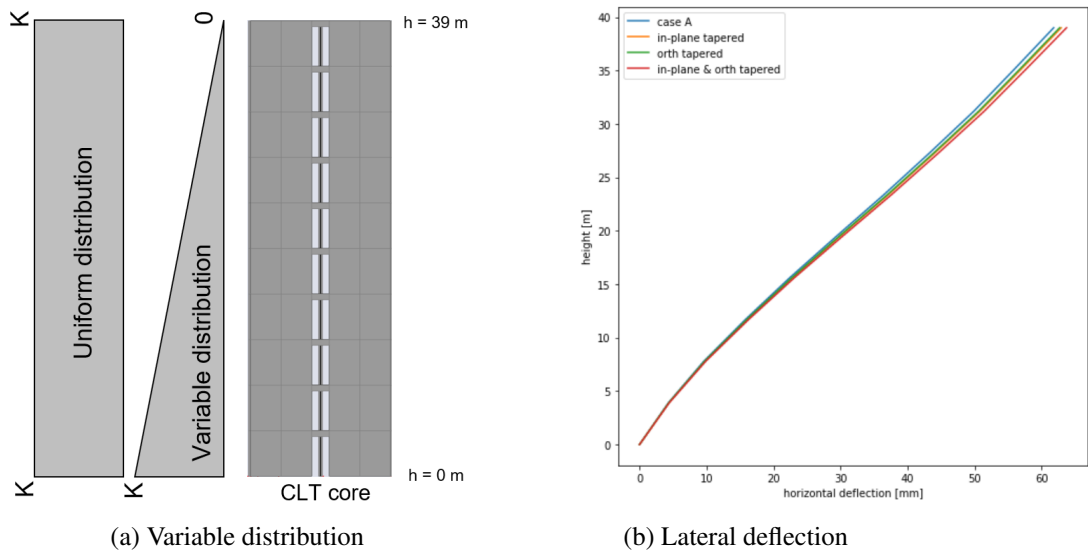


Figure 5.13. Influence of variably distributed vertical connections on the lateral deflection

Table 5.10. Maximum values of the lateral deflection for tapered vertical connections

	deflection [mm]	% with regards to case A
Case A	61.8	-
tapered vertical in-plane	62.9	+1.8%
tapered vertical orthogonal	62.7	+1.4%
tapered vertical in-plane & orthogonal	63.7	+3.1%

It can be seen that decreasing the amount of screws over the height decreases interaction between the walls resulting in an increased lateral deflection. However reducing the amount of screws by 50% in the vertical connections increases lateral deflections 3.1% still providing a high degree of interaction between core walls, showing that a large part of the slip in the vertical joints originate from the lower section of the core where forces are at a maximum.

5.1.4 Conclusion results case A

The current design of case A which has been designed based ULS criteria does not meet the imposed limit on deflections, however for such a non-slender structure the dynamic behaviour is

not governing in this case.

The castelations are able to reduce deflections by 0.8% using mechanical interlocking without increasing the amount of steel used. Gap opening at ground level is one of the most critical connection design aspects of a CLT core and is responsible for 6.8% of lateral deflections. Both the vertical in-plane as orthogonal connection provide a high degree of composite interaction between core walls. Further increasing the vertical stiffness's will not have large effects on the composite interaction of the core system.

Global stiffness of a CLT core incorporating vertical joints can be estimated using analytical calculation methods. However carefull design choices need to be made when determining the effective flange widths of the core. Additionally depending on the type of connection between core and floors interaction between corner sections of the core may or may not occur.

5.1.5 Discussion results case A

During the modelling of the floor to core connection attention needs be paid as to how the connection is realised. For instance modelling of the connection as rigid in the vertical direction will not only prevent slip in the vertical joints but will also induce a bending moment in the floor plates, resulting in a behaviour much like a moment resistant frame connecting corner sections of the core.

5.2 Results case B

In this section the results of case B are discussed, after which a sensitivity analysis is performed.

5.2.1 Static response

In this section the static behaviour of case B is discussed. The deflection under SLS loading can be seen in figure 5.14. The maximum deflection of case B is equal to 52.9 mm, which is a reduction of 14.4 % in comparison to the maximum deflection of case A, which is 61.8 mm. From the figure below it can also be noted that case B which is designed on ULS does not provide sufficient stiffness to meet the SLS requirement on maximum deflection, equal to 40 mm.

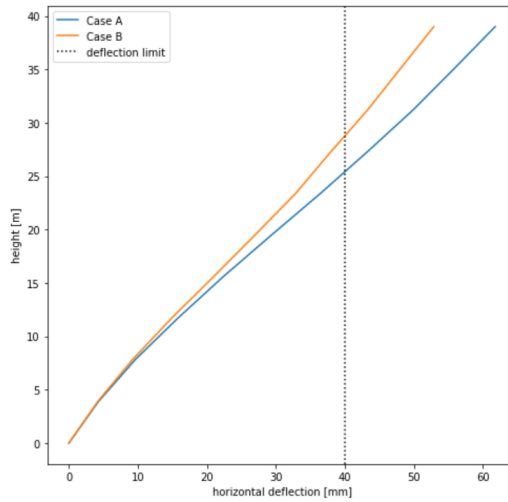


Figure 5.14. Deflection of case B

Contributions to the total deflection

The different contributions to the total deflection of case B can be seen in figure 5.15. Similar observation can be made as discussed in section 5.1.1 with regards to the behaviour of the core and its respective contributions, however the average contributions of the core have decreased due to the addition of the outrigger.

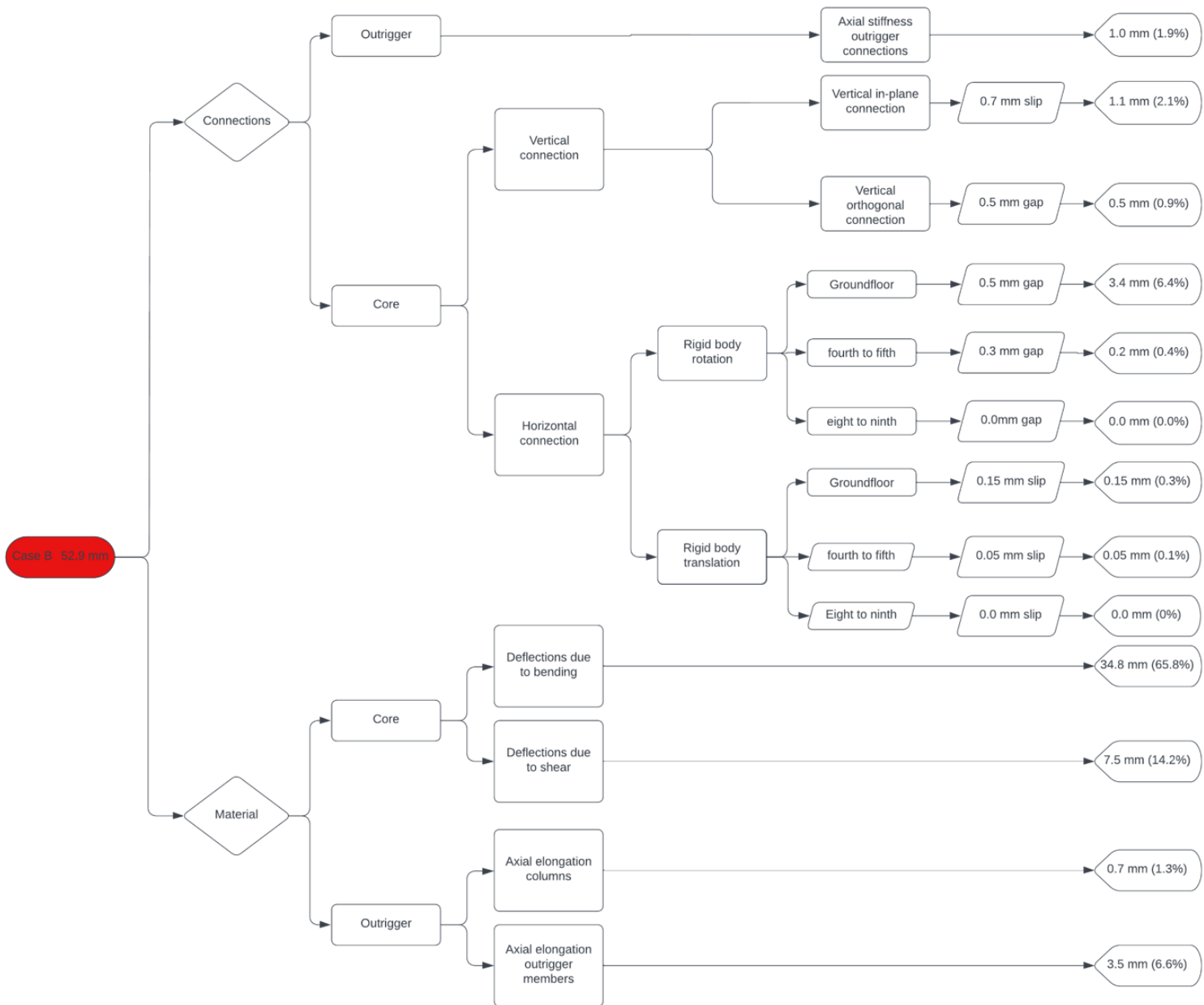


Figure 5.15. Origin of translations case B

Forces in the connections

In this section the influence of the addition of the outrigger on the forces in the core connections are discussed.

Comparing the axial forces in the horizontal connection as shown in table 5.11. It can be seen that a reduction of maximum forces is present due to the addition of the outrigger.

Table 5.11. *Maximum axial force horizontal connections*

	tensile force [kN]	compressive force [kN]
Case B		
ground floor	+1290(-8.2%)	-2168(-4.2%)
fourth to fifth	+271(-44%)	-796(-10%)
eight to ninth	+102(-58.9%)	-390(-2.7%)
Case A		
ground floor	+1405	-2263
fourth to fifth	+484	-884
eight to ninth	+248	-401

Table 5.12. *Maximum shear force horizontal connections*

	Case A	Case B
shear force [kN/m]		
ground floor	390	372 (-4.5%)
fourth to fifth	287	269(-6.3%)
eight to ninth	103	92 (-10.6%)

Table 5.13. *Maximum shear force vertical connections*

	Case A	Case B
shear force [kN/m]		
in-plane	328	261 (-20.4%)
orthogonal	250	202 (-19.2%)

From table 5.13 it can be seen that the forces in the vertical connections of the core have been reduced by approximately 20%. Since the connection has been designed based on ULS the spacing between the screws can be increased by 20% which would provide enough strength to carry the design loads. What is interesting to note however is that increasing the spacing by 20% does not have a large effect on the interaction factors of the core as can be seen in table 5.14.

Table 5.14. *Interaction factors*

		K [kN/mm]	s [mm]	γ
Vertical orthogonal	$\gamma_{1.1}$	89.4	260	0.988
Vertical orthogonal	$\gamma_{1.2}$	89.4	260	0.976
Vertical in-plane	γ_2	46.2	130	0.968
+20% spacing				
Vertical orthogonal	$\gamma_{1.1}$	89.4	312	0.985(-0.3%)
Vertical orthogonal	$\gamma_{1.2}$	89.4	312	0.972(-0.4%)
Vertical in-plane	γ_2	46.2	156	0.962(-0.6%)

Calculating the analytical deflection of the CLT core similar as in section 5.1.1 results in a deflection of 78.9 mm, compared to the 78.6 mm previously found, which is only 0.3 mm higher. The influence of increasing the spacing on the global deflections has been verified with numerical models in

which the deflections are increased by 0.2 mm when the spacing in the vertical orthogonal and in-plane connections is increased by 20%.

Behaviour of the outrigger

In this section the behaviour of the outrigger is discussed, first the deflections of the outrigger are discussed and secondly the forces in the outrigger are discussed. Contributions to the deflections and forces in the outrigger are subdivided into contributions due to lateral wind loading and contributions due to vertical loading of the structure.

In figure 5.16 the vertical displacement of the outrigger is shown due to wind loads, vertical loading and finally a combination of wind and vertical loads. In table 5.15 the vertical displacement of the nodes are given due to lateral wind loading, from this table it can be seen that the displacement of the inner and outer column row is approximately equal to 1 mm. For the loaded side the displacement is upwards while for the opposite side the displacement is downwards resulting in tensile and compressive loads in the columns respectively.

While in table 5.15 it can be seen that the displacement due to vertical loading of the inner column row is equal to 12.5 mm while the displacement of the outer column row is 9 mm. The larger displacement in the inner column row is due to a higher load transfer in the column which causes a larger axial deformation. Additionally it can be seen that the axial shortening in the core is 2 mm due to vertical loads, resulting in an average axial shortening difference between columns and core of 8.8 mm.

Table 5.15. *Vertical displacements of the outrigger*

	left outer column	left inner column	left side core	right side core	right inner column	right outer column
wind loading	0.9 mm ↑	0.9 mm ↑	2.5 mm ↑	1.9 mm ↓	1.1 mm ↓	0.9 mm ↓
vertical loading	9.0 mm ↓	12.5 mm ↓	2.0 mm ↓	2.0 mm ↓	12.5 mm ↓	9.0 mm ↓
combination	8.1 mm ↓	11.6 mm ↓	0.5 mm ↑	3.9 mm ↓	13.6 mm ↓	9.9 mm ↓

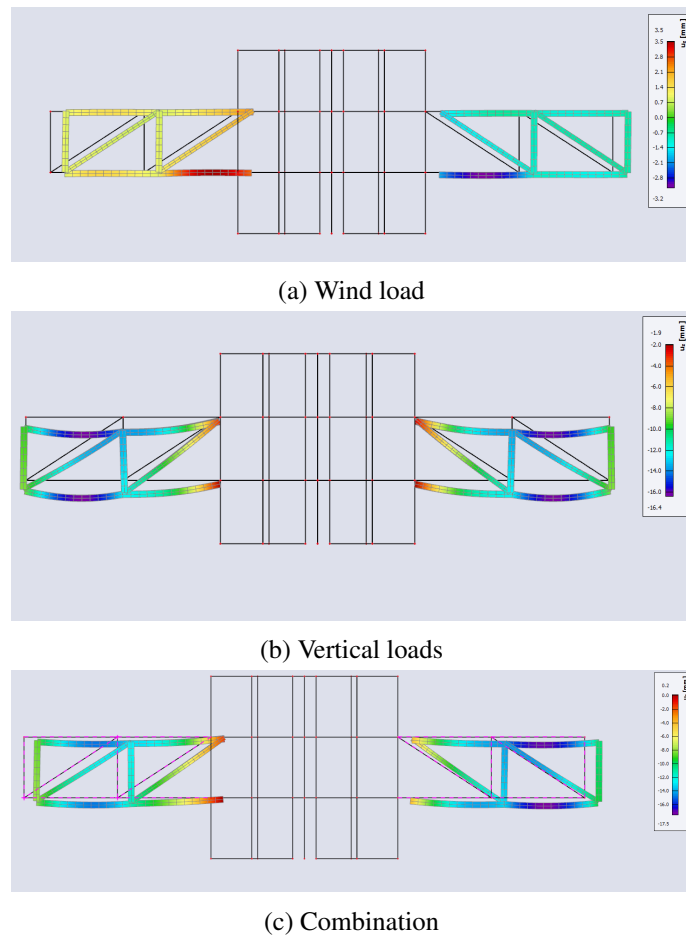
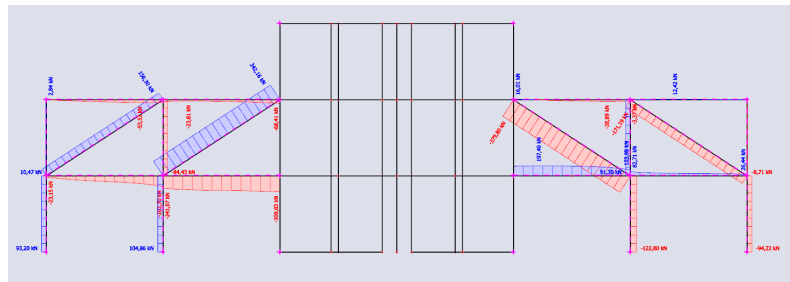


Figure 5.16. *Vertical displacement of the outrigger*

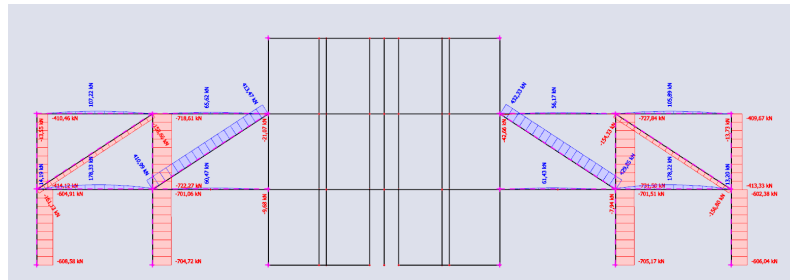
In figure 5.17 the axial force in outrigger members is shown. In figure 5.17a the forces are shown due to lateral wind loading, it can be seen that compressive forces in the diagonals are slightly larger than tensile forces. Which is likely due to the axial stiffness of the connection, which is only activated in tension resulting in a lower outrigger stiffness for the tensile side, resulting in a slightly larger compressive force in the columns. Additionally it can be seen that inner column row transfers a higher load than the outer column row. The total bending moment which is transferred from core to columns is equal to 6105 kNm.

Vertical loading of the structure results in a tensile force of approximately 420 kN in the inner diagonal while the outer diagonal transfers a compressive force of 150 kN as can be seen in figure 5.17b.

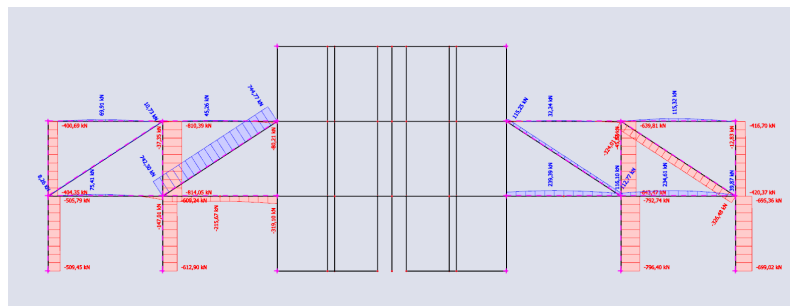
Combining both lateral and vertical loads it is shown that compressive forces in the column are not decreased enough to reach the tensile regime, as can be seen in figure 5.17c. Additionally it can be seen that the force in the outer diagonal on the left side of the core is reduced after combining vertical and lateral loading, while the tensile force on the inner diagonal is increased. At the right side of the core the force in the inner diagonal is reduced while the force in the outer diagonal is increased.



(a) Wind load



(b) Vertical loads



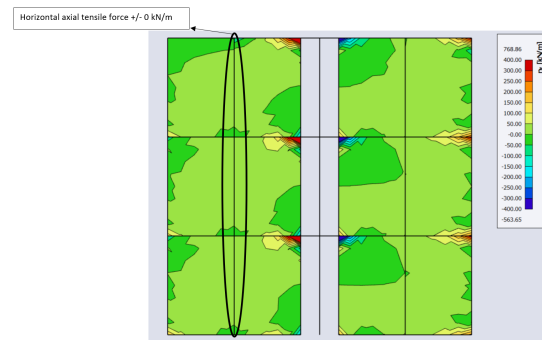
(c) Combination

Figure 5.17. Forces in members of the outrigger

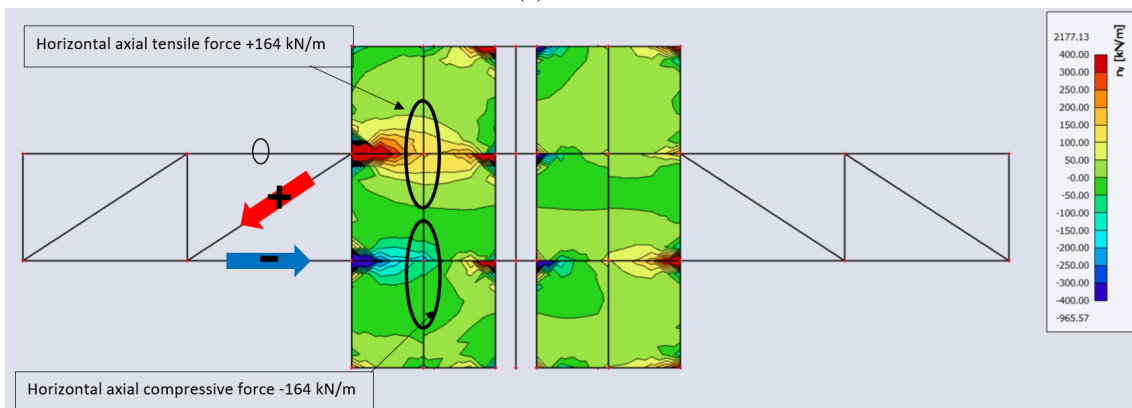
Behaviour of the core at outrigger level

In this section the behaviour of the core at outrigger level is assessed. Due to the addition of the outrigger, forces within the core may change with regards to case A.

During the design of the vertical connections, orthogonal and in-plane, the assumption has been made that wall sections remain in contact during loading since only compressive horizontal forces are present. The horizontal forces at outrigger level and adjacent floors, floor six, seven and eight, are shown in figure 5.18.



(a) Case A



(b) Case B

Figure 5.18. Horizontal axial forces n_y in the core at outrigger level

In figure 5.18a it can be seen that for case A without outrigger the horizontal forces ' n_y ' in the vertical in-plane connection is equal to zero. When the outrigger is introduced forces in the horizontal direction at outrigger level differ, see figure 5.18b. It can be seen that at the left hand side a compressive and tensile force is introduced, in the lower beam and diagonal respectively, with the values shown in figure 5.17c. The compressive force can be transferred through contact between the in-plane wall sections. While the tensile force, with a maximum value of 164 kN/m, in the in-plane connection needs to be taken up by the inclined and straight screws.

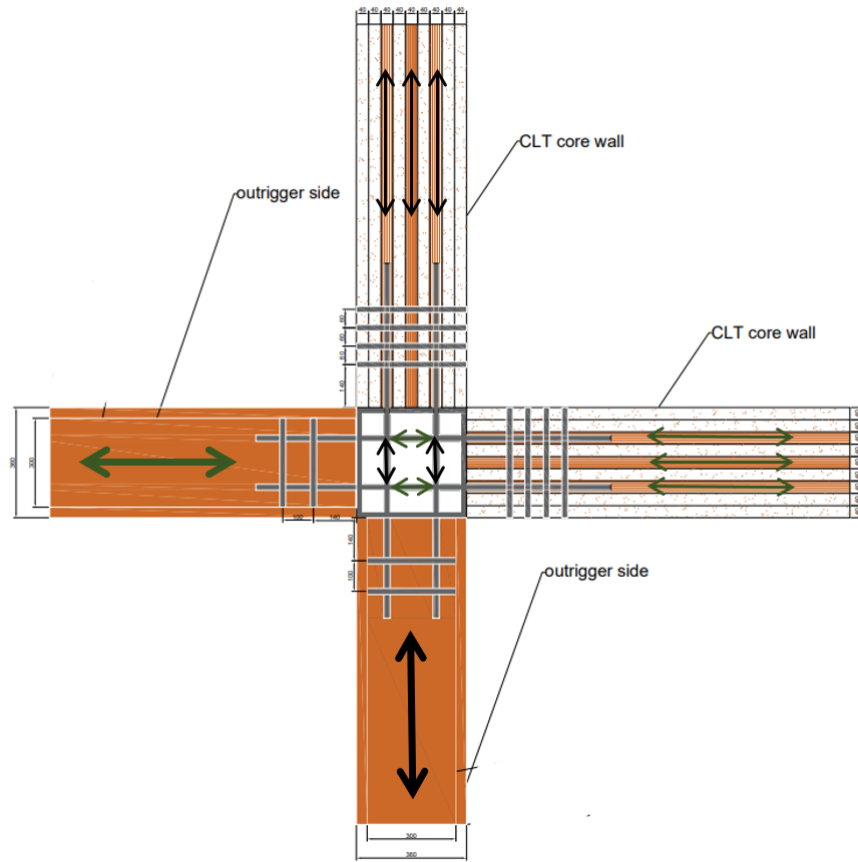


Figure 5.19. Force transfer outrigger to core , top view

The horizontal forces are transferred through the three horizontally orientated layers with a total thickness of 120 mm as can be seen in figure 5.19. Additionally it can be seen that the outrigger transfers forces to the in-plane CLT core wall, indicated with black and green direction. It can be seen in equation 5.2 and 5.3 that the horizontal layers are sufficiently strong to carry the transfer the tensile loads.

$$f_{t,0,d} = k_{mod} * \frac{f_{t,0,k}}{\gamma_M} = 10.1 \text{ N/mm}^2 \quad (5.2)$$

$$\sigma_{t,d} = \frac{N_{t,y}}{A} = 1.4 \text{ N/mm}^2 \leq f_{t,0,d} \quad (5.3)$$

In equations 5.4 and 5.5 it can be seen that the compressive stresses can be transferred through the horizontal layers, based on a maximum horizontal compressive force of 200 kN/m.

$$f_{c,0,d} = k_{mod} * \frac{f_{c,0,k}}{\gamma_M} = 15.1 \text{ N/mm}^2 \quad (5.4)$$

$$\sigma_{c,d} = \frac{N_{c,y}}{A} = 1.7 \text{ N/mm}^2 \leq f_{c,0,d} \quad (5.5)$$

5.2.2 Dynamic response

The first eigenfrequencies for case B can be seen in figure 5.20, with the type of modes similar to the ones found for case A. However a shift in frequency is observed when compared to case A as can be seen in table 5.16.

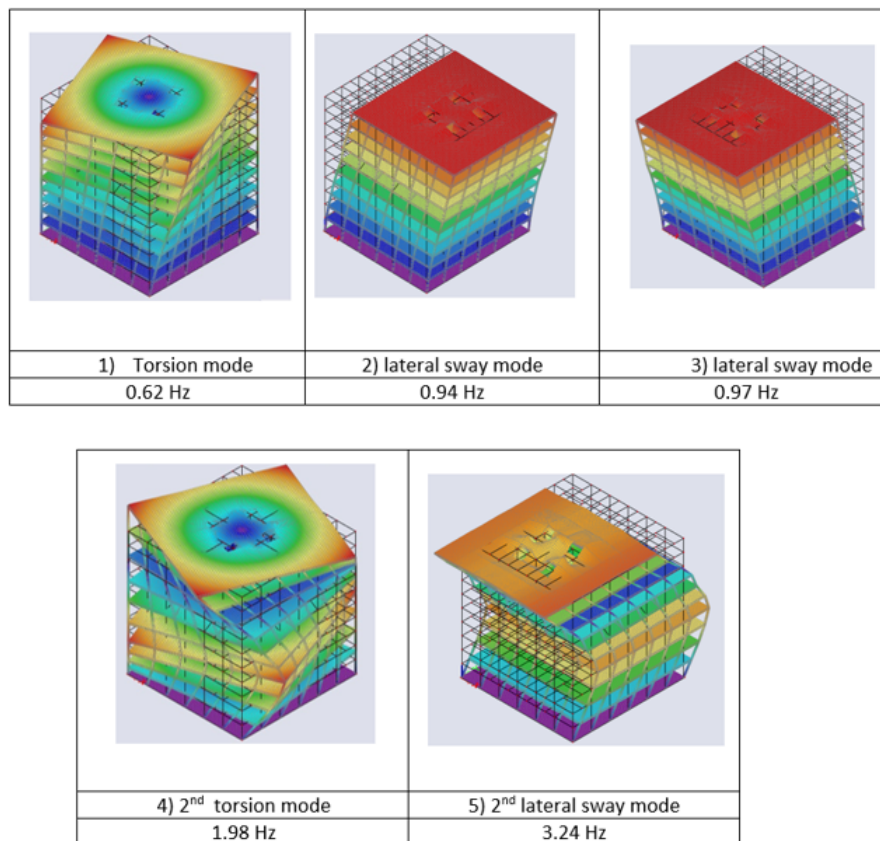


Figure 5.20. *Dynamic response case B*

Table 5.16. *Eigenfrequencies lateral sway modes case B*

	x-direction [Hz]	y-direction [Hz]
Case A	0.86	0.89
Case B	0.94(+9.3%)	0.97(+9.0%)

The increase in eigenfrequencies results in a decreased peak lateral acceleration as can be seen in table 5.17. The peak accelerations are reduced by 10.1 % due to the addition of the outriggers.

Table 5.17. *Peak lateral acceleration case B*

	acceleration [m/s^2]
case A	0.076
case B	0.069 (-10.1%)

Similar to case A the first mode is a torsional mode and is disregarded in the calculation of the along wind peak lateral acceleration on the basis of being anti-symmetric while the wind load is symmetric.

Simplified calculation

A simplified model is made in the software matrixframe using the previously calculated analytical bending stiffness of the core as shown in section 5.1.1. Results are shown in table 5.18 with assumptions for the model shown in Appendix B.

Table 5.18. *Result analytical vs numerical calculation outrigger*

type	deflection [mm]	deflection [mm]
	analytical/simplified	numerical
horizontal connections included	no	yes
without outrigger	78.6	61.8
with outrigger	53.3(-32%)	49(-20.7%)

The simplified model provides a upper bound value of the influence of the addition of an outrigger to a CLT core building.

5.2.3 Sensitivity analysis case B

During the sensitivity analysis the influence of different design parameters on the stiffness of the structure are assessed. Starting with the member size of both the outrigger and column, secondly the stiffness of the connections of the outrigger, thirdly the height of the outrigger and finally the orientation of the system itself.

Column size

In this section the influence of the inner and outer column connected to the outriggers is assessed, the related columns can be seen in figure 5.21.

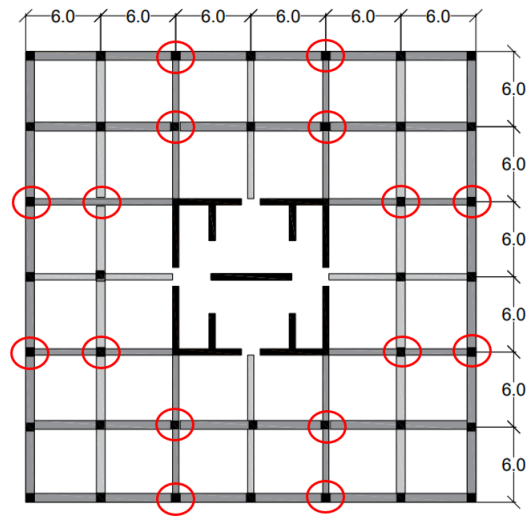


Figure 5.21. Columns connected to the outrigger

The influence of the column size on the global stiffness is assessed three separate models, the first model which is the regular case B design, which has a column size of 400x400 mm. The second model use a column size in which the cross sectional area is increased by 25% resulting in a column of 450x450 mm. The third model makes use of a column size of which the cross sectional area is increased by 50 % compared to case B, 490x490 mm. The numerical results of the different models are shown in table 5.19.

Table 5.19. Influence of the column size on the lateral deflection

Case B	column size	maximum deflection	% with regards to case B
	400x400 mm	52.9 mm	-
25% increase	450x450 mm	52.9mm	0%
50% increase	490x490 mm	52.9mm	0%

From the results it is immediately apparent that the column size does not influence the lateral deflection, at least not for the cases that the column size is increased by 25% and 50%.

Outrigger size

similar to the column size sensitivity discussed in the previous section the influence of the size of the outrigger is checked on the lateral deflection. Case B is compared to a model with a 25 % increased member size of the outrigger and a model with a 50% increased member size of the outrigger. The numerical results of the different models are shown in table 5.20.

Table 5.20. Influence of the outrigger size on the lateral deflection

Case B	column size	diagonal size	beam size	deflection	% with regards to case B
	400x400 mm	360x300mm	300x400mm	52.9 mm	-
25% increase	450x450 mm	360x375mm	360x415mm	52.5mm	-0.8%
50% increase	490x490 mm	360x500mm	360x450mm	52.2mm	-1.3%

From the results it is shown that increasing the cross sectional areas of the outrigger by 25% and 50% leads to a reduction of lateral deflection by 0.8% and 1.3% respectively. The models used do not include changes to the stiffness related to the connection of the outrigger, additionally column size of the columns outside of the outrigger remain the same as in case B.

Connection stiffness

The influence of the connection stiffness of the outrigger is assessed by comparing case B to a model with double the amount of dowels and a rigid model. The connections of the outrigger can be seen in figure 5.22.

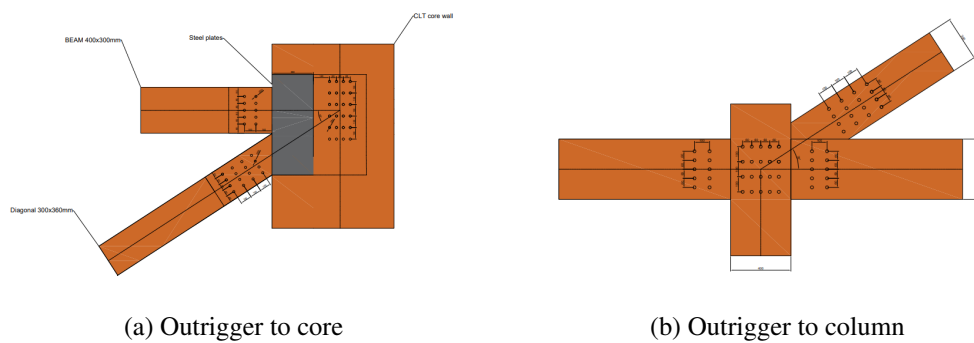


Figure 5.22. Overview outrigger connections

The modelling assumptions used in the model are shown in table 5.21.

Table 5.21. Boundary conditions outrigger connection , sensitivity analysis

	dowel rows	u_x	u_y	u_z	ϕ_x	ϕ_y	ϕ_z
Case B							
beam	2	rigid	262 kN/mm/m	rigid	rigid	pinned	pinned
diagonal	4	rigid	420 kN/mm/m	rigid	rigid	pinned	pinned
double stiffness							
beam	4	rigid	524 kN/mm/m	rigid	rigid	pinned	pinned
diagonal	8	rigid	840 kN/mm/m	rigid	rigid	pinned	pinned
rigid							
beam	-	rigid	rigid	rigid	rigid	pinned	pinned
diagonal	-	rigid	rigid	rigid	rigid	pinned	pinned

The results of the models are shown in figure 5.23 and table 5.22

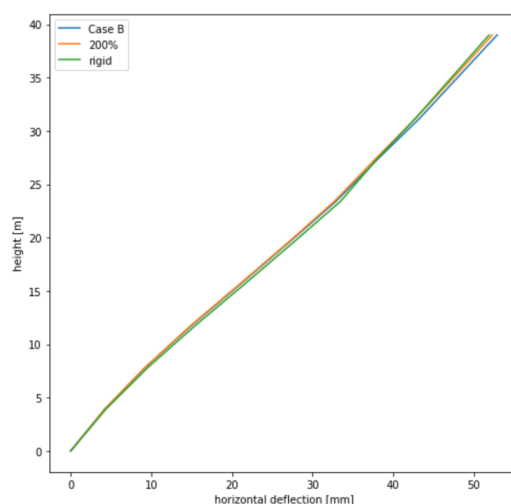


Figure 5.23. Influence of the connection stiffness of the outrigger on lateral deflection

Table 5.22. Influence of the connection stiffness of the outrigger on the lateral deflection

	deflection [mm]	% with regards to case B
Case B	52.9	-
double stiffness	52.3	-1.1%
Rigid	51.9	-1.9%

From the results shown above deflection is reduced by 1.1% if the amount of dowels is doubled and thus the stiffness of the connection is doubled. Additionally it is shown that if the connections are modelled as rigid the deflections can be reduced by 1.9%.

Combined member size and connection stiffness

In this section the influence of a combined increase of the column and outrigger size and the connection stiffness on the global stiffness is assessed. The column and outrigger sizes are increased by 25% and 50% similar as in the section 5.2.3. The stiffness of the connections are also increased by 25% and 50% as shown in table 5.23 which is equal to an additional one or two rows of dowels respectively.

Table 5.23. Boundary conditions outrigger connection , sensitivity analysis

	dowel rows	u_x	u_y	u_z	ϕ_x	ϕ_y	ϕ_z
Case B							
beam	2	rigid	262 kN/mm/m	rigid	rigid	pinned	pinned
diagonal	4	rigid	420 kN/mm/m	rigid	rigid	pinned	pinned
+25% stiffness							
beam	2.5	rigid	327.5 kN/mm/m	rigid	rigid	pinned	pinned
diagonal	5	rigid	525 kN/mm/m	rigid	rigid	pinned	pinned
+50% stiffness							
beam	3	rigid	393 kN/mm/m	rigid	rigid	pinned	pinned
diagonal	6	rigid	630 kN/mm/m	rigid	rigid	pinned	pinned

Results of the different models are shown in table 5.24.

Table 5.24. *Influence of the connection stiffness of the outrigger on the lateral deflection*

	deflection [mm]	% with regards to case B
Case B	52.9	-
+25%	52.3	-1.1%
+50%	51.8	-2.1%

Increasing both the member sizes and amount of dowels in the connection related to the outrigger system by 25% and 50% reduces deflections by 1.1% and 2.1% respectively.

Material stiffness

The influence of the material stiffness is assessed by changing the outrigger and adjacent columns from GL28h to GL32h to check to influence of the increased modulus of elasticity. The different material strengths grades have different mean values for the Youngs modulus, according to table 2.2 the values for $E_{0,g,mean}$ are 12600 and 14200 Mpa for GL28h and GL32h respectively.

The maximum deflection for the case that GL32h is used is equal to 52.7 mm which is only 0.2mm less then the case in which GL28h is used. Since the cost of GL32h is higher then that of GL28h, it is not likely that changing the material properties leads to an cost effective method of decreasing deflections.

Type of outrigger

Two different types of outrigger are assessed namely a truss type and a shear wall type. The shear wall is constructed of similar build up of CLT connecting the core to the columns. It should be noted that the assumption is made that a similar connection as the panel to foundation connection will be sufficient in transferring the forces from core to outrigger wall and vice versa. The orientation is that of vertical core wall rotated by 90 degrees, such that the vertical fibres lay in horizontal direction. The deflection of both types of outriggers can be seen in figure 5.24.

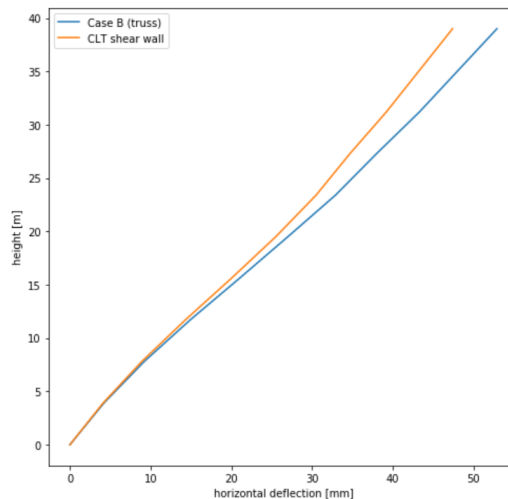


Figure 5.24. Deflection of CLT the shear wall outrigger

The maximum deflection of the wall outrigger is 47.4 mm which is 5.5 mm or 10.4 % lower than the deflection of case B which shows the effectiveness of the system. It should be noted however that such a system drastically reduces the open floor area of the storey at which the system is applied. Having openings in the outrigger wall will allow for transportation across rooms but will likely have large effects on the effectiveness of the system. Additionally the amount of timber needed for this system is higher than that of the truss.

Additionally changing the type of outrigger will have the following influence, while stiffness is increased compared to a truss type outrigger the type of force on the connection between core and outrigger is changed. For the truss type an axial and compressive force is transferred to the core while a shear wall will transfer a bending moment, the values of the resulting horizontal force can be seen in figure 5.25. Comparing the force per meter length to that of the truss the following observations can be made. The maximum tensile force per meter length for the shear wall outrigger is equal to 1200 kN/m, while the maximum tensile force (750 kN) in the truss is transferred through the diagonal of the outrigger at a vertical member height of 360 mm resulting in a maximum tensile force per meter length of 1747 kN/m. Therefore it can be said that introduction of a shear wall as an outrigger will reduce tensile requirements on the dowels compared to a truss type. A shear wall type is able to more effectively spread out the stresses over the height of the connection, while a truss results in higher local stresses.

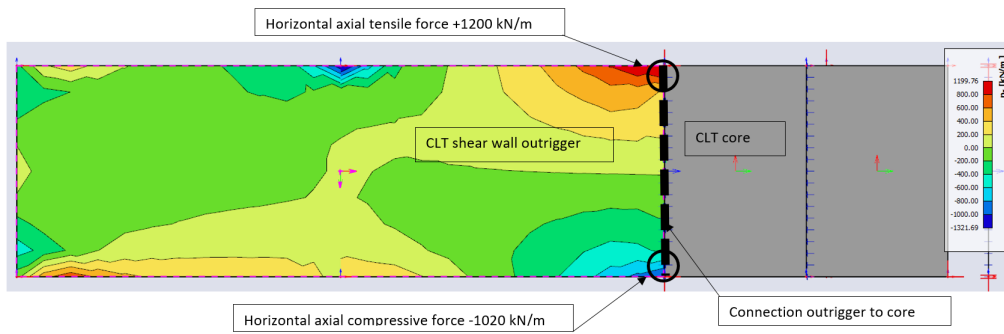


Figure 5.25. Horizontal force in the outrigger to core connection

Location of the outrigger

The influence of the location of the outrigger is assessed by placement of the outrigger at the fourth, fifth, sixth, seventh (Case B), see figure 5.26b, and eighth floor. The deflection of the different cases is shown in figure 5.26a and the maximum deflection is shown in table 5.25.

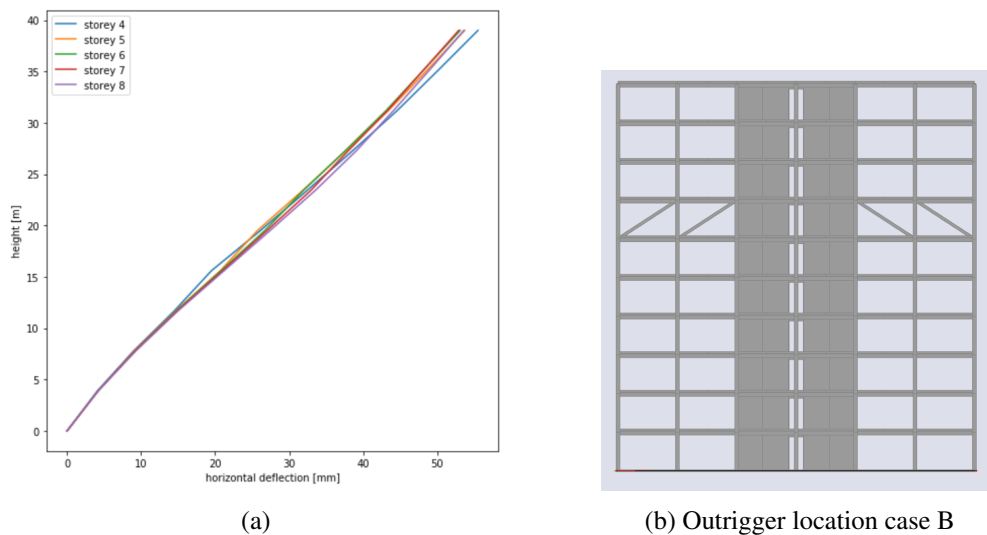


Figure 5.26. Lateral deflection of the structure with different heights of the outrigger

Table 5.25. Influence of the location of the outrigger on the lateral deflection

	deflection [mm]	% with regards to case B
Case B(seventh floor)	52.9	-
fourth floor	55.5	+5.4%
fifth floor	53.7	+1.5%
sixth floor	53.1	+0.4%
eighth floor	53.6	+1.3 %

According to literature the optimum height of the outrigger was at 49 % of the building height for displacement optimization. From the results shown above for a glulam outrigger to a CLT core the optimum height can be found at seventh floor for a 10 storey building, which is at 58.5 % of the

building. This shows there is an upwards shift of the optimum location for an outrigger in a timber building versus a concrete/steel building.

Outrigger truss configuration

Different outrigger truss configurations are modelled to investigate the influence it has on the deflection of the structure. The different configurations modelled are shown in figure 5.27.

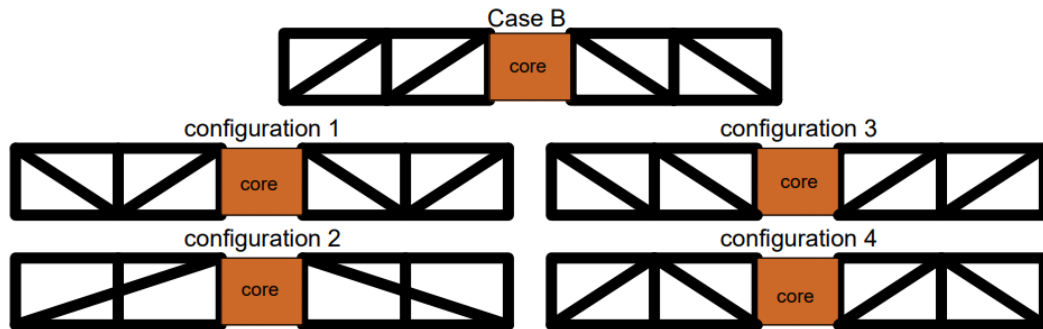


Figure 5.27. One storey outrigger configurations

Modelling of the connection and member sizes is based on the member size of the diagonal of 360 by 300 mm with the spring stiffness as calculated in section 3.10.

The deflections of the different truss configuration can be seen in figure 5.28. The maximum deflection of the different configurations are found in table 5.26.

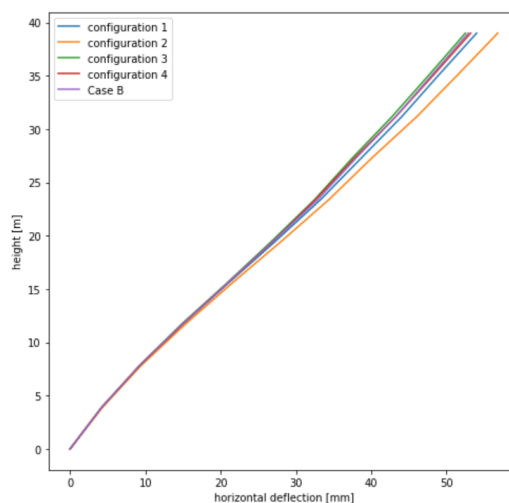


Figure 5.28. Lateral deflection of the outrigger truss configurations

Table 5.26. Influence of the location of the outrigger on the lateral deflection

	deflection [mm]	% with regards to case B
Case B	52.9	-
configuration 1	54.0	+2.0%
configuration 2	56.8	+7.4%
configuration 3	52.5	-0.8%
configuration 4	53.2	+0.6%

Configuration 3 provides the lowest maximum deflection of the structure and reduces overall deflection by 0.8%. Difference between the configurations is noticeable, especially configuration 2 has a large negative effect on the maximum stiffness. This is largely due to the reduced angle of the diagonal from 33° to 18°.

Two storey outrigger truss configuration

In this section the influence of the outrigger configuration for a two storey tall truss will be assessed. From the forces in the truss of the Case B design as shown in figure 3.30 most of the forces on the tensile (left) side are transferred to the inner column, which reduces the lever arm of the bending moment and as a result the effectiveness of the system is reduced. Therefore it is proposed to increase the height of the outrigger to two storey to have a member directly connecting the core to the outer column, while not reducing the angle of the diagonal. Four different designs are made which are shown in figure 5.29.

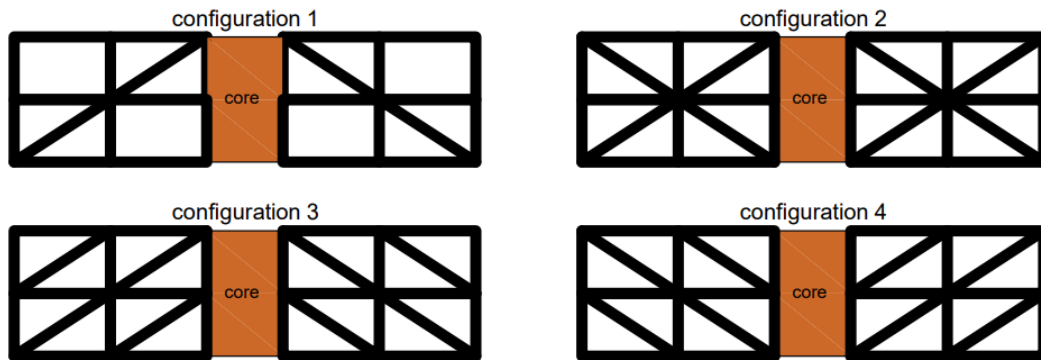


Figure 5.29. Two storey outrigger configurations

The lateral deflection of the different configurations can be seen in figure 5.30 and the values for the maximum deflections can be found in table 5.27.

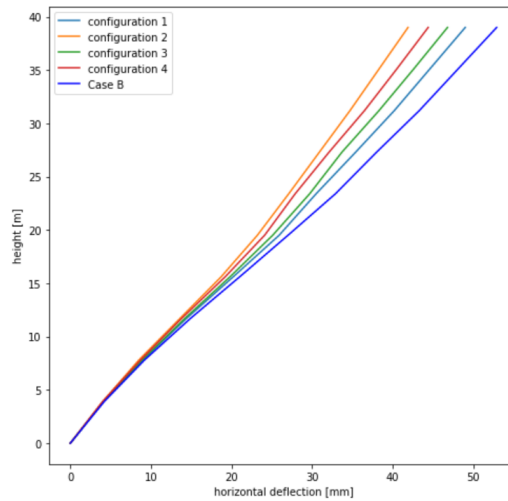


Figure 5.30. Lateral deflection of the two storey tall outrigger truss configurations

Table 5.27. Influence of the location of the outrigger on the lateral deflection

	deflection [mm]	% with regards to case B
Case B	52.9	-
configuration 1	49	-7.4%
configuration 2	41.9	-20.8%
configuration 3	46.8	-11.5%
configuration 4	44.4	-16.6%

The deflection of the outrigger system can be reduced by increasing the storey height of the truss, allowing for a direct line between the outer column and the core. By shifting the outer diagonal one storey down in comparison to the design of case B, as shown in figure 5.29 configuration 1, the deflections of the structure can be reduced by 7.4 %. Configuration two reduces the maximum deflections by 20.8 % to 41.9 mm, which is almost sufficient for the 40 mm deflection limit.

The maximum deflection of the structure can be decreased by 32.2 % when compared to case A without outrigger, while a single storey outrigger reduces deflections by 15.1 %. Which highlights the significance of have a two storey tall outrigger.

Effectiveness of the outrigger system

In this section the influence of the outrigger stiffness on the lateral deflections and peak lateral accelerations is discussed. For each of the before mentioned outriggers the effective bending stiffness is calculated in Appendix L, which includes the calculation method and relevant data needed from each different case. The effective bending stiffness of 10 different cases is determined, four two storey outriggers, six one storey outriggers of which one shear wall type outrigger. The ratio of effective bending stiffness of outrigger to core is determined and plotted on the x-axis with the maximum lateral deflections and normalized lateral deflections on the y-axis as shown in figure 5.31a and 5.31b respectively, after which an exponential curve is fitted to the processed

data. A similar approach is used to determine the influence of the stiffness ratio on the peak lateral acceleration as can be seen in figure 5.31c and in figure 5.31d with normalized values

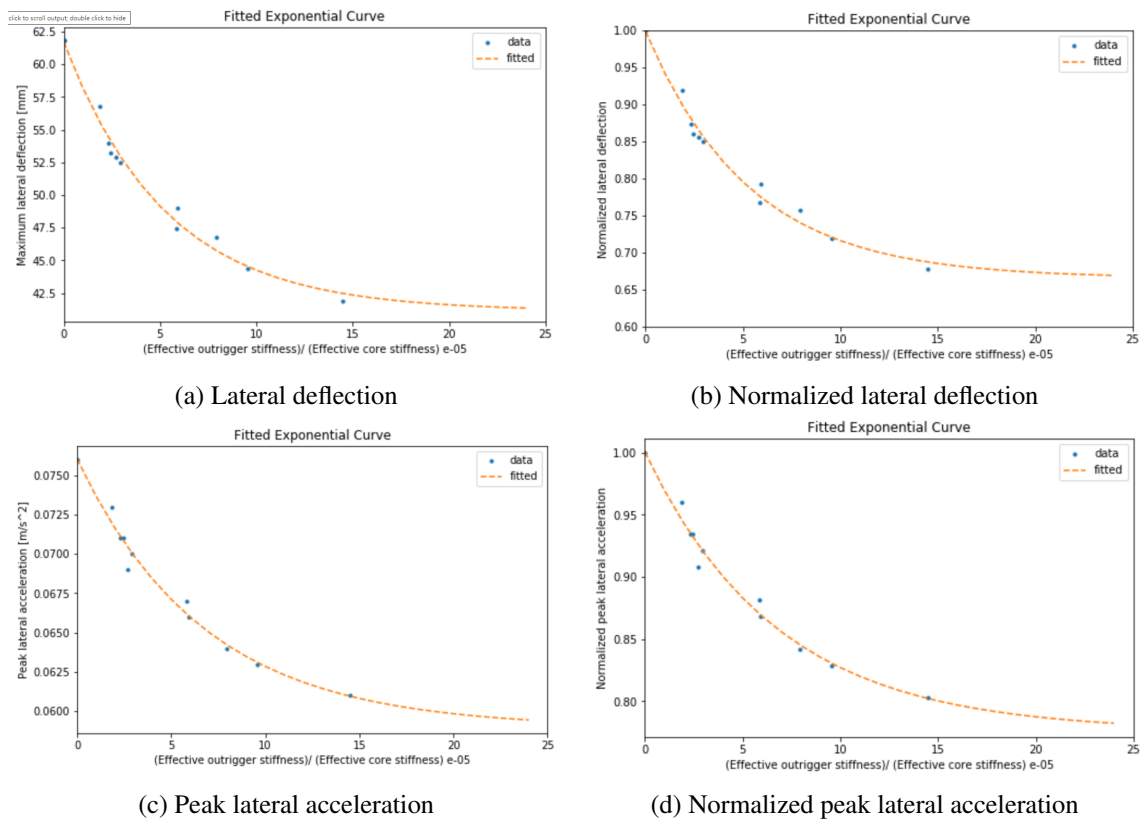


Figure 5.31. Fitted curves influence of stiffness ratio

In figure 5.31a it can be seen that for a stiffness ratio close to zero the deflection is equal to the deflection of case A, 61.8 mm. For a high outrigger stiffness and as a result a higher stiffness ratio the maximum lateral deflection is close to 41 mm and 0.66 for a normalized deflection. For the case of accelerations the normalized value for the peak lateral acceleration becomes 0.77. In this case the outrigger can be assumed as an infinitely rigid beam. Even though some scatter occurs it can be seen that an exponential fit closely follows the data points plotted in the figure. From the graph it can be seen that increase the stiffness ratio from 0 to 10×10^{-5} will have a large effect on the later deflection, namely 28% reduction. While increasing the stiffness ratio from 10 to 20×10^{-5} will only result in a reduction in deflections of 5%. Similar observations can be made for the influence of the stiffness ratio on the peak lateral accelerations.

By mirroring the normalized exponential relationships around the x-axis and changing the values on the y-axis from 0 to 100% an estimation of the effectiveness of a specific outrigger design can be made according to figure 5.32 on terms of maximum lateral deflection and peak lateral accelerations. In which 0% represents the case that the outrigger has no bending stiffness, i.e. non-existent. While 100% represents the case that the outrigger has an infinitely high bending stiffness.

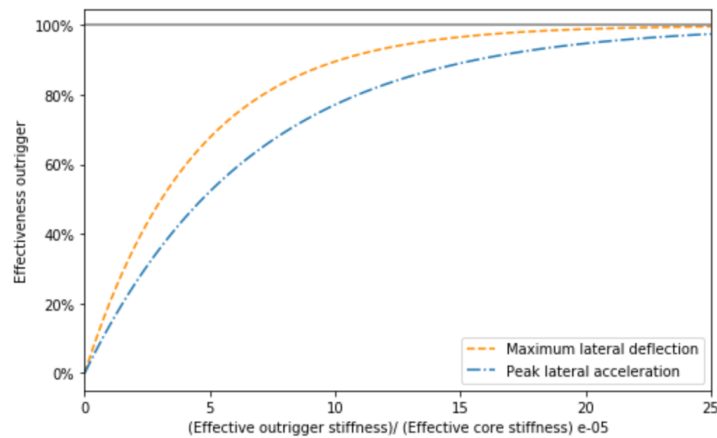


Figure 5.32. *Effectiveness outrigger*

5.2.4 Conclusion results case B

The following conclusions are made based on the results from case B.

- A 10 storey CLT core with a one storey timber outrigger designed based on ULS does not provide sufficient stiffness to meet the SLS requirement on deflections.
- Similar to case A the most critical connection in terms of deflections is the connection between the core and foundation. In which rigid body translations are responsible for 6.4% of the total deflections.
- Implementation of the outrigger leads to a reduction in forces in the core. Redesign of the vertical orthogonal and in-plane connection, by increasing the spacing by 20%, increases global deflections only by 0.4%.
- Introducing an outrigger to a CLT core system introduces horizontal loads in the core at outrigger level, these loads need to be taken up in the vertical in-plane connection between CLT panels.
- Peak lateral accelerations are decreased by 10% due to the addition of the outrigger system while the first eigenfrequencies for lateral sway modes are increased by 9 %.
- Increased member size of the column showed to have little effects on lateral deflections, while an increase in member size of the outrigger truss by 25 % and 50% reduced deflections by 0.8% and 1.3%.
- Increasing the stiffness of the connections in the outrigger truss by doubling the amount of dowels reduces deflections by 1.1%.
- A combined increase of outrigger member size and connection stiffness by 25% and 50% reduces deflections by 1.1% and 2.1% respectively.
- A CLT shear wall type outrigger is able to reduce deflections more effectively than a truss type outrigger. However the open floor area is drastically reduced by implementing a closed outrigger system.
- Optimum location of the outrigger was found to be at 58.5 % of height of the structure for a 10 storey timber building.

- Reducing the angle of the diagonal of the outrigger reduces the overall effectiveness of the system. An increase of deflections of 8% is observed when the diagonal connects the outer column directly to the core, instead of outer column to inner column and inner column to core.
- Two storey outriggers are able to more than double the reduction of lateral deflections compared to a single storey outrigger. A reduction of deflections of 32.2 % and 15.1% is observed when a two and one storey outrigger is implemented in the CLT core building compared to the deflections of the core itself.
- Due to the addition of the outrigger forces in the vertical connections in the core are reduced by 20%. Decreasing the amount of screws by 20% does not have a large influence on the interaction factor between walls, the increase in lateral deflections is 0.4%.
- The influence of the outrigger to core effective bending stiffness ratio on both the lateral deflections and peak lateral accelerations was evaluated. An exponential fit provided a close fit to the data points.
- An estimation can be made of the effectiveness of a specific stiffness ratio in terms of reducing deflections and lateral accelerations. With lower and upper bound effectiveness representing zero and infinite bending stiffness of the outrigger respectively.

5.2.5 Discussion results case B

Connection design of the different configurations of outriggers both one and two storey configurations is based upon the design for case B. The numerical results showed that the dowelled connection provided adequate strength to support the loads from various outrigger configurations.

5.3 Results case C

In this section the results of Case C are discussed, additionally the design of case C is discussed based on sensitivity analysis results of case A and B.

Design of case C

Design of case C is based upon the results obtained from the sensitivity analysis of case A and B as shown in chapters 5.1.3 and 5.2.3 respectively. To further decrease the deflections to a value of 40 mm or lower the following changes are made to case B to obtain case C.

- It has been shown that a two storey outrigger is able to more than double the reduction in deflections compared to a single storey outrigger. Therefore it is proposed to implement a two outrigger with an X-configuration similar to configuration 2 as shown in figure 5.29, reducing the deflections to 41.9 mm.
- From both case A and case B it has been shown that the connection between foundation and core is critical and is responsible for 6.8% and 6.4% of total deflections due to rigid body rotation of the core. Therefore it is proposed to increase the stiffness of the horizontal ground floor connection by doubling the amount of dowels , from three to six rows of dowels. Which

decreases the deflections to 40.5 mm.

- Finally the member size of the diagonals and beams in the outrigger is increased by 25% in combination with an increased connection stiffness of 25%, which is equal to an additional dowel row in both members. Which decreases deflections further to below 40 mm.

5.3.1 Static response

In figure 5.33 it can be seen that case C provides sufficient global stiffness to meet the requirements on maximum deflection of 40 mm.

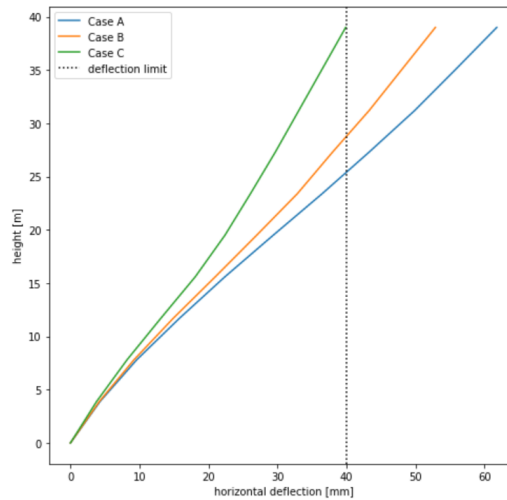


Figure 5.33. Deflection case C

In table 5.28 the results of the maximum deflection for the different case studies can be seen.

Table 5.28. Maximum deflections of case studies

	deflection [mm]	% with regards to case A
case A	61.8	-
case B	52.9	14.4%
case C	39.9	35.4%

Forces in the connections

In this section the influence of the addition of the two storey outrigger with X-configuration on the forces in the core connections are discussed.

Comparing the axial forces in the horizontal connection as shown in table 5.29. It can be seen that a reduction of maximum forces is present due to the addition of the outrigger two storey outrigger, reducing strength requirements on the horizontal core to core and core to foundation connection. Additionally the reduced forces in the horizontal connection result in a smaller vertical gap opening lowering the rigid body translations of the core.

Table 5.29. *Maximum axial force horizontal connections, case C*

	tensile force [kN]	compressive force [kN]
Case C		
ground floor	+1197(-14.8%)	-2109(-6.8%)
fourth to fifth	+133(-73%)	-593(-33%)
eight to ninth	+78(-69%)	-382(-4.5%)
Case B		
ground floor	+1290(-8.2%)	-2168(-4.2%)
fourth to fifth	+271(-44%)	-796(-10%)
eight to ninth	+102(-59%)	-390(-2.7%)
Case A		
ground floor	+1405	-2263
fourth to fifth	+484	-884
eight to ninth	+248	-401

Table 5.30. *Maximum shear force horizontal connections, case C*

	Case A	Case B	Case C
shear force [kN/m]			
ground floor	390	372 (-4.5%)	337 (-13.6%)
fourth to fifth	287	269(-6.3%)	261(-9%)
eight to ninth	103	92 (-10.6%)	92(-10.6%)

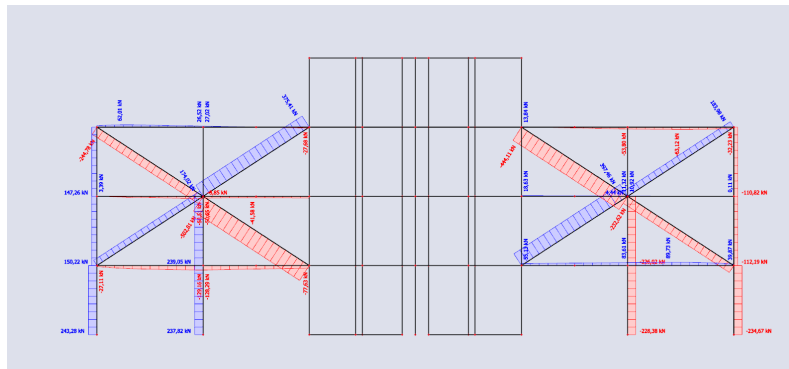
Table 5.31. *Maximum shear force vertical connections, case C*

	Case A	Case B	case C
shear force [kN/m]			
in-plane	328	261 (-20.4%)	218 (-33.5%)
orthogonal	250	202 (-19.2%)	170 (-32%)

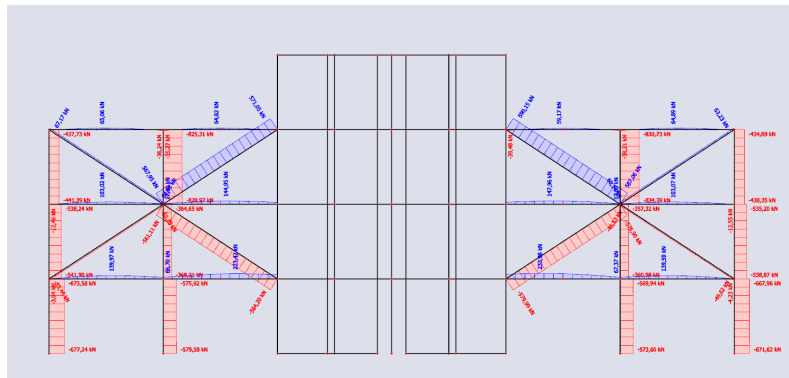
By implementation of the two storey outrigger (case C) the connection forces are further reduced compared to the case of a single storey outrigger (Case B) as can be seen in the tables above. In table 5.31 it can be seen that maximum shear forces in the vertical connections of the core are reduced by approximately 33%, further reducing strength requirements of the vertical connection of the core compared to a single storey outrigger. Spacing of the screws of the vertical core connections could be reduced further to decrease the amount of steel used, without having a large influence on the interaction factor of the different connections.

Forces in the outrigger

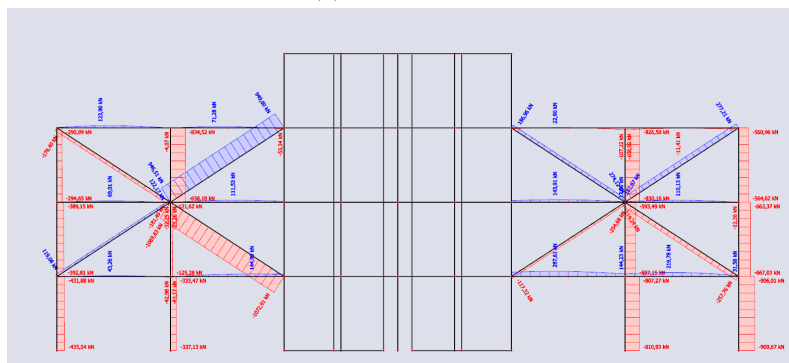
In this section the forces in the outrigger of case C are discussed. In figure 5.34c the maximum forces in the outrigger are shown while in 5.34a and 5.34b the forces due to wind and vertical loading are shown respectively.



(a) Wind load



(b) Vertical loads



(c) Combination

Figure 5.34. Forces in members of the outrigger of case C

It can be seen in figure 5.34a that the total amount of bending moment transferred from core to columns is around 14200 kNm, which is more than twice the amount of case B which was 6100 kNm respectively.

Behaviour of the core at outrigger level

In this section the behaviour of the core at outrigger level is assessed due to the addition of a two storey outrigger with X-configuration. The maximum forces can be seen in figure 5.35 with a tensile force in the upper outrigger to core connection and a horizontal force in the lower outrigger to core connection.

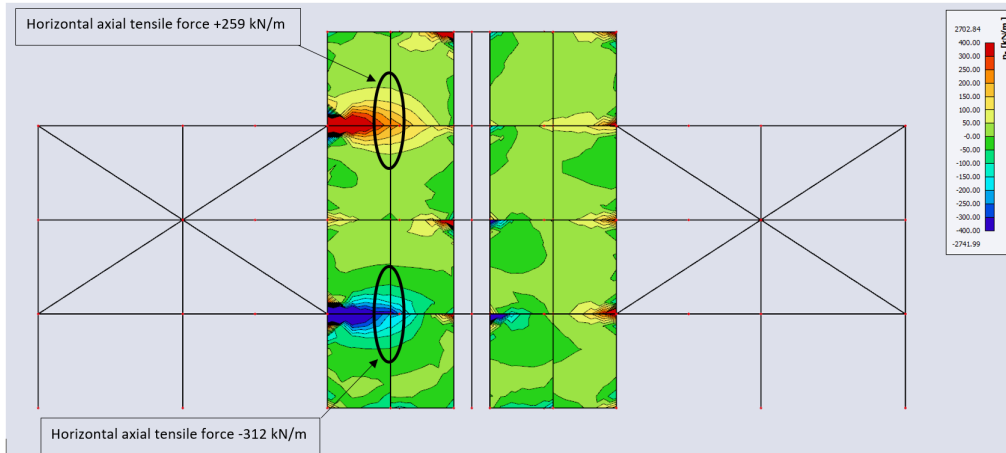


Figure 5.35. Horizontal axial forces n_y in the core at outrigger level, case C

The maximum horizontal stresses in the horizontally orientated layers are shown in equation 5.6 and 5.7. The forces induced by the outrigger can be transferred through the in-plane CLT panels. The current design of the vertical in-plane connection is sufficiently strong to carry the maximum horizontal tensile loads. However if the forces in the connection are increased further local reinforcement is needed to transfer the tensile loads from panel to panel.

$$\sigma_{t,d} = \frac{N_{t,y}}{A} = 2.2 \text{ N/mm}^2 \leq f_{t,0,d} \quad (5.6)$$

$$\sigma_{c,d} = \frac{N_{c,y}}{A} = 2.6 \text{ N/mm}^2 \leq f_{c,0,d} \quad (5.7)$$

5.3.2 Dynamic response

The first eigenfrequencies for case C can be seen in figure 5.36, the fifth mode is changed from second lateral sway mode to third torsional mode. The eigenfrequency of the lateral sway modes is increased by approximately 27-28% compared to case A as can be seen in table 5.32.

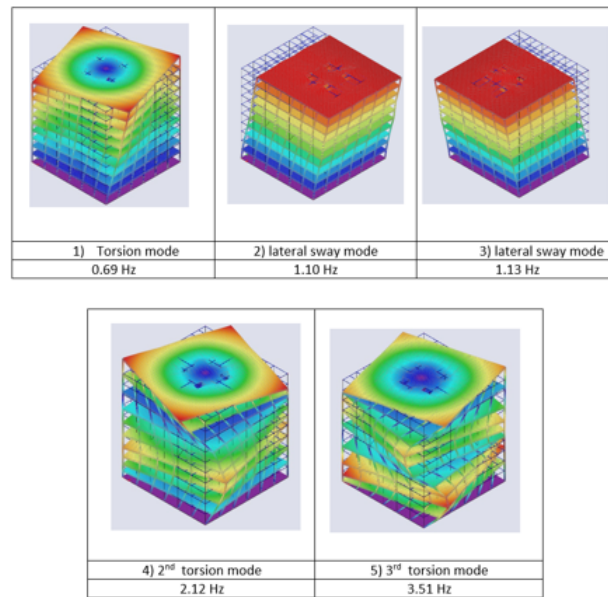


Figure 5.36. *Dynamic response case C*

Table 5.32. *Eigenfrequencies lateral sway modes case C*

	x-direction [Hz]	y-direction [Hz]
Case A	0.86	0.89
Case B	0.94(+9.3%)	0.97(+9.0%)
Case C	1.10(+27.9%)	1.13(+26.9%)

The increase in eigenfrequencies results in a decreased peak lateral acceleration as can be seen in table 5.33. The peak accelerations are reduced by 25 % due to the addition of the two storey outrigger.

Table 5.33. *Peak lateral acceleration case C*

	acceleration [m/s^2]
case A	0.076
case B	0.069 (-10.1%)
case C	0.057 (-25%)

Similar to case A and B the first mode is a torsional mode and is disregarded in the calculation of the along wind peak lateral acceleration on the basis of being anti-symmetric while the wind load is symmetric.

5.3.3 Conclusion results case C

The following conclusions are made based on the results from case C.

- A 10 storey CLT core with a two storey timber outrigger is able to provide sufficient stiffness

to meet the SLS requirement on deflections. The maximum later deflection is equal to 39.9 mm which is a reduction of 35.4% compared to case A.

- Due to the addition of the two storey outrigger forces in the vertical connections in the core are reduced by 33%.
- An overall reduction of forces in the connections can be observed when introducing a two storey outrigger compared to a single storey outrigger. Further decreasing the strength requirements on the connections of the core.
- The transfer of bending moment from core to columns is increased from 6100 kNm to 14200 kNm by implementing a two storey outrigger compared to single storey outrigger.
- Introducing an outrigger to a CLT core system introduces horizontal loads in the core at outrigger level, these loads need to be taken up in the vertical in-plane connection between CLT panels. By introducing a two storey outrigger the horizontal tensile stress is increased from 1.4 N/mm^2 to 2.2 N/mm^2 compared to a single storey outrigger in the horizontally orientated layers. Horizontal compressive stresses are increased from 1.7 N/mm^2 to 2.6 N/mm^2 . Tensile strength requirements on the vertical in-plane connection between core panels is further increased compared to a single storey outrigger.
- Peak lateral accelerations are decreased by 25% due to the addition of the two storey outrigger system while the first eigenfrequencies for lateral sway modes are increased by 27%.

6. Discussion

Limitations

The influence of the foundation is not included, therefore the results provided throughout the report reflect only on the behaviour of the structure. Not including the foundation reduces the accuracy of the results provided in this report, however the influence of the addition of the outrigger can still be assessed with a reasonable accuracy.

Throughout the design of the different case studies a similar core layout is used. The influence of increasing the core size has not been assessed in the sensitivity analysis. Increasing the core size will have a positive influence on the global stiffness of the structure, but will come at the cost of available net floor area, an increased amount of material and an increased amount of connections that are needed.

For the case studies in this research only the influence of a single outrigger is assessed, since the structure is only 10 storeys tall. Adding more outriggers will come at the cost of open floor area. If the use of the building is changed from office to residential the need for open floor area is reduced and more shear walls and/or outriggers can be placed.

In this research the scatter of different aspects of the design such as stiffness, geometrical and material strength on component and global level has not been taken into account. However the scatter of these parameters especially the former two can have significant influence on some of the comparisons made in this research. Comparison between different case studies, connections and design parameters as shown in section 5 showing low differences can be significantly influenced by such scatters.

Behaviour of the CLT core structure

The core is build-up of different CLT walls which are connected using double inclined STS. The designed connections are able to provide high interaction between core walls which increases global stiffness and provides better use of the CLT panels. Sliding between panels is minimized due to the high connection stiffnesses and respective high interaction factors, which are close to 1.

At foundation level uplifting forces are present due to the lateral wind-loading. Since the core is not post-tensioned gap opening occurs which will result in lateral deformations due to rigid body rotations, a gap opening at foundation of 0.6 mm results in lateral deflection of 4.2 mm at the top of the structure, being responsible for 6.8% of total deflections for case A. Additionally due to shear forces in the horizontal connections sliding occurs resulting in rigid body translations. However with the introduction of the castellations rigid body translations can be kept to a minimum. These phenomena together describe the composite behaviour of a CLT core with both vertical and

horizontal connections.

Behaviour of the outrigger structure

By introducing a timber outrigger to a CLT core a part of the bending moment in the core is transferred through the outrigger to the columns which transfers the force to the foundation. The outrigger restricts rotation of the core which induces an inflection point in the deflection graph resulting in a decreased global deflection of the structure. By introducing an outrigger the global structure becomes stiffer resulting in a higher natural frequency which in turn results in a lower peak lateral acceleration. The effectiveness of the system depends on the stiffness of the outrigger. Increasing the effective stiffness of the outrigger will increase the overall effectiveness of the system.

The in this research presented relationship between the ratio of the effective bending stiffness of the outrigger to core and deflection and accelerations is determined based on the numerical data from the different case studies and sensitivity analyses. However the following influences have not been taken into account in the determination of the relationship. First the influence of the building height, secondly the lever arm of the outrigger and finally the influence of the effective core stiffness. Nevertheless the current model presented can provide an estimation of the reduction of lateral deflections or peak lateral accelerations due to the addition of an outrigger for outriggers placed around mid height of the building. Additionally with the fitted curves as shown in figure 5.37 the overall effectiveness of the outrigger can be estimated on terms of reducing lateral deflections and accelerations where 0% is equal to an outrigger with zero bending stiffness while 100% is equal to an infinitely rigid outrigger. From the figure below it can be seen that an outrigger design reaches a higher maximum lateral deflection effectiveness than a peak lateral acceleration effectiveness for a similar stiffness ratio.

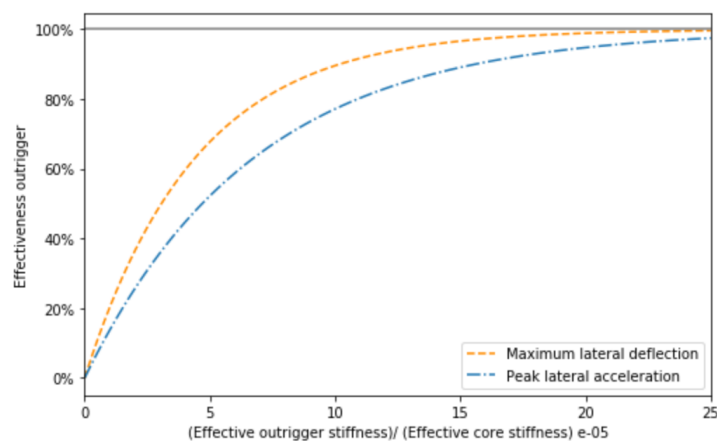


Figure 5.37. *Effectiveness outrigger*

The curves shown in figure 5.37 could help structural engineers in getting a feeling for a specific core and outrigger design and provide an estimation of how much a design could be improved based on the stiffness ratio in terms of deflections and accelerations.

The outrigger is able to transfer forces from the core to the outer columns, as a result the strength requirements on the connections of the core are reduced. By having a stiffer outrigger the system is more effective in transferring forces from the core to the columns, further reducing force requirements on the connections of the core.

The single storey outrigger is able to provide interaction between the core and columns which reduces the bending moment in the core by 6106 kNm. The bending moment is transferred as compressive and tensile loads through the diagonals and beams from the core to the columns. This tensile loads results in horizontal tensile forces being present in the vertical in-plane connection between CLT panels in the core. By increasing the stiffness of the outrigger the amount of forces transferred is increased to 14200 kNm for case C compared to case B resulting in an increase of horizontal forces in the core by 58%. Increasing the stiffness of the outrigger will increase bending moments transferred from core to column which will in turn result in higher tensile stresses in the vertical connections of the core at outrigger level.

In section 5.2.3 the influence of different two-storey outriggers has been assessed. Comparing a single diagonal connecting the core to the columns, for a one storey outrigger as shown in figure 5.38a and a two storey outrigger as shown in figure 5.38c, an outrigger with an increased angle from 18° to 33° respectively is able to more effectively transfer forces from the core to columns. This is due to the fact that an increased angle results in a higher percentage of vertical forces transferred to the columns, increasing the effectiveness of the system and reducing lateral deflections from 56.8 to 49 mm for a one and two storey outrigger respectively.

Additionally it has been shown that a single outrigger diagonal directly connecting the outer column to the core of a two-storey outrigger compared to one-storey outrigger with similar angels is able to increase effectiveness of the system without increasing the material use. The deflections are reduced from 52.9 to 49 mm by introducing outrigger configurations as shown in figure 5.38b and 5.38c respectively. Finally it is shown that an X-type outrigger configurations is the most effective method of transferring forces from core to columns. This is due to the fact that not one but two diagonals directly connect the core to outer columns, of which one in tension and one in compression, resulting in an increased stiffness of the system.

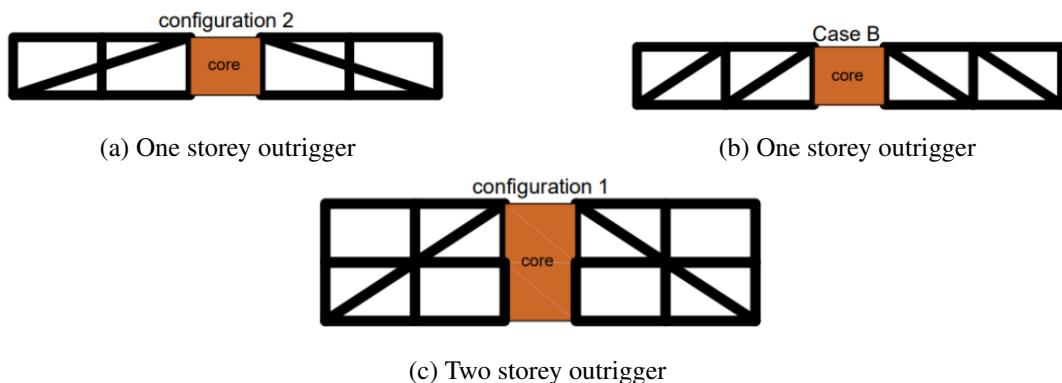


Figure 5.38. *Outrigger with a single diagonal connecting core to column*

Horizontal connections of the core

The height of a CLT panel is maximized in order to reduce the amount of horizontal connections, which in turn reduces the lateral deflections due to rigid body translation and rotation. The horizontal connection of CLT panel to CLT panel consists of both dowels as castellations. During the calculation of the combined stiffness it has been assumed fabrication margins of both the castellations and dowels holes do not lead to initial rigid body translations when loaded, therefore the provided combined stiffness is used.

The castellated joint design is able to increase the shear stiffness by a factor 6.5 compared to a single dowel row connection. If the building height is increased both the amount of horizontal connections and the forces on the horizontal connection will increase which will increase the effectiveness of the castellations in reducing the rigid body translations, provided a similar core layout is used. Therefore the higher the structure the bigger the influence castellations will have on reducing global deflections due to rigid body translations.

The horizontal connection at foundation level showed to be a critical design aspect in the serviceability design of CLT core. The reason that especially the connection at foundation level is critical is due the high tensile forces and the respective effect of vertical gap opening on the lateral displacement. A horizontal connection at foundation level will double the lateral deflection compared to a horizontal connection at half the height of the structure with similar vertical gap opening, the lower the horizontal connection the higher the effect on lateral displacements. In both case A and B small gap openings, below 1 mm, are responsible for approximately 6.5% of the total lateral deflections due to translations of the core.

A possible alternative to the horizontal connection between core and foundation has been designed by making use of glued-in rods as described in section Appendix K. The glued-in rod connection could provide an increase in axial stiffness by a factor 5 while shear stiffness is reduced by a factor 5 compared to the dowelled connection. However since gap opening at foundation is critical glued-in rods could reduce global deflections of a structure. Nevertheless placement of the glued-in rods could prove difficult due to the limited amount of space.

Vertical connections of the core

As discussed in section 5.2.1 increasing the spacing, reducing the stiffness per meter length, in the vertical core connections by 20% has minimal influence on the lateral deflections. In figure 5.39 the influence of the connection stiffness per meter length on the interaction factor γ can be seen, showing an exponential distribution. From figure 5.39a it can be seen that the influence of reducing connection stiffness by 20% is minimal while a more significant influence can be seen if the connection stiffness is reduced by 50%, similar to the influence of having a variable distributed vertical joint design as shown in section 5.1.3. The values of the interaction factors for different connection stiffness values can be seen in table 5.34, highlighting the low influence of reducing stiffness by 20% and showing a more significant but still low influence if stiffness is reduced by 50%. Decreasing the stiffness further than 50% could have drastic effects on the interaction factor

and thus composite interaction of the core due to the exponential function of interaction factor vs stiffness. It can also be seen from figure 5.39 that if the connection stiffness is doubled from 344 to 688 kN/mm/m a limited increase occurs in the orthogonal interaction factors. Which explains the low influence of decreasing the spacing of the vertical orthogonal connection on the global stiffness as previously shown in section 5.1.3.

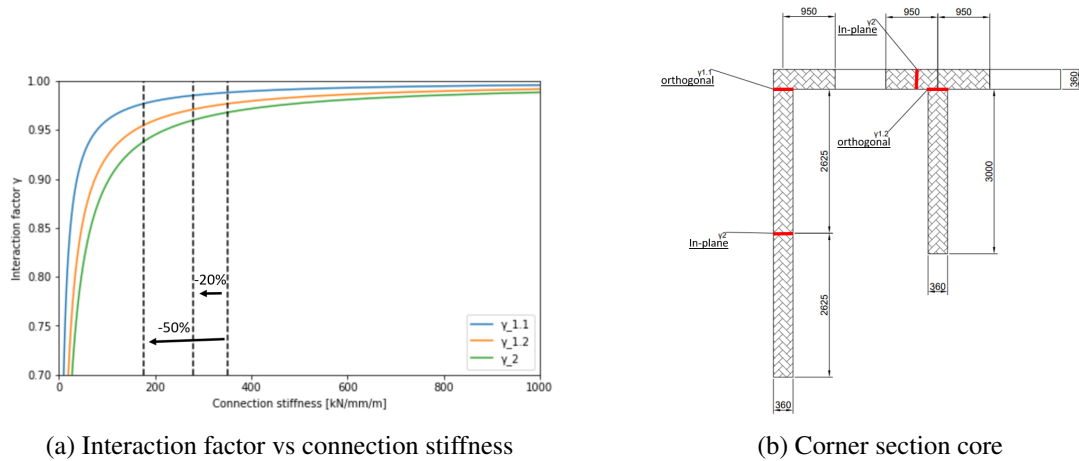


Figure 5.39. Interaction factors CLT core

Table 5.34. Influence of connection stiffness on interaction factors

	$\gamma_{1.1}$ orthogonal connection	$\gamma_{1.2}$ orthogonal connection	γ_2 in-plane
Case A			
Connection stiffness [kN/mm/m]	344	344	355
Interaction factor γ	0.988	0.976	0.968
-20%			
Connection stiffness [kN/mm/m]	275 (-20%)	275(-20%)	284(-20%)
Interaction factor γ	0.985(-0.3%)	0.971(-0.5%)	0.961(-0.7%)
-50%			
Connection stiffness [kN/mm/m]	172(-50%)	172(-50%)	177.5(-50%)
Interaction factor γ	0.976(-1.2%)	0.954(-2.3%)	0.939(-3.0)

In section 5.1.3 the influence of the vertical orthogonal connection of the core is shown. It was shown that by modelling the vertical orthogonal connection as free the lateral deflections increased by 52.3% showing the significance of providing interaction between the web and flange of the core. In figure 5.40a the effective core contributing to the bending stiffness of the structure can be seen. In the case of zero interaction between the webs and flanges, the webs are fully responsible for providing stability against lateral loading.

In section 5.1.3 the influence of the vertical in-plane connection of the core is shown. It was shown that by modelling the vertical in-plane connection as free the lateral deflections increased by 158.6% showing the significance of providing interaction between the webs of the core. In figure 5.40b the effective core contributing to the bending stiffness of the structure can be seen. In the case of

zero interaction between the webs the effective length of the web is reduced by half with the lower section of the web acting independently, additionally the effective flange width is reduced due to the limited available width.

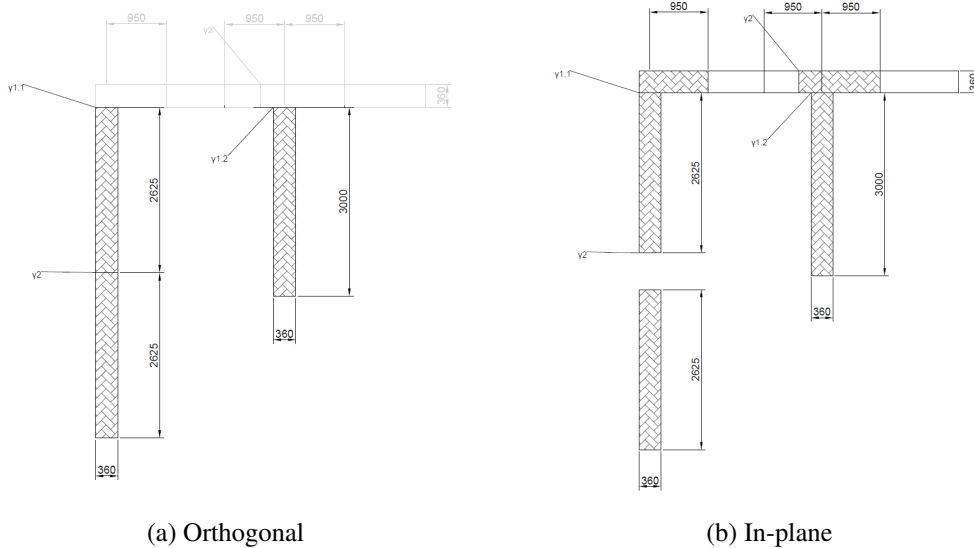


Figure 5.40. *Effect of zero interaction of the vertical connections of the core*

Connections of the outrigger

From the sensitivity analysis on the influence of the connection stiffness of the outrigger in section 5.2.3 it was shown that increasing the connection stiffness decreases global deflections. By increasing the axial connection stiffness the axial slip of the outrigger joints under tension is reduced providing an increased stiffness of the outrigger system and reducing overall deflections. During modelling of the outrigger connections the assumption has been made that the slip only occurs when the joint is under tension, as when under compression direct contact between members would restrict slip in joints. Therefore increase the connection stiffness only effects joints under tension.

Floor to core connection

In all graphs for deflections a slight inflection point can be seen at which the structures starts bending in the opposite direction of the wind loading, which is especially apparent for the different results of case A. The reason for this inflection point is the connection between corners of the core and the floor, providing interaction between corner sections and restricting deformations, similar to a moment resisting frame. In figure 5.41a the deflection of case A with and without floors can be seen, while in figure 5.41b the normalized deflection of case A with and without the floors can be seen.

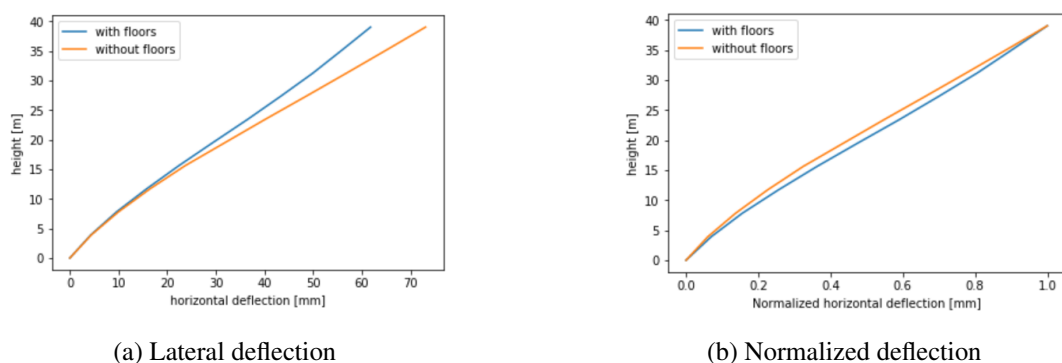


Figure 5.41. *Deflection of case A with and without floors*

From the figures above it can be seen that the inflection point is due to the addition of the floors as they will increase interaction between corners of the core and will reduce overall lateral deflections.

By adding stiffness in the vertical direction to the floor-to-core connection, the floors are able to transfer bending moments between the corner sections of the core, similar to a moment resisting frame. This interaction between corners improves the overall bending stiffness of the core. However special attention needs to be paid during the design phase as to how this connection is realized and how this influences the behaviour of the core system due to lateral wind loading.

Dynamic behaviour

The influence of the outrigger is assessed by performing a modal analysis with estimations of the peak lateral acceleration made according to EC1-4. The estimation of the damping capacity is based on results of previous timber buildings as discussed in section 2.6.1, a damping ratio of 1.9% has been used. During the calculations for the lateral peak accelerations a similar damping ratio has been used for all case studies. Therefore the additional connections and materials used to construct the outrigger has not been taken into account to assess the influence the outrigger has on the global damping ratio.

Throughout this research dynamic response of the structure is assessed due to lateral wind-loading. When designing a similar structure for earthquake loading, using vertical connections in the core consisting of double inclined screws can provide the necessary ductility and help dissipate energy.

The first eigen frequencies for lateral sway modes for case A are below the estimation for steel and concrete buildings and approximations provided by Reynolds[50]. However values are similar to the first two eigenfrequencies of the Treet. By introducing the timber outrigger to the CLT core as done in case B and case C the first eigenfrequencies for lateral sway are increased by 9% and 27 % for a one and two storey outrigger respectively, which is a result of the increased global stiffness. For the case that a two storey timber outrigger is introduced as in case C the value of the eigenfrequency of the first lateral sway mode is in between the lower and upper bound approximations as shown in figure 2.32.

The dynamic behaviour of the different case studies has been determined by use of numerical software, modal analysis and estimations by EC1-4. The first five eigenmodes of the structure are determined, of which the first mode a torsional mode. Since the wind-load is assumed to act symmetrically on the structure, the anti-symmetric torsional mode will not or hardly be excited. Therefore for the calculation of the peak lateral acceleration, the first lateral sway mode is used, which is the first symmetric mode of the structure. Similar results for the first five eigenmodes in which the first mode is a torsional one were found in the thesis research performed by Boellaard, B.[4], in which a CLT core with timber outriggers was assessed.

7. Conclusions and recommendations

7.1 Conclusions

In this section the research question are answered, starting with the two sub questions after which the main research question is answered.

Sub research questions

The two sub research questions have been defined as follows:

What are the critical parameters of a CLT core building with timber outriggers?

How can a timber outrigger system of a CLT core building be optimized?

Core design

The following conclusions can be made regarding the design and optimization of a CLT core, answering the sub questions.

1. The most critical and influential connection is the horizontal connection between the CLT core and foundation. Since small vertical gap opening at foundation level resulting in rigid body rotation results in relatively large deformation at the top of the structure. Reducing the gap opening at ground level is an effective method of reducing the lateral deflections of a CLT core building. In case study A and B vertical gap opening at foundation is responsible for 6.8% and 6.4% of the total deflections respectively in SLS loading.
2. Introduction of castellations in the horizontal CLT to CLT connection can effectively reduce rigid body translations by mechanical interlocking of the core while not increasing the amount of steel used in the connection.
3. Both the vertical in-plane and orthogonal connection between CLT panels using double inclined STS provided a high composite interaction between core walls, due to their respective high interaction factors.
4. A 10 storey CLT core building designed based on ULS does not provide sufficient stiffness to meet SLS requirements. Provided a similar slenderness of the core is used

5. For vertical connections of the core having high interaction factors close to 1, decreasing the connection stiffness does not have large effects on the global behaviour. Namely an decreased connection stiffness in the vertical direction by 20% results in an increase of lateral deflections by only 0.4%.

Outrigger design

The following conclusions can be made regarding the design and optimization of a timber outrigger connected to a CLT core, answering the sub questions.

1. The optimum location of the outrigger to minimize lateral deflections was found to be at 58.5% of the building height.
2. Introduction of a shear wall type outrigger reduces lateral deflection more effectively than a single storey truss, however effective floor area is decreased while material use is increased.
3. Introduction of a two storey timber truss outrigger is able to more than double the reduction on lateral deflection compared to a single storey timber truss outrigger.
4. Increasing the angle of the outrigger diagonal can result in a higher transfer of bending moments from core to columns, compared to a lower angle of the diagonal, while not increasing the amount of material needed.
5. Increasing the stiffness of an outrigger results in a higher force transfer from core to column, reducing bending moments in the core and decreasing global deflections of the structure.
6. An exponential relationship has been derived between the ratio of the effective bending stiffness of the outrigger and the core and the maximum lateral deflections.
7. An exponential relationship has been derived between the ratio of the effective bending stiffness of the outrigger and the core and the peak lateral accelerations.
8. An estimation can be made of the effectiveness of a specific stiffness ratio of the outrigger and the core in terms of reducing deflections and lateral accelerations. With lower and upper bound effectiveness representing zero and infinite bending stiffness of the outrigger respectively.

Main research questions

The results and observations found during this investigation can be used to answer the main research question, which is as follows:

How does a timber outrigger system influence the structural behaviour of a cross laminated core building?

Influence of the outrigger

Introducing a timber outrigger to a CLT core system has the following effects, answering the main research question.

1. Lateral deflections of a CLT core building can be reduced by implementation of a timber outrigger, a higher stiffness of the outrigger will result in a larger reduction of deflections. For the specific case presented throughout this research lateral deflections are reduced by 14 and 34 % for a one and two storey outrigger respectively compared to a CLT core building.
2. Peak lateral accelerations of a CLT core building can be reduced by implementation of a timber outrigger, a higher stiffness of the outrigger will result in a greater reduction of peak lateral accelerations. For the specific case presented throughout this research peak lateral accelerations are reduced by 9 and 25 % for a one and two storey outrigger respectively compared to a CLT core building.
3. Introducing an outrigger generates horizontal tensile forces in the core, which must be considered when designing the core connections. A higher stiffness of the outrigger will increase the amount of the horizontal forces that are transferred to the core, increasing the strength requirements on the vertical core connections.
4. The addition of an outrigger can reduce the force requirements on connections of the core. The efficiency of the outrigger in transferring loads from the core to the columns directly impacts the magnitude of the reduction in forces in the core connections. In other words, the more efficient the outrigger is, the greater the reduction in forces in the connections of the core. With the exception of the vertical connection at outrigger level as mentioned in the previous point.

7.2 Recommendations

In this section recommendations are given on future research within CLT core buildings and timber outriggers.

1. It has been shown that the connection between core and foundation is critical. It would be interesting to check what the influence of a post-tensioned cable connecting the core to the foundation is on material use, deflections and peak lateral accelerations.
2. A possible alternative to the connection between the core and foundation was given by making use of glued-in rods. It would be interesting to perform an optimization of the design of such a connection in which the maximum tensile and shear strength is determined per meter length, for instance by optimizing the diameter of the rods or by placement of the rods.
3. The effective flange width found from numerical results showed large differences with the effective flange width as provided by Masoudnia et al., [59], 1900 and 490 mm respectively. Comparison between numerical and experimental results of different CLT thicknesses and lay-ups in combination with CLT webs could provide a more accurate estimation of the effective flange width for more than 5-layer CLT.
4. For the design of the vertical connections between the core panels the assumption has been made that the strength and stiffness models provided by brown et al, [27] can be used for long screws, in this research up to 1200 mm. However in the experimental tests performed inclined screws had a maximum length of 200 mm. It would therefore be interesting to experimentally verify the strength and stiffness models for lengths above 200 mm.
5. For the calculation of the dynamic response of the different case studies a similar damping ratio is used. However it would be interesting to quantify the influence of adding an outrigger and its respective connections would have on the damping ratio.
6. In this research a design has been made of the horizontal connection between CLT panels combining both internal steel plates and dowels with castellations. Current scientific literature is very limited regarding this subject, therefore it would be interesting to verify the response of such a system by performing experimental tests.
7. The in this research presented relationship between the ratio of the effective bending stiffness of the outrigger to core and deflection is determined based on the numerical data from the different case studies and sensitivity analyses. Similarly as for the relation between stiffness ratio of the outrigger and core and peak lateral accelerations. By increasing the amount of data incorporated the accuracy of the models can be improved. Incorporation of different effective bending stiffnesses of the core, lever arms of the outrigger and building heights could help increase the understanding of the relationship between the stiffness ratio and

lateral deflections or accelerations and possibly provide upper and lower bound estimations of the relationship.

References

- [1] Mir M Ali and Kyoung Sun Moon. “Structural developments in tall buildings: current trends and future prospects”. In: *Architectural science review* 50.3 (2007), pp. 205–223.
- [2] Ivana Kuzmanovska et al. “Tall timber buildings: Emerging trends and typologies”. In: *2018 World Conference on Timber Engineering*. 2018.
- [3] EC Slooten. *Feasibility study of a wood-concrete hybrid super tall building and optimization of its wind-induced behaviour*. 2018.
- [4] B Boellaard. “Design of an outrigger structure for tall timber buildings”. Master thesis. Eindhoven University of Technology, Eindhoven, the Netherlands . . . , 2012.
- [5] Raimondo Da Col and Waugh Thistleton Architects. “From Murray Grove to Dalston Lane”. In: *Europäischer Kongress EBH 2017*. 2017.
- [6] Rune B Abrahamsen and Kjell Arne Malo. “Structural design and assembly of “Treet”—A 14-storey timber residential building in Norway”. In: *World conference on timber engineering*. Vol. 2014. 8. 2014.
- [7] Rune ABRAHAMSEN. *Mjøstårnet—Construction of an 81 m tall timber building*. 2017. 2019.
- [8] Sheryl Staub-French et al. “Construction process innovation on brock commons tallwood house”. In: *Construction Innovation* (2021).
- [9] Mohamed Kasbar et al. “Construction productivity assessment on Brock Commons Tallwood House”. In: *Construction Innovation* (2021).
- [10] David B McKeever. “Engineered wood products: a response to the changing timber resource”. In: *Pacific Rim Wood Market Report* 123.5 (1997), p. 15.
- [11] E Karacabeyli and S Gagnon. “Canadian CLT handbook: 2019 edition”. In: *FPInnovations: Pointe-Claire, QC, Canada* (2019).
- [12] Hans Joachim Blaß and Carmen Sandhaas. *Timber engineering-principles for design*. KIT Scientific Publishing, 2017.
- [13] Robert H Falk and Francois Colling. “Laminating effects in glued-laminated timber beams”. In: *Journal of structural engineering* 121.12 (1995), pp. 1857–1863.
- [14] Reza Rahgozar, Ali Reza Ahmadi, and Yasser Sharifi. “A simple mathematical model for approximate analysis of tall buildings”. In: *Applied Mathematical Modelling* 34.9 (2010), pp. 2437–2451.
- [15] Wael Alhaddad et al. “A comprehensive introduction to outrigger and belt-truss system in skyscrapers”. In: *Structures*. Vol. 27. Elsevier. 2020, pp. 989–998.
- [16] Hi Sun Choi and Leonard Joseph. “Outrigger system design considerations”. In: *International Journal of High-Rise Buildings* 1.3 (2012), pp. 237–246.

- [17] Soobum Lee and Andrés Tovar. “Outrigger placement in tall buildings using topology optimization”. In: *Engineering Structures* 74 (2014), pp. 122–129.
- [18] BS Taranath. “Optimum belt truss locations for high-rise structures”. In: (1975).
- [19] Hyun-Su Kim and Joo-Won Kang. “Smart outrigger damper system for response reduction of tall buildings subjected to wind and seismic excitations”. In: *International journal of steel structures* 17.4 (2017), pp. 1263–1272.
- [20] Solomon Tesfamariam and Sourav Das. “Resilient Tall Timber Building Design: Damped-Outrigger System”. In: (2021).
- [21] ML Batchelar and KA McIntosh. “Structural joints in glulam”. In: *Proceedings of the 5th World conference in Timber Engineering, Montreux*. 1998, pp. 17–20.
- [22] Kjell Arne Malo, Rune B Abrahamsen, and MA Bjertnæs. “Some structural design issues of the 14-storey timber framed building “Treet” in Norway”. In: *European Journal of Wood and Wood Products* 74.3 (2016), pp. 407–424.
- [23] Robert Wiktor. “Glulam connections using epoxy glued-in rebars”. PhD thesis. University of British Columbia, 1994.
- [24] Zhibin Ling et al. “Load-slip behaviour of glue laminated timber connections with glued-in steel rod parallel to grain”. In: *Construction and Building Materials* 227 (2019), p. 117028.
- [25] T Smith et al. “Feasibility and detailing of post-tensioned timber buildings for seismic areas”. In: (2008).
- [26] Matteo Izzi et al. “Seismic behaviour of Cross-Laminated Timber structures: A state-of-the-art review”. In: *Engineering Structures* 170 (2018), pp. 42–52.
- [27] Justin R Brown et al. “Experimental testing of a low-damage post-tensioned C-shaped CLT core-wall”. In: *Journal of Structural Engineering* 147.3 (2021), p. 04020357.
- [28] Gabriele Granello et al. “Pres-lam buildings: state-of-the-art”. In: *Journal of Structural Engineering* 146.6 (2020), p. 04020085.
- [29] Xiaofeng Sun, Minjuan He, and Zheng Li. “Experimental and analytical lateral performance of posttensioned CLT shear walls and conventional CLT shear walls”. In: *Journal of Structural Engineering* 146.6 (2020), p. 04020091.
- [30] Ida Shahnewaz et al. “In-plane stiffness of cross-laminated timber panels with openings”. In: *Structural Engineering International* 27.2 (2017), pp. 217–223.
- [31] Tugce Akbas et al. “Analytical and experimental lateral-load response of self-centering posttensioned CLT walls”. In: *Journal of Structural Engineering* 143.6 (2017), p. 04017019.
- [32] Justin R Brown et al. “Experimental study on orthogonal joints in cross-laminated timber with self-tapping screws installed with mixed angles”. In: *Engineering Structures* 228 (2021), p. 111560.
- [33] Afrin Hossain, Marjan Popovski, and Thomas Tannert. “Group effects for shear connections with self-tapping screws in CLT”. In: *Journal of Structural Engineering* 145.8 (2019), p. 04019068.

- [34] Roberto Scotta et al. “A dissipative connector for CLT buildings: concept, design and testing”. In: *Materials* 9.3 (2016), p. 139.
- [35] Zheng Li et al. “Mechanical performance of pre-fabricated metal dovetail connections for Cross-Laminated Timber (CLT) structures”. In: *Construction and Building Materials* 303 (2021), p. 124468.
- [36] Justin R Brown, Minghao Li, and Francesco Sarti. “Structural performance of CLT shear connections with castellations and angle brackets”. In: *Engineering Structures* 240 (2021), p. 112346.
- [37] Xiaoyue Zhang, Marjan Popovski, and Thomas Tannert. “High-capacity hold-down for mass-timber buildings”. In: *Construction and Building Materials* 164 (2018), pp. 688–703.
- [38] Roberto Tomasi and Ian Smith. “Experimental characterization of monotonic and cyclic loading responses of CLT panel-to-foundation angle bracket connections”. In: *Journal of Materials in Civil Engineering* 27.6 (2015), p. 04014189.
- [39] Andrea Polastri et al. “Structural characterization of multistory buildings with CLT cores”. In: *Proceedings 13th World Conference on Timber Engineering, Quebec City, Canada*. 2014.
- [40] Boris Azinović et al. “Glued-in rods in cross laminated timber–Numerical simulations and parametric studies”. In: *Construction and building materials* 212 (2019), pp. 431–441.
- [41] Gbenga Solomon Ayansola, Thomas Tannert, and Till Vallee. “Experimental investigations of glued-in rod connections in CLT”. In: *Construction and Building Materials* 324 (2022), p. 126680.
- [42] Carl-Johan Johansson and Charlotte Bengtsson. *GIROD-Glued-in rods for timber structures*. na, 2002.
- [43] Gbenga Solomon Ayansola, Thomas Tannert, and till Vallee. “Glued-in multiple steel rod connections in cross-laminated timber”. In: *The Journal of Adhesion* 98.6 (2022), pp. 810–826.
- [44] E Serrano, R Steiger, and P Lavisci. “5 GLUED-IN RODS”. In: *Core document* (2008), p. 37.
- [45] Lisa-Mareike Ottenhaus, Minghao Li, and Tobias Smith. “Structural performance of large-scale dowelled CLT connections under monotonic and cyclic loading”. In: *Engineering Structures* 176 (2018), pp. 41–48.
- [46] Justin R Brown and Minghao Li. “Structural performance of dowelled cross-laminated timber hold-down connections with increased row spacing and end distance”. In: *Construction and Building Materials* 271 (2021), p. 121595.
- [47] Birgit Östman, Daniel Brandon, and Håkan Frantzich. “Fire safety engineering in timber buildings”. In: *Fire Safety Journal* 91 (2017), pp. 11–20.
- [48] Andrea Frangi, Mario Fontana, and Markus Knobloch. “Fire design concepts for tall timber buildings”. In: *Structural Engineering International* 18.2 (2008), pp. 148–155.
- [49] Xuan Zhao et al. “Numerical Analysis on Global Serviceability Behaviours of Tall CLT Buildings to the Eurocodes and UK National Annexes”. In: *Buildings* 11.3 (2021), p. 124.

- [50] Thomas Reynolds et al. “Design parameters for lateral vibration of multi-storey timber buildings”. In: *International Network on Timber Engineering Research Proceedings (INTER 2016)*. 2016.
- [51] Angela Feldmann et al. “Dynamic properties of tall timber structures under wind-induced vibration”. In: *World Conference on Timber Engineering (WCTE 2016)*. 2016.
- [52] Bryan Stafford Smith, Alex Coull, and Bryan S Stafford-Smith. *Tall building structures: analysis and design*. Vol. 5. Wiley New York, 1991.
- [53] P Aondio, P Glaser, and H Kreuzinger. “FE calculation of glued cross laminated timber-part 1: theory”. In: *Bauingenieur* 95.1 (2020), pp. 22–25.
- [54] Caroline Johansson and Erik Johansson. “A sensitivity study regarding different CLT modeling assumptions and their influence on high-rise timber buildings-A sensitivity study regarding different CLT modeling assumptions and their influence on high-rise timber buildings”. In: (2021).
- [55] M Wallner-Novak, J Koppelhuber, and K Pock. “Cross-laminated timber structural design–Basic design and engineering principles according to Eurocode”. In: *ProHolz: Innsbruck, Austria* (2014).
- [56] Tigist Znabei. “A Post-tensioned Cross-Laminated Timber core for buildings”. In: (2020).
- [57] Sylvain Gagnon and Ciprian Pirvu. *CLT handbook: cross-laminated timber*. FPIinnovations, 2011.
- [58] J Brown. “Seismic Performance of CLT Core-Wall Systems and Connections”. PhD thesis. PHD Thesis. University of Canterbury, Canterbury, New Zealand . . . , 2021.
- [59] Reza Masoudnia, Ashkan Hashemi, and Pierre Quenneville. “Predicting the effective flange width of a CLT slab in timber composite beams”. In: *Journal of Structural Engineering* 144.7 (2018), p. 04018084.

Appendix A

Wind velocity

The mean wind velocity $v_m(z)$ is calculated according to equation A.1, making use of equation A.2, A.3 and A.4. It should be noted that all equations to determine the wind loads are extracted from the most recent version of the eurocode NEN-EN1 991-1-4.

$$v_m(z) = c_r(z)c_0(z)v_b \quad (\text{A.1})$$

where

- $v_m(z)$ is the mean wind velocity;
- $c_r(z)$ is the terrain roughness factor;
- $c_0(z)$ is the orography factor, equal to 1.0 for Netherlands;

$$v_b = c_{dir}c_{season}v_{b,0} \quad (\text{A.2})$$

where

- v_b is the basic wind velocity at a reference height of 10 m;
- $v_{b,0}$ is the fundamental value of the basic wind velocity, equal to 27m/s for Rotterdam, area 2 according to EC1;
- c_{dir} is the wind direction influence factor;
- c_{season} is the seasonal influence factor;

$$c_r(z) = k_r \ln\left(\frac{z}{z_0}\right) \quad (\text{A.3})$$

where

- z_0 is the terrain roughness length;
- k_r is the terrainfactor dependant on the roughnesslength z_0 using equation A.4

$$k_r = 0.19\left(\frac{z_0}{0.05}\right)^{0.07} \quad (\text{A.4})$$

Peak wind pressure

The peak wind pressure $q_p(z)$ dependent on height z is calculated using equation A.5.

$$q_p(z) = (1 + 7I_v(z)) \frac{1}{2} \rho v_m^2(z) \quad (\text{A.5})$$

where

ρ is the density of air during storm conditions;
 $I_v(z)$ is the turbulence intensity, according to equation A.6.

$$I_v(z) = \frac{k_l}{c_0 \ln\left(\frac{z}{z_0}\right)} \quad (\text{A.6})$$

where

k_l is the turbulence factor, equal to 1 according to national annexes;

Table A.1. Results Peak wind pressure calculation

parameter	value	assumption
h and z	40 meters	value is taken at 40 meters height
c_{dir}	1	
c_{season}	1	
$v_{b,0}$	27 m/s	wind-area 2 South-holland
v_b	27 m/s	
z_0	0.5 m	urban area
k_r	0.223	
c_r	0.978	
v_m	26.4 m/s	
k_l	1	
I_v	0.228	
ρ	1.25 kg/m ³	
q_p	1.13 kN/m ²	

Wind pressure

The wind pressure is determined based on the force coefficient method which determines the characteristic global wind load on a building for the different surfaces, the calculation is performed using equation A.7.

$$F_w = c_s c_d \sum_{surfaces} c_f q_p(z) A_{ref} \quad (\text{A.7})$$

where

$c_s c_d$ is the structural factor;
 c_f is the force coefficient;

A_{ref} is the reference area;
 $q_p(z)$ is the peak wind pressure;

$$c_s c_d = \frac{1 + 2k_p I_v(z) \sqrt{B^2 + R^2}}{1 + 7I_v(z)} \quad (\text{A.8})$$

where

k_p is the peak factor;
 I_v is the turbulence-intensity factor;
 B^2 is the background response factor;
 R^2 is the resonance response factor;

$$k_p = \sqrt{2 \ln(vT)} + \frac{0.6}{\sqrt{2 \ln(vT)}} \geq 3 \quad (\text{A.9})$$

where

v is the estimation of the wind gust frequency;
 T is the average period of the reference wind velocity, $T = 600 \text{seconds}$;

$$v = n_{1,x} \sqrt{\frac{R^2}{B^2 + R^2}} \quad (\text{A.10})$$

where

$n_{1,x}$ is the natural frequency;

$$B^2 = \frac{1}{1 + \frac{3}{2} \sqrt{\left(\frac{b}{L(z)}\right)^2 + \left(\frac{h}{L(z)}\right)^2 + \left(\frac{b}{L(z)} \frac{h}{L(z)}\right)^2}} \quad (\text{A.11})$$

where

b is the width of the structure;
 h is the height of the structure;
 $L(z)$ is the turbulence length scale;

$$L(z) = L_t \left(\frac{z}{z_t}\right)^\alpha \quad (\text{A.12})$$

where

L_t is the reference scale length, 300 meter;
 z_t is the reference height, 200 meter;

and

$$\alpha = 0.67 + 0.05 \ln(z_0) \quad (\text{A.13})$$

$$R^2 = \frac{\pi^2}{2\delta} S_L K_s \quad (\text{A.14})$$

$$\delta = \delta_s + \delta_a \quad (\text{A.15})$$

where

δ_s is the logarithmic decrement of the structural damping, assumed 0.19;

Logarithmic decrement of the of the aerodynamic damping,

$$\delta_a = \frac{c_f \rho v_m(z)}{2n_{1,x} \mu_e} \quad (\text{A.16})$$

$$\mu_e = \rho_b d \quad (\text{A.17})$$

where

ρ_b is the volumetric mass of the building, estimated as 90 kg/m³;

and

$$c_f = c_{f,0} \psi_r \psi_\lambda \quad (\text{A.18})$$

where

$c_{f,0}$ is the force coefficient for rectangular cross section without correction factor, from figure A.1;

ψ_r is the reduction factor for rectangular cross section with rounded corners, equal to 1;

ψ_λ is the reduction factor for end effects, equal to 1;

The spectral density function for the distribution of the wind speed frequencies can be calculated

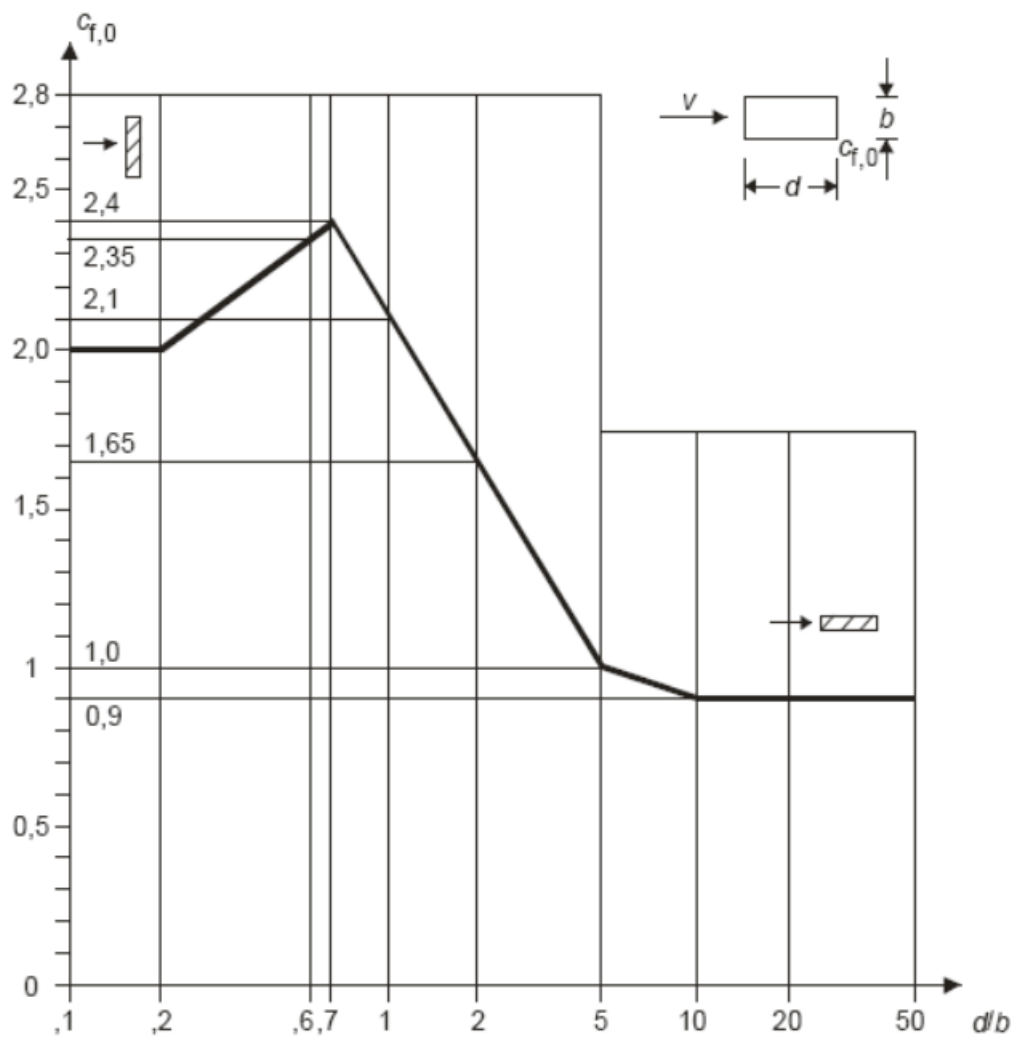


Figure A.1. Force coefficient for rectangular cross section with sharp corners

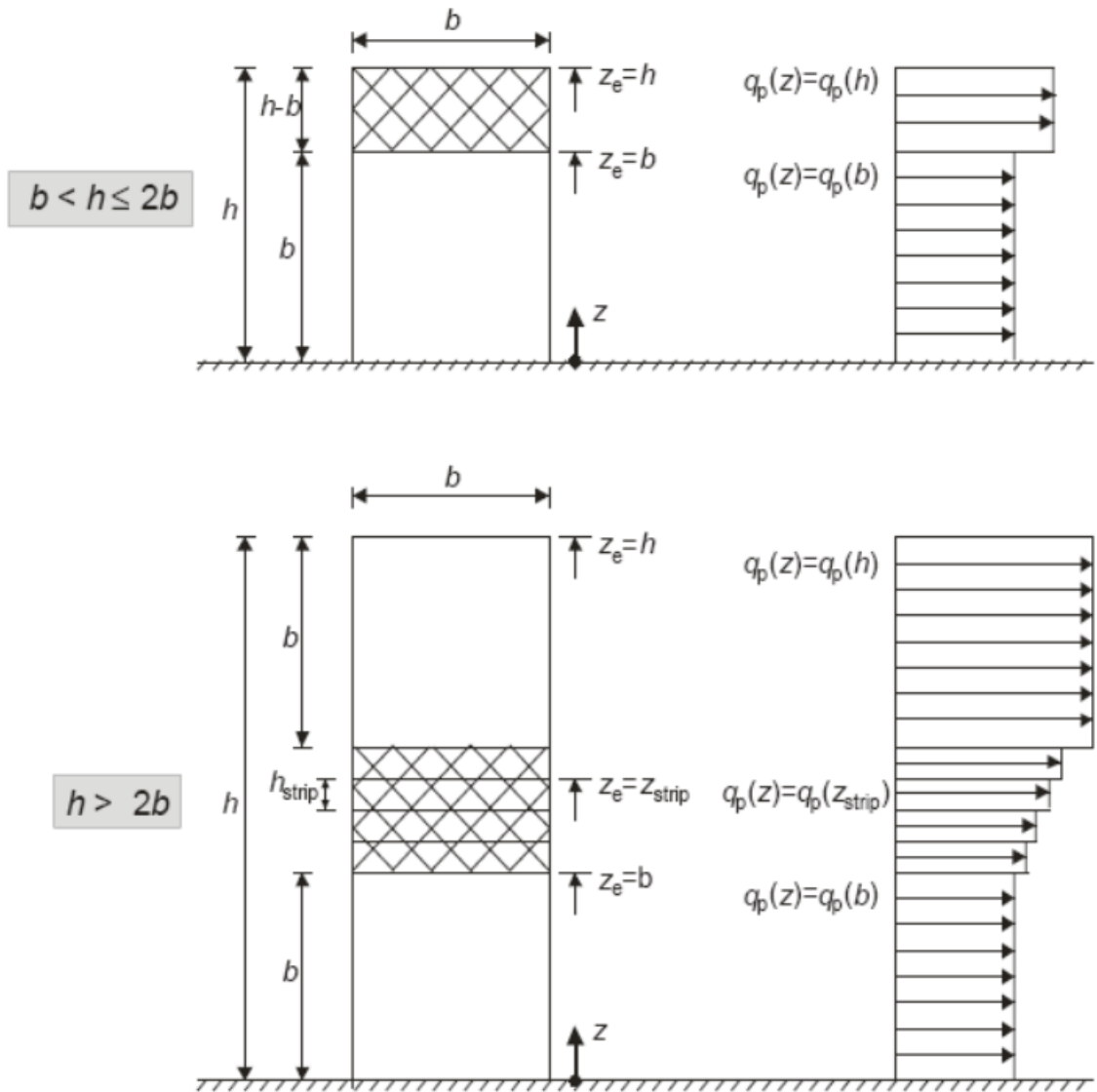


Figure A.2. Reference height according to NEN1991-1

according to equation A.19.

$$S_l = \frac{6.8 f_l(z, n)}{(1 + 10.2 f_l(z, n))^{5/3}} \quad (\text{A.19})$$

$$f_l = \frac{n_{1,x} L(z)}{v_m(z)} \quad (\text{A.20})$$

$$K_s = \frac{1}{1 + \sqrt{(G_y \phi_y)^2 + (G_z \phi_z)^2 + \left(\frac{\pi}{2} G_y \phi_y G_z \phi_z\right)^2}} \quad (\text{A.21})$$

$$\phi_y = \frac{c_y b n}{v_m} \quad (\text{A.22})$$

$$\phi_z = \frac{c_z h n}{v_m} \quad (\text{A.23})$$

where

c_y and c_z are decay constants;

Table A.2. Results calculation windpressure

parameter	value	assumption
$n_{1,x}$	1.34 Hz	based on equation 2.8
b	36 meters	
h	40 meters	
c_y	11.5	
c_z	11.5	
ϕ_y	21.01	
ϕ_z	23.4	
G_y	1/2	
G_z	3/8	
k_y	1	
k_z	3/2	
K_s	0.016	
α	0.635	
L_t	300 m	
z_t	200 m	
L	107.9	
f_l	5.48	
S_l	0.044	
μ_e	3240 kg/m ²	
c_f	2.4	square floorplan
δ_a	0.01	
δ	0.2	
R^2	0.017	
B^2	0.565	
v	0.229 Hz	
k_p	3.33	
$c_s c_d$	0.716	

characteristic wind load

As an initial assumption it is assumed that a constant characteristic wind load is acting on the structure, for this the wind load at 40 meters high is used. Equation A.24 is used to calculate the characteristic windload.

$$w_{e,total} = c_s c_d c_f q_p \quad (\text{A.24})$$

$$w_{e,total} = 0.716 \cdot 2.4 \cdot 1.13 = 1.94 \text{ kN/m}^2 \quad (\text{A.25})$$

Appendix B

Analytical calculation of deflections

In this section an analytical calculation of the deflections is made to verify the numerical results provided in the report.

Assumptions

For the analytical calculation of the stiffness of the structure some assumptions are made to reduce calculation efforts. The interaction between corner sections of the core is assumed to be equal to zero, each corner behaves separately. The horizontal connections of the CLT core are not taken into account, therefore the related rigid body rotations and translations are omitted.

Effective width

To calculate the moment of inertia of the corner section the effective width of the flanges should be taken into account. The effective width takes into account a reduced flange width due to shear lag effect. according to experimental research performed by Masoudnia et al.,[[59]] the effective flange width of a CLT panel can be calculated according to equation B.1. It should however be noted that the effective flange widths are determined without taking into account different geometrical properties of the web, throughout the before mentioned research a constant web is used, namely an LVL beam with dimensions 300x600 mm. The test setup used to determine the effective flange width of a specific CLT configuration can be seen in figure B.1.

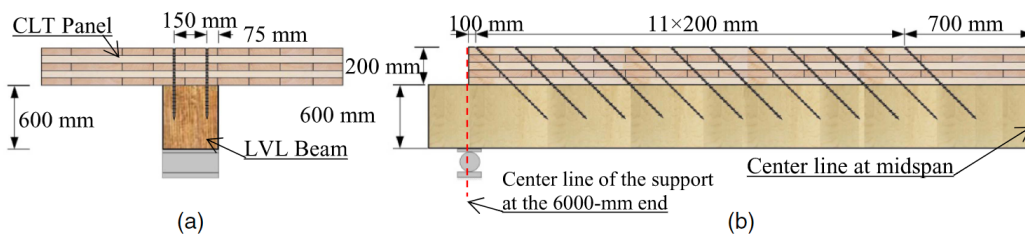


Figure B.1. Test setup used to determine the effective width of a CLT-LVL composite beam [59]

$$b_{eff} = \alpha \beta 23400 \left(\frac{(\sum \text{Longitudinal layer thickness})^2}{\sum \text{Transverse layer thickness}} \right)^{-0.67} \quad (\text{B.1})$$

where

- α is the coefficient for MoE, 0.95, 1.00, 1.30 for 6, 8 and 10 GPa respectively
- β is the coefficient for plank width, 1.00

For a CLT layup of [0/0/90/0/90/0/90/0/0], a layer thickness of 40mm and a Young's modulus of 11 GPa the effective flange width is equal to 490 mm. Additionally the effective flange width of the core has been determined by numerical calculations. According to the numerical calculations the effective flange width of the core is equal to 1900 mm for the case that flanges extend on both sides of web, while the effective flange width for the corner section is equal to 950 mm.

Results between both methods deviate substantially which would have large results on the analytical calculation of the bending stiffness of the core. Since the experimentally proposed effective flange width is based on 5-layer CLT in which only the layup and thickness of the CLT flanges is varied the numerically found effective flange width will be used to analytically calculate the deflections and assess the influence of the different connections. Since the geometrical and material properties of the web will have significant influence on the effective flange width.

Composite beam theory

Since the core is made of several vertical panels mechanically jointed the composite stiffness can be calculated according to NEN-EN1995-1-1, which takes into account the stiffness of the different connections by incorporating an interaction factor γ . The composite stiffness for a beam shown in figure B.2 can be calculated according to equation B.2. In equation B.2 the steiner part is multiplied by interaction factor, where $\gamma = 1$ equals a fully composite interaction and $\gamma = 0$ equals no interaction. In table B.1 the interaction factors for the vertical in-plane and orthogonal connections are provided, taken into account the effective flange widths as shown in figure B.3b. It should be noted that in equation B.3 the length is taken as the length of a beam between two hinges, therefore the length should be taken as twice the building height.

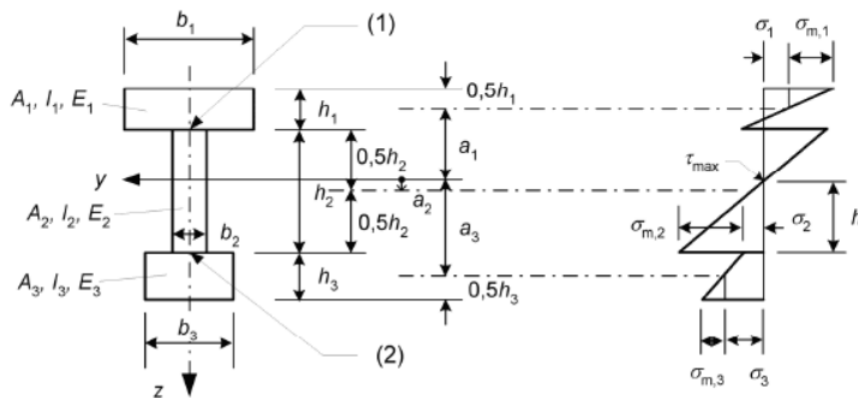


Figure B.2. Mechanically jointed beam according to NEN-EN1995-1-1

$$(EI_{eff}) = \sum (E_i I_i + \gamma_i E_i A_i a_i^2) \quad (B.2)$$

$$\gamma_i = \frac{1}{1 + \frac{\pi^2 E_i A_i s_i}{K_i l^2}} \quad (\text{B.3})$$

where

- s_i is the spacing between fastener rows
- K_i is the slip factor of a fastener row
- l is the length of the "beam", in this case clamped CLT core, between two hinges, therefore the height is doubled from 39 meters to 78 meters
- E is taken as the average youngs modulus of the CLT in which 6 vertically orientated layers and 3 horizontally orientated layers are present, 7500 N/mm^2

Table B.1. Interaction factors

		K [kN/mm]	s [mm]	γ
Vertical orthogonal	$\gamma_{1.1}$	89.4	260	0.988
Vertical orthogonal	$\gamma_{1.2}$	89.4	260	0.976
Vertical in-plane	γ_2	46.2	130	0.968

In figure B.3 the shear lag effect on a corner section of the CLT core is shown. In figure B.3b the different interaction factors for the different connections between CLT panels can be seen. Namely $\gamma_{1.1}$ which is an orthogonal connection at the corner of the core, $\gamma_{1.2}$ which is an orthogonal connection between a web and a flange and finally γ_2 is used to indicate the interaction factor for the in-plane connection. The reason to use two different orthogonal interaction factors $\gamma_{1.1}$ and $\gamma_{1.2}$ is because of the different available flange widths.

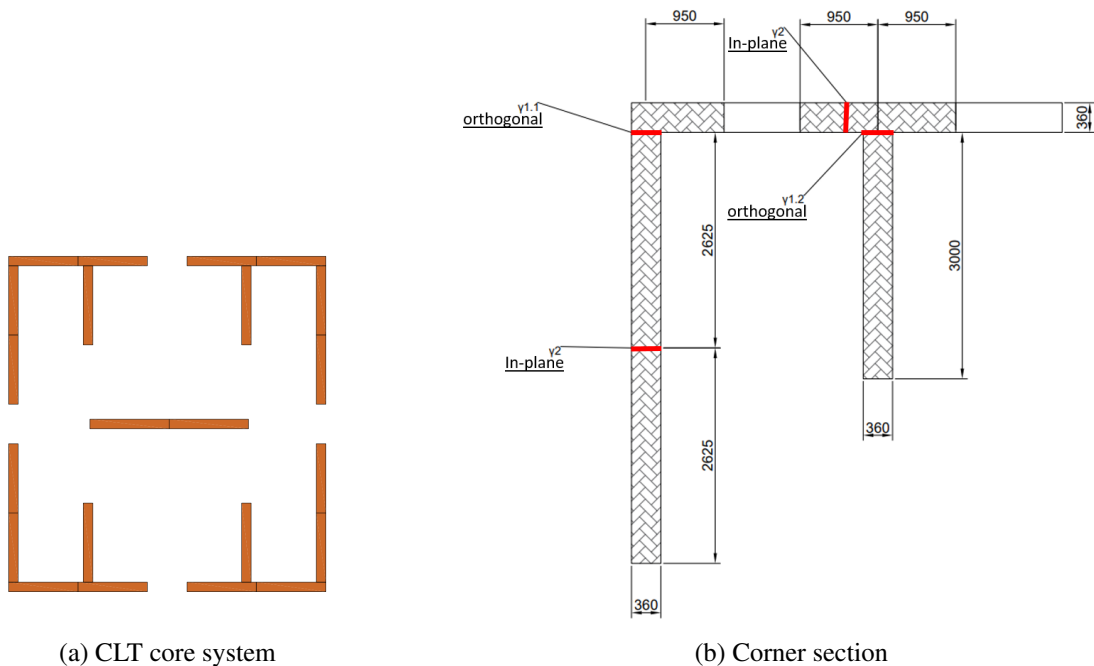


Figure B.3. Shear lag effect CLT core

Results

The deflection of a clamped beam can be calculated according to equation B.4. The wind load is taken as distributed q-load equal to 69.84 kN/m and the bending stiffness of the core is taken as four times the individual stiffness of the corner sections as shown in figure B.3b.

$$u = \frac{ql^4}{8EI} \quad (\text{B.4})$$

Table B.2. Result analytical calculation

	$I_{eff} \text{ mm}^4$	deflection mm
model	$3.42 * 10^{13}$	78.6
vertical orthogonal interaction		
$\gamma = 0$	$2.06 * 10^{13}$	130.4
$\gamma = 1$	$3.44 * 10^{13}$	78.3
vertical in-plane interaction		
$\gamma = 0$	$1.46 * 10^{13}$	185.2
$\gamma = 1$	$3.47 * 10^{13}$	77.8

Table B.3. Result analytical vs numerical calculation

type	deflection [mm]	
	analytical	numerical
horizontal connections included	no	yes
model	78.6	61.8
vertical orthogonal interaction		
$\gamma = 0$	130.4(+65.9%)	94.1(+52.3%)
$\gamma = 1$	78.3 (-0.4%)	61.2(-1%)
vertical in-plane interaction		
$\gamma = 0$	185.2(+135%)	158.6(+156.6%)
$\gamma = 1$	77.8(-2.7%)	60.6(-1.9%)

The results shown in table B.2 show that while the calculated value for the deflection is higher in the analytical model than in the numerical model the influence of the different connections can be assessed analytically with a reasonable accuracy. In both models it is shown that the influence of the vertical in-plane connection is larger than the orthogonal connection especially for the case that γ is equal to zero.

The following assumptions for the analytical model could be the cause for the difference in deflection between both models. First of all the assumption is made that the corners of the core behave separately, however in the numerical model connections of the floors to core provide some interaction between the corner sections which increases the global bending stiffness. Secondly the influence of the effective flange width of the core has a large effect on the analytical calculation of the composite bending stiffness, and since literature on the topic is relatively scarce an estimation is made with some simple numerical models.

Outrigger structure

The deflection of the outrigger core structure is approximated by a simple model in developed in matrixframe. In this model again the influence of the horizontal core connections are neglected. The previously analytically calculated stiffness of the core is used in the model combined with columns and a beam clamped to the core which represents the outrigger, the matrixframe model is shown in figure B.4. Similar to the numerical models the influence of foundation on lateral deflections is not taken into account.

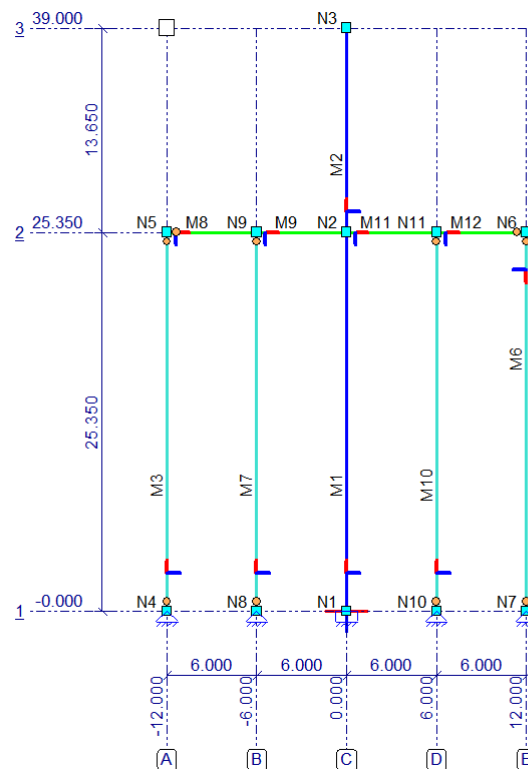


Figure B.4. *Matrixframe outrigger structure*

The upper bound value of the moment of inertia of the outrigger is calculated as the moment of inertia of two beams spaced 3.9 meters apart as shown in figure B.5 and is equal to $9.1 \times 10^{11} \text{ mm}^4$. Since only a single outrigger and column is modelled in the out of plane direction the stiffness of the core is halved similar to the lateral wind loading. As it is assumed half of the core takes half the loading. Columns are modelled as gl28h with dimensions 400x400mm. Loading of the system is placed directly on the core.

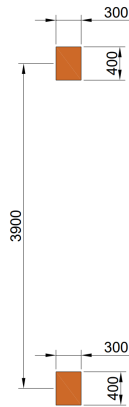


Figure B.5. *Bending stiffness outrigger*

The input for the matrixframe model is shown in table B.4.

Table B.4. *Input matrixframe*

	$I [mm^4]$
core	$1.72 * 10^{13}$
outrigger	$9.1 * 10^{11}$

The lateral deflection of the outrigger structure in matrixframe can be seen in figure B.6a, with the maximum value equal to 44.6 mm. Which is a 43.3 % reduction of the maximum deflection compared to case with only a CLT core a shown in table B.2. The imposed column forces due to compression and tension are equal to 150 and 245 kN for the outer and inner column row respectively, as can be seen in figure B.6b.

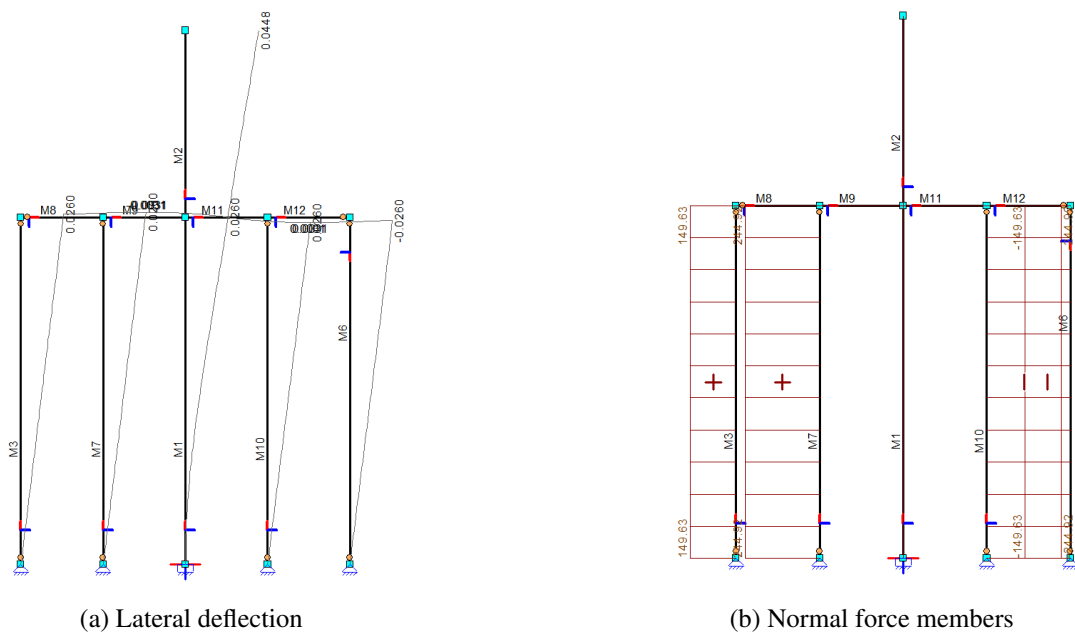


Figure B.6. *Results matrixframe outrigger beam model*

Additionally a model is made in which the truss is not simplified to a beam and modelled as shown in figure B.7.

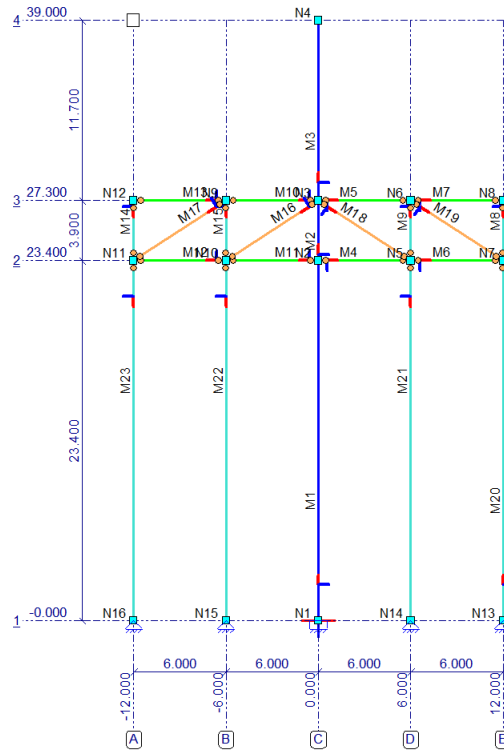


Figure B.7. *Matrixframe outrigger structure with truss*

The resulting lateral deflection can be seen in figure B.8a, in which the maximum horizontal deflection is equal to 53.3 mm. Which is a 32 % reduction of the maximum deflection compared to case with only a CLT core a shown in table B.2. The imposed column forces due to compression and tension are equal to 146 and 115 kN for the outer and inner column row respectively, as can be seen in figure B.8b.

Appendix C

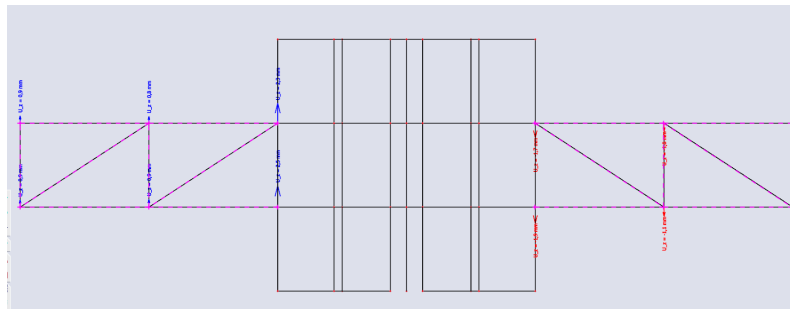
Behaviour of the outrigger

In this section the behaviour of the outrigger is examined. Contributions to the deflections and forces in the outrigger are subdivided into contributions due to lateral wind loading and contributions due to vertical loading of the structure.

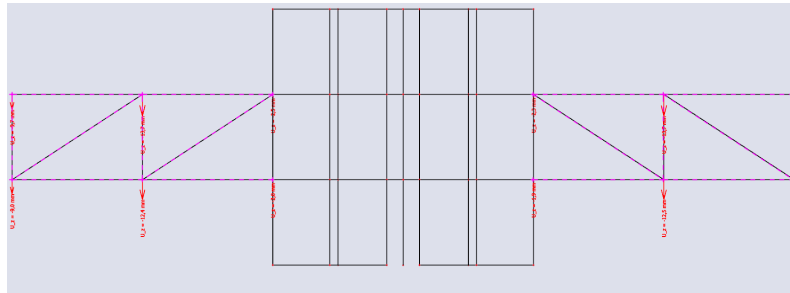
In figure C.1 the vertical displacement of the outrigger nodes are given. In figure C.1a the vertical displacement of the nodes are given due to lateral wind loading, from this figure it can be seen that the displacement of the inner and outer column row is approximately equal to 1 mm. For the loaded side the displacement is upwards while for the opposite side the displacement is downwards.

While in figure C.1b it can be seen that the displacement due to vertical loading of the inner column row is equal to 12.5 mm while the displacement of the outer column row is 9 mm. The larger displacement in the inner column row is due to a higher load transfer in the column which causes a larger axial deformation.

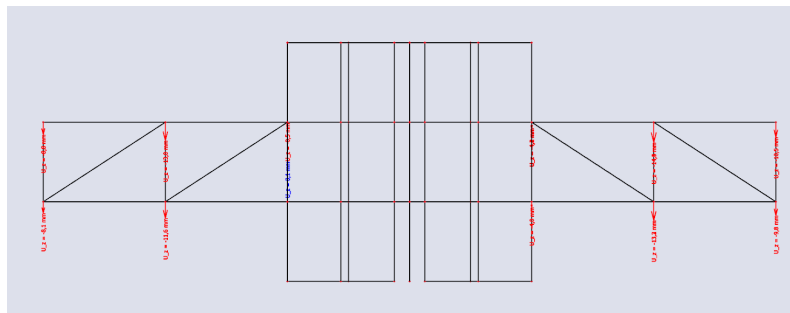
In figure C.2 the displacement of the members is shown.



(a) wind load



(b) vertical loads



(c) combination

Figure C.1. Vertical displacement of the outrigger nodes

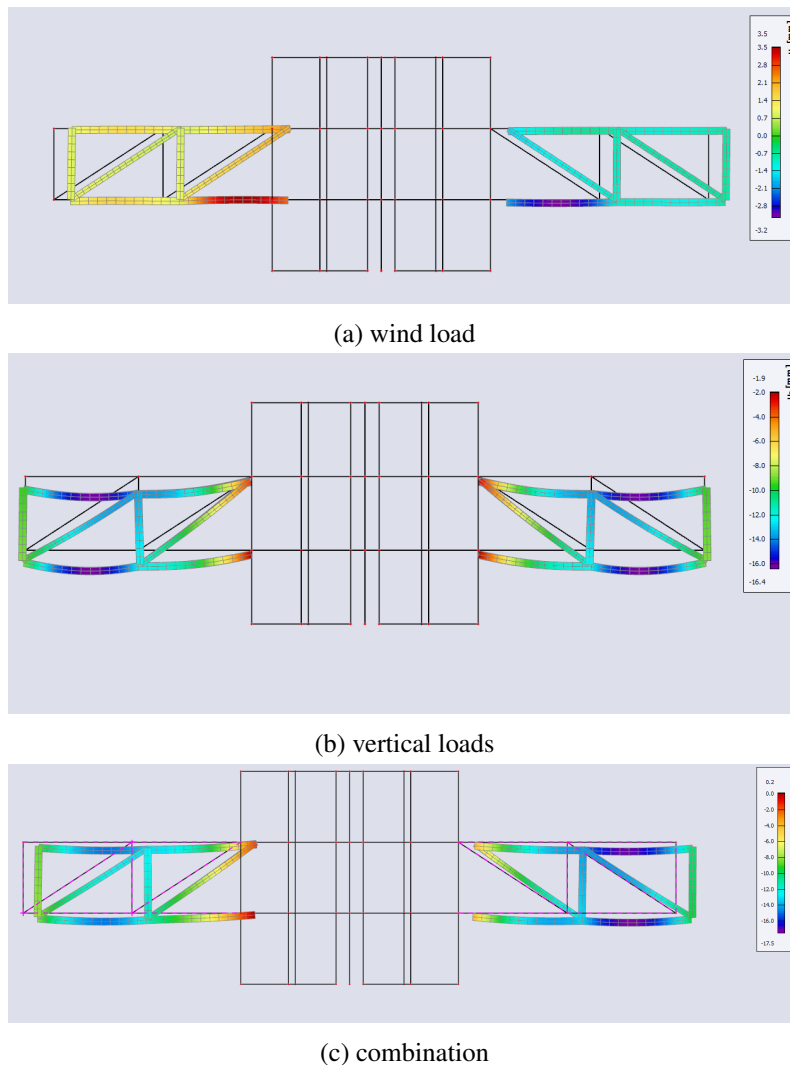
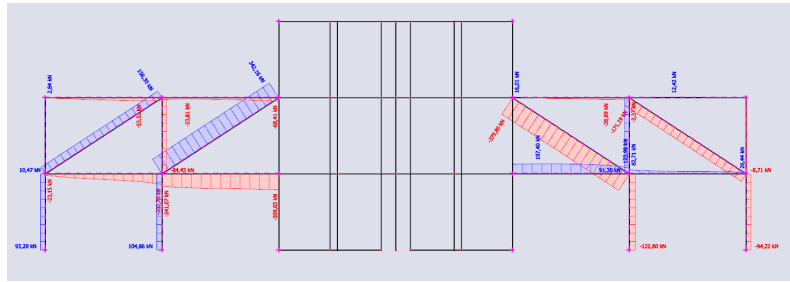


Figure C.2. Vertical displacement of the outrigger

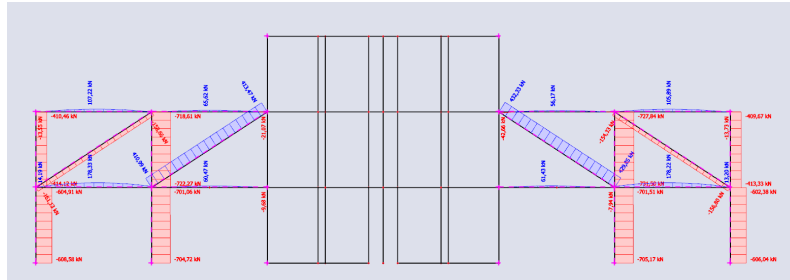
In figure C.3 the axial force in outrigger members is shown. In figure C.3a the forces are shown due to lateral wind loading, it can be seen that compressive forces in the diagonals are slightly larger than tensile forces. Which is likely due to the axial stiffness of the connection, which is only activated in tension, resulting in a slightly larger compressive force in the columns. Additionally it can be seen that inner column row transfers a higher load than the outer column row.

Vertical loading of the structure results in a tensile force of approximately 420 kN in the inner diagonal while the outer diagonal transfers a compressive force of 150 kN as can be seen in figure C.3b.

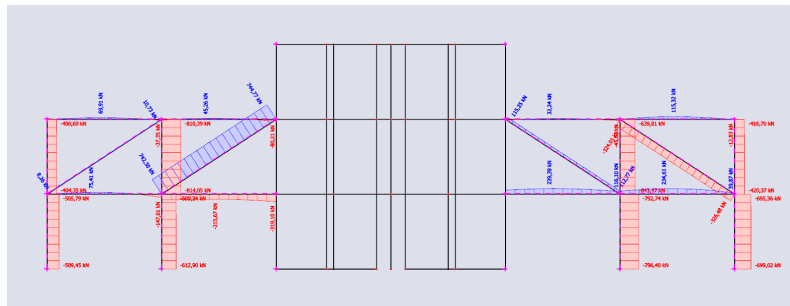
Combining both lateral and vertical loads it is shown that compressive forces in the column are not decreased enough to reach the tensile regime, as can be seen in figure C.3c. Additionally it can be seen that the force in the outer diagonal on the left side of the core is reduced after combining vertical and lateral loading, while the tensile force on the inner column is increased. At the right side of the core the force in the inner diagonal is reduced while the force in the outer diagonal is



(a) wind load



(b) vertical loads



(c) combination

Figure C.3. Forces in members of the outrigger

increased.

Appendix D

Origin of deflections

In this appendix the origin of deflections are discussed.

Case A

In figure D.1 the lateral translation of 61.8 mm for case A is subdivided into the different categories such as material and connections. It can be seen that the contribution due to bending and shear deformation is 70.6% and 18% respectively.

Secondly the contributions due to the influence of the different connections of the core is shown, which is subdivided into the horizontal and vertical connections. The total contribution of the horizontal connection towards rigid body translation is equal to 0.6% while the rigid body rotation is responsible for 8.1%. It is shown that even a slight gap opening of 0.6 mm at ground level can increase deflections by 6.8%, again highlighting the significance of providing a rigid connection at ground level.

Additionally the slip of the different connections is shown in the in-plane shear direction and the gap opening for the horizontal connection is given which results in rigid body translation of the core.

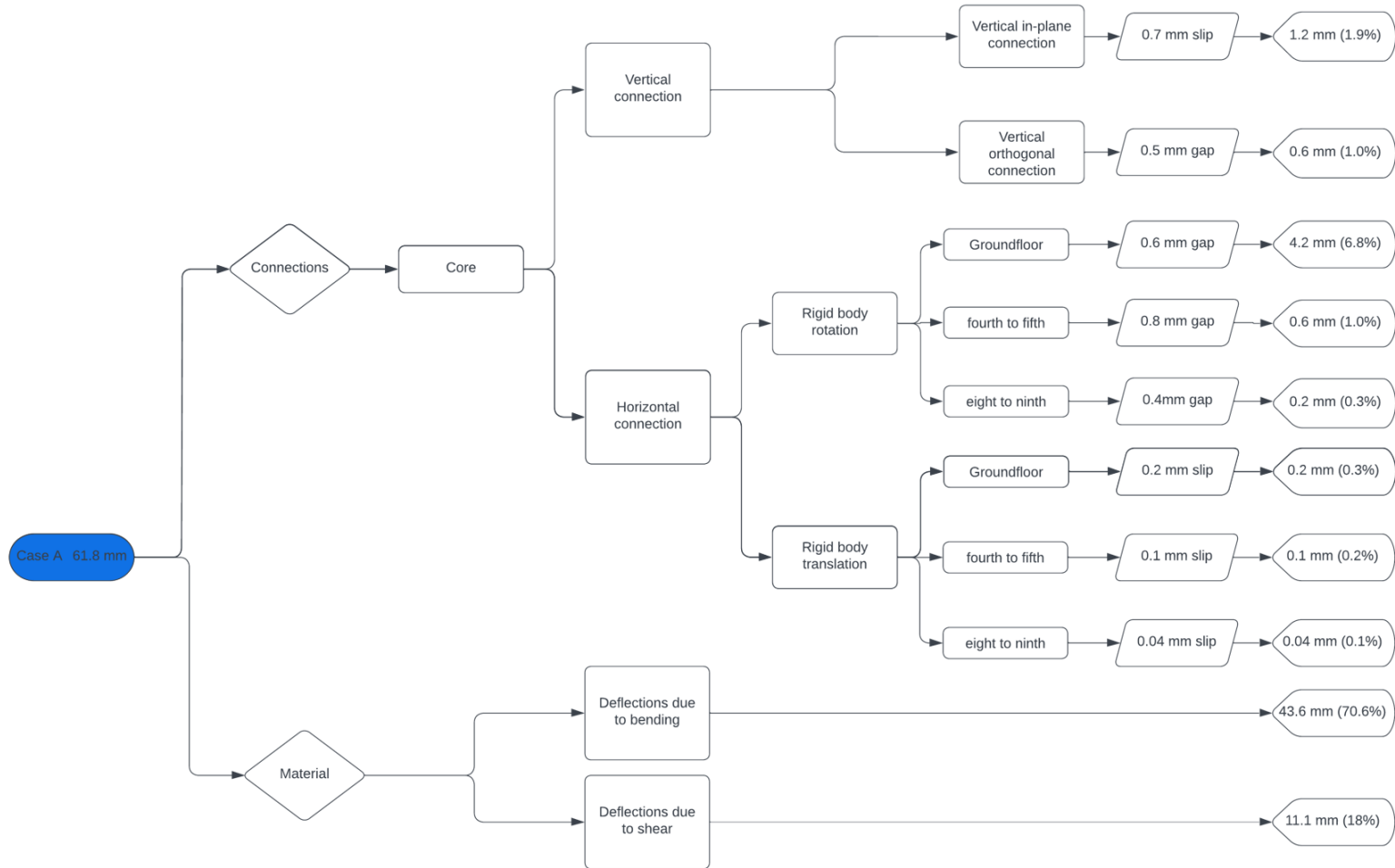


Figure D.1. *Origin of translations case A*

Case B

The different contributions to the total deflection of case B can be seen in figure D.2. Similar observation can be made as discussed in the previous section with regards to the behaviour of the core and its respective contributions, however the average contributions of the core have decreased due to the addition of the outrigger.

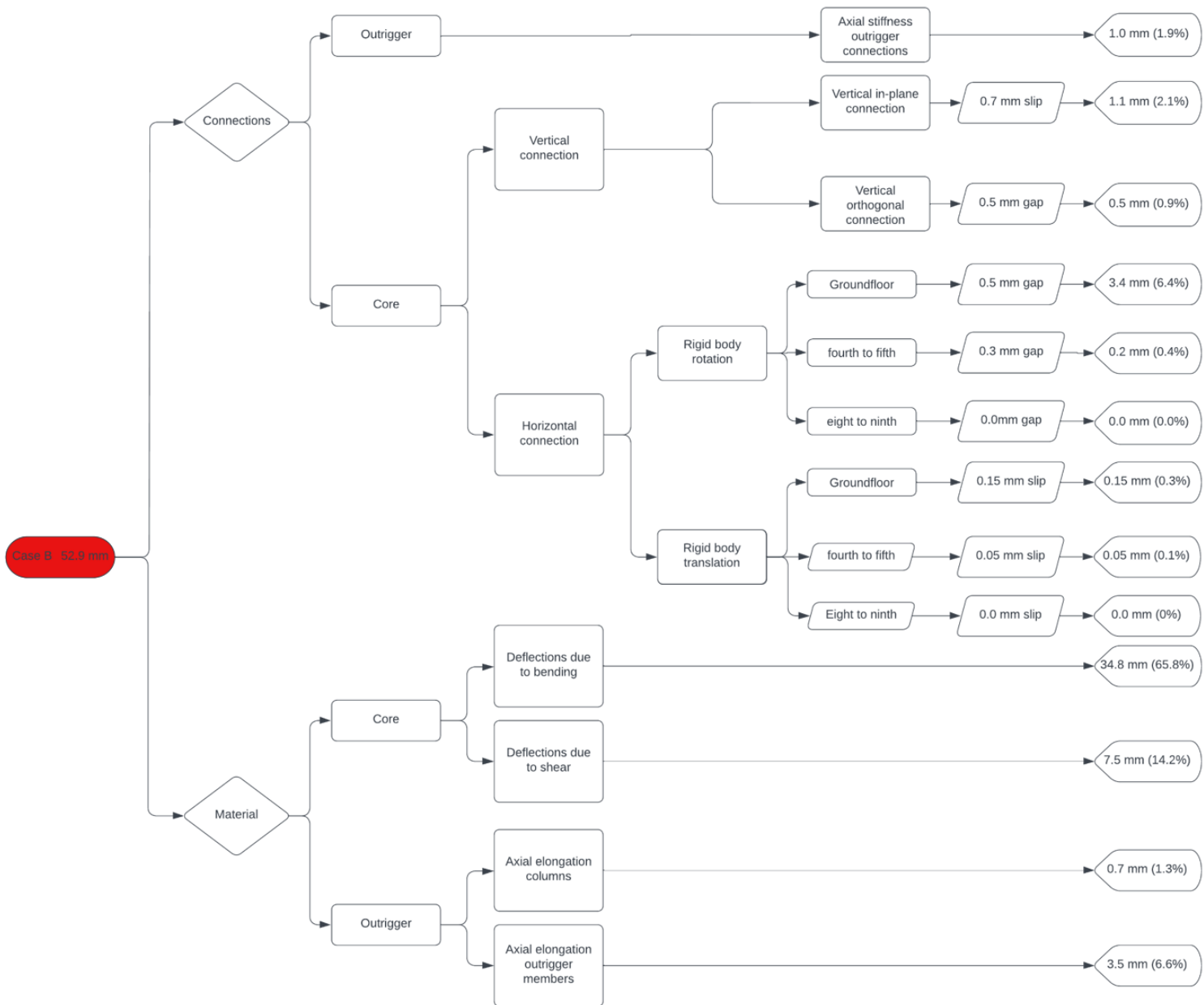


Figure D.2. Origin of translations case B

Appendix E

Verification CLT wall

The maximum compressive force in the core wall is equal to 2263 kN/m, extracted from SCIA.

compression

The compressive resistance of the wall can be checked according to equation E.3.

$$\sigma_{c,0,d} \leq k_{c,1} f_{c,0,d} \quad (\text{E.1})$$

where

$k_{c,1}$ is the factor considering the effect of moisture on the compressive strength, 1 for CLT;

The effective area of the CLT is given by equation E.4.

$$A_{eff} = bh_{eff} \quad (\text{E.2})$$

where

h_{eff} is the effective height, cumulative height of all layers orientated in the load direction;

tensile resistance

$$\sigma_{t,0,d} \leq k_l f_{t,0,d} \quad (\text{E.3})$$

where

k_l is the length modification factor, assumed equal to 1, version used does not contain these factors as of yet;

The effective area of the CLT is given by equation E.4.

$$A_{eff} = bh_{eff} \quad (\text{E.4})$$

where

h_{eff} is the effective height, cumulative height of all layers orientated in the load direction;

Shear resistance

The shear resistance of the CLT panel loaded in-plane is verified by making use of the effective cross section method. The effective cross section method reduces thickness of the outer laminates by 20%. Resulting in a total effective width t_{eff} of 344 mm for a 9 layer CLT with 40 mm laminates. The horizontal and vertical in-plane shear resistances per meter can be calculated using equation E.6.

$$V_{Ed} \leq V_{Rd} \quad (E.5)$$

$$V_{Rd,hor} = k_v(t_{eff}f_{v,d}1000) \quad (E.6)$$

With k_v , the adjustment factor for shear strength, equal to equation 1 for CLT.

The value for the design shear strength can be calculated with equation E.7.

$$f_{v,d} = \frac{f_{v,k}}{\gamma_m} k_{mod} \quad (E.7)$$

Lateral flexural buckling

Stability and buckling strength of the core wall need to be checked to ensure buckling does not take place. The calculation methods used in this section are provided by prEN1995-1-1.

For the calculation of a wall buckling will only occur in the weak out of plane direction, therefore only the following calculations are used

$$\lambda_{c,y,rel} = \sqrt{\frac{f_{c,0,k}}{\sigma_{y,crit}}} \quad (E.8)$$

The critical stresses $\sigma_{y,crit}$ for the y-axis can be calculated according to equation E.9.

$$\sigma_{y,crit} = \frac{\pi^2}{A} \frac{E_{0,05} I_{y,eff}}{l_{y,eff}^2} \quad (E.9)$$

where

$E_{0,05}$

is the fifth percentile of the axial modulus of elasticity;

$l_{y,eff}$

are the effective lengths of the members for buckling around the y-axis;

$I_{y,eff}$ is the effective moment of inertia around the y-axis based on vertically orientated layers only;

The buckling resistance of the wall can be verified according to equation E.10 , with $\lambda_{c,rel,0} = 0.3$ for CLT.

$$\frac{\sigma_{c,0,d}}{k_{c,y} f_{c,0,d}} \leq 1 \quad (E.10)$$

with

$$k_{c,y} \lambda_{c,y,rel}^2 \leq 0.5 \quad (E.11)$$

where

$k_{c,y}$ is the factor for the effects of imperfections;

$$k_{c,y} = \frac{1}{\phi_{c,y} + \sqrt{\phi_{c,y}^2 - \lambda_{c,y,rel}^2}} \quad (E.12)$$

with

$$\phi_{c,y} = 0.5[1 + \beta_c(\lambda_{c,y,rel} - \lambda_{c,rel,0}) + \lambda_{c,y,rel}^2] \quad (E.13)$$

and

where

$\phi_{c,y}$ are the intermediate parameters for the calculations of $k_{c,y}$;
 β_c is the material specific imperfection factor for compressive members, as calculated in equation E.14;

$$\beta_c = \beta_{c,0} k_{creep} \quad (E.14)$$

where

$\beta_{c,0}$ is the initial imperfection factor for members under compression;

The factor to account for the effects of creep k_{creep} , can be calculated according to equation E.15.

$$k_{creep} = 1 + \psi_G k_{def} \quad (E.15)$$

where

ψ_G is the share of permanent loads in the considered load combination, with $\psi_G \leq 1$;

k_{def} is the deformation factor;

In table E.1 an overview is given of values used for the calculation of the different strength criterion's with the unity checks given in table E.2.

Table E.1. *Input data calculation wall section*

t	layer thickness	40 mm
b	width	2625 mm
$l_{y,eff}$	height of a storey	3.9 m
$f_{c,0,k}$	compressive strength parralel to the fibres	21 Mpa
$f_{t,0,k}$	tensile strength parallel to the fibres	14 Mpa
$f_{v,k}$	shear strength out of plane loading	3.5 Mpa
$f_{v,xy,k}$	shear strength perpendicular to plane loading	5.5 Mpa
$E_{0.05}$	fifth percentile value of youngs modulus	10.5 Gpa
$\lambda_{c,rel,0}$		0.3
$\beta_{c,0}$	initial imperfection for members under compression	0.1
k_{def}	deformation factor	0.6
ψ_G	share permanent loads	0.5
k_{mod}	modification factor	0.9
γ_m	partial factor	1.25

Table E.2. *Unity checks CLT core wall*

compression	$\frac{\sigma_{c,0,d}}{f_{c,0,d}k_{c,1}}$	0.62
tension	$\frac{\sigma_{t,0,d}}{f_{t,0,d}k_l}$	0.58
shear horizontal in-plane	$\frac{V_{Ed}}{V_{Rd}}$	0.2
shear vertical in-plane	$\frac{V_{Ed}}{V_{Rd}}$	0.26
buckling resistance	$\frac{\sigma_{c,0,d}}{f_{c,0,d}k_{c,y}}$	0.64

Appendix F

Verification columns

Compression

For the verification of compressive forces in columns, as well as diagonals of the truss connecting the core to perimeter columns compression is solely parallel to the grain. Therefore the following checks can be used.

The compressive stresses in the columns have to satisfy equation F.1.

$$\sigma_{c,0,d} \leq k_{c,1} f_{c,0,d} \quad (\text{F.1})$$

where

$k_{c,1}$ is a strength factor dependent on the moisture content and material, 1.2 for GLT in SC1 conditions, 0.83 for LVL designed in SC2 or 3 conditions and 1 for all other cases;

Tension

The tensile forces within the column have to satisfy equation F.2.

$$\sigma_{t,0,d} \leq k_l f_{t,0,d} \quad (\text{F.2})$$

where

k_l is the length modification factor;

Shear

The shear stresses within the column need to satisfy equation F.3 to ensure shear failure does not occur.

$$\tau_d \leq k_v f_{v,d} \quad (\text{F.3})$$

With k_v , the adjustment factor for shear strength, equal to 1 for LVL and equal to equation F.4 for GLT.

$$k_v = \min\left\{k_{h,v}k_{var}\frac{f_{v,k,ref}}{f_{v,k}}; 1\right\} \quad (\text{F.4})$$

Where the depth modification factor $k_{h,v}$ can be calculated according to equation F.5.

$$k_{h,v} = \min\left\{\left(\frac{600\text{mm}}{h}\right)^{0.1}; 1.1\right\} \geq 1 \quad (\text{F.5})$$

where

$f_{v,k,ref}$ is the reference characteristic shear strength, 2.5 for GLT;

Bending

the Bending stresses within the columns need to satisfy the equation given, F.6 and F.7.

$$\frac{\sigma_{m,y,d}}{f_{m,y,d}} + k_{red}\frac{\sigma_{m,z,d}}{f_{m,z,d}} \leq 1 \quad (\text{F.6})$$

$$k_{red}\frac{\sigma_{m,y,d}}{f_{m,y,d}} + \frac{\sigma_{m,z,d}}{f_{m,z,d}} \leq 1 \quad (\text{F.7})$$

where

k_{red} is a reduction factor, equal to 0.7 for rectangular cross-sections;

Bending and Compression

Combined bending and compression needs to be checked in the columns to ensure failure does not occur, both equation F.8 and equation F.9 need to be satisfied.

$$\left(\frac{\sigma_{c,0,d}}{f_{c,0,d}}\right)^p + \frac{\sigma_{m,y,d}}{f_{m,y,d}} + k_{red}\frac{\sigma_{m,z,d}}{f_{m,z,d}} \leq 1 \quad (\text{F.8})$$

$$\left(\frac{\sigma_{c,0,d}}{f_{c,0,d}}\right)^p + k_{red}\frac{\sigma_{m,y,d}}{f_{m,y,d}} + \frac{\sigma_{m,z,d}}{f_{m,z,d}} \leq 1 \quad (\text{F.9})$$

where

p is the factor accounting for the probabilistic effects on combined bending and compressive strength, equal to 2 for rectangular cross-sections;

Lateral flexural buckling

Stability and buckling strength of the columns need to be checked to ensure buckling does not take place. The calculation methods used in this section are provided by pr EN1995-1-1.

The relative slenderness for in-plane buckling can be calculated according to equation F.10 and F.11 for buckling around the y-axis and z-axis respectively.

$$\lambda_{c,y,rel} = \sqrt{\frac{f_{c,0,k}}{\sigma_{y,crit}}} \quad (\text{F.10})$$

$$\lambda_{c,z,rel} = \sqrt{\frac{f_{c,0,k}}{\sigma_{z,crit}}} \quad (\text{F.11})$$

The critical stresses $\sigma_{y,crit}$ and $\sigma_{z,crit}$ for the y-axis and z-axis can be calculated according to equation F.12 and F.13 respectively.

$$\sigma_{y,crit} = \frac{\pi^2 E_{0,05} I_y}{A l_{y,ef}^2} \quad (\text{F.12})$$

$$\sigma_{z,crit} = \frac{\pi^2 E_{0,05} I_z}{A l_{z,ef}^2} \quad (\text{F.13})$$

where

$E_{0,05}$ is the fifth percentile of the axial modulus of elasticity;
 $l_{y,ef}, l_{z,ef}$ are the effective lengths of the members for buckling around the y-axis and z-axis respectively;

If $\lambda_{c,y,rel} \leq \lambda_{c,rel,0}$ and $\lambda_{c,z,rel} \leq \lambda_{c,rel,0}$, with $\lambda_{c,rel,0} = 0.3$ for LVL and GLT, equations F.8 and F.9 need to be satisfied, else equations F.14 and F.15 need to be satisfied.

$$\frac{\sigma_{c,0,d}}{k_{c,y} f_{c,0,d}} + \frac{\sigma_{m,y,d}}{f_{m,y,d}} \leq 1 \quad (\text{F.14})$$

$$\frac{\sigma_{c,0,d}}{k_{c,z} f_{c,0,d}} + \frac{\sigma_{m,z,d}}{f_{m,z,d}} \leq 1 \quad (\text{F.15})$$

with

$$k_{c,y/z} \lambda_{c,y/z,rel}^2 \leq 0.5 \quad (\text{F.16})$$

and

$$\frac{\sigma_{m,y/z,d}}{f_{m,y/z,d}} \leq 0.25 \quad (\text{F.17})$$

where

$k_{c,y}, k_{c,z}$ are the factors for the effects of imperfections;

$$k_{c,y} = \frac{1}{\phi_{c,y} + \sqrt{\phi_{c,y}^2 - \lambda_{c,y,rel}^2}} \quad (\text{F.18})$$

$$k_{c,z} = \frac{1}{\phi_{c,z} + \sqrt{\phi_{c,z}^2 - \lambda_{c,z,rel}^2}} \quad (\text{F.19})$$

with

$$\phi_{c,y} = 0.5[1 + \beta_c(\lambda_{c,y,rel} - \lambda_{c,rel,0}) + \lambda_{c,y,rel}^2] \quad (\text{F.20})$$

and

$$\phi_{c,z} = 0.5[1 + \beta_c(\lambda_{c,z,rel} - \lambda_{c,rel,0}) + \lambda_{c,z,rel}^2] \quad (\text{F.21})$$

where

$\phi_{c,y}, \phi_{c,z}$ are the intermediate parameters for the calculations of $k_{c,y}$ and $k_{c,z}$;
 β_c is the material specific imperfection factor for compressive members, as calculated in equation F.22;

$$\beta_c = \beta_{c,0} k_{creep} \quad (\text{F.22})$$

where

$\beta_{c,0}$ is the initial imperfection factor for members under compression;

The factor to account for the effects of creep k_{creep} , can be calculated according to equation F.23.

$$k_{creep} = 1 + \psi_G k_{def} \quad (\text{F.23})$$

where

ψ_G is the share of permanent loads in the considered load combination, with $\psi_G \leq 1$;
 k_{def} is the deformation factor;

Table F.1. *Input data column calculation*

h	width	400 mm
b	depth	400 mm
$f_{c,0,k}$	characteristic compressive strength	28 Mpa
$E_{0.05}$	fifth percentile of the axial modulus of elasticity	10500 Mpa
$l_{y,ef}$	effective buckling length	3.9 m
$\lambda_{c,rel,0}$	threshold value for buckling	0.3
$\beta_{c,0}$	initial imperfection for members under compression	0.1
k_{def}	deformation factor	0.6
ψ_G	share of permanent loads	0.5
γ_m	partial factor for material property	1.25
k_{mod}	modification factor taking into account load duration and moisture content	0.9

Table F.2. *Unity checks column*

shear	$\frac{\tau_d}{k_v f_{v,d}}$	0.047
compression	$\frac{\sigma_{c,0,d}}{f_{c,0,d} k_{c,1}}$	0.72
buckling	$\frac{\sigma_{c,0,d}}{f_{c,0,d} k_{c,y}}$	0.9

Appendix G

Validation of the numerical modelling methods

In this appendix a validation is made of the numerical modelling methods by comparing the deflections of a numerical and experimental model of a C-shaped post-tensioned core wall, as tested by Brown et al., [27]

Description of the experimental model

Since the experimental data makes use of several different configurations the choice is made to use CW-6 to verify the numerical methods and assumptions. The reason to use CW-6 is solely based on the fact that it provides the largest stiffness to the structure.

The CLT used for the C-shaped CLT core wall consists of a 175 mm thick five-ply (45/20/45/20/45) panel, consisting of SG8 grade Douglas fir laminations, according to NZS3603, a New Zealand standard from 1993. The connection stiffness and yield strength are listed in table G.1, figure G.1 shows the dimensions of the experimental test setup.

Table G.1. *Connection stiffness experimental tests CW-6 [27]*

joint	F_y (kN/m)	K_{ser} (kN/mm/m)
In-plane	150	121
Wall 1/3 joint	68	55
wall 2/4 joint	63	51

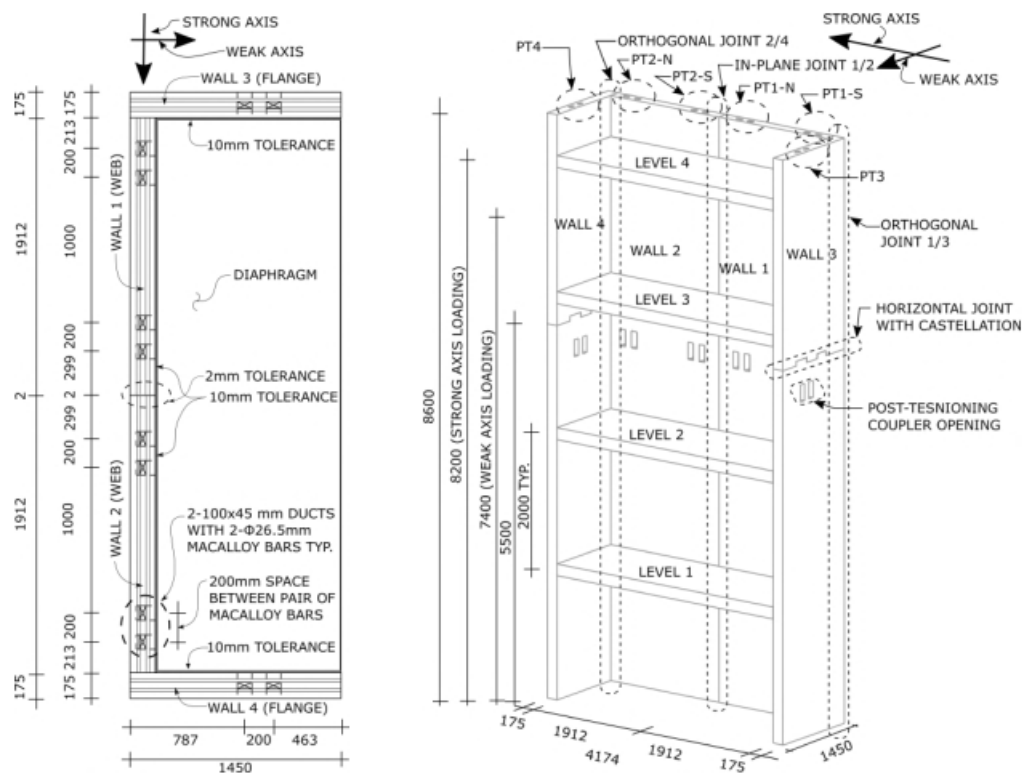


Figure G.1. Dimensions of the experimental test setup [27]

The following should be noted from figure G.1, total height of the test setup is 8600 mm which includes 4 floor levels, the goal of adding floors in this test setup is not to transfer loads from flange to flange but to resist out of plane deformations. Floors are connected to the walls through angle profile consisting of slotted holes allowing for horizontal and vertical displacement, gaps of 10 mm between the walls and floors are used eliminate strut action.

The test setup uses a steel beam as support and anchorage for the post tension cables, additionally shear keys are placed at the end of each wall section to not allow for rigid body translations of the walls. Next to the supports at the base of the wall section actuators on each flange along the weak direction at a height of 7400 mm provided resistance against torsion.

In the web and flanges cut outs are made in which tendons are placed and post tensioned up to 75 kN. Location of the cut outs are marked in figure G.1, diameter of the rods are 26.5 mm with a yield strength of 835 N/mm^2 .

Description of the numerical validation model

In this section a description is given of modelling methods and assumptions used for the numerical validation model. The CLT, connections, floors, steel tendons, supports and loads are described.

CLT

One of the most important aspects of modelling CLT structures correctly is incorporating the correct stiffness matrix in the models. Since the layup and properties of the CLT is known a calculation can be made in which the different stiffness terms on the diagonal matrix can be quantified. These calculations can be done analytically or by the use of the software "CLTdesigner". For both cases a similar matrix is obtained which can later be used as input in SCIA. User defined material can be made in SCIA with the previously derived stiffness matrix.

To ensure the stiffness matrix coincides with the intended direction in the models the local coordinate system of all the vertical CLT elements need to follow similar convention as those can be seen in figure 2.37a, x-axis in the longitudinal direction, y-axis in the transverse direction and the z-axis in the out-of-plane direction.

Connections

During the modelling of the connections the follow assumptions have been made, the vertical connections, i.e. the STS connections, can be modelled as vertical springs bonding the elements together. The horizontal connections consisting of castellated joints can be modelled as rigid in the horizontal connection, since experimental test have shown that deformation of the castellation is negligible.

Floors

The floors are modelled using the following constraints. The connection between the floor and web of the core is free in all aspects, expect for translation in lateral direction, this will ensure the floors do not move through the wall section and will provide the web with lateral support. The connection between the floor and flange section is modelled as a pinned connection. Allowing the floor to rotate without introducing out-of-plane bending stresses in the core.

Steel tendons

To model the steel tendons a different technique needs to be used than simply applying post-tensioned cables, since this is not possible in the used version of SCIA. Therefore it is proposed to use discrete springs which connect the vertical panels to each other. The springs modelled are tension only springs and are therefore non-linear. The springs are modelled over a width equal to 26.5 mm which is equal to the diameter of the cables used in the experimental test. The steel tendons have a yield strength of 835 N/mm^2 and a Youngs modulus of 170 GPa. Combining this with the data given in table G.2 the spring stiffness representing the cables can be calculated according to equation G.1.

Table G.2. Spring stiffness of the cables

Youngs modulus (E) [GPa]	yield strength (f_y) [N/mm^2]	length cables (l_c) [mm]	Spring stiffness per meter (k_c) [kN/mm/m]
170	835	5600	631.8

$$k_c = \frac{E1/4\pi\phi^2}{l_c\phi} \quad (G.1)$$

The springs representing the cables are modelled at the following locations, in vertical plane at foundation level and at 5500 mm height (horizontal castellated joint). While in horizontal plane the springs are placed at the positions of the ducts in the experimental model as shown in figure G.1 on the left hand side and in the numerical model as shown in figure G.2.

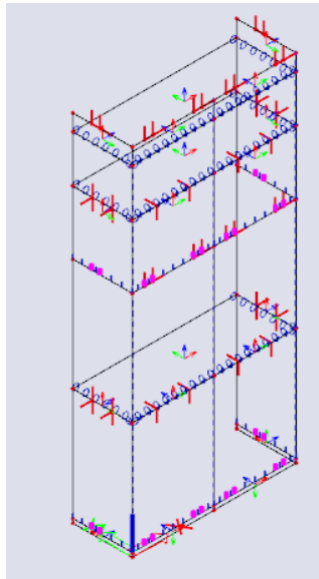


Figure G.2. Spring placement (pink) in the numerical model

Supports

The following supports are modelled in SCIA. As discussed previously the experimental model makes use of a steel beam which supports the entire structure. The steel beam is moment resistantly fixed to the concrete floor and does provide the structure with additional translations and or rotations. Therefore the beam is modelled with fixed supports along the length and a high enough stiffness so that deformations do not occur. Furthermore two lateral supports are placed at 7400 mm height at each flange in the weak axis direction, providing the structure with rotational restraints. The applied supports on the model can be seen in figure G.3, in blue.

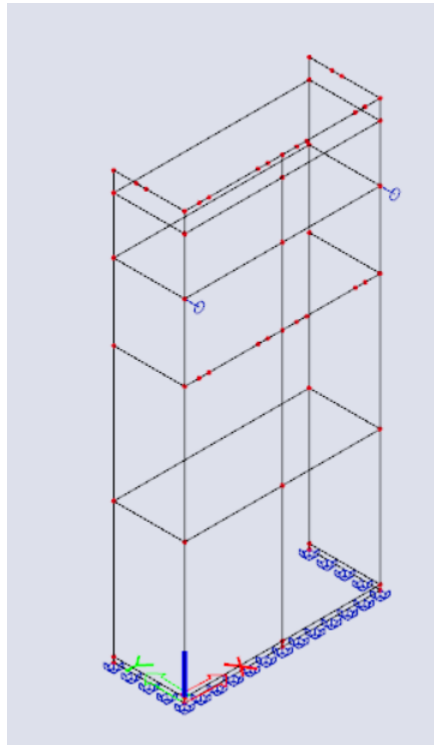


Figure G.3. *Support on the numerical verification model*

Loads

Loads on the structure consist of a horizontal pointload at 8200 mm height at the intersection of web and flange, lateral loading is in the strong direction of the structure. Additionally selfweight of the structure has been turned on. Finally pointloads at the location of the discrete springs are placed at a height 8600 mm (top of the structure) to simulate the post tensioned force in the cables. Loading of the structure can be seen in green in figure G.4

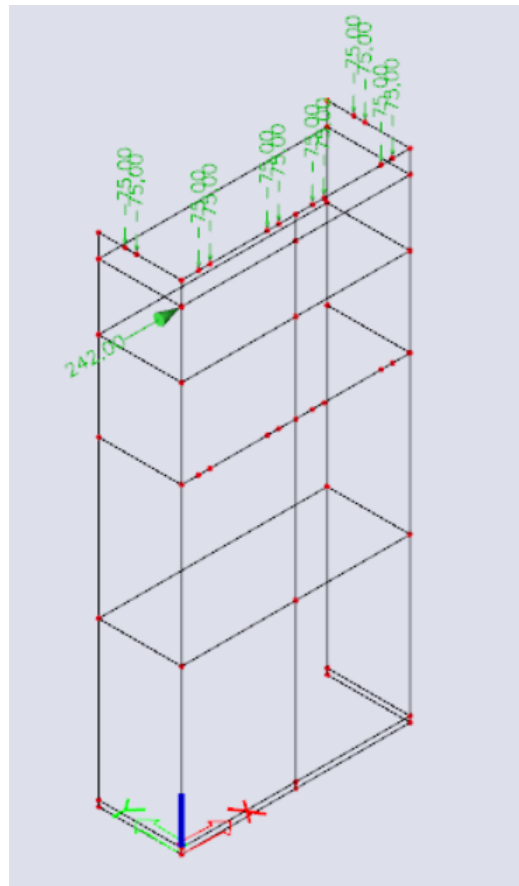


Figure G.4. *Loads on the numerical validation model*

Overview of the numerical validation model

Combining all the before mentioned aspects of modelling the C-shaped wall the following model in figure G.5 is obtained.

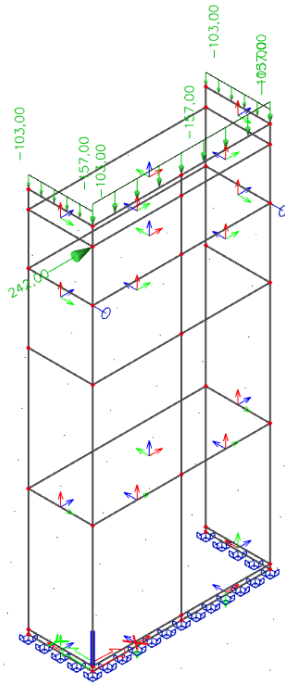


Figure G.5. C-shaped CLT wall numerical model

The orientation of the degrees of freedoms for 2D joints in scia can be seen in figure G.6. Additionally an overview of the connection constraints is given in table G.3

Table G.3. Overview connection constraints

	u_x	u_y	u_x	ϕ_x	ϕ_y	ϕ_z
In-plane vertical	121 kN/mm/m	rigid	rigid	rigid	-	-
Orthogonal vertical	51 kN/mm/m	rigid	rigid	rigid	-	-
horizontal	rigid	*631.8 kN/mm/m	rigid	rigid	-	-
floor to web	free	rigid	free	free	-	-
floor to flange	rigid	rigid	rigid	free	-	-

*non-linear springs are used to model the horizontal joints where the springs are only activated in tension using the springstiffnesses as shown in table G.1.

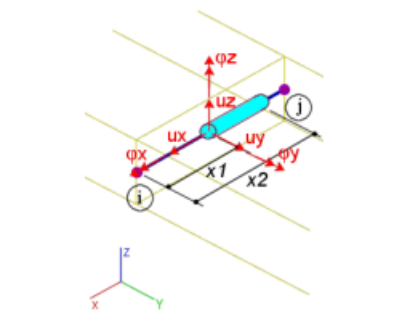


Figure G.6. Orientation joint degree of freedoms SCIA

Results of the numerical validation model

Running a non-linear analysis in SCIA the global displacements of the C-shaped CLT wall can be obtained, result is shown in figure G.7. When checking the lateral displacement in the direction of the load at the height of the load, the height at which experimental measurements are taken, a maximum displacement of 23.4 mm is obtained.

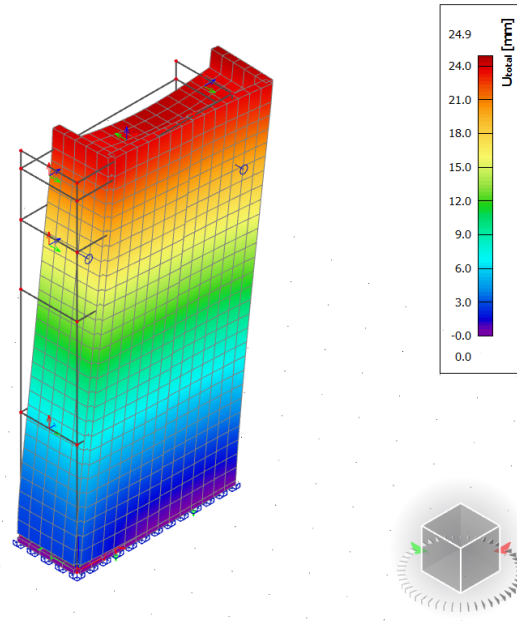


Figure G.7. Global displacement of the C-shaped CLT wall

From the global displacement as previously shown two distinct features of the model need to be mentioned. In figure the shear deformation of the in-plane joint can be seen, which is as expected. Figure G.8b shows that in the left side of the base the compressive force is overcome by tensile forces induced by the overturning moment, resulting in activation of the tensile springs and the opening of a small gap. On the compressive side of the base contact is maintained between the wall section and the beam, confirming that implementation of the non-linear springs is correct.

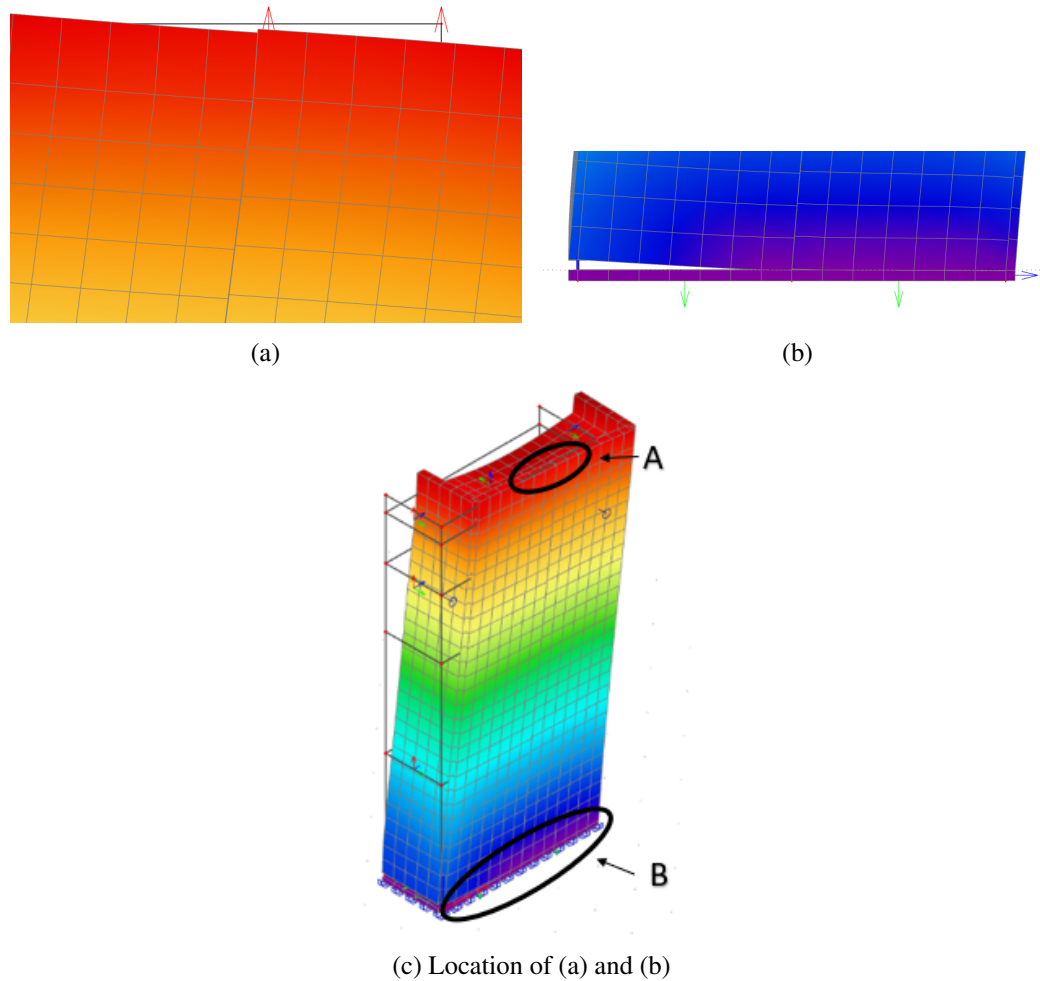


Figure G.8. (a) *Shear deformation in-plane joint*, (b) *Tensile deformation vertical springs*

The results of the experimental model and that of the numerical model can now be compared. From the experimental test a maximum horizontal displacement of 27.2 mm is found. Comparing this with the maximum displacement of the numerical test, 23.4 mm, a difference of 3.8 mm is observed. One of the causes of differences between the numerical and experimental modeling is that of the horizontal joints, of which one exists between CLT panels. In the numerical model these connections are rigid in the horizontal in-plane panel direction, however in the experimental model castellated joints are used. The Castellated joints can be modelled as rigid since the stiffness is approximately similar to that of the base material, however during fabrication a margin of 2 mm was used, resulting in free sliding of 4 mm when panels are joined (the rigid body translation of the panels due to the castellation has been confirmed by Brown et al.). Taking this into account when comparing the numerical and experimental tests a difference of only 0.2 mm (0.8%) is noted. This confirms that the modelling methods and assumptions used are able to provide results with very high accuracy.

Discussion of the numerical validation model

During the numerical modelling of the experimental model some assumptions have been made which could cause differences in the output of both models. First the modelling of the post-tensioned cables have been simplified to discrete springs. This results in the following differences. The force distribution of the panels in the numerical model differ with those in the experimental model. In the numerical model the tensile force flows from the panel through the discrete spring to the adjacent panel, while in the experimental model the tensile force is transferred through the cable entirely. Additionally the cut outs in which the cables are placed are not modelled in the numerical model but are present in the experimental model. Another difference is in the way panels are connected and there specific placement, SCIA makes use of shell elements to model plates which are connected on a 2D line, while in the experimental tests the flanges are extended on which the web is connected as can be seen in figure G.1. Additionally modelling walls as shell elements and introducing an equivalent stiffness does not allow the through-thickness behaviour of the wall to be inspected. In the numerical model the influence of the reduced stiffness of the castellations is neglected and the horizontal connection is modelled as rigid in both horizontal directions. Another reason for the difference in results is the lack of experimental data and the deviation in material properties, more specifically stiffness properties of both the material and of the different connections.

Appendix H

Calculation methods connections

In this appendix the calculation methods for the different connections are shown.

Vertical in-plane connection

The characteristic lateral shear resistance of a fastener can be calculated according to equation H.1.

$$F_{V,k} = k_{WD}F_{D,k} + F_{rp,k} \quad (\text{H.1})$$

where

k_{WD} is the reduction factor for wooden dowels, equal to 1 for steel fasteners.

The six failure modes which shall be considered in the determining the shear resistance of an fastener loaded in single shear can be seen in figure H.1.

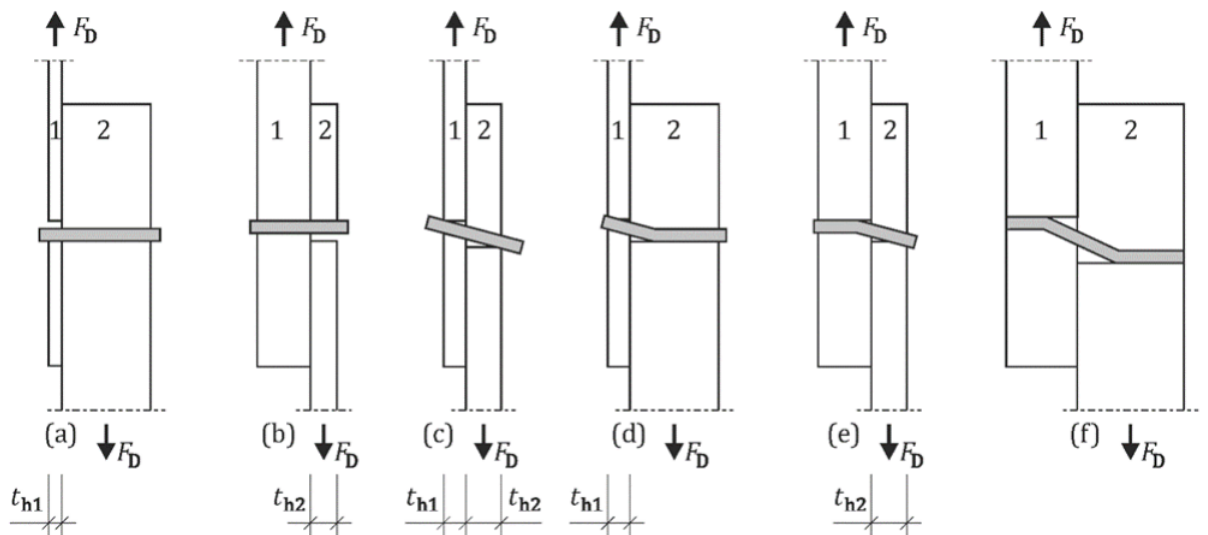


Figure H.1. Failure modes of a fastener loaded in single shear

The characteristic and design value of the dowel-effect per shear plane $F_{D,k}$ and $F_{D,Rd}$ can be calculated according to equation H.2 and H.3 respectively.

$$F_{D,k} = \min \begin{cases} F_{v,Rk,a} \\ F_{v,Rk,b} \\ F_{v,Rk,c} \\ F_{v,Rk,d} \\ F_{v,Rk,e} \\ F_{v,Rk,f} \end{cases} \quad (\text{H.2})$$

$$F_{D,Rd} = \frac{k_{mod}}{\gamma_M} F_{D,k} \quad (\text{H.3})$$

With the detailed calculations of the different failure modes as shown in figure H.1 can be calculated according to equation H.4, H.5, H.6, H.7, H.8 and H.9 for the modes a, b, c, d, e and f respectively

$$F_{v,Rk,a} = f_{h,1,k} t_1 d \quad (\text{H.4})$$

$$F_{v,Rk,b} = f_{h,2,k} t_2 d \quad (\text{H.5})$$

$$F_{v,Rk,c} = \frac{f_{h,1,k} t_1 d}{1 + \beta} \left[\sqrt{\beta + 2\beta^2 \left(1 + \frac{t_2}{t_1} + \left(\frac{t_2}{t_1}\right)^2\right) + \beta^3 \left(\frac{t_2}{t_1}\right)^3} - \beta \left(1 + \frac{t_2}{t_1}\right) \right] \quad (\text{H.6})$$

$$F_{v,Rk,d} = 1.05 \frac{f_{h,1,k} t_1 d}{2 + \beta} \left[\sqrt{2\beta(1 + \beta) + \frac{4\beta(2 + \beta)M_{y,k}}{f_{h,1,k} d t_1^2}} - \beta \right] \quad (\text{H.7})$$

$$F_{v,Rk,e} = 1.05 \frac{f_{h,1,k} * t_2 d}{1 + 2\beta} \left[\sqrt{2\beta(1 + \beta) + \frac{4\beta(1 + 2\beta)M_{y,k}}{f_{h,1,k} d t_2^2}} - \beta \right] \quad (\text{H.8})$$

$$F_{v,Rk,f} = 1.15 \sqrt{\frac{2\beta}{1 + \beta}} \sqrt{2M_{y,k} f_{h,1,k} d} \quad (\text{H.9})$$

where

β is the ratio of embedment strengths, $\frac{f_{h,2,k}}{f_{h,1,k}}$.

d is the diameter of the fastener, in mm.

t_1 is the thickness of member 1, in mm.

t_2 is the thickness of member 2, in mm.

For screws with a diameter $3.5\text{mm} \leq d \leq 20\text{mm}$ the characteristic yield moment $M_{y,k}$ can be calculated according to equation H.10.

$$M_{y,k} = 0.3(f_{u,k})d^{2.6} \quad (\text{H.10})$$

where

$f_{u,k}$ is the characteristic ultimate strength of the screw, in N/mm^2 .

The characteristic embedment strength $f_{h,i,k}$ of screws with wood screw thread for CLT can be calculated according to equation H.11.

$$f_{h,i,k} = \frac{0.019\rho_k^{1.24}d^{-0.3}}{2.5\cos(\epsilon)^2 + \sin(\epsilon)^2} \quad (\text{H.11})$$

where

ϵ is the angle between the fastener and the orientation of the fibres, as can be seen in figure H.2.

ρ_k is the characteristic density of the timber, in kg/m^3 .

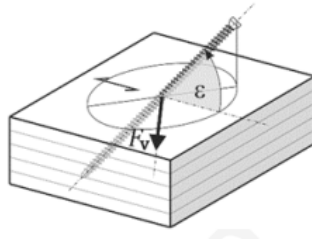


Figure H.2. Angle between fastener and fibre direction

The characteristic rope-effect $f_{rp,k}$ per shear plane per fastener can be calculated according to equation H.12.

$$F_{rp,k} = \min(k_{rp,1}F_{ax,t,k}, k_{rp,2}F_{D,k}) \quad (\text{H.12})$$

where

$k_{rp,1}$ is the factor for the rope effect, generally 0.25.

$k_{rp,2}$ is the limitation factor for the rope effect, equal to 1 for screws

The axial design capacity $F_{ax,t,k}$ of a connection can be calculated according to H.13.

$$F_{ax,t,k} = \min(F_{P,k}, F_{W,k}, F_{T,k}) \quad (\text{H.13})$$

where $F_{T,k}$ is the characteristic tensile resistance according to equation H.14.

$$F_{T,k} = \frac{0.9\pi d^2}{4} f_{u,k} \quad (\text{H.14})$$

$F_{P,k}$ is the characteristic head pull-through resistance according to equation H.15.

$$F_{P,k} = f_{head} A_{head} \quad (\text{H.15})$$

with

$$A_{head} = \frac{d_{head}^2 \pi}{4} \quad (\text{H.16})$$

where

d_{head} is the diameter of the fastener head.

$F_{W,k}$ is the characteristic withdrawal resistance according to equation H.17.

$$F_{W,k} = \pi d_l f_{w,k} \quad (\text{H.17})$$

where

l_w is the anchorage depth, in mm.

$f_{w,k}$ is the characteristic withdrawal parameter, according to equation H.18.

$$f_{w,k} = 8.2 k_w k_{mat} d^{-0.33} \left(\frac{\rho_k}{350} \right)^{k_p} \quad (\text{H.18})$$

where

k_w is equal to 1 for $\epsilon = 90^\circ$.

k_{mat} is a material parameter dependent on the number of layers, 1.15 for 7 or more layers.

Horizontal connection

In this section the calculation for the dowels in the horizontal joints between CLT panels and CLT panel to foundation is shown.

Lateral resistance of fasteners per shear plane

The characteristic and design lateral resistance per shear plane $F_{v,k}$ and $F_{v,d}$ of a single fastener should be calculated according to equation H.19 and H.20 respectively.

$$F_{v,k} = k_{WD}F_{D,k} + F_{rp,k} \quad (\text{H.19})$$

$$F_{v,d} = k_{mod} \frac{F_{v,k}}{\gamma_M} \quad (\text{H.20})$$

where

- $F_{v,k}$ is the characteristic dowel-effect contribution per shear plane.
- $F_{v,d}$ is the design dowel-effect contribution per shear plane.
- $F_{rp,d}$ is the characteristic rope-effect contribution, 0 for dowels.
- k_{WD} is the reduction factor for wooden dowels, 1 for all fasteners except wooden dowels.

To allow the tensile forces to be transferred at the horizontal connection a dowelled joint with two steel plates is designed. The following assumptions are used in the calculation and design of the joint. For the failure mode of a dowel in a connection of four shear planes the individual failure modes according to figure H.1 can be used, however compatibility between the modes needs to be ensured. Furthermore if a steel plates are used with a thickness equal or larger than the dowel diameter and a hole clearance of maximum 0.1d is used it can be assumed that the plates provide sufficient clamping of the fastener, according to prEN1995-1-1.

To allow for compatibility of the outer timber section and inner steel plates, which provides clamping, failure modes (a), (d) and (f) are used in the shear resistance of outer shear planes as can be seen in equation H.21.

$$F_{V,Rk,outer} = \min \begin{cases} F_{V,Rk,a} = f_{h,1,k} t_1 d \\ F_{V,Rk,d} = 1.05 \frac{f_{h,1,k} t_1 d}{2+\beta} \left[\sqrt{2\beta(1+\beta) + \frac{4\beta(2+\beta)M_{y,k}}{f_{h,1,k} d t_1^2}} - \beta \right] \\ F_{V,Rk,f} = 1.15 \sqrt{\frac{2\beta}{1+\beta}} \sqrt{2M_{y,k} f_{h,1,k} d} \end{cases} \quad (\text{H.21})$$

For the outer shearplane the assumption has been made that the embedment of the horizontal orientated layer is the same as that of the vertically orientated layer since the embedment length in

equation H.23.

$$f_{h,\alpha,k} = \frac{0.082(1 - 0.01d)\rho_k}{k_{mat}} \quad (\text{H.23})$$

with

$$k_{mat} = k_{90}\sin^2\alpha + \cos^2\alpha \quad (\text{H.24})$$

$$k_{90} = 1.35 + 0.015d \quad (\text{H.25})$$

The angle α denotes the angle between loading and orientation of the fibres, 90° and 0° for transverse and longitudinal layers respectively.

For the steel member the embedment strength $f_{h,steel,k}$ can be taken as 600 Mpa if $d/t \geq 1$.

The factor β can then be calculated using equation H.26.

$$\beta = \frac{f_{h,steel,k}}{f_{h,\alpha,k}} \quad (\text{H.26})$$

The angle α denotes the angle between the loading and the orientation of the longitudinal fibres as can be seen in figure H.4, in which 1 is the wide face, 2 is the edge face and 3 is the end grain.

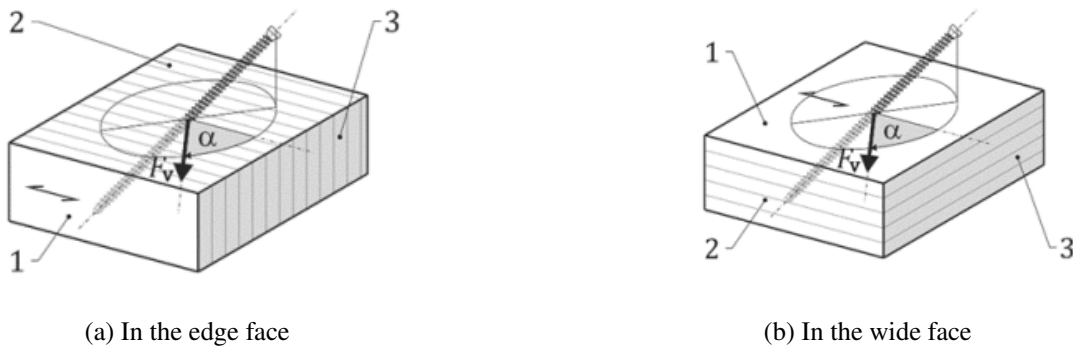


Figure H.4. Definition of angle α

The characteristic yield moment $M_{y,k}$ should be calculated according to equation H.27.

$$M_{y,k} = 0.3f_{u,k}d^{2.6} \quad (\text{H.27})$$

where

$f_{u,k}$ is the characteristic tensile strength of the wire, in N/mm^2 .

The effective number of dowels n_{ef} can be calculated using equation H.28. By making use of the effective number of fasteners splitting along the grain of a row of fasteners is accounted for.

$$n_{ef} = \min \begin{cases} n \\ n^{0.9} \sqrt[4]{\frac{a_1}{13d}} \end{cases} \quad (\text{H.28})$$

where

n is the number of fasteners in a row parallel to the grain.

a_1 is the spacing parallel to the grain, in mm .

d is the diameter of the fastener, in mm .

Slip modulus

The slip modulus of a individual dowel per shear plane can be calculated according to equation H.29. it should be noted that for steel to timber connections in which the fastener is rigidly embedded in the steel the value of the mean slip modulus may be doubled. Additionally for the core wall to core wall the value of the total stiffness is halved since the calculations determine the stiffness of a single side of the connection.

$$K_{SLS,mean} = \rho_{mean}^{1.5} d / 23 \quad (\text{H.29})$$

Spacing and edge distances

For dowels the spacing and end distances are indicated in figure H.5.

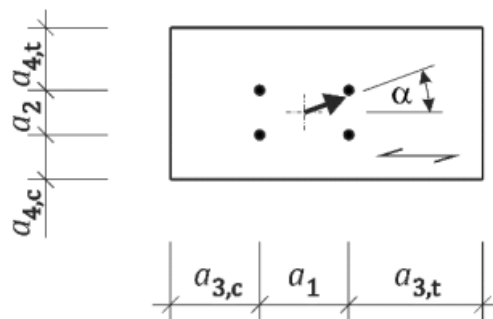


Figure H.5. Spacing and edge distances for fasteners in timber

For predrilled holes the minimum edge distances and spacing for dowels can be found in table H.1.

Table H.1. Recommended minimum spacing and edge distance for lateral loaded dowel connection

a_1	5d
a_2	3d
$a_{3,t}$	max(7d; 80mm)
$a_{3,c}$	4d
$a_{4,t}$	4d
$a_{4,c}$	3d

Column to foundation

In this section the calculation methods for the column to foundation connection are shown.

Bonded-in rods

This section will discuss the strength that bonded-in rods can provide. The bonded-in rod connection is a possible connection technique for CLT core to outrigger or of the outriggers them self.

The anchorage length of the bonded-in rods should satisfy equation H.30.

$$l_b \geq \max \begin{cases} 0.5d^2 \\ 10d \end{cases} \quad (\text{H.30})$$

The required minimum characteristic bond line strength $f_{vr,k}$

Table H.2. Characteristic bond line strength for different effective anchorage lengths

	$l_{b,ef} \leq 250mm$	$250mm \leq l_{b,ef} \leq 500mm$	$500mm \leq l_{b,ef} \leq 1000mm$
$f_{vr,k}$ in N/mm^2	4.0	$5.25 - 0.005l_{b,ef}$	$3.5 - 0.0015l_{b,ef}$

Tension failure of the glued-in rod

The calculation method for the tension failure of the glued-in rods will be shown in the following section. Here the axial resistance of the rods (threaded or ribbed) and the axial resistance of the parent material (CLT, GLT or LVL) are calculated. From these two axial resistance the governing failure mode can be derived and the maximum tensile load on the connection can be determined.

The design resistance of the bonded rod $F_{ax,Rd}$ is calculated according to equation H.31.

$$F_{ax,Rd} = \max \begin{cases} F_{t,d} \\ F_{b,d} \end{cases} \quad (\text{H.31})$$

with

$$F_{t,d} = \min \begin{cases} \frac{1}{\gamma_{M,0}} A_s f_{y,k} \\ \frac{1}{\gamma_{M,2}} 0.9 A_s f_{u,k} \end{cases} \quad \text{for threaded rods} \quad (\text{H.32})$$

and

$$F_{t,d} = \frac{1}{\gamma_{M,0}} A_s f_{y,k} \quad \text{for ribbed rods} \quad (\text{H.33})$$

and

$$F_{b,d} = \frac{k_{mod}}{\gamma_M} F_{b,k} \quad (\text{H.34})$$

with

$$F_{b,k} = \min \begin{cases} \pi d l_{b,ef} f_{vr,k} \\ E_s A_s \varepsilon_{u,timber} \end{cases} \quad (\text{H.35})$$

and

$$l_{b,ef} = \min \begin{cases} l_b \\ 40d \\ 1000mm \end{cases} \quad (\text{H.36})$$

with

- $F_{b,Rd}$ is the design value of the bondline resistance, in N .
- $F_{b,k}$ is the characteristic value of the bondline resistance, in N .
- A_s is the nominal stress area for threaded and ribbed rods, in mm^2 .
- $f_{y,k}$ is the characteristic yield strength of the bonded-in rod, in N/mm^2 .
- $f_{u,k}$ is the characteristic ultimate strength of the bonded-in rod, in N/mm^2
- d is the diameter of the bonded-in rod, in mm .
- l_b is the anchorage length, in mm
- $l_{b,ef}$ is the effective anchorage length, in mm
- $f_{vr,k}$ is the characteristic bond-line strength, in N/mm^2
- $\gamma_{M,0}$, $\gamma_{M,2}$ and γ_M are the partial factors for material properties.
- $\varepsilon_{u,timber}$ is the failure strain of the timber parallel to the grain, 2.4‰ for softwood.

The axial design resistance of the timber member $F_{t,0,Rd}$ in this case column, can be calculated according to equation H.37.

- l_b is the anchorage length.
- $M_{y,k}$ is the characteristic yield moment of the rod.
- n is the number of bonded in rods.

Spacing

To ensure the previously shown axial and shear resistance of the connection can be obtained adequate spacing between rods needs to be maintained. Otherwise the strength of the connection will be compromised. Spacing should be based on table H.3 with the use of figure H.7.

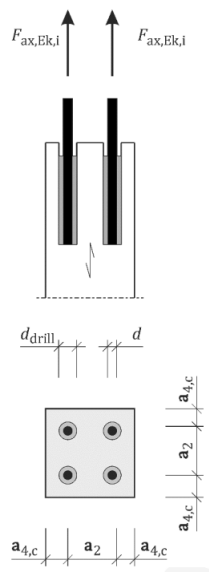


Figure H.7. Spacing notation bonded-in rods

Table H.3. Spacing for glued-in rods

Rods bonded-in	axially loaded rods	Laterally loaded rods
Parallel to the grain	$a_2 = 5d, a_{4,c} = 2.5d$	$a_2 = 5d, a_{4,c} = 2.5d, a_{4,t} = 4d$
Perpendicular to the grain	$a_1 = 4d, a_2 = 4d, a_{3,c} = 2.5d, a_{4,c} = 2.5d$	see eurocode

Beam to column

In this section the calculation methods for the beam to column connection is provided.

Lateral resistance of fasteners per shear plane

The characteristic lateral resistance per shear plane $F_{v,k}$ of a single fastener should be calculated according to equation H.1. The possible failure modes for fasteners under single shear can be seen in figure H.1. It is preferred that a ductile failure occurs instead of brittle, therefore the joint should develop at least one plastic hinge during failure as can be seen in the modes (d), (e) and (f)

Therefore failure mode f is chosen to ensure ductile failure of the beam to column joint. As a

simplification and to ensure ductile failure mode (f) the characteristic value for a steel-to-timber connection of the dowel-effect contribution per shear plane $F_{D,k}$ can be calculated using equation H.40.

$$F_{D,k} = 1.15 * 2\sqrt{M_{y,k}f_{h,k}d} \min \left\{ \begin{array}{l} t_h/t_{h,req} \\ 1 \end{array} \right. \quad (\text{H.40})$$

To ensure that failure mode (f) occurs for a steel-to-timber connection in double shear the minimum required embedment depth $t_{h,req}$ should be taken from equation H.41.

$$t_{h,req} = 1.15 * 4\sqrt{\frac{M_{y,k}}{f_{h,\alpha,k}d}} \quad (\text{H.41})$$

The characteristic embedment strength $f_{h,k}$ for screws can be calculated according to equation H.42.

$$f_{h,\alpha,k} = \frac{0.019\rho_k^{1.24}d^{-0.3}}{2.5\cos(\epsilon)^2 + \sin(\epsilon)^2} \quad (\text{H.42})$$

For screws with a diameter $3.5\text{mm} \leq d \leq 20\text{mm}$ the characteristic yield moment $M_{y,k}$ can be calculated according to equation H.16.

The characteristic rope-effect $F_{rp,k}$ per shear plane per fastener can be calculated according to equation H.43.

$$F_{rp,k} = \min(k_{rp,1}F_{ax,t,k}, k_{rp,2}F_{D,k}) \quad (\text{H.43})$$

where

$k_{rp,1}$ is the factor for the rope effect, generally 0.25.

$k_{rp,2}$ is the limitation factor for the rope effect, equal to 1 for screws

The axial design capacity $F_{ax,t,k}$ of a connection can be calculated according to H.44.

$$F_{ax,t,k} = \min(F_{P,k}, F_{W,k}, F_{T,k}) \quad (\text{H.44})$$

where $F_{T,k}$ is the characteristic tensile resistance according to equation H.45.

$$F_{T,k} = \frac{0.9\pi d^2}{4} f_{u,k} \quad (\text{H.45})$$

$F_{P,k}$ is the characteristic head pull-through resistance according to equation H.46.

$$F_{P,k} = f_{head} A_{head} \quad (\text{H.46})$$

with

$$A_{head} = \frac{d_{head}^2 \pi}{4} \quad (\text{H.47})$$

where

d_{head} is the diameter of the fastener head.

$F_{W,k}$ is the characteristic withdrawal resistance according to equation H.48.

$$F_{W,k} = \pi d l_w f_{w,k} \quad (\text{H.48})$$

where

l_w is the anchorage depth, in mm.

$f_{w,k}$ is the characteristic withdrawal parameter, according to equation H.49.

$$f_{w,k} = 8.2 k_w k_{mat} d^{-0.33} \left(\frac{\rho_k}{350} \right)^{k_p} \quad (\text{H.49})$$

where

k_w is equal to 1 for $\epsilon = 90^\circ$.

k_{mat} is a material parameter dependent on the number of layers, 1.15 for 7 or more layers.

Strength of the steel to column connection

The axial design capacity $F_{ax,t,k}$ of the connection can be calculated according to H.50.

$$F_{ax,t,k} = \min(F_{P,k}, F_{W,k}, F_{T,k}) \quad (\text{H.50})$$

where $F_{T,k}$ is the characteristic tensile resistance according to equation H.45, $F_{P,k}$ is the characteristic head pull-through resistance according to equation H.46 and $F_{W,k}$ is the characteristic withdrawal resistance according to equation H.48.

Appendix I

Connection of the floors

Floor to beam connection

For the floor to beam connection the connection will consist of shear compression and shear tension screws spaced at a distance of $40d$. Calculation of the strength and stiffness is performed using equations 3.13 until 3.20 and 3.23 until 3.27 respectively. Table I.1 contains the floor to beam forces extracted from SCIA. The reason that an increased spacing is possible is due to the fact longer screws can be used which have a higher strength, resulting in a lower total number of screws.

Table I.1. *Forces acting on the floor to beam connection*

	load [kN/m]
In-plane shear force	45
Normal force (tension)	53

Table I.2. *Input data floor to beam connection*

d	diameter of the screw	inclined screws 13 mm
d_c	diameter of the core of the screw	8 mm
l	length of the fastener	700 mm
l_t	screw thread length	675 mm
ρ_k	characteristic density CLT	385 kg/m ³
ρ_m	mean density CLT	420 kg/m ³
f_{uk}	characteristic tensile strength	1000 N/mm ²
f_l	withdrawal strength parameter	11.7 Mpa
f_{rs}	rolling shear strength	0.9 Mpa
ϕ		45°
θ		45°
b	width	400 mm
n	number of fasteners per row	1*

* SC and ST screws are placed at an alternating pattern spaced $10d$ apart

The output for the shear and axial strength stiffness of the connection is shown in table I.3. It should be noted that for the connection between two floor panels and a beam insufficient space is available to place double inclined screws in both direction, resulting in the fact that the axial resistance and stiffness will be different dependent on the direction of loading, with tension resulting in a slightly higher strength and stiffness compared to compression.

Table I.3. *Output floor to beam connection*

	$F_{v,D}$ [kN/m]	K [kN/mm/m]
In-plane shear	46	53
axial single floor	46	53
axial double sided tension	56	61

Figure I.1 contains drawings of a single floor panel to beam connection while figure I.2 contains the connection of two floor plates to a single beam.

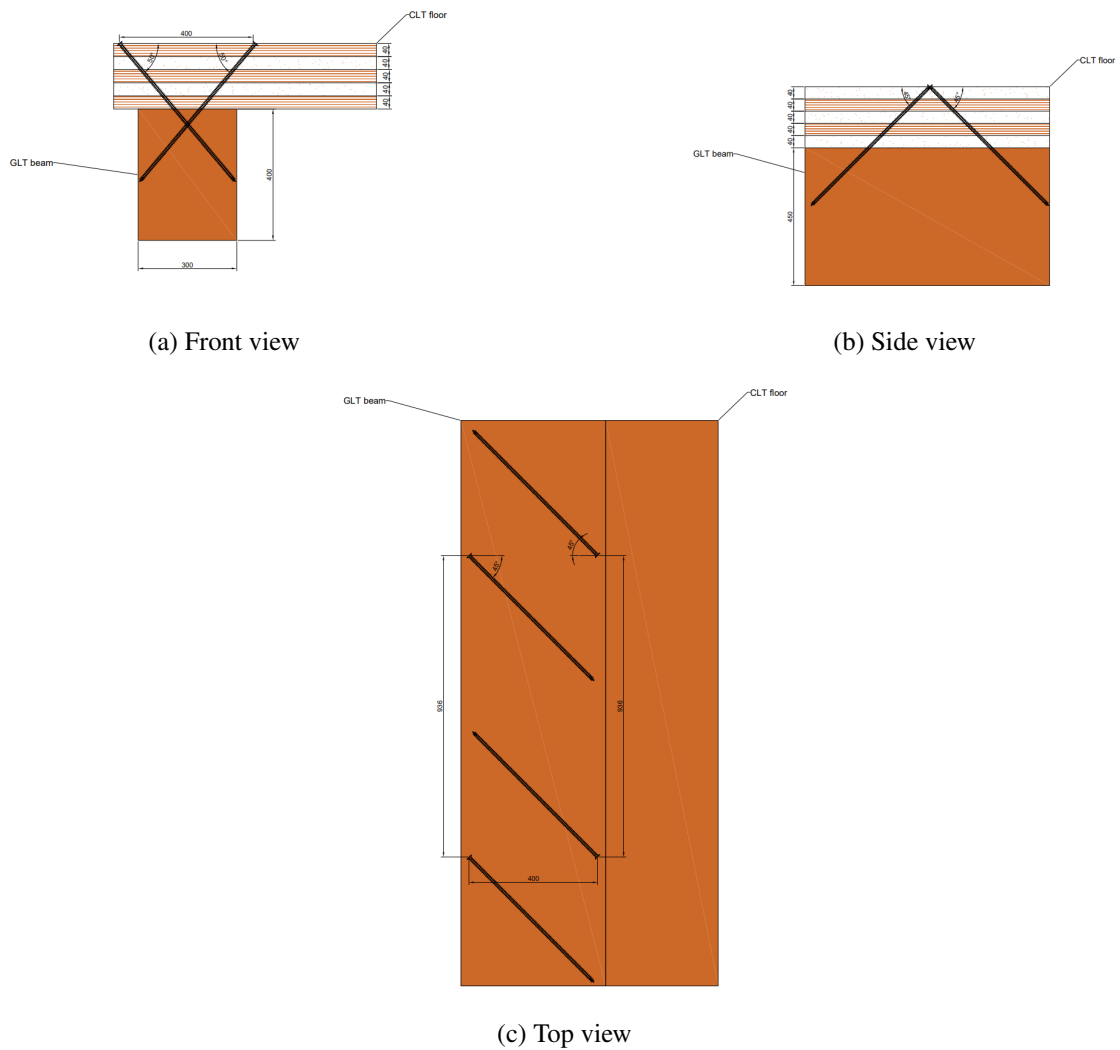


Figure I.1. *Floor to beam connection of a single floor panel*

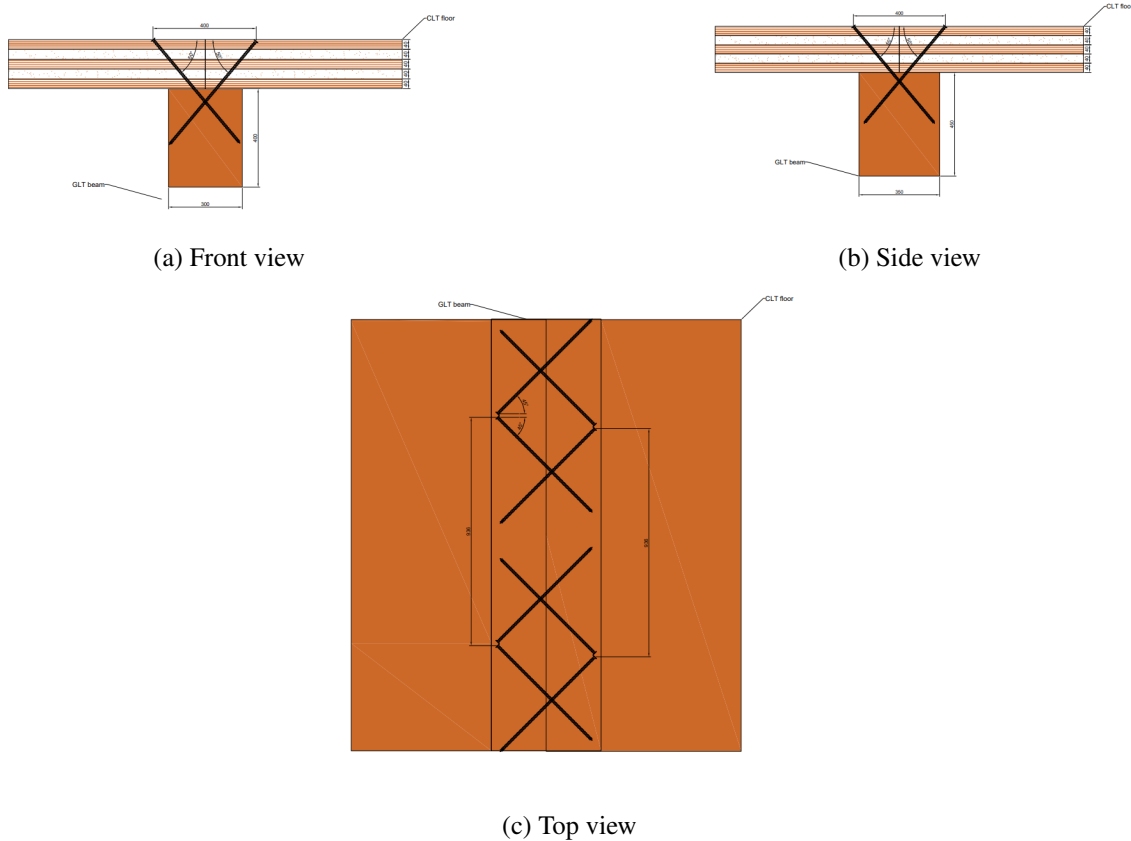


Figure I.2. Floor to beam connection of two floor panels

Table I.4 contains the modelling assumptions i.e. stiffnesses of the the joint in the different degrees of freedom.

Table I.4. *Stiffness modelling assumptions floor to beam connection*

	u_x	u_y	u_z	ϕ_x
double floor	53 kN/mm/m	56 kN/mm/m in tension	rigid	free
single floor	53 kN/mm/m	53 kN/mm/m	rigid	free

Floor to floor connection

Similar to the floor to beam connection the floor to floor connection consist of both shear compression and shear tension screws placed under a double 45° angle. This will provide a high stiffness and strength to the connection independent of the direction of loading. Calculations are performed using similar equations as the floor to beam connection as discussed in the previous section 7.2.

Table I.5 contains the floor to floor forces extracted from SCIA.

Table I.5. *Forces acting on the floor to floor connection*

	load [kN/m]
In-plane shear force	33
tensile force	-

Table I.6 contains the input data used for the analytical calculation of the strength and stiffness of the floor to floor connection.

Table I.6. *Input data floor to floor connection*

d	diameter of the screw	inclined screws 13 mm
d_c	diameter of the core of the screw	8 mm
l	length of the fastener	350 mm
l_t	screw thread length	325 mm
ρ_k	characteristic density CLT	385 kg/m ³
ρ_m	mean density CLT	420 kg/m ³
f_{uk}	characteristic tensile strength	1000 N/mm ²
f_l	withdrawal strength parameter	11.7 Mpa
f_{rs}	rolling shear strength	0.9 Mpa
ϕ		45°
θ		45°
b	width	200 mm
n	number of fasteners per row	1X

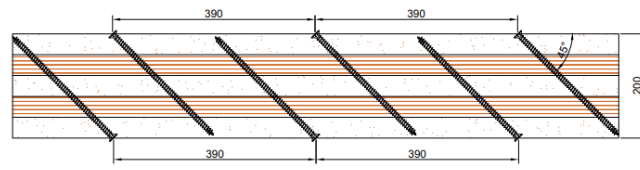
*for inclined screws an X-configuration consist of a shear-tension and shear compression-screw

The output data for the strength and stiffness in in-plane shear direction for double inclined screws spaced 30d can be found in table I.7.

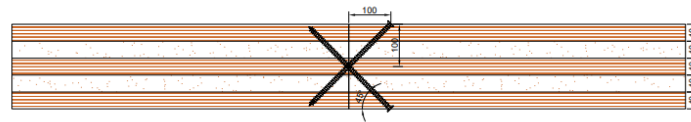
Table I.7. *Output floor to floor connection*

	$F_{v,D}$ [kN/m]	K [kN/mm/m]
In-plane shear	43	52

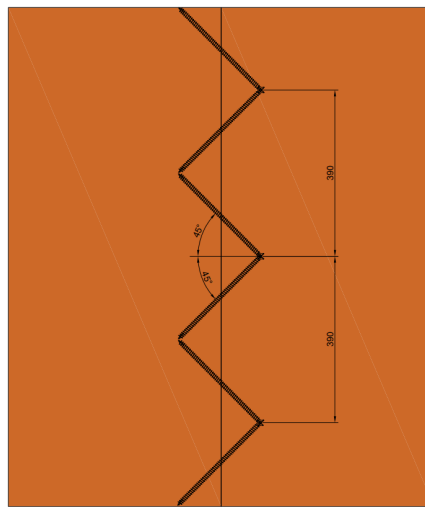
In figure I.3 detailed drawings are shown for the floor to floor connection showing the double inclined screws spaced 30d.



(a) Front view



(b) Side view



(c) Top view

Figure I.3. *Floor to floor connection*

Table I.8 contains the modelling assumptions i.e. stiffnesses of the the joint in the different degrees of freedom. For modelling of the floor to floor the in-plane axial stiffness u_y is modelled as rigid based on the fact only compressive forces are present within the floors and u_z the out-of-plane shear stiffness is also modelled as rigid, based on the assumption adjacent panels have similar deflections i.e. symmetry.

Table I.8. *Stiffness modelling assumptions floor to floor connection*

u_x	u_y	u_z	ϕ_x
52 kN/mm/m	rigid	rigid	free

Floor to core connection

The floor to core connection will consist of a STS connection under double 45° angle again provide high strength and stiffness independent on the direction of loading. Calculation is similar to that

used for the floor to beam and floor to floor connections shown in sections 7.2 and 7.2 respectively.

Table I.9 contains the floor to core forces extracted from SCIA.

Table I.9. Forces acting on the floor to core connection

	load [kN/m]
In-plane shear force	78.8
Out-of-plane shear force	38.4
Normal force (tension)	86.9
Normal force (compression)	66.6

The input for the calculation of the strength and stiffness of the connection in different directions are shown in table I.10.

Table I.10. Input data floor to core connection

		inclined screws
d	diameter of the screw	13 mm
d_c	diameter of the core of the screw	8 mm
l	length of the fastener	350 mm
l_t	screw thread length	325 mm
ρ_k	characteristic density CLT	385 kg/m ³
ρ_m	mean density CLT	420 kg/m ³
f_{uk}	characteristic tensile strength	1000 N/mm ²
f_l	withdrawal strength parameter	11.7 Mpa
f_{rs}	rolling shear strength	0.9 Mpa
ϕ		45°
θ		45°
b	width	200 mm
n	number of fasteners per row	1X

*for inclined screws an X-configuration consist of a shear-tension and shear compression-screw

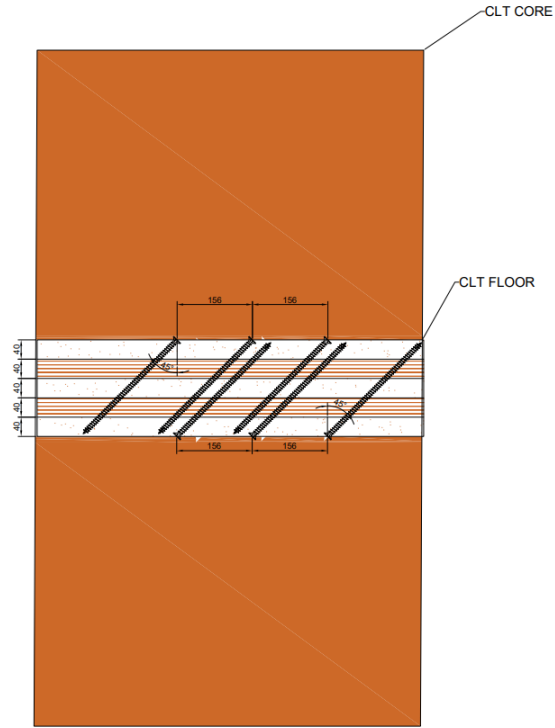
The analytically calculated strengths and stiffnesses for the different directions are shown in table I.11. It should be noted that the axial resistance and stiffness is higher than that of the in-plane and out-of-plane shear directions. This is the result of having two shear tension screws per row which provide a higher stiffness and strength than a combination of shear tension and shear compression.

Table I.11. Output floor to core connection

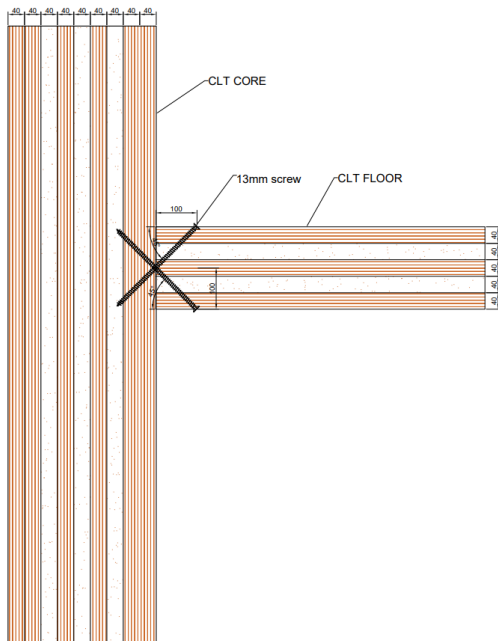
	F [kN/m]	K [kN/mm/m]
In-plane shear	108	129
out-of-plane shear	108	129
axial tension	181	194

In figure I.4 detailed drawings are shown for the floor to floor connection showing the double

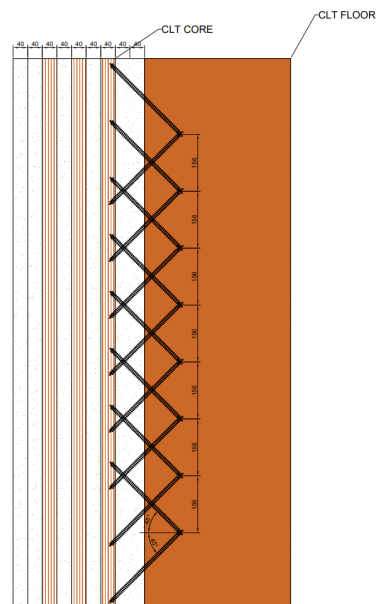
inclined screws spaced 12d.



(a) Front view



(b) Side view



(c) Top view

Figure I.4. Floor to core connection

Table I.10 contains the modelling assumptions i.e. stiffnesses of the joint in the different degrees of freedom. The directions u_x and u_y are modelled according to the results of the calculation as they influence the behaviour of the diaphragm floor, while u_z is modelled as rigid, which is the out-of-plane shear directions, as the influence on the global behaviour will be negligible. Additionally the rotational stiffness is modelled as pinned.

Table I.12. *Stiffness modelling assumptions floor to core connection*

u_x	u_y	u_z	ϕ_x
129 kN/mm/m	194 kN/mm/m (tension only)	rigid	free

Appendix J

Column to beam

Connection of the beams

At the intersection of the connection with columns as shown in section 3.9.7 the connection between columns and beams needs to be realised. The beams are loaded in bending due to floor loads which needs to be transferred through the joint as shear force, additionally lateral wind-loads need to be transferred from the facade to the beam as a normal force. The connection between the column and beam is performed by making use of a metal hanger with internal wings manufactured by Rothoblaas, as can be seen in figure J.1. The calculation method used is similar to that provided in section 3.9.4 with regards to straight screws except for the material used namely GL28h instead of CLT, therefore some changes are applied according to prEN1995-1-1.



(a) 3D view



(b) Metal hanger with internal wings

Figure J.1. *Beam to column joint*

At both the column and beam side of the connection screws will be used to connect the members with the metal hanger. Some benefits of using the metal hanger with internal wings are the following. Since the wings are internal most of the connection is concealed and beams with similar widths as columns can be connected together. The method allows for quick assembly and is relatively inexpensive for the connection of large size beams.

Table J.1. *Forces on the beam to column connection*

	force [kN]
Normal force (compression)	218
Normal force (tension)	-
shear force	101

The calculation method for the beam to column connection is shown in section Beam to column of Appendix H. The input for the calculation is shown in table J.2.

Table J.2. *Input data beam to column*

		beam side	column side
b	width	300 mm	400 mm
h	height	400 mm	400 mm
d	diameter of the fastener	12 mm	12 mm
d_{head}	diameter of the head of the fastener	20.75 mm	20.75mm
l_w	anchorage length	138mm	178mm
f_{head}	head pull through parameter	10.5 Mpa	10.5 Mpa
$f_{u,k}$	ultimate characteristic strength fastener	800 Mpa	800 Mpa
ρ_k	characteristic density	350 kg/m ³	350 kg ³
ϵ	angle between fibres and direction of fastener	90°	90°
t_h	embedment depth	138 mm	178 mm
k_{wd}		1	1
$k_{rp,1}$	factor for the rope effect	0.25	0.25
$k_{rp,2}$	limitation factor for the rope effect	1	1
k_p		1	1
k_{mat}	material parameter for the number of laminations	1.15	1
k_w		1	1

The obtained strengths for the beam and column side of the connection can be seen in table J.3. Both sides of the connection are able to transfer the shear force with a total of 24 screws on each side, by reducing the length of the screws at the column side from 200 mm to 150mm material use can be reduced while still providing sufficient strength.

Table J.3. *Shear resistance beam to column joint*

	number of screws	$F_{v,D}$
beam side	24	103 kN
column side	24	137 kN

In figure J.2 a detailed drawing is shown of the beam to column joint which is easily repeatable and can be partially attached off site to the columns after which the beams can be placed and fastened to the connector. Additionally the connections can be used at the intersection of the column to column connection as shown in section 3.9.7.

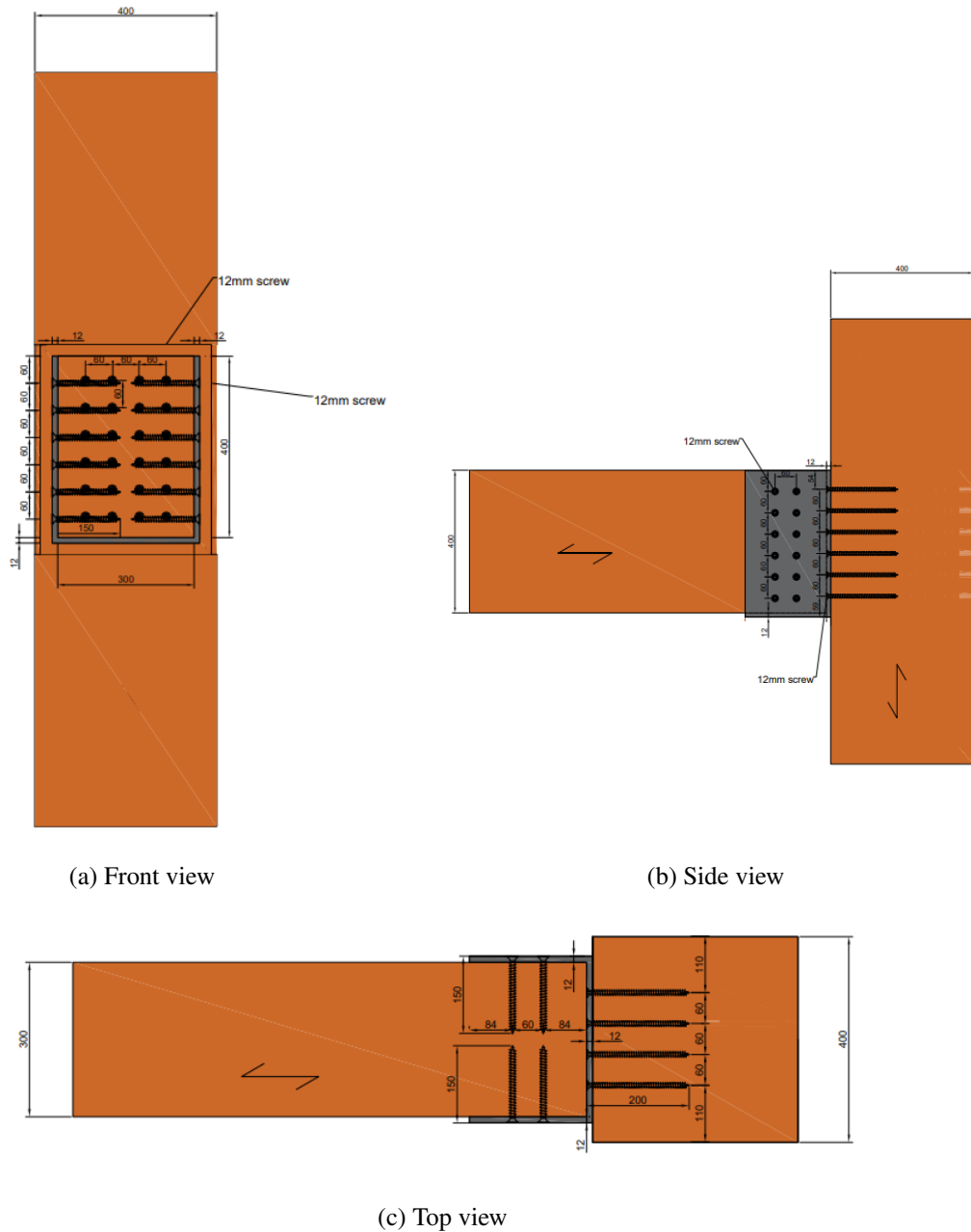


Figure J.2. Beam to column joint

The connection will be assumed as pinned in the numerical model. The corners of the steel connectors do not provide a stiff connection to resist translations and rotations. The modelling assumptions can be found in table J.4.

Table J.4. Numerical boundary conditions column to beam connection

	u_x	u_y	u_z	ϕ_x	ϕ_y	ϕ_z
Boundary conditions	rigid	rigid	rigid	rigid	free	free

Beam to core connection

The core to beam connection will be connected by a similar metal hanger with internal steel wings as in the column to beam design shown in the previous section 7.2. According to Rothoblaas the connection can be realised in both Glulam as well as CLT. It should be noted that the calculation method used in the previous section is not changed due to the change from glulam column to CLT core, methods are similar for both material types. However the parameter k_{mat} is changed from 1.15 to 1, which accounts for the number of layers.

The forces in the beam to core connection are shown in table J.5 below.

Table J.5. *Forces on the beam to core connection*

	force [kN]
Normal force (compression)	106
Normal force (tension)	34.5
shear force	61.8

The input data used for the calculation is shown in table J.6

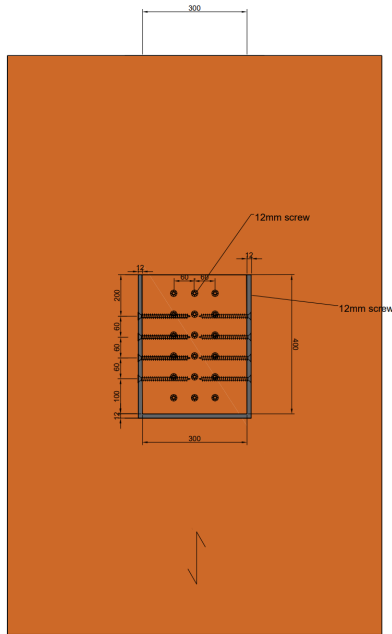
Table J.6. *Input data beam to core*

		beam side	core side
d	diameter of the fastener	12 mm	12 mm
d_{head}	diameter of the head of the fastener	20.75 mm	20.75mm
l_w	anchorage length	140mm	140mm
f_{head}	head pull through parameter	10.5 Mpa	10.5 Mpa
$f_{u,k}$		800 Mpa	800 Mpa
ρ_k	characteristic density	350 kg/m^3	350 kg^3
ϵ	angle between fibres and direction of fastener	90°	90°
t_h	embedment depth	140 mm	140 mm
k_{wd}	reduction factor wooden dowels	1	1
$k_{rp,1}$	factor for the rope effect	0.25	0.25
$k_{rp,2}$	limitation factor for the rope effect	1	1
k_p		1	1
k_{mat}	material parameter for the number of laminations	1.15	1
k_w		1	1

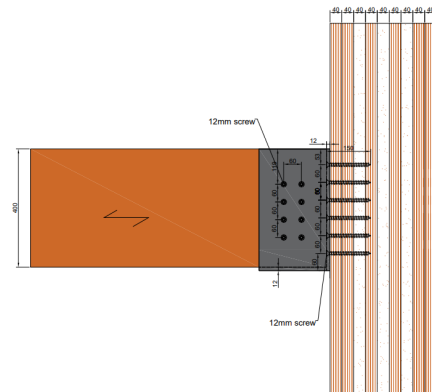
In figure J.3 a detailed drawing is shown of the beam to core connection. To enable both the beam to core and horizontal connection of the CLT panels as shown in section 3.9.5 an increased edge distance of the dowels need to be taken to ensure no overlapping occurs between the screws of the beam to core connection and the dowels of the horizontal CLT panel connection. The reduced strength requirements of the joint resulted in a reduction of the amount of screws used in comparison with the beam to column connection. The resistance of the connection can be found in table J.7.

Table J.7. Shear resistance beam to column joint

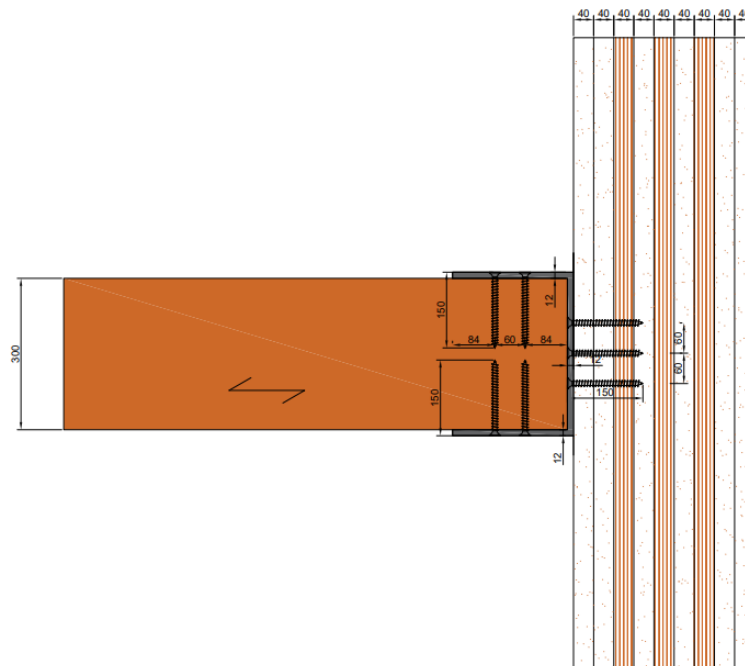
	number of screws	$F_{v,D}$	$F_{t,D}$
beam side	16	71.1 kN	71.1 kN
core side	18	91.4 kN	46 kN



(a) Front view



(b) Side view



(c) Top view

Figure J.3. Beam to core connection

Similar to the beam to column connection discussed in the previous section the beam to core connection will be modelled as pinned, with the modelling assumptions as shown in table J.8.

Table J.8. *Numerical boundary conditions beam to core connection*

	u_x	u_y	u_z	ϕ_x	ϕ_y	ϕ_z
Boundary conditions	rigid	rigid	rigid	rigid	free	free

Appendix K

Alternative connection core to foundation

Glued-in rods

For the sake of comparison a simple alternative design is made for the connection between the CLT core and foundation. The connection is made with glued-in rods instead of dowels and internal steel plates.

The resistance of the glued-in rods is based on the design for the column to column and column to foundation connection with the shear and tensile resistance for a single 30 mm rod as shown in table J.1. The reason that the bonded-in rods are placed in the vertically orientated layers is to ensure sufficient tensile strength. If rods are placed in horizontally orientated layers the design tensile capacity of the rods is limited to the effective area times the tensile strength ($f_{t,0,k} = 14$ vs $f_{t,90,k} = 0.12$) which drastically reduces tensile performance compared rods placed in vertically orientated layers.

Table J.1. *Required amount of glued in rods, placed in vertically orientated layers*

	Design resistance single rod [kN]	Design force con- nection [kN/m]	number of rods re- quired per m
Tension	91.5	1400	16
Shear	5.8	390	77

From the table above it can be seen that shear strength is governing in the determination of the required amount of rods. Which is due to the low embedment strength of the vertically orientated layers. However a possible solution to reduce the amount of rods is to place rods in horizontally orientated layers as well to increase shear resistance. In table J.2 the design shear and tensile resistance of the rods placed in horizontally orientated layers can be seen.

Table J.2. *Required amount of glued in rods, placed in horizontally orientated layers*

	Design resistance single rod [kN]	Design force con- nection [kN/m]	number of rods re- quired per m
Tension	0.6	1400	-
Shear	32.8	390	12

It can be stated that with the 16 rods in vertically orientated layers only 10 rods are needed in horizontally orientated layers to transfer the remaining shear force.

With a total of 26 rods in a single meter the stiffness is calculated and shown in table J.3

Table J.3. *Stiffness of the glued in rod connection*

	[kN/mm]	number of rods per m	[kN/mm/m]
K_{ax}	242	26	6292
$K_{v,0}$	11.8	16	188.8
$K_{v,90}$	2.4	10	24

To the total shear stiffness of the horizontal connection to the foundation is equal to $K_{v,tot} = 212.8 \text{ kN/mm/m}$ and the axial stiffness is equal to $K_{ax} = 6292 \text{ kN/mm/m}$. While the stiffnesses for the dowelled connection are equal to $K_{v,tot} = 1231 \text{ kN/mm/m}$ and $K_{ax} = 1231 \text{ kN/mm/m}$

It can be said that a design based on ULS of bonded-in rods provides an axial stiffness that is much higher than that of the dowelled connection, approximately 5 times higher. However the shear stiffness of the connection is approximately 5 times smaller than that of the dowelled connection. However as shown in section 5.1.1 the rigid body translation are governing in the lateral deflections due to the horizontal connection.

The rigid body translations are multiplied by a factor 5 while the rigid body translations are divided by a factor of 5. Resulting in a total deflection due to the horizontal connection of 1.9 mm if glued-in rods are used, compared to 4.4 mm for dowelled connections.

Special attention needs to be paid as to how the rods are placed in the CLT taking into account orientation of the layers, edge distances, internal spacing and end distances. Difficulties could occur due to the limited width of the member resulting in a lack of space to place the rods and provide sufficient spacing between rods.

For instance for a 30 mm rod a minimum internal spacing of 120 mm needs to be maintained which would in this case result in approximately 8 rows per meter CLT wall. For this case each row would have at least 3 glued-in rods to provide sufficient strength to the connection.

It can be concluded that if enough rods can be placed in a CLT panel which meet the requirements on spacing and edge distance, providing sufficient strength, a glued-in rod connection to the foundation is able to increase stiffness and reduce deflections originating from the foundation to core connection compared to a dowelled connection.

Appendix L

Calculation effective stiffness outrigger

In this appendix the calculation method used to determine the stiffness of an outrigger is shown. The calculation of the effective stiffness of the outrigger of case B is shown after which the effective stiffness of all other outrigger presented in this research will be shown. It should be noted that throughout the calculation only the effects of wind loading have been taken into account, in this way deflections of the outrigger can be obtained without the influence of axial differential shortening between core and columns.

By using superposition the deflection u at the outer column can be calculated according to equation J.1, in which the first term is the deflection due to bending at the outer column, the second term is the deflection due to bending at the inner column row and the third term is the rotation due to bending at the inner column row multiplied by the lever arm to the outer column row.

$$u = \frac{F_1 l_1^3}{3EI_{eff,outrigger}} + \frac{F_2 l_2^3}{3EI_{eff,outrigger}} + l_2 \frac{F_2 l_1^2}{2EI_{eff,outrigger}} \quad (J.1)$$

where

- F_1 is the outer column force due to wind loading only
- F_2 is the inner column force due to wind loading only
- L_1 is the length from core to outer column row, 12 meters
- L_2 is the length from core to inner column row, 6 meters

Rewriting the equation with the effective bending stiffness of the outrigger $EI_{eff,outrigger}$ as the unknown yields equation J.2

$$EI_{eff,outrigger} = \frac{F_1 l_1^3}{3u} + \frac{F_2 l_2^3}{3u} + l_2 \frac{F_2 l_1^2}{2u} \quad (J.2)$$

The next step consists of calculating the deflections due to bending. The procedure can be seen in figure J.1 for the outrigger on the left side of the core, the first step consists of determining the position of the outrigger if zero bending would occur, which is for the left hand side an upward shift of the core and a rotation of the core. Secondly the vertical displacement of the outrigger at the column locations is determined and is subtracted from the displacement if zero bending would occur.

With the displacement due to bending at the outer column and forces in both columns known the

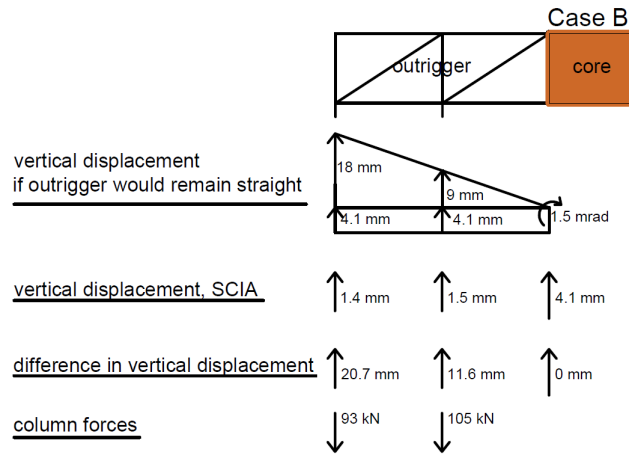


Figure J.1. Procedure for calculating the deflections due to bending of the outrigger

effective bending stiffness of the outrigger can be calculated using equation J.2. Finally an average is taken of the bending stiffness of the left and right side of the core. Differences are present due to the non-linear connections which are only activated in tension. The deflections and rotations of the core and columns can be seen in table J.1, with forces shown in table J.2. The effective bending stiffness of the left, right and average of the outriggers can be seen in table J.3

Table J.1. Vertical deflections and rotations of the column and core

	left outer column row	left inner column row	left side core	left side core rotation [mrad]	right side core rotation [mrad]	right side core deflection [mm]	right inner column row	right outer column row
	deflection [mm]	deflection [mm]	deflection [mm]				deflection [mm]	deflection [mm]
single storey outrigger								
Case B	1.4↑	1.5↑	4.1↑	1.5○	1.7○	3.1↓	1.8↓	1.4↓
Configuration 1	1.4↑	1.3↑	4.3↑	1.6○	1.8○	3.2↓	2.1↓	1↓
Configuration 2	1.3↑	0.2↑	4.8↑	1.6○	1.7○	3.6↓	0.4↓	1.3↓
Configuration 3	1.7↑	1.8↑	3.8↑	1.5○	1.7○	3.1↓	1.3↓	1.4↓
Configuration 4	1.2↑	2.3↑	3.9↑	1.6○	1.7○	3.1↓	1.2↓	1.3↓
Shear wall	2.2↑	2.5↑	3.2↑	1.1○	1.4○	2.4↓	2.3↓	2.2↓
Two storey outrigger								
Configuration 1	2.1↑	1.1↑	3.7↑	1.2○	1.4○	2.8↓	1.4↓	2.5↓
Configuration 2	3↑	2.9↑	2.1↑	1○	1.2○	1.8↓	2.8↓	2.9↓
Configuration 3	2.5↑	1.8↑	3.2↑	1.1○	1.3○	2.5↓	2.1↓	2↓
Configuration 4	3.1↑	2↑	2.8↑	1○	1.2○	2.3↓	1.5↓	2.4↓

Table J.2. *Vertical forces in the column*

	left column [kN]	outer row	left column [kN]	inner row	right column [kN]	inner row	right column row[kN]	outer
single storey outrigger								
Case B	93		105		-123		-94	
Configuration 1	95		86		-144		-68	
Configuration 2	88		13		-20		91	
Configuration 3	115		122		-83		-94	
Configuration 4	75		159		-82		-89	
Shear wall	149		175		-154		-149	
Two storey outrigger								
Configuration 1	171		88		-116		-202	
Configuration 2	243		238		-228		-235	
Configuration 3	203		150		-173		-226	
Configuration 4	252		164		-120		-200	

Table J.3. *Effective bending stiffness outrigger*

	$EI_{eff,outriggerleft}$ $*10^{12}$ [Nmm ²]	$EI_{eff,outriggerright}$ $*10^{12}$ [Nmm ²]	$EI_{eff,outriggerav}$ $*10^{12}$ [Nmm ²]
single storey outrigger			
Case B	3.5	3.5	3.5
Configuration 1	3.2	2.7	3.0
Configuration 2	2.3	2.5	2.4
Configuration 3	4.4	3.1	3.8
Configuration 4	3.3	3.0	3.1
Shear wall	8.3	6.7	7.5
Two storey outrigger			
Configuration 1	7.1	8.0	7.6
Configuration 2	16.5	13.3	14.9
Configuration 3	10.4	10.0	10.2
Configuration 4	14.9	9.6	12.2

Finally the ratio of the effective bending stiffness of the outrigger vs the effective bending stiffness of the core is determined as shown in table J.4, taking into account two outriggers are placed on each side of the core. The effective bending stiffness of the core is taken from table B.2 in Appendix B and is equal to $EI_{eff,core} = 2.57 * 10^{17}$.

Table J.4. Ratio effective bending stiffness outrigger vs effective bending stiffness core

	maximum lateral deflection [mm]	Peak lateral acceleration [m/s^2]	$\frac{2*E I_{eff,outriggerav}}{E I_{eff,core}} * 10^{-5}[-]$
single storey outrigger			
Case B	52.9	0.069	2.71
Configuration 1	54	0.071	2.3
Configuration 2	56.8	0.073	1.87
Configuration 3	52.5	0.070	2.93
Configuration 4	53.2	0.071	2.44
Shear wall	47.4	0.067	5.83
Two storey outrigger			
Configuration 1	49	0.066	5.91
Configuration 2	41.9	0.061	11.6
Configuration 3	46.8	0.064	7.94
Configuration 4	44.4	0.063	9.55

The obtained data can now be plotted in a graph as shown in figure J.2 with the stiffness ratio on the x-axis and the maximum lateral deflection for each case on the y-axis. Besides the data shown in table J.4 an additional point is added for which the outrigger stiffness is equal to zero and the maximum lateral deflection is equal to 61.8 mm, equal to the results of case A, a CLT core without outrigger.

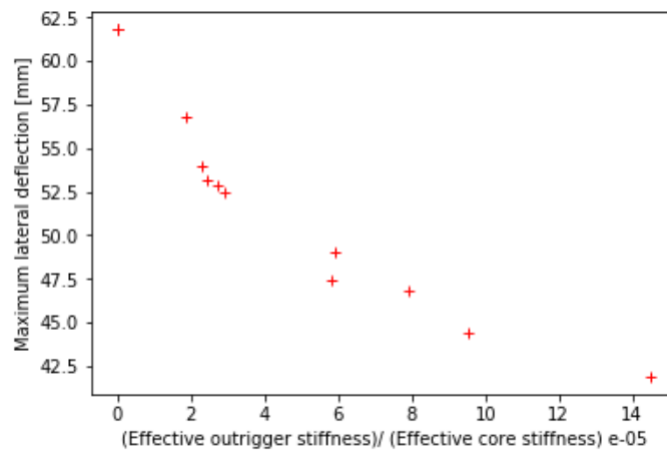
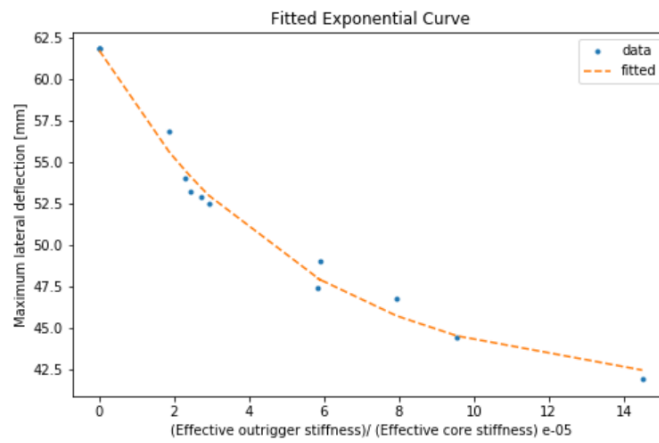
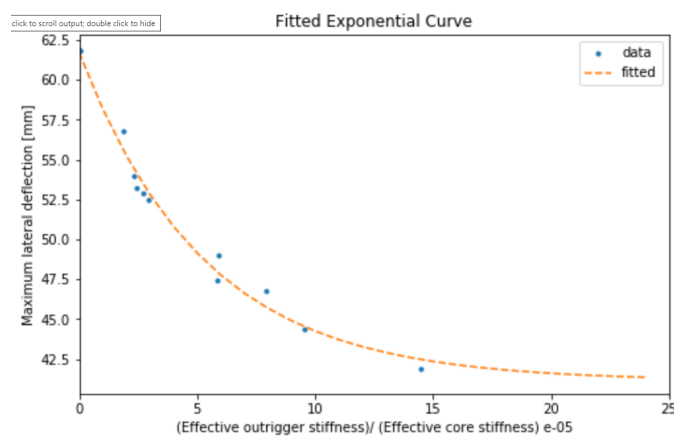


Figure J.2. Deflection vs stiffness ratio

An exponential fit is made of the data as shown in figure J.3a which is then extrapolated as shown in figure J.3b.



(a)



(b) Extrapolated

Figure J.3. Fitted curve deflection vs stiffness ratio

The fitted curves as shown in figure J.3 follow equation J.3.

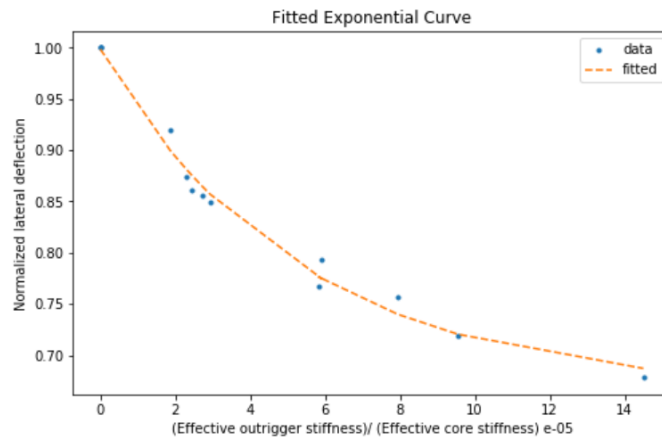
$$Y = 20.57789 * e^{-0.188645*x} + 41.1 \quad (J.3)$$

where

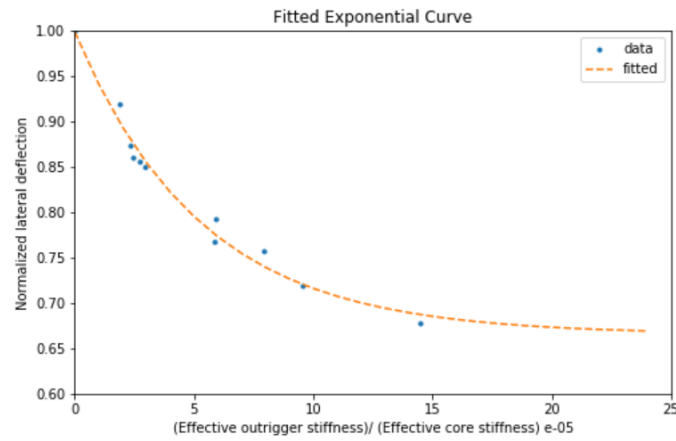
x is the ratio of the effective bending stiffness of the outrigger divided by the effective bending stiffness of the core, multiplied by 10^5 ;

Y is the maximum lateral deflection, in mm;

Finally a normalized plot is made in which the maximum lateral deflection is normalized with values starting at 0 and ending at 1 as shown in figure J.4.



(a)



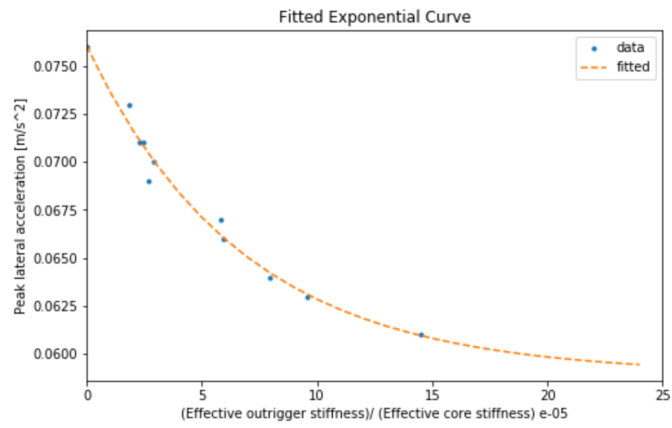
(b) Extrapolated

Figure J.4. Normalized fitted curve deflection vs stiffness ratio

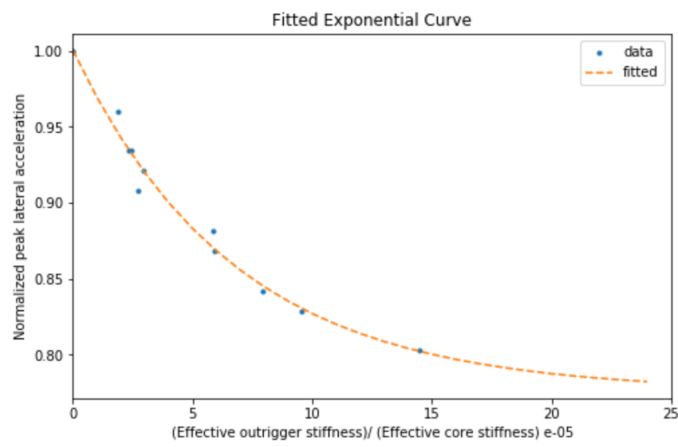
The fitted curves as shown in figure J.4 follow equation J.4.

$$Y = 0.332975 * e^{-0.188645*x} + 0.66551 \quad (J.4)$$

Similarly as the deflections the influence of the stiffness ratio on lateral accelerations can be assessed. The resulting figures for the lateral accelerations and normalized lateral accelerations can be seen in figure J.5a following equation J.5 and J.5b following equation J.6 respectively.



(a) Peak lateral acceleration



(b) Normalized peak lateral acceleration

Figure J.5. Fitted curves influence of stiffness ratio on peak lateral accelerations

$$Y = 0.01707 * e^{-0.14775*x} + 0.05896 \quad (J.5)$$

$$Y = 0.22466 * e^{-0.14775*x} + 0.77576 \quad (J.6)$$

The fitted curves are able estimate the influence on lateral of an outrigger based on the ratio of the effective stiffness of the outrigger vs the effective stiffness of the core.